

ACTA MEDICA (HRADEC KRÁLOVÉ)

2004, Vol. 47, No. 4

CONTENTS

REVIEW ARTICLES

Jiří Patočka, Kamil Kuča, Daniel Jun

Acetylcholinesterase and butyrylcholinesterase – important enzymes of human body.....215

Ana Lucía Seminario, Romana Ivančáková

Natal and neonatal teeth229

ORIGINAL ARTICLES

Jaroslav Mokry, Dana Čížková, Jan Österreicher

Subependymal zone: immunohistochemically distinct compartment in the adult mammalian forebrain235

Luděk Joska, Miroslav Marek

Passivation of dental amalgams and mercury release243

Lucie Bartošová, Gabriela Kunešová, Kamil Kuča, Josef Vachek

Therapeutic efficacy of different antidotal mixtures against poisoning with GF-agent in mice249

Caner Arslan, Sibel Özyazgan, Kazım Beşirli, Emir Cantürk, Gökçe Şirin, Kürşat Bozkurt, Gökhan Akkan

What are the reactivities of coronary arteries harvested from the hearts exposed to cold ischemic preservation?.....253

Demetrio Tamiolakis, Ioannis Venizelos, Maria Lambropoulou, Theodoros Jivannakis, Evagelia Seliniotaki, Panagiotis Tsikouras, Vasilios Limberis, Angelos Tsalkidis, Nikolas Papadopoulos

Gains and losses of HLA class II (DR) and CD4 in atypical hyperplasia, carcinoma in situ and infiltrating ductal carcinoma of the breast257

Hamid Nasri, Azar Baradaran

Correlation of serum magnesium with dyslipidemia in maintenance hemodialysis patients.....263

Ziad Albahri, Eliška Marklová, Hubert Vaníček, Lenka Minxová, Petr Dědek, Sylva Skálová, Marika Talábová, Jaroslava Vávrová, Eva Rencová

Our experience with diagnostics of congenital disorders of glycosylation267

Lubica Cibičková, Norbert Cibiček, Petr Žďánský, Pavel Kohout

The impairment of gastroduodenal mucosal barrier by coffee.....273

CASE REPORTS

Tulay Ozer, Ali Borazan, Mubin Hosnuter, Eksal Kargi, Ahmet Savranlar, Ahmet Yilmaz

Calciphylaxis involving both the upper and lower extremities277

Pavel Hladík, Robert Čáp, Tomáš Holeček

Acute stomach volvulus – case report281

BRIEF COMMUNICATIONS

Viera Danielisová, Miroslava Némethová, Jozef Burda

Iron deposition in the brain following the ischemia in a rat model of ischemic tolerance285

Jiří Knížek

Theoretical basis of new methodology of mathematical-statistical decision making with the help of biomarkers from mass spectra289

BIOPHYSICAL DAYS

Ladislav Doležal, Jan Hálek

A contribution to sonograph image quality estimation using point spread function293

Stanislav Ďoubal, Petr Klemra, Vladimír Semecký, Jiří Lamka, Monika Kuchařová

Non-linear mechanical behavior of visco-elastic biological structures – measurements and models297

Josef Hanuš, Jiří Záhora

Mechanical properties of selfexpandable stents.....301

Zuzana Hlinomazová, Ivo Hrazdira

Standardisation in ultrasonography: principle and diagnostic significance305

Martin Huf, Hana Kolářová, Robert Bajgar, Jaroslav Maceček, Marek Tomečka, Pavla Nevřelová, Jiří Mosinger, Pavel Tomek, Miroslav Strnad

Spectral characteristics of the supramolecular complexes of polypyrrolic sensitizers and cyclodextrin carriers: usage in photodynamic therapy of tumors.....309

Hana Kolářová, Martin Huf, Jaroslav Maceček, Pavla Nevřelová, Marek Tomečka, Robert Bajgar, Jiří Mosinger, Miroslav Strnad

The cellular uptake of sensitizers bound to cyclodextrin carriers.....313

Katarína Kozlíková, Juraj Martinka

Age and sex variability of initial parts of the QRS complex displayed in isointegral maps of young people317

Galina Laputková, Michal Legiš, Ján Sabo

Influence of D-glucose on lipid solid support membrane system as attempt for biosensing of medically relevant molecules323

Jaroslav Maceček, Hana Kolářová, Jitka Psotová, Robert Bajgar, Martin Huf, Pavla Nevřelová, Marek Tomečka, Jiří Mosinger

Assessment of cellular damage by comet assay after photodynamic therapy in vitro327

Josef Pešák, Tomáš Grézl, Ludmila Hurtová, Lenka Modráčková and working group

Report on the course of study BZ-1003-BR following the changes in airways in stutterers with the help of pulse oscillometry (Master Screen IOS)331

Jana Staničová, Andrej Musatov, Neal C. Robinson

Stability of bovine cytochrome c oxidase as studied after exposure to high hydrostatic pressure335

Daniel Šuta, Martin Komárek, Milan Jilek, Josef Syka

Software for the analysis of species-specific vocalizations.....339

Zdeňka Zapletalová, Roman Kubínek, Milan Vůjtek, Radko Novotný

Examination of dentin surface using AFM (our experience).....343

ACETYLCHOLINESTERASE AND BUTYRYLCHOLINESTERASE - IMPORTANT ENZYMES OF HUMAN BODY

Jiří Patočka^{1,2}, Kamil Kuča¹, Daniel Jun¹

Purkyně Military Medical Academy in Hradec Králové, Czech Republic; Department of Toxicology¹; University of South Bohemia, Faculty of Health and Social Studies, České Budějovice, Czech Republic; Department of Radiology and Toxicology²

Summary: The serine hydrolases and proteases are a ubiquitous group of enzymes that is fundamental to many critical life-functions. Human tissues have two distinct cholinesterase activities: acetylcholinesterase and butyrylcholinesterase. Acetylcholinesterase functions in the transmission of nerve impulses, whereas the physiological function of butyrylcholinesterase remains unknown. Acetylcholinesterase is one of the crucial enzymes in the central and peripheral nerve system. Organophosphates and carbamates are potent inhibitors of serine hydrolases and well suited probes for investigating the chemical reaction mechanism of the inhibition. Understanding the enzyme's chemistry is essential in preventing and/or treating organophosphate and carbamate poisoning as well as designing new medicaments for cholinergic-related diseases like as Alzheimer's disease.

Key words: *Acetylcholine; Acetylcholinesterase; Butyrylcholinesterase; Molecular forms; Cholinergic receptor; Organophosphates; Nerve agents; Carbamates; Reactivator; Oximes; Inhibition; Reactivation; Alzheimer's disease; Cholinolytics; Cholinomimetics*

1. Introduction

Acetylcholinesterase (AChE) is one of the most crucial enzymes for nerve response and function. AChE catalyzes the hydrolysis of acetylcholine esters with a relative specificity for acetylcholine. Acetylcholine is a common neurotransmitter found in the central and peripheral nervous system. When acetylcholine is released from an axon terminal, it moves across the synaptic cleft to bind to a receptor on the other side of the synapse. In the peripheral nervous system, acetylcholine is located at the „neuromuscular junction“ where it acts to control muscular contraction. Acetylcholine is also used in the autonomic nervous system. The intracellular effects of acetylcholine are mediated by the activation of nicotinic and muscarinic acetylcholine receptors (AChRs). AChE terminates transmission of neuronal impulses by rapid hydrolysis of acetylcholine (11).

2. Acetylcholine receptors

AChRs in the mammalian CNS can be divided into muscarinic and nicotinic subtypes based on the ability of the natural alkaloids, muscarine and nicotine, to mimic the effects of acetylcholine as a neurotransmitter (81). AChRs also mediate synaptic transmission at the neuromuscular

junction. The channel-linked AChR that mediates rapid, excitatory actions of acetylcholine is called nicotinic AChR (nAChR) because it can be activated by nicotine. The non-channel linked AChR that mediates the slow actions of acetylcholine, which can be either inhibitory or excitatory, is called muscarinic AChR (mAChR) because it can be activated by muscarine.

2.1 Nicotinic AChRs

The nAChRs arguably has the longest history of experimental study of any receptor, and is the prototype of ligand-gated ion channel. The nAChRs mediate the passage of potassium and sodium ions across synaptic membranes. Two classes of receptors exist: the neuromuscular nAChRs, which mediate signals between nerve and muscle cells, and the neuronal nAChRs, which are found throughout the nervous system. Until recently, studies of the neuropsychopharmacological effects of acetylcholine have focused on mAChRs, while nAChRs have been evaluated primarily for their role in mediating neuromuscular and autonomic transmission. However, over the last decade, this trend has changed following preclinical and clinical studies indicating that neuronal nAChRs may have a substantial role in mediating antinociception, cognitive performance, modulating

affect, and enhancing the release of other neurotransmitters.

These receptors comprise five homologous subunits, arranged either as a homopentameric or a pseudo-pentameric structure, depending on the types of subunits present (64). The small molecule acetylcholine (ACh), the activating ligand of these receptors, binds to two sites in a receptor, inducing a conformational change that is transmitted allosterically from the binding site through the subunits. The channels open as a result, permitting potassium and/or sodium ion passage across the membrane.

2.1.1 Classification of nAChRs

The muscle nAChR is a ligand-gated ion channel (LGIC) receptor composed of 5 subunits: two α_1 subunits, and one each of β_1 , δ and γ (or ϵ , depending on the stage of development). Several genes have been identified in rat and chick neural or sensory tissue that encode for neuronal nAChR subunits that are distinct from those in the muscle nAChR, providing for a multitude of potential subtypes of neuronal nAChRs. The wide distribution of some of these transcripts in mammalian brain indicates that neuronal nAChRs represent a major neurotransmitter receptor superfamily related to other LGICs including serotonin (5HT₃), GABA_A, N-methyl-D-aspartate (NMDA), and glycine.

Receptor nomenclature in the nAChR area has been derived from classical pharmacology approaches. Paton and Zaimis (1952) showed that the antagonist decamethonium (C10) was more effective than hexamethonium (C6) in blocking muscle nAChRs, whereas C6 was effective in autonomic ganglia. This led to the description of 'C10' (muscle) and 'C6' (neuronal) receptors (19). Muscle nAChRs are selectively activated by phenyltrimethylammonium salts and are pseudo-irreversibly blocked by alpha-bungarotoxin (alpha-BgT), toxic peptide from the venom of snake *Bungarus multicinctus*. Ganglionic nAChRs are preferentially activated by 1,1-dimethyl-4-phenylpiperazinium (DMPP), competitively blocked by trimethaphan, and are resistant to snake alpha-toxins, yet sensitive to neuronal bungarotoxin (n-BgT: also known as kappa-BgT, alpha-BgT 3.1, or toxin F) (101).

Brain nAChRs are a class of LGIC composed of alpha and beta subunits with specific structural, functional and pharmacological properties. They participate in the physiological and behavioural effects of acetylcholine and mediate responses to nicotine. They are associated with numerous transmitter systems and their expression is altered during development and ageing as well as in diseases such as autism, schizophrenia, Alzheimer's disease, Parkinson's disease and Lewy body dementia. Nicotinic receptors containing a number of different subunits are highly expressed during early human development (27).

In mammalian brain, two major neuronal nAChR subclasses can be delineated using radioligand binding (93): those that bind a-BgT with high affinity (a-BgT-sensitive

nAChRs, with $K_d \sim 0.5$ nM using [¹²⁵I]a-BgT) and those that do not (a-BgT-insensitive nAChRs). a-BgT-sensitive nAChRs have low affinity for (-)-nicotine, whereas a-BgT-insensitive nAChRs have high affinity ($K_d = 0.5$ – 5 nM) for [³H](-)-nicotine, [³H]ACh, [³H]methylcarbamylcholine (MCC), and [³H]cytisine). All four of these [³H]agonist ligands are thought to interact with the same acetylcholine binding sites on the nAChR (82).

2.1.2 Molecular diversity of nAChRs

The nAChRs are encoded by a family of related but distinct genes that share a common origin and have a long phylogenetic history. The current number of neuronal nAChR subunits in mammals is eleven (α_2 – α_7 , α_9 , α_{10} , β_2 – β_4), with an additional subunit, α_8 , identified in avian species. Nine subunits (α_2 – α_{10}) code for subunits based on the presence of adjacent cysteine residues in the predicted protein sequences, in a region homologous to the putative agonist binding site of the muscle subunit (α_1) while three are referred to as non-alpha or beta subunits (β_2 – β_4). Each of the nAChR subunits displays a characteristic phenotype of structural features extending from the N-terminus to the C-terminus: 1) a large (~200 amino acids) N-terminal hydrophilic domain containing the multiple loops of the neurotransmitter binding site; 2) the highly variable C-terminal hydrophilic domain that faces the cytoplasm, where it can be phosphorylated; and 3) a set of four closely spaced transmembrane domains—termed M1–M4—immediately following the large extracellular domain. The M2 domain is believed to form the wall of the ion channel. The amino acid sequences of the neuronal nAChR genes except α_7 and α_8 are between 40–60% similar (22). The α_7 and α_8 genes share approximately 70% similarity, with a much lower level (<30%) of similarity to the other nAChR genes. The α_9 subunit is the most unique of the alpha-subunits displaying less than 50% similarity to α_2 – α_8 (67). Comparison of the nAChR sequences also reveals that several pairs of subunits display homologies that are instructive in considering their function. For example the β_2 and β_4 are highly homologous, consistent with their ability to substitute for one another in forming functional channels when paired with α_2 , α_3 , or α_4 subunits.

Some human brain disorders believed to be associated with abnormal brain maturation involve deficits in both $\alpha_4\beta_2$, in the case of autism, and α_7 possibly in addition to $\alpha_4\beta_2$ nAChRs in the case of schizophrenia. In ageing and age-related neurodegenerative disorders nAChR deficits are predominantly associated with α_4 -containing receptors, although some studies also indicate the involvement of α_3 and α_7 subunits (27).

2.1.3 Topology of ligand binding sites on nAChR

The nAChR presents two very well differentiated domains for ligand binding that account for different choli-

nergic properties. In the hydrophilic extracellular region of both alpha subunits there exist the binding sites for agonists such as the neurotransmitter acetylcholine and for competitive antagonists such as d-tubocurarine. Agonists trigger the channel opening upon binding while competitive antagonists compete for the former ones and inhibit its pharmacological action. Identification of all residues involved in recognition and binding of agonist and competitive antagonists is a primary objective in order to understand which structural components are related to the physiological function of the AChR. These sites are mainly located on both alpha subunits in a pocket approximately 30–35 Å above the surface membrane. Since both alpha subunits are sequentially identical, the observed high and low affinity for agonists on the receptor is conditioned by the interaction of the alpha subunit with the delta or the gamma chain, respectively.

The principal component for the agonist/competitive antagonist binding sites involves several aromatic residues, in addition to the cysteine pair at 192–193, in three loops-forming binding domains (loops A–C). Other residues such as the negatively charged aspartates and glutamates (loop D), Thr or Tyr (loop E), and Trp (loop F) from non-alpha subunits were also found to form the complementary component of the agonist/competitive antagonist binding sites. Neurotoxins such as alpha-, kappa-bungarotoxin and several alpha-conotoxins seem to partially overlap with the agonist/competitive antagonist binding sites at multiple point of contacts. The alpha subunits also carry the binding site for certain acetylcholinesterase inhibitors such as eserine and for the neurotransmitter 5-hydroxytryptamine which activate the receptor without interacting with the classical agonist binding sites. The link between specific subunits by means of the binding of acetylcholine molecules might play a pivotal role in the relative shift among receptor subunits. This conformational change would allow for the opening of the intrinsic receptor cation channel transducing the external chemical signal elicited by the agonist into membrane depolarisation. The ion flux activity can be inhibited by non-competitive inhibitors. For this kind of drugs, a population of low-affinity binding sites has been found at the lipid-protein interface of the AChR. In addition, several

high-affinity binding sites have been found to be located at different rings on the M2 transmembrane domain, namely luminal binding sites. In this regard, the serine ring is the locus for exogenous non-competitive inhibitors such as chlorpromazine, triphenyl methyl phosphonium, the local anaesthetic QX-222 or phencyclidine (6).

2.2 Muscarinic AChRs

The mAChRs were first defined on the operational basis of selective agonism by muscarine and antagonism by atropine (86). The mAChRs are present in neurons of the central and peripheral nervous system, cardiac and smooth muscle and various exocrine glands (51). There are 5 subtypes (M1–M5) of the receptor that have a tissue specific pattern of expression (110). The M2 receptor is localized primarily in cardiac tissue and is also expressed at low levels in the hippocampus, cortex, striatum, thalamus, basal forebrain, brainstem, lung, vas deferens and uterus. The acetylcholine receptor channel is placed at the junction between the neuronal synapse and the muscle fiber. If the synapse becomes excited, the acetylcholine filled vesicles secrete their neurotransmitter into the synaptic cleft. This neurotransmitter opens the AChR channels resulting in an ionic current through the channels. The currents in turn excites the muscle fibers which then contract.

In the periphery, mAChRs mediate smooth muscle contraction, glandular secretion, and modulation of cardiac rate and force. In the CNS, mAChRs mediate motor control, temperature regulation, cardiovascular regulation and memory (96).

2.2.1 Classification of mAChRs

Five intronless genes encode all the mAChRs in vertebrates. The coding genes are fairly similar across species and exhibit sequence and structural homologies. Structurally, the muscarinic receptors are glycoproteins that display seven transmembrane pass domains similar to the G-protein-coupled receptor superfamily (96). The sequence homology also holds between muscarinic receptor subtypes across species, to the extent that they are classified as species homologues, i.e. when greater than 90 % of the amino

Tab. 1: Muscarinic acetylcholine receptor subtypes, G protein coupling, transductional mechanism and functional response.

	M1	M2	M3	M4	M5
Preferred G-Protein	Gq/11	Gi/o	Gq/11	Gi/o	Gq/11
The 2nd Messengers	PLC IP ₃ /DAG Ca ²⁺ /PKC	AC(-)	PLC IP ₃ /DAG Ca ²⁺ /PKC	AC(-)	PLC IP ₃ /DAG Ca ²⁺ /PKC
Functional Response	M-current inhibition	K ⁺ channel activation, Ca ²⁺ channel inhibition, decreases heart rate and force, decreased neurotransmitter release (presynaptic)	Smooth muscle contraction, gland secretion, decreased neurotransmitter release (presynaptic)	Ca ²⁺ channel inhibition	n/a

acid sequence is identical between receptors from different species. It is known that the minor sequence differences between species have a major impact on the pharmacological profiles but in the case of mAChR family, small sequence differences between mammalian species do not alter the pharmacological profiles and the order of potency mAChR agonists (42). In addition to being activated in the presence of agonists, mAChRs can interact with G-proteins in the absence of agonist, leading to activation of the G-protein pathway. This type of activation in the absence of a ligand is called constitutive activity (62). The summary of the major properties of mAChR subtypes is shown in Tab. 1.

3. Cholinesterases

Cholinesterase (ChE) is a generic term used for a family of related enzymes that hydrolyze choline esters at a faster rate than other esters under optimal conditions. These are serine hydrolases that belongs to the esterase family within higher eukaryotes. This family acts on different types of carboxylic esters (2). There are two types of ChE in the human body, with several variations and a confusing set of names. One type of ChE is acetylcholinesterase (AChE) (or acetylcholine acetyl-hydrolase, EC 3.1.1.7) also known as true, specific, genuine or type I ChE. This enzyme is found in erythrocytes, nerve endings, lungs, spleen and in the all compartments of brain. This enzyme is a membrane-bound glycoprotein and exists in several molecular forms. The other subgroup, butyrylcholinesterase (BuChE) (or acetylcholine acyl-hydrolase, EC 3.1.1.8) also known as plasma, serum, benzoyl, false, butyryl, nonspecific, or type II ChE. BuChE exists in plasma and has more than eleven isoenzyme variants. BuChE is also present in liver, smooth muscle, intestines, pancreas, heart and white matter of brain (70).

3.1 Butyrylcholinesterase

The enzyme is found in mammalian blood plasma, liver, pancreas, intestinal mucosa and the white matter of the central nervous system. It is sometimes referred to as serum ChE as opposed to red cell cholinesterase i.e. AChE. It hydrolyzes butyrylcholine 4 times more rapidly than acetylcholine. The BuChE does not hydrolyze D- β -methyl acetylcholine whereas AChE does. The enzyme is more active with butyryl and propionyl choline than with acetylcholine (68).

In humans, BuChE is synthesized in many tissues, including the liver, lungs, heart and brain. For a long time the physiological function of BuChE was vague. Nowadays the roles for BuChE have been suggested, for example, in lipoprotein metabolism (60), myelin maintenance (41), cellular adhesion and neurogenesis (61), as a scavenger of toxic molecules (100) and in the processing of the amyloid precursor protein (9). In human brain, the enzyme is found in neurones (29), glia (115) and in the plaques and tangles of Alzheimer' disease (AD) (47). Furthermore, the activity of

BuChE in the brain increases with age and is raised in AD (87). The BuChE plays important role in metabolism of some compounds. It hydrolyses also non-choline esters e.g. local anesthetics procaine, amethocaine or bupivacaine (45), suxamethonium (77), cocaine (20) and some other compounds, such as aspirin (69). The ability of BuChE to hydrolyze cocaine can be very important. Exogenously administered BuChE can accelerate cocaine metabolism in such a way as to potentially lessen the behavioral and toxic effects of cocaine. Therefore, BuChE may be useful as a treatment for cocaine addiction and toxicity. Because BuChE is alike as AChE inhibited by organophosphate compounds, the reduction in plasma activity is a means of monitoring exposure of individuals to organophosphates (98). The pre-treatment with purified exogenous human or equine serum BuChE is tested as a new therapeutic agent for protection against nerve agents and antidote against organophosphate lethality, without producing the adverse side effects associated with conventional treatments (8, 73).

3.1.1 BuChE genotypes

Several genetic variants of human BuChE are reportedly associated with prolonged apnoea in patients given the muscle relaxant drug succinylcholine (16). An estimation of the serum BuChE activity, dibucaine number (DN) and fluoride number (FN) have, in the past, been sufficient to identify most of the known BuChE phenotypes associated with succinylcholine sensitivity (37). However, several additional BuChE variants have been discovered in the last 10–20 years, which complicates the phenotyping of individuals. The molecular basis for a number of these variants has been reported, and it has become clear that multiple mutations within a single BuChE gene are not rare (12). The gene for BuChE is at chromosome 3q26.1–q26.2 and has several variants, such as the atypical (dibucaine-resistant), fluoride-1 and -2 (fluoride-resistant), and silent alleles, as well as the K, J and H variants, which result in reduced activity of BuChE (3, 46). The atypical allele, well known for the associated succinylcholine hypersensitivity, is found in approximately 4% of Caucasians. The various silent alleles are associated with no esteratic activity and are very rare (4). The most common coding region polymorphism is the K variant, found in about 33% of Caucasians and Orientals, i.e. with an allelic frequency of 18%. It has a DNA point mutation from guanine to adenine at nucleotide 1615 in exon 4, changing alanine 539 to threonine, near the carboxy terminus of the 574 amino acid protein. The K variant of BuChE results in 30% less plasma activity, due to fewer circulating enzyme molecules (94). The mutation, however, does not affect the esteratic activity, protein turnover or tetramer formation. Of these polymorphisms, only the K variant has been seriously studied as a gene associated with the development of AD (63, 74). The atypical allele has also been investigated. However, no AD association was found among the six atypical carriers. Genetic variation is one of several factors determining the level and

quality of plasma cholinesterase activity and it is very possible that individual differences can have till this time unexpected connections¹.

3.1.2 Molecular structure of BuChE

The molecule of BuChE contains 574 amino acids per subunit and nine carbohydrate chains attached to 9 asparagines. The four subunits of ChE appear to be identical and create tetramer molecule of BuChE. The active site serine is the 198th residue from the amino terminus. The sequence of human serum ChE is 53.8% identical with the sequence of acetylcholinesterase from *Torpedo californica* and 28% identical with the carboxyl-terminal portion of bovine thyroglobulin (66). Human serum ChE contains 8 half-cystines in each subunit of 574 amino acids. Six of these form three internal disulfide bridges: between Cys65–Cys92, Cys252–Cys263, and Cys400–Cys519. The disulfide bridges in human BuChE have exactly the same location as in *Torpedo californica* acetylcholinesterase. There is one potential free sulfhydryl in human ChE at Cys66, but this sulfhydryl could not be alkylated. Comparison of human ChE, and *Torpedo* and *Drosophila* acetylcholinesterases to the serine proteases suggests that the cholinesterases constitute a separate family of serine esterases, distinct from the trypsin family and from subtilisin (65).

The BuChE gene is at least 73 kb long, includes 1,722 basepairs of the coding sequence corresponding to the protein found circulating in human serum and contains four exons. Exon 1 contains untranslated sequences and two potential translation initiation sites at codons-69 and 47. Exon 2 (1525 basepairs) contains 83% of the coding sequence for the mature protein, including the N-terminal and the active-site serine, and a third possible translation initiation at codon-28. Exon 3 is 167 nucleotides long. Exon 4 (604 basepairs) codes for the C-terminus of the protein and the 3' untranslated region where two polyadenylation signals were identified. Intron 1 is 6.5 kb long, and the minimal sizes of introns 2 and 3 are estimated to be 32 kb each. Southern blot analysis of total human genomic DNA is in complete agreement with the gene structure established by restriction endonuclease mapping of the genomic clones: this strongly suggests that the BuChE gene is present in a single copy (7).

3.2 Acetylcholinesterase

Acetylcholinesterase (AChE) is likewise as BuChE a serine hydrolase that belongs to the esterase family within higher eukaryotes. This family acts on different types of carboxylic esters. Acetylcholinesterase's biological role is the termination of impulse transmissions at cholinergic sy-

napses within the nervous system by rapid hydrolysis of the neurotransmitter, acetylcholine (99).

3.2.1 Molecular structure of AChE

The monomer of AChE with a molecular weight around 60,000 is an ellipsoidal molecule approximately 45 x 60 x 65 Å, which consists of a 12 stranded central mixed beta sheet surrounded by 14 alpha helices (106). Studies have indicated several major domains within the protein: a catalytic active site composed of two subsites, the aromatic gorge in which the catalytic active site lies, and a peripheral anionic site, distinct from the catalytic active site, which plays a role in the confirmation of the residues within the aromatic gorge and active site.

3.2.2 Active site of AChE

The active site is composed of two subsites: the esteric subsite which contains the catalytic triad, and the anionic subsite that accommodates the positive quaternary compartment of acetylcholine. The esteric subsite contains the catalytic machinery of the enzyme: a catalytic triad of Ser 200, His 440, and Glu 327. This catalytic triad is similar to other serine proteases, except that this triad is the first to show Glu as the third member as opposed to Asp. The anionic subsite is defined by Trp 84, Phe 330, and Phe 331. Its role is to orient the charged part of the substrate that enters the active center. This role is the main function of the Trp residue (106). The recent rendition of the x-ray structure for AChE places the active catalytic site deep within a gorge-like fold of the protein. The aromatic gorge in the protein is approximately 20 Å deep and penetrates halfway into the enzyme. The active site lies at the base of this gorge only 4 Å above the base, leading some to label this the active gorge. The aromatic gorge is a more appropriate term, though, because 40% of its lining is composed of 14 aromatic residues located in the gorge which are highly conserved from different species of acetylcholinesterases (50). The high aromatic content of the walls and floor may explain why studies have proposed hydrophobic and anionic binding sites independent of the active site. Only a few acidic residues are present within the gorge. The aromatic residues clearly play an important role in the stabilization of the complex. Electrostatic as well as hydrophobic effects are of importance here (15). Electrostatic computations reveal the enzyme to be a single massive dipole. Electrostatic potential map of AChE suggests that this enzyme, possibly like other enzymes with charged substrates, steers its substrate toward its gorge and into the active site.

The most interesting aspect of this enzyme is the peripheral anionic site on its surface. A peripheral site was initially suggested by Changeux (21) to be involved in allo-

¹Many Persian Gulf veterans returned from that war only to develop unexplained illnesses for which the causes remain elusive. Recently, a committee of the Institute of Medicine reported that they were unable to find an association between such illnesses and a number of chemical exposures in the Gulf, including pyridostigmine bromide (anti-nerve gas pills) and organophosphate pesticides, both of which act by blocking the acetylcholinesterase necessary for nerves and muscles to work properly. However, it is possible that relationships between anticholinesterases and unexplained illnesses were obscured by genetic variations in sensitivity to these compounds. Butyrylcholinesterase is a plasma protein that binds these anticholinesterases and prevents their actions on muscles and nerve.

steric inhibition of the enzyme. The peripheral anionic site on AChE, located at the active center gorge entry, encompasses overlapping binding sites for allosteric activators and inhibitors; yet, the molecular mechanisms coupling this site to the active center at the gorge base to modulate catalysis remain unclear. The peripheral site has also been proposed to be involved in heterologous protein associations occurring during synaptogenesis or upon neurodegeneration (17). Site-directed labeling and mutagenesis studies place the location of this peripheral anionic site at or near the rim of the aromatic gorge (10). This site has the ability to bind to many different types of ligands, and by doing so effects the conformation of the active center. Hence ligand association with this site may prevent access of substrates to the gorge by steric obstruction to restrict entry to the gorge, by charge repulsion imparted through the association of a cationic ligand, or by allosteric mechanism in which the active center conformation is altered. Several bis- and tris-quaternary ligands bind to the peripheral site, and bis-quaternary ligands with large interquaternary distances (cca 14 Å) prevent binding of both active center and peripheral site ligands. Six residues have established activity within this site: Trp 286, Tyr 72, Tyr 124, Glu 285, and Asp 74 and Tyr 341, which are located on the opposite side of the gorge entrance to the previous four. Residues Trp 286, Tyr 72 and Tyr 124 are critical for dictating specificity. Likewise do the residues Trp 86, Phe 337, Tyr 342 and Glu 202. Occupation of the peripheral site may affect the conformation of the active center and the configuration of bound ligands at the active center. The above mentioned domains are responsible for the selectivity of AChE for substrates and inhibitors. Specificity for acyl chain length and the discrimination for substrate activation or inhibition are governed largely by the two Phe's 295 and 297 whose side chains outline the acyl pocket (79).

The peripheral anionic site is involved in a „cross-talk“ mechanism with the active site. This mechanism is an interaction between the Trp 286 and Trp 86 residues. When Trp 286 is bonded on the periphery, it effects the Trp 86 in the active site and causes distinct conformations of the active site to occur, thus changing the functionality of the enzyme. Asp 74 also plays a role in allosteric modulation of the enzyme. This residue acts with Tyr 341, as well as other residues along the aromatic gorge, and terminates at Tyr 337. The sensitivity of these residues and the plasticity of the active center are probably the result of evolutionary design aimed to confer optimal catalytic activity under a wide variety of conditions that are characteristic for the operation of acetylcholinesterase in the synaptic cleft (79).

3.2.3 Hydrolysis of acetylcholine

The hydroxyl group on the serine executes a nucleophilic attack on an electrophilic carbon atom of the substrate, in this case the ester linkage between choline and the acyl group to temporarily form a covalent acyl bond between the enzyme and the substrate. The imidazole nitrogen of histi-

dine may form a transient hydrogen bond with the hydroxyl group of the serine, promoting the nucleophilic reaction. The imidazole group may then facilitate the transfer of the acyl group from the serine hydroxyl to water. This is followed by a rapid hydrolysis of the acylated enzyme yielding acetic acid, and the restoration of the esteratic site. The pathway is similar to a pipeline, where substrate goes in one end and the products come out the other through conformational changes, along with the hydrophobic and electrostatic forces (104). Acetylcholine is the neurotransmitter common to many synapses throughout mammalian nervous systems. AChE is bound to cellular membrane of excitable tissues at cholinergic synaptic junctions, endoplasmic reticulum, among other membranes, which are usually associated with nerve impulse conduction. AChE is also found in red blood cells.

The optimum pH for AChE is 7.0 with the isoionic point near the pH of 5.35. The specificity at substrate concentrations of 1×10^{-3} M and constant enzyme level (approximately optimal for acetylcholine), produce the following relative rates of hydrolysis for several ester substrates: acetylcholine, 100; propionylcholine, 96; butyrylcholine, negligible; and triacetin, 11. A typical activator for AChE is 0.02 M Mg^{2+} , which is stimulatory in purified preparations.

3.2.4 Substrate Inhibition

Various explanations have been proposed to account for the different responses of AChE and BuChE to excess substrate. Rosenberry (92) suggested that the rate limiting step in catalysis was formation of an induced fit complex, and substrate inhibition was brought about by interference with this step. It has also been proposed that substrate inhibition is due to deacylation being retarded by binding of a second acetylcholine molecule to the anionic subsite of the acyl enzyme (59). The inhibition of AChE by excess of substrate is one of the key features that distinguishes it from BuChE. BuChE exhibits the converse substrate activation, and both phenomena are likely to be related to the binding of substrate, and to the catalytic mechanism of the enzymes. It is not known whether substrate inhibition has a biological role, or is simply a consequence of the structure and molecular mechanism of AChE action.

It has been suggested that AChE is allosterically regulated by the binding of acetylcholine to the peripheral site through conformational changes at the active centre (21). During development, the electrophoretic mobility and sedimentation coefficient of rat brain G4 AChE remain constant, but its kinetic parameters including substrate inhibition are changed (54). Amphiphilic AChE from mosquito showed no substrate inhibition when freshly extracted, however upon conversion to its non-amphiphilic derivatives, with thiocyanate (a chaotropic anion), the substrate inhibition returned (30). These results indicate that the environment may confer a slight conformational change in AChE, which results in substrate inhibition. The importance of the peripheral site in substrate inhibition has been

supported by Radic et al. (89), based on studies of competition of substrate with the peripheral site ligand propidium.

3.2.5 Molecular forms of AChE

The enzyme in its natural state is a monomer with a molecular weight around 60,000 and often forms aggregates which continue to produce catalytic activity. The enzyme monomer is an alpha/beta protein that contains 537 amino acids with Asp1 as the N-terminal and Cys537 as the C-terminal.

Cholinesterases show a polymorphism of quaternary structures, of similar catalytic activity but differing in their hydrodynamic parameters and ionic or hydrophobic interactions. In the past the different polymorphic forms have been separated by sedimentation on density gradients, or by electrophoretic techniques, with or without detergent, which has led to a number of naming strategies. In this paper molecular forms are referred to using the recently agreed upon nomenclature of Massoulié (71).

Catalytic subunits, which may vary in glycosylation, can oligomerise into dimers or tetramers, giving rise to the globular (G) forms: G1, G2 and G4. The globular forms can further be divided depending on their amphiphilicity, due to the possibility of cell membrane attachment by either a glycosylphosphatidylinositol (GPI) anchor or the hydrophobic P subunit. Attachment of a collagen-like tail (Q subunits) to one, two or three catalytic tetramers gives the A4, A8 and A12 asymmetric forms which bind to the basal lamina. Free cysteine residues form inter-subunit disulphide bonds, to covalently dimerise catalytic subunits, and to attach catalytic subunits to P and Q polypeptide anchors. Tetramers are formed by electrostatic and hydrophobic interaction between two disulphide bonded dimers (40).

4. Anticholinesterases

For a long time the anticholinesterases of the most interest were the organophosphate and carbamate compounds employed as insecticides and nerve agents with military importance (1). Recently there are also inhibitors of AChE with practical use as therapeutics against Alzheimer's disease.

Although the catalytic triad of AChE is housed deep within the gorge, pharmacological observations demonstrate that AChE can be efficiently targeted by numerous inhibitors. Several regions in the complex structure of AChE can contribute to the overall picture of ligand affinity. These include all the protein domains through which the ligand proceeds to reach the active site in the bottom of gorge, such as the rim area surrounding the entering part of gorge and the amino acid residues lining its walls (104). In addition, the peripheral anionic site and/or the hydrophobic domains within the active site itself may be involved in ligand interactions. This heterogeneity of potential sites might explain the existence of multiple inhibitors of AChE. In-

hibition can be either reversible, by competitively blocking the substrate reaching the active site or quasi-irreversible, by covalent reaction with the active site serine, inactivating the catalytic ability of the enzyme.

Competitive inhibition takes place by blocking substrate at the active site (tacrine, edrophonium), non competitive inhibition occurs by binding to the peripheral site (propidium, gallamine). The bis-quaternary ligands as for example decamethonium or BW284c51 bind across both active and peripheral sites.

The longest known and most widely used inhibitor is the natural alkaloid physostigmine. This carbamoylates the active site serine residue, greatly slowing the acyl-enzyme hydrolysis reaction compared with the acetylated enzyme. Organophosphorus compounds such as diisopropyl fluorophosphate (DFP) are very potent inhibitors of AChE and they are used as agricultural insecticides or as nerve gases in chemical warfare. These compounds react with the active site serine forming a very stable covalent phosphoryl-enzyme complex. Carbamates and organophosphates are the most important groups of AChE inhibitors.

4.1 Carbamates

The longest known and the most widely used inhibitor of AChE is the natural alkaloid physostigmine (eserine). Physostigmine comes from the calabar bean (*Physostigma venenosum*) which grows in West Africa. The structure of physostigmine, first carbamate found in nature, was discovered by Stedman and Barger (105). When anticholinesterase activity of physostigmine was found and the meaning of N-methyl carbamic group as essential moiety for biological activity was recovered, thousands of different carbamates were synthesized. With a few exceptions they are either N-methyl or N,N-dimethyl carbamates. The N-methyl carbamates predominate in number and importance. Some of them, mainly discharged and lipophilic carbamates found exercise as insecticides (carbaryl, moban, dimetan, isolan, and hundreds of others), another found exercise in human and veterinary medicine (miotine, pyridostigmine, syntostigmine, etc.). Some carbamates were very toxic also for mammals including human and about their use as chemical weapons was speculated (T 1123) (85). Chemical structures of some important carbamates and carbamate pesticides are given in Fig. 1.

Carbamates act by carbamylating of AChE and abolishing its physiological function. The kinetic of AChE inhibition by carbamate can be illustrated by the Scheme 1.

Enzyme acetylcholinesterase (E) and carbamate (CX) create intermediate complex (ECX) with dissociation constant K_d which lose leaving group of carbamate (X) and the result of this procedure is carbamoylated enzyme (EC). This step of reaction is characterized by rate constant of carbamylation (k_2). The stability of carbamylated AChE (EC) is dependent on the character of carbamate. EC decarbamylated spontaneously by velocity character-

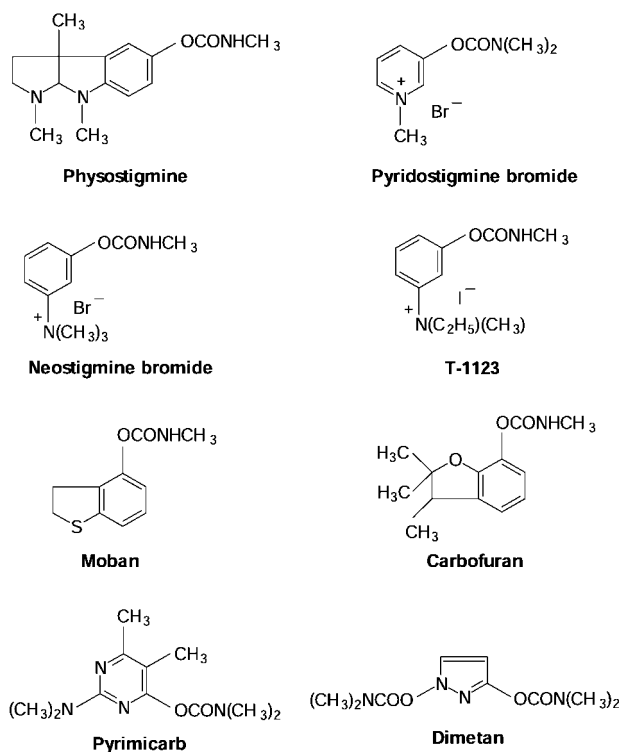


Fig. 1: Chemical structures of some important carbamates and carbamate pesticides.

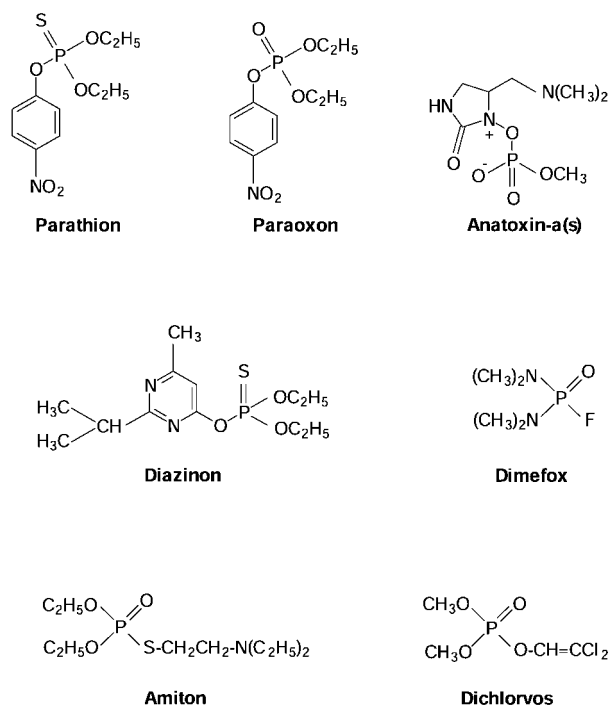
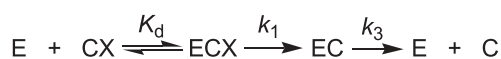
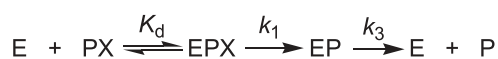


Fig. 2: Chemical structures of some organophosphates and organophosphate pesticides.



Scheme 1.



Scheme 2.

Tab. 2: Rates of spontaneous regeneration of carbamylated cholinesterases.

Carbamyl Group	Cholinesterase	Half-life	Reference
CH ₃ NH-CO-	AChE, eel	38 min	a
(CH ₃) ₂ N-CO-	AChE, eel	27 min	b
(CH ₃) ₂ N-CO-	AChE, bovine	56 min	b
(CH ₃) ₂ N-CO-	BuChE, human	3-5 hr	b

References: ^a Wilson et al., 1961, ^b Aldridge and Reiner, 1972

Tab. 3: Rates of spontaneous regeneration of phosphorylated cholinesterases.

Phosphoryl Group	Cholinesterase	Half-life	References
(CH ₃ O) ₂ -P(O)-	AChE, rat	121 min	a
(CH ₃ O) ₂ -P(O)-	AChE, rabbit	82 min	b
(C ₂ H ₅ O) ₂ -P(O)-	AChE, rat	44 hr	a
(C ₂ H ₅ O) ₂ -P(O)-	AChE, eel	27 days	c
(C ₂ H ₅ O) ₂ -P(O)-	BuChE, human	30 days	d
(C ₂ H ₅ O) ₂ -P(O)-	AChE, sheep	48 hr	e
(C ₂ H ₅ O) ₂ -P(O)-	AChE, hen	2 hr	d

^a Vandekar and Heath (1957), ^b Aldridge (1953), ^c Wilson (1951), ^d Davison (1955), ^e Blaber and Creasey (1960)

ized by a rate constant of decarbamylation (k_3). The half lives ($t_{0.5} = \ln 2/k_3$) of typical carbamylated AChEs are then, for example, between 20–60 min. It comes to this, that inhibition of AChE by carbamates has character of pseudoirreversible reaction. Rates of spontaneous regeneration of some carbamylated AChEs are summarized in Tab. 2.

4.2 Organophosphates

Organophosphates are typically synthetically prepared compounds. The only one organophosphate known in nature is anatoxin-a(s), toxic product of some cyanobacteria. All other toxic organophosphates were produced by human, either as pesticides or as nerve agents for warfare. First highly toxic organophosphates were prepared in Germany and Great Britain near before World War Two. Their extensive research and development come in fifth and sixth decade of the past century. The hazard problems which brought using of these compounds for environment and for mankind are known very well and there are not resolved comfortable.

Organophosphates react with AChE, likewise as carbamates, according to Scheme 2.

Acetylcholinesterase (E) creates with organophosphate (PX) intermediate complex (EPX) with dissociation constant K_d which loses leaving group of organophosphate (X) and the result of this procedure is phosphorylated enzyme (EP). EP is mostly quite stable and its velocity of dephosphorylation, characterized by a rate constant of dephosphorylation (k_3), is very slow. The half lives ($t_{0.5} = \ln 2/k_3$) of typical phosphorylated AChEs range several hours till several days. It comes to this, that inhibition of AChEs by organophosphates is practically irreversible and dephosphorylation step of this reaction is negligible. Rates of spontaneous regeneration of some phosphorylated AChEs are summarized in Tab. 3.

4.2.1 Organophosphate pesticides

Organophosphate pesticides were used in the fight with different pests in agriculture and forestry for a long time. A major objection to organophosphate pesticides has been their high mammalian toxicity and the resulting hazards associated with their use. While the objection is valid for what might be called the first generation of organophosphates (schradan, paraoxon, parathion), it does not hold to nearly the same extent for the second generation compounds (malathion, diazinon, fenitrothion) (72). Therefore many of them are used till this time. Chemical structures of some important organophosphates and organophosphate pesticides are given in Fig. 2.

4.2.2 Organophosphate nerve agents

Among lethal chemical weapons agents, the nerve agents have an entirely dominant role. Nerve agents acquired their name because they affect the transmission of

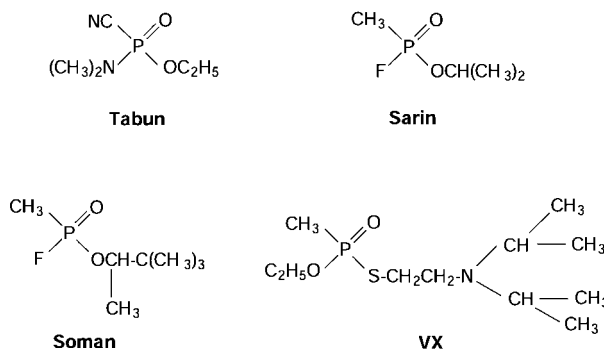
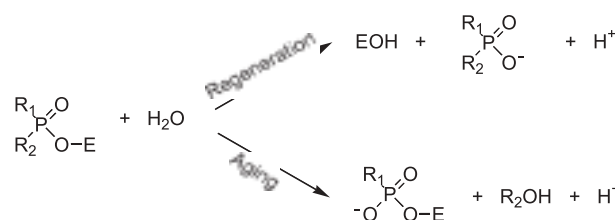


Fig. 3: Chemical structures of some military important organophosphates.



Scheme 3.

nerve impulses in the nervous system. All nerve agents belong chemically to the group of organo-phosphorus compounds. They are stable and highly toxic and have rapid effects both when absorbed through the skin and via respiration. It was not until the early 1930's that German chemists observed that organophosphorus compounds could be poisonous. In 1934, Dr Gerhard Schrader, a chemist at IG Farben, was given the task of developing a pesticide. Two years later a phosphorus compound with extremely high toxicity was produced for the first time. This phosphorus compound, given name tabun, was the first of the substances later referred to as nerve agents (57). Chemical structures of some important organophosphate nerve agents are given in Fig. 3.

4.3 Spontaneous regeneration and aging

Phosphorylated AChEs can undergo spontaneous hydrolysis to yield free enzyme (34, 109). The reaction follows first order kinetic with respect to [EP] because the concentration of water is relatively very high, and it remains constant. Spontaneous regeneration is a chemical reaction depending upon an enzyme, temperature, pH and ionic strength and namely on the kind of phosphoryl group (Tab. 3). A phosphorylated AChE may dephosphorylate and be regenerated, or it may dealkylate, in which case it is permanently inhibited and does not regenerate spontaneously or with reactivators.

The dealkylation of phosphorylated AChE is also known as aging. Like spontaneous regeneration, the rate of aging depends on the AChE in question and on the nature

of the phosphoryl group. Also aging follows first-order kinetics. The aging half-time of the diethyl phosphoryl enzyme is 41 hr compared with 4.6 hr for the diisopropyl phosphoryl AChE (52). Some groups age with alarming speed. For example, the aging half-life of the phosphorylating group of the phosphonate nerve agent, soman, is only 6 min at 25 °C, pH 7.4 using bovine erythrocyte AChE. By substituting cyclohexyl for the 1,2,2-trimethylpropyl (pinacolyl) group of soman, the aging half-life increased to 4000 min or by 666 times (26). Clearly then the rate of aging is very dependent on the alkyl groups substituted on the phosphorus.

4.4 Reactivators

The idea that certain compounds might greatly accelerate spontaneous regeneration of phosphorylated AChE is connected with Wilson's (111) experiments with hydroxylamine and choline. The hydroxylamine pointed to the necessity of finding compounds with improved nucleophilic properties, while the choline indicated that quaternary nitrogen might amplify the nucleophilic attack (112). The therapeutic potential of such compounds stimulated a search which culminated with the discovery of pyridine-2-aldoxime methiodide (2-PAM) by Wilson and Ginsburg (112) and Childs et al. (23). At present time several hundreds of such compounds are known and these are named as reactivators

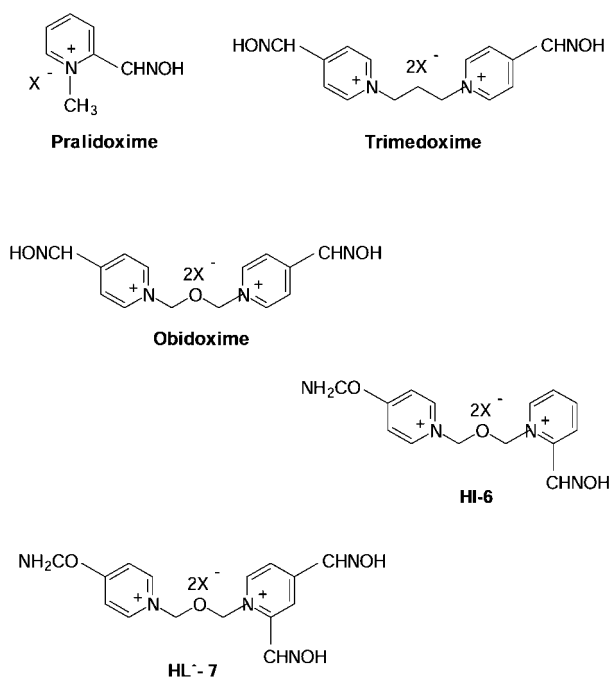


Fig. 4: Chemical structures of some pyridine oxime reactivators.



Scheme 4.

of phosphorylated AChE (56). 2-PAM has become an informal standard against which the efficacy of other reactivators is measured. The best-known reactivators are aldoximes derived from pyridine, and some of them found exercise in human medicine as antidotes against organophosphate poisoning. There are mainly bis-quaternary dialdoximes (trimedoxime, obidoxime) and bisquaternary monoaldoximes (HI-6, HI-67). Chemical structures of some important reactivators of phosphorylated AChE are given in Fig. 4.

The kinetic of reactivation is proceed according to the Scheme 4.

Phosphorylated enzyme (EP) create with reactivator (R) transient complex (EPR). The product of this reaction is regenerated enzyme (E) and phosphorylated oxime (PR). That themselves are powerful inhibitors of ChE, but they are unstable and decompose in a matter of minutes or hours (49).

5. Nerve Agent Antidotes

The effects of nerve agent exposure can be mitigated by the use of antidotes. Recent antidotes for nerve agent poisoning include administration of atropine together with reactivator of phosphorylated AChE (91). Atropine has been known for some time to be a competitive antagonist to muscarinic receptors and attenuates the effects of excess acetylcholine in the synaptic cleft. Atropine decreases secretions, reverses the spasms and contractions of smooth muscles and helps restore normal neurotransmission. Nevertheless, atropine is not able to restore AChE activity and its physiological function. This efficiency have only oxime reactivators. Reactivation of organophosphate-inhibited AChE by oximes is the primary reason for their effectiveness in the treatment of organophosphate poisoning (35).

6. Nerve Agent Pyridostigmine Pretreatment (NAPP)

The therapeutic agent pyridostigmine bromide has been used to treat *myasthenia gravis*, a chronic disease of neuromuscular transmission (78). Pyridostigmine is an AChE inhibitor in a manner analogous to organophosphorous agents with several important exceptions. The U. S. Army found that when given to animals in advance of nerve agent exposure, pyridostigmine has several beneficial effects. First, pyridostigmine reversibly carbamoylates the active site of AChE and does not significantly impair neuro-transmission. In addition, pyridostigmine is a competitive antagonist to phosphorylating agents and offers AChE a degree of protection against nerve agents. When animals are pretreated with pyridostigmine to a minimal level of carbamoylated AChE (20-40% of available AChE) and then exposed to lethal doses of nerve agents, the animal spontaneously regenerates enough AChE to carry on vital func-

tions. However, administration of atropine and 2-PAM chloride are still required when excess nerve agent remains to phosphorylate the AChE previously protected by pyridostigmine. Whereas NAPP affords protection against tabun and soman in animal models (55, 58), it provides little or no protection against sarin, GF, and VX exposure (5, 108).

7. Alzheimer's disease and AChE

Alzheimer's Disease (AD) is a neurodegenerative disorder affecting mainly aging populations in industrialised nations. This civilization disease effects only in the United States more than 4 million people. AD is characterized by loss of memory and cognition and its etiology is unknown. Approximately 90% of the cases are classified as sporadic late onset. By age 85 one out of two people has AD. Clinical picture of AD is characterised by three major pathological signs: beta-amyloid plaques, neurofibrillary tangles, and synaptic loss (43). A deficiency in cholinergic neurotransmission is considered to be one of the major causes of memory impairments in patient (13, 31, 107).

A role for the cholinergic system in human memory was suggested in the early 1970s, by demonstrating that the cholinergic antagonist scopolamine impaired learning in man (28, 38). Whereas the AChE inhibitor physostigmine was found to increase long term memory processes (32). Around the same time it was discovered that post mortem AD brain tissue showed reduction in the cholinergic neuronal markers choline acetyltransferase and AChE (31) and the loss of AChE in AD has more recently been refined to selective loss of membrane bound G4 (97). All these findings led to the formulation of a „cholinergic hypothesis“, i.e. that AD is associated with an impairment in cholinergic transmission (39, 113), linking abnormalities in the cholinergic system to certain functional and pathological changes in AD (18, 88). Since then abnormalities have been found in other parts of the cholinergic system: ACh synthesis (102), choline uptake (95), and in some cases, muscarinic receptors (114).

The importance of AChE in AD was emphasised by Smith and Cuello (103), suggesting that different cell groups where lesions occur in AD share a common feature, they all contain AChE. Cholinesterases were also found in senile plaques (44), even at the initial stages of their formation (76), and in neurofibrillary tangles (75). Mesulam and co-workers have reported that AChE in plaques and tangles shows a lower pH optimum, a reduced sensitivity to the inhibitors BW284c51, tacrine, and physostigmine (75). The AChE plays important role in the etiology, diagnostic and therapy of AD (84).

7.1 AChE inhibitors as Alzheimer's disease drugs

Current therapeutic strategies for the treatment of AD aim mainly to alleviate cognitive deficit by activating defective cholinergic transmission. Work has mainly centred on

inhibitors of AChE who represent at present standard of care for the symptomatic treatment of mild to moderate Alzheimer's disease. Cholinesterase inhibitors are a class of compounds used as chemical weapons on the one hand and simultaneously as a class of drugs that have been used for a number of years to slow the progression of Alzheimer's disease (83). The idea behind them is based on the fact that in Alzheimer's, there is a lack of a acetylcholine in the brain that shows degenerative changes of neurons. A drug that inhibits ChE means that more acetylcholine is available to carry out nerve cell communications. First clinical experiments of Alzheimer's disease treatment were due largely with physostigmine (14, 24) but the first medicament used in clinical practice was tacrine (Cognex) (33, 80). Chemical structures of some other inhibitors of AChE tested as potential drugs of Alzheimer's disease are given in Fig. 5.

In short- and long-term studies, the three cholinesterase inhibitors most commonly used, donepezil, rivastigmine, and galantamine, have demonstrated efficacy in improving not only cognition but also function and behavior in patients suffering from mild to severe cases of Alzheimer's disease and other forms of dementia (25). However, the benefits of cholinesterase inhibitors in treating the broad spectrum of symptoms associated with Alzheimer's disease

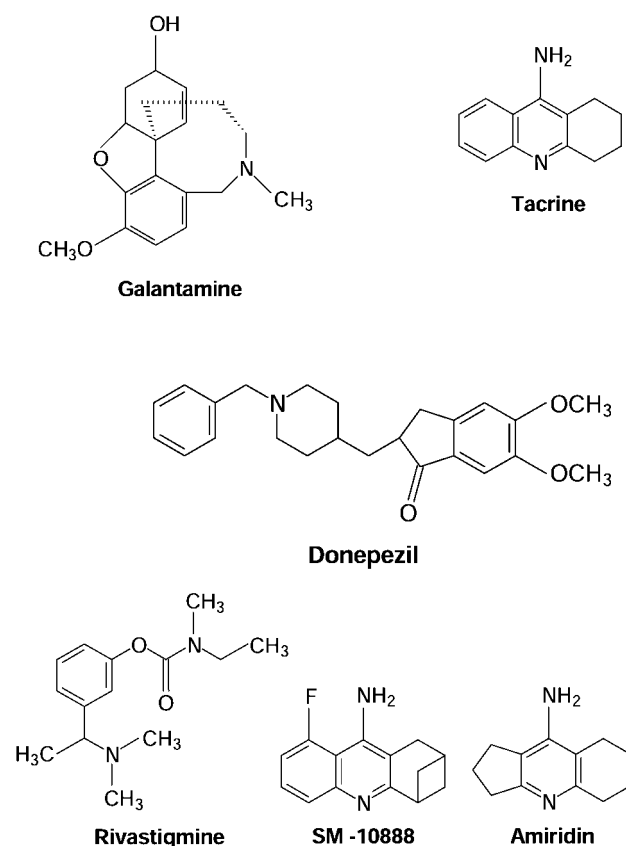


Fig. 5: Chemical structures of some acetylcholinesterase inhibitors used as Alzheimer's disease medicaments.

are not sustained indefinitely, and the illness continues to progress even while patients are receiving treatment. Additionally, while temporary stabilization may occur, there is typically only a modest improvement from baseline, and side effects from treatment with ChE inhibitors can be too severe for some patients to tolerate. Therefore, additional therapies for Alzheimer's disease still need to be developed that include more tolerable agents with alternative mechanisms of action and broader efficacy (36). Recently, evidence was presented that AChE accelerates assembly of amyloid- β -peptides into the amyloid fibrils that form the senile plaques characteristic of AD (53). It was suggested that a hydrophobic environment close to the peripheral binding site of the enzyme, at or near the entrance to the active-site gorge, might be involved in this process (48, 90).

References

- Aldridge WN, Reiner E. Enzyme Inhibitors as Substrates. Interaction of Esterases with Esters of Organophosphorus and Carbamic Acids. North Hollan Publ Comp, Amsterdam, 1972.
- Aldridge WN. Serum esterases. I. Two type sof esterase (A and B) hydrolysing p-nitrophenylacetate, propionate and butyrate, and a method for their determination. *Biochem J* 1953;53:110-24.
- Allderdice PW, Gardner HAR, Galutira D, Lockridge O, LaDu BN, McAlpine PJ. The cloned butyrylcholinesterase (BCHE) gene maps to a single chromosome site, 3q26. *Genomics* 1991;11:452-4.
- Altland K, Goedde HW. Heterogeneity in the silent gene phenotype of pseudocholinesterase of human serum. *Biochem Genet* 1970;4:321-38.
- Anderson DR, Harris LW, Woodard CL, Lennox WJ. The effect of pyridostigmine pretreatment on oxime efficacy against intoxication by soman or VX in rats. *Drug Chem Toxicol* 1992;15:285-94.
- Arias HR. Topology of ligand binding sites on the nicotinic acetylcholine receptor. *Brain Res Brain Res Rev* 1997;25:133-91.
- Arpagaus M, Kott M, Vatsis KP, Bartels CF, La Du BN, Lockridge O. Structure of the gene for human butyrylcholinesterase. Evidence for a single copy. *Biochemistry* 1990;29:124-31.
- Ashani Y, Shapira S, Levy D, Wolfe AD, Doctor BP, Raveh L. Butyrylcholinesterase and acetylcholinesterase prophylaxis against soman poisoning in mice. *Biochem Pharmacol* 1991;41:37-41.
- Balasubramanian AS. Amyloid beta peptide processing, insulin degrading enzyme and butyrylcholinesterase. *Neurochem Res* 2001;26:453-6.
- Barak D, Kronman C, Ordentlich A et al. Acetylcholinesterase peripheral anionic site degeneracy conferred by amino acid arrays sharing a common core. *J Biol Chemistry* 1994;269:6296-305.
- Barnard EA. Enzymatic destruction of acetylcholine. In Hubbard JI (ed.): *The Peripheral Nervous System*, New York, USA: Plenum Press, 1974;201-24.
- Barta C, Sasvari-Szekely M, Devai A, Kovacs E, Staub M, Enyedi P. Analysis of mutations in the plasma cholinesterase gene of patients with a history of prolonged neuromuscular block during anesthesia. *Mol Genet Metab* 2001;74:484-8.
- Bartus RT, Dean RL, Beer B, Lippa AS. The cholinergic hypothesis of geriatric memory dysfunction. *Science* 1982;217:408-14.
- Becker R, Giacobini E, Elble R, McIlhany M, Sherman K. Potential pharmacotherapy of Alzheimer's disease. A comparison of various forms of physostigmine administration. *Acta Neurol Scand Suppl* 1988;116:19-32.
- Berman HA, Leonard K. Ligand exclusion on acetylcholinesterase. *Biochemistry* 1990;29:10640-9.
- Boeck AT, Fry DL, Sastre A, Lockridge O. Naturally occurring mutation, Asp70His, in human butyrylcholinesterase. *Ann Clin Biochem* 2002;39:154-6.
- Bourne Y, Taylor P, Radic Z, Marchot P. Structural insights into ligand interactions at the acetylcholinesterase peripheral anionic site. *EMBO J* 2003;22: 1-12.
- Bowen DM, Allen SJ, Benton JS et al. Biochemical assessment of serotonergic and cholinergic dysfunction and cerebral atrophy in Alzheimer's disease. *J Neurochem* 1983;41:266-72.
- Brown DA. Neurotoxins and the ganglionic (C6) type of nicotinic receptor. *Adv Cytopharmacol* 1979;3:225-30.
- Carmona GN, Jufer RA, Goldberg SR et al. Butyrylcholinesterase accelerates cocaine metabolism: in vitro and in vivo effects in nonhuman primates and humans. *Drug Metab Dispos* 2000;28:367-71.
- Changeux JP. Responses of acetylcholinesterase from *Torpedo marmorata* to salts and curarizing drugs. *Mol Pharmacol* 1966;2:369-92.
- Chen Z, White MM. Forskolin modulates acetylcholine receptor gating by interacting with the small extracellular loop between the M2 and M3 transmembrane domains. *Cell Mol Neurobiol* 2000;20:569-77.
- Childs AF, Davies DR, Green AL, Rutland JP. The reactivation by oximes and hydroxamic acids of cholinesterase inhibited by organo-phosphorus compounds. *Br J Pharmac* 1955;10:462-5.
- Coelho F, Birks J. Physostigmine for Alzheimer's disease. *Cochrane Database Syst Rev* 2001;2:CD001499.
- Corey-Bloom J. Galantamine: a review of its use in Alzheimer's disease and vascular dementia. *Int J Clin Pract* 2003;57:219-23.
- Coult DB, Marsh DJ, Read G. Dealkylation studies on inhibited acetylcholinesterase. *Biochem J* 1956;98:869-73.
- Court JA, Martin-Ruiz C, Graham A, Perry E. Nicotinic receptors in human brain: topography and pathology. *J Chem Neuroanat* 2000;20:281-98.
- Crow TJ, Grove-White IG. An analysis of the learning deficit following hyoscine administration to man. *Brit J Pharmacol* 1973;49:322-7.
- Darvesh S, Grantham DL, Hopkins DA. Distribution of butyrylcholinesterase in the human amygdala and hippocampal formation. *J Comp Neurol* 1998;393:374-90.
- Dary O, Wedding RT. Absence of substrate inhibition and freezing-inactivation of the mosquito acetylcholinesterase are caused by alterations of hydrophobic interactions. *Biochim Biophys Acta* 1990;1039:103-9.
- Davies P, Maloney AJ. Selective loss of central cholinergic neurons in Alzheimer's disease. *Lancet* 1976;2:1403.
- Davis KL, Mohs RC, Tinklenberg JR, Pfefferbaum A, Hollister LE, Kopell BS. Physostigmine: improvement of long-term memory processes in normal humans. *Science*. 1978;201:272-4.
- Davis KL, Powchik P. Tacrine. *Lancet* 1995;345:625-30.
- Davison AN. Return of cholinesterase activity in the rat after inhibition by organophosphorus compounds. *Biochem J* 1955;60:339-46.
- Dawson RM. Review of oximes available for treatment of nerve agent poisoning. *J Appl Toxicol* 1994;14:317-31.
- Doody RS. Current treatments for Alzheimer's disease: cholinesterase inhibitors. *J Clin Psychiatry* 2003;64(Suppl 9):11-7.
- Doutin D, Brodeur J. An automated method for simultaneous determination of serum pseudocholinesterase activity, dibucaine number and fluoride number. *Clin Biochem* 1970;3:245-54.
- Drachman DA, Leavitt J. Human memory and the cholinergic system. *Arch Neurol* 1974;30:113-21.
- Dunnett SB, Fibiger HC. Role of forebrain cholinergic systems in learning and memory: relevance to the cognitive deficits of aging and Alzheimer's dementia. *Prog Brain Res* 1993;98:413-20.
- Duval N, Krejci E, Grassi J, Coussen F, Massoulie J, Bon S. Molecular architecture of acetylcholinesterase collagen-tailed forms; construction of a glycolipid-tailed tetramer. *EMBO J*. 1992;11:3255-61.
- Earl CJ, Thompson RHS. Cholinesterase levels in the nervous system in tri-ortho-cresyl phosphate poisoning. *Br J Pharmacol* 1952;7:685-94.
- Eglen RM, Hegde SS, Watson N. Muscarinic receptor subtypes and smooth muscle function. *Pharmacol Rev* 1996;48:531-65.
- Fine RE. The biochemistry of Alzheimer disease. *Alzheimer Dis Assoc Disord* 1999;13(Suppl 1):S82-7.
- Friede RL. Enzyme histochemistry of neuroglia. *Prog Brain Res* 1965;15:35-47.
- Galenko-Yaroshevskii AP, Derlugov LP, Ponomarev VV, Dukhanin AS. Pharmacokinetics and pharmacodynamics of a new local anesthetic agent. *Bull Exp Biol Med* 2003;136:170-3.
- Gaughan G, Park H, Priddle J, Craig I, Craig S. Refinement of the localization of human butyrylcholinesterase to chromosome 3q26.1-q26.2 using a PCR-derived probe. *Genomics* 1991;11:455-8.
- Geula C, Mesulam MM. Cholinesterases and the pathology of Alzheimer disease. *Alzheimer Dis Assoc Disord* 1995;9(Suppl. 2):23-8.
- Giacobini E. Cholinergic function and Alzheimer's disease. *Int J Geriatr Psychiatry*. 2003;18(Suppl 1):S1-S5.
- Hackley BE, Jr, Steinberg GM, Lamb JC. Formation of potent inhibitors of AChE by reaction of pyridinaldoximes with isopropyl methylphosphonofluoridate (GB). *Arch Biochem* 1959;80:211-4.
- Harel M, Schalk I, Ehret-Sabatier L et al. Quaternary ligand binding to aromatic residues in the active-site gorge of acetylcholinesterase. *Proc Natl Acad Sci USA* 1993;90:9031-5.
- Hirota SA. A quick guide to muscarinic acetylcholine receptors. *BioPharm J* 2001;5:6-8.
- Hobbiger FW. Chemical reactivation of phosphorylated human and bovine true cholinesterase. *Br J Pharmac* 1956;11:295-303.

53. Inestrosa NC, Alvarez A, Perez CA et al. Acetylcholinesterase accelerates assembly of amyloid-beta-peptides into Alzheimer's fibrils: possible role of the peripheral site of the enzyme. *Neuron* 1996;16:881-91.
54. Inestrosa NC, Ruiz G. Membrane-bound form of acetylcholinesterase activated during postnatal development of the rat somatosensory cortex. *Dev Neurosci* 1985;7:120-32.
55. Kassa J, Krejčová G, Samnaliev I. A comparison of the neuroprotective efficacy of pharmacological pretreatment and antidotal treatment in soman-poisoned rats. *Acta Med (Hradec Králové)* 2003;46:101-7.
56. Kassa J. Review of oximes in the antidotal treatment of poisoning by organophosphorus nerve agents. *J Toxicol* 2002;40:803-16.
57. Khurana D, Prabhakar S. Organophosphorus intoxication. *Arch Neurol* 2000;57:600-2.
58. Krejčová G, Kassa J. Neuroprotective efficacy of pharmacological pretreatment and antidotal treatment in tabun-poisoned rats. *Toxicology* 2003;185:129-39.
59. Krupka RM. The mechanism of action of acetylcholinesterase: substrate inhibition and the binding of inhibitors. *Biochemistry* 1963;2:76-82.
60. Kutty KM, Payne RH. Serum pseudocholinesterase and very-low-density lipoprotein metabolism. *J Clin Lab Anal* 1994;8:247-50.
61. Layer PG, Willbold E. Novel functions of cholinesterases in development, physiology and disease. *Prog Histochem Cytochem* 1995;29:1-94.
62. Leff P, Scaramellini C, Law C, McKechnie K. A three-state receptor model of agonist action. *Trends Pharmacol Sci* 1997;18:355-62.
63. Lehmann DJ, Johnston C, Smith AD. Synergy between the genes for butyrylcholinesterase K variant and apolipoprotein E4 in late-onset confirmed Alzheimer's disease. *Hum Molec Genet* 1997;6:1933-6.
64. Le Novère N, Corringer PJ, Changeux J-P. The diversity of subunit composition in nAChRs: evolutionary origins, physiologic and pharmacologic consequences. *J Neurobiol* 2002;53:447-56.
65. Lockridge O, Adkins S, La Du BN. Location of disulfide bonds within the sequence of human serum cholinesterase. *J Biol Chem* 1987;262:12945-52.
66. Lockridge O, Bartels CF, Vaughan TA, Wong CK, Norton SE, Johnson LL. Complete amino acid sequence of human serum cholinesterase. *J Biol Chem* 1987;262:549-57.
67. Lustig LR, Peng H. Chromosome location and characterization of the human nicotinic acetylcholine subunit alpha (alpha) 9 (CHRNA9) gene. *Cytogenet Genome Res* 2002;98:154-9.
68. Main A, Soucie W, Buxton I, Arinc E. The Purification of Cholinesterase from Horse Serum. *Biochem J* 1974;143:733-44.
69. Masson P, Froment MT, Fortier PL, Visicchio JE, Bartels CF, Lockridge O. Butyrylcholinesterase-catalyzed hydrolysis of aspirin, a negatively charged ester, and aspirin-related neutral esters. *Biochim Biophys Acta* 1998;1387:41-52.
70. Massoulie J, Sussman J, Bon S, Silman I. Structure and functions of acetylcholinesterase and butyrylcholinesterase. *Prog Brain Res* 1993;98:139-46.
71. Massoulie J. The origin of the molecular diversity and functional anchoring of cholinesterases. *Neurosignals* 2002;11:130-43.
72. Matsumura F. *Toxicology of Insecticides*. Plenum Press, New York 1975.
73. Matzke SM, Oubre JL, Caranto GR, Gentry MK, Galbicka G. Behavioral and immunological effects of exogenous butyrylcholinesterase in rhesus monkeys. *Pharmacol Biochem Behav* 1999;62:523-30.
74. McIlroy SP, Crawford VLS, Dynan KB, McGleenon BM, Vahidassr MD, Lawson JT, Passmore AP. Butyrylcholinesterase K variant is genetically associated with late onset Alzheimer's disease in Northern Ireland. *J Med Genet* 2000;37:182-5.
75. Mesulam MM, Geula C, Moran MA. Anatomy of cholinesterase inhibition in Alzheimer's disease: effect of physostigmine and tetrahydroaminoacridine on plaques and tangles. *Ann Neurol* 1987;22:683-91.
76. Moran MA, Mufson EJ, Gomez-Ramos P. Colocalization of cholinesterases with beta amyloid protein in aged and Alzheimer's brains. *Acta Neuropathol (Berl)*. 1993;85:362-9.
77. Morgan AA. Apnoea following suxamethonium: the genetic study of four generations of a family. *J Med Genet* 1982;19:22-5.
78. Newsom-Davis J. Therapy in myasthenia gravis and Lambert-Eaton myasthenic syndrome. *Semin Neurol* 2003;23:191-8.
79. Ordentlich A, Barak D, Kronman C, et al. Dissection of the human acetylcholinesterase active center determinants of substrate specificity. Identification of residues constituting the anionic site, the hydrophobic site, and the acyl pocket. *J Biol Chem* 1993;268:17083-95.
80. Ott BR. Medical treatment of Alzheimer's disease: past, present, and future. *Med Health R I* 2002;85:210-2.
81. Palacios JM, Boddeke HW, Pombo-Villar E. Cholinergic neuropharmacology: an update. *Acta Psychiatr Scand Suppl* 1991;366:27-33.
82. Paterson D, Nordberg A. Neuronal nicotinic receptors in the human brain. *Prog Neurobiol* 2000;61:75-111.
83. Patočka J. Acetylcholinesterase inhibitors - From nervous gas to Alzheimer's disease therapeutics. *Chem Listy* 1998;92:1016-9.
84. Patočka J, Strunecká A, Řipová D: Cholinesterázy a jejich význam v etiologii, diagnostice a terapii Alzheimerovy nemoci. *Čs Fyziol* 2001;50:4-10.
85. Patočka J.: T-1123, highly toxic carbamate with military significance (In Bulgarian). *Voenno Med Delo* 1990;44:14-19.
86. Paton WD, Zaimis E. The methonium. *Pharmacol Rev* 1952;4:219-53.
87. Perry EK, Perry RH, Blessed G, Tomlinson BE. Changes in brain cholinesterases in senile dementia of Alzheimer type. *Neuropathol Appl Neurobiol* 1978;4:273-7.
88. Perry EK. The cholinergic system in old age and Alzheimer's disease. *Age Ageing* 1980;9:1-8.
89. Radic Z, Reiner E, Taylor P. Role of the peripheral anionic site on acetylcholinesterase: inhibition by substrates and coumarin derivatives. *Mol Pharmacol* 1991;39:98-104.
90. Reyes AE, Perez DR, Alvarez A et al. A monoclonal antibody against acetylcholinesterase inhibits the formation of amyloid fibrils induced by the enzyme. *Biochem Biophys Res Commun* 1997;232:652-5.
91. Ricordel I, Meunier J. Chemical weapons: antidotes. View about the real means, perspectives. (in French) *Ann Pharm Fr* 2000;58:5-12.
92. Rosenberry TL. Catalysis by acetylcholinesterase: evidence that the rate-limiting step for acylation with certain substrates precedes general acid-base catalysis. *Proc Natl Acad Sci USA* 1975;72:3834-8.
93. Rubboli F, Court JA, Sala C, Morris C, Chini B, Perry E, Clementi F. Distribution of nicotinic receptors in the human hippocampus and thalamus. *Eur J Neurosci*. 1994;6:1596-604.
94. Rubinstein HM, Lubrano T, La Du BN. DNA mutation associated with the human butyrylcholinesterase K-variant and its linkage to the atypical variant mutation and other polymorphic sites. *Am J Hum Genet* 1992;50:1086-103.
95. Rylett RJ, Ball MJ, Colhoun EH. Evidence for high affinity choline transport in synaptosomes prepared from hippocampus and neocortex of patients with Alzheimer's disease. *Brain Res* 1983;289:169-75.
96. Scarpero HM, Dmochowski RR. Muscarinic receptors: what we know. *Curr Urol Rep*. 2003;4:421-8.
97. Schegg KM, Harrington LS, Neilsen S, Zweig RM, Peacock JH. Soluble and membrane-bound forms of brain acetylcholinesterase in Alzheimer's disease. *Neurobiol Aging* 1992;13:697-704.
98. Schneider F, Steenland K, Hernandez B, Wilson B, Krieger R, Spencer J, Margetich S. Monitoring peach harvest workers exposed to azinphosmethyl residues in Sutter County, California, 1991. *Environ Health Perspect* 1994;102:580-5.
99. Schumacher M, Camp S, Maulet Y, Newton M, MacPhee-Quigley K, Taylor SS, Friedmann T, Taylor P. Primary structure of Torpedo californica acetylcholinesterase deduced from its cDNA sequence. *Nature*. 1986;319:407-9.
100. Schwarz M, Glick D, Loewenstein Y, Soreq H. Engineering of human cholinesterases explains and predicts diverse consequences of administration of various drugs and poisons. *Pharmacol Ther* 1995; 67: 283-322.
101. Shen WX, Jobling P, Horn JP. The sensitivity of nicotinic synapses in bullfrog sympathetic ganglia to alpha-bungarotoxin and neuronal-bungarotoxin. *Br J Pharmacol* 1994;113:898-902.
102. Sims NR, Bowen DM, Allen SJ, Smith CC, Neary D, Thomas DJ, Davison AN. Presynaptic cholinergic dysfunction in patients with dementia. *J Neurochem* 1983;40:503-9.
103. Smith AD, Cuello AC. Alzheimer's disease and acetylcholinesterase-containing neurons. *Lancet* 1984;1:513.
104. Soreq H, Gnatt A, Loewenstein Y, Seville LF. Excavations into the active-site gorge of acetylcholinesterase. *TIBS* 1992;17:353-8.
105. Stedman E, Barger G. Physostigmine (eserine). Part III. *J Chem Soc* 1925; 127:247-58.
106. Sussman JL, Harel M, Frolov F et al. Atomic structure of acetylcholinesterase from Torpedo californica: a prototypic acetylcholine-binding protein. *Science* 1991;253:872-9.
107. Terry RD, Masliah E, Salmon DP et al. Physical basis of cognitive alterations in Alzheimer's disease: synapse loss is the major correlate of cognitive impairment. *Ann Neurol* 1991;30:572-80.
108. Tuovinen K, Kaliste-Korhonen E, Raushel FM, Hanninen O. Success of pyridostigmine, physostigmine, eptastigmine and phosphotriesterase treatments in acute sarin intoxication. *Toxicology* 1999;134:169-78.
109. Vandekar M, Heath DF. The reactivation of cholinesterase after inhibition in vivo by some dimethyl phosphate esters. *Biochem J* 1957;67:202-8.
110. Volpicelli LA, Levey AI. Muscarinic acetylcholine receptor subtypes in cerebral cortex and hippocampus. *Prog Brain Res* 2004;145:59-66.
111. Wilson IB. Acetylcholinesterases. XI. Reversibility of tetraethylpyrophosphate inhibition. *J Biol Chem* 1951;190:111-7.
112. Wilson IB, Ginsburg S. Reactivation of acetylcholinesterase inhibited by alkyl phosphates. *Arch Biochem Biophys* 1955;54:269-71.
113. Weinstock M. Possible role of the cholinergic system and disease models. *J Neural Transm Suppl*. 1997;49:93-102.

114. Whitehouse PJ, Au KS. Cholinergic receptors in aging and Alzheimer's disease. *Prog Neuropsychopharmacol Biol Psychiatry* 1986;10:665-76.
115. Wright CI, Geula C, Mesulam MM. Neuroglial cholinesterases in the normal brain and in Alzheimer's disease: relationship to plaques, tangles, and patterns of selective vulnerability. *Ann Neurol* 1993;34:373-84.

Submitted April 2004.

Accepted July 2004.

*Prof. RNDr. Jiří Patočka, DrSc.,
Purkyně Military Medical Academy,
Department of Toxicology,
500 01 Hradec Králové,
Czech Republic.
e-mail: patocka@pmfhk.cz*

NATAL AND NEONATAL TEETH

Ana Lucía Seminario, Romana Ivančaková

Charles University in Prague, Faculty of Medicine in Hradec Králové, Czech Republic: Department of Dentistry

Summary: Tooth eruption follows a chronology corresponding to the date when the tooth erupts into the oral cavity. This date has been established in the literature and is subject to small variations depending on hereditary, endocrine and environmental features. Any disturbance during the development of the teeth -systemic or local- can affect not only the morphology, structure of dental hard tissues or number of teeth but also the time of eruption. The presence of a tooth in the mouth at birth or during the first month of life has been studied and denominated as natal and neonatal teeth. The aim of this paper is to review current information on this topic and to give treatment alternatives if it is necessary.

Key words: *Natal and neonatal teeth; Supernumerary teeth; Riga-Fede disease*

Introduction

The success in the diagnosis, treatment and clinical procedures in dentistry involves good knowledge of dental structures morphology and the dynamics of growing and development of the dentition. Child development from conception through the first year of life is marked by many changes. Tooth eruption at about 6 months of age is a milestone both in terms of functional and psychological changes in the child's life and in emotional terms for the parents.

The expectations about the eruption of the first teeth are great and even greater when the teeth appear early in the oral cavity. When teeth are observed at birth or during the first month of life, being denoted natal and neonatal teeth, respectively, the interest, curiosity and concern of clinicians are similar to that of the parents.

Because of its rare occurrence, in the past this anomaly of eruption was associated with folklore, superstition, being related to good or bad omens. This explains the many reports about this topic since 59 B.C., as observed in cuneiform inscriptions detected in the 19th century.

Today, these teeth also stimulate the interest of both parents and health professionals because of their clinical characteristics, among them their great mobility, which raises concern about the possibility of their being swallowed or aspirated by the infant during nursing. The objective of the study was to present a review of the literature and clinical management techniques for natal and neonatal teeth.

Definition

Several terms have been used in the literature to designate teeth erupting before the normal time, such as con-

genital teeth, fetal teeth, predecidual teeth and dentitio praecox. According to the definition presented by Massler and Savara (1950) (36), taking only the time of eruption as preference, natal teeth are those observable in the oral cavity at birth and neonatal teeth are those that erupt during the first 30 days of life. This definition has been accepted and used by most authors.

History

The presence of natal and neonatal teeth has been reported and associated with interesting beliefs during time. The first reports came from Roman times with Titus Livius (59 BC) and Caius Plinius Secundus (23 BC) (23). The first considered the presence of natal teeth to be a prediction of disastrous events while the second believed that a splendid future awaited male infants with natal teeth, whereas the same phenomenon was bad omen for girls. In many African tribes children born with teeth were murdered soon after birth because they were believed they bring misfortune to all they would contact.

In England, the belief was that babies born with teeth would grow to be famous soldiers whereas in France and Italy the belief was that this condition would guarantee the conquest of the world. Historical figures such as Hannibal, Luis XIV, Mazarin, Richelieu, Richard II and Napoleon may also have been favoured by the presence of natal teeth (2,23,36).

Prevalence

Massler and Savara (36) reported a frequency of 1:2000 birth, 95% of them were deciduous teeth and only 5% su-

pernumerary. The literature reports incidence goes from 1:2000 to 1:3500 births (4). Kates, Needleman and Holmes (29) made a study with 18,155 infants and showed a prevalence of 1:716 live births. Leung (34) evaluated 50,892 infants over 17 years and found a prevalence of 1:3392 natal teeth. Even when there is not established (20), some investigators as Kates et al. (29) reported a higher prevalence of natal teeth in females with 66%. The variation in prevalence depends on the different population studied and on the methods employed in each study.

Aetiology

Many theories have been reported in order to explain the etiology of this phenomenon. The presence of natal and neonatal teeth is definitely a disturbance of histological chronology whose aetiology is still unknown. Some investigators suggest that natal teeth may be associated with some syndromes such as Ellis-van Creveld (Chondroectodermal dysplasia) (16,26), Hallerman-Streif (17), Pachyonychia congenita (13,45), Wiedemann-Rautenstrauch (51), cleft palate and cleft lip (16,21) and Soto (9).

It has been assumed that early eruption of primary teeth is the result of abnormal position of the germ during its development in the alveolar bone (5,40). Stewart and Prescott (50) believed that the superficial position of the dental germ increased rate of eruption due to febrile incidents, hormonal stimulation and heredity. Hals (22) thought that natal teeth were the result of hereditary influences. Bodentoff and Gorlin reported a family association in 14.5% of cases whereas Kates, Needleman and Holmes (29) found a positive family history in 7 of 38 cases of natal and neonatal teeth.

Osteoblastic activity has also been reported as a possible factor of this anomaly. Clergueau-Guerithault (26) suggested that the eruption of natal and neonatal teeth could be dependent on osteoblastic activity within the area of the tooth germ.

Clinical characteristics

Most of natal and neonatal teeth reported are early erupted teeth of normal deciduous dentition. The prevalence of supernumerary teeth has been suggested as ranging from 1 to 10% (29). Rusmah (43) described natal and neonatal teeth as conical or normal in size and shape and opaque yellow-brownish in colour. Bigeard (9) reported that dimensions of the crown are smaller than those reported by Lautrou (32) for primary teeth under normal conditions.

Histological reports about natal and neonatal teeth have shown that despite the normal structure of enamel of these teeth, early eruption interrupts the mineralization process of enamel (6,22). Hence, enamel has often been described as dysplastic or hypomineralized and has a tendency to wear and discolour (10).

Soni et al. (47) have published a microradiographical and polarized light microscopy (PLM) study of natal and neonatal teeth. They found enamel hypoplasia and dentinal disturbances including formation of irregular dentin and osteodentin in the cervical portions and interglobular dentin in the coronal region.

Meryem et al. (38) evaluated the surface topography of mandibular natal and neonatal incisors at the ultrastructural level using the scanning electron microscope (SEM). They found the hypoplastic enamel, depressed areas and the incisal edge of natal tooth lacked of enamel. In addition, root formation of the teeth was not complete which correlated with findings that teeth may erupt without root formation.

There is an interesting histological report on an upper natal molar made by Friend (18). He demonstrated that the alteration in amelogenesis detected in this tooth was due to premature exposure of it to the oral cavity, which finally resulted in metaplastic alteration of the epithelium of the normally columnar enamel to a stratified squamous configuration. This squamous aspect of enamel was visualized in the study made by Biggeard et al. (9).

The terms natal and neonatal teeth proposed by Massler and Savara (36) were limited only to the time of eruption, they did not consider the anatomical, morphological or structural characteristics of the teeth. Spouge and Feasby (49) in 1966 proposed a classification of these teeth based on their clinical characteristics. These teeth were then classified into:

Mature - when they are fully developed in shape and comparable in morphology to the deciduous teeth.

Immature - when their structure and development are incomplete.

The term mature may suggest that the tooth is well-developed compared to the remainder of the primary dentition and that its prognosis is relatively good. In contrast, the term immature assumes the presence of an incomplete structure and implies a worse prognosis for the tooth in question. On the basis of the literary data, Hebling (1977) (24), recently classified natal teeth into 4 clinical categories:

1. Shell-shaped crown poorly fixed to the alveolus by gingival tissue and absence of a root.
2. Solid crown poorly fixed to the alveolus by gingival tissue and little or no root.
3. Eruption of the incisal margin of the crown through gingival tissue.
4. Edema of gingival tissue with an unerupted but palpable tooth.

Diagnosis

It is important to determine if the tooth belongs to normal deciduous dentition or if it is supernumerary. Most of natal and neonatal teeth are primary teeth of the normal dentition and not supernumerary teeth (14). The use of cli-

nical and radiographic methods has been suggested by many authors (8,34,43). Radiographic verification shows adjacent structures of tooth and the presence or absence of germ in the primary tooth area (3).

Natal and neonatal teeth are usually located in the region of the lower incisors and are duplicated in 61% (2,11,29). Multiple natal teeth are extremely rare (41). However, some authors reported a case of natal teeth in which a second upper molar and lower canine were involved (37,52). Cysts of the dental lamina and Bohn nodules may be confused with neonatal teeth, the diagnosis can be made by radiographic examination (28,41,55).

Diagnosis is important for the maintenance of natal and neonatal teeth of the normal dentition. Premature loss of a primary tooth causes a loss of space and collapse of the developing mandibular arch with consequent malocclusion in permanent dentition (31).

Treatment and complications

The management of natal teeth depends on many factors. If it is a supernumerary tooth, then extraction is the best choice of treatment. If the tooth is excessively mobile and has poor implantation it is better to extract it and avoid risk of deglutition or inhalation. Hooley (25) found that 67% of natal and neonatal teeth would exfoliate prematurely, due to inadequate root formation and mobility of these teeth in the mouth. Bjueggren (10) published a report of 121 cases; he found that 38% of the natal and neonatal teeth exfoliated in the first year of life. When extraction is decided, it is necessary to be sure that the underlying dental papilla and Hertwig's epithelial root sheath are removed by a gentle curettage, otherwise, root development with continued (15). Ryba, Kramer, and Southam (44,48) reported that if there is remaining dental papilla, with the persistence of part of the radicular epithelial sheath of Hertwig there is a possibility of continuous dentin formation.

Extraction of these teeth is usually a simple procedure. But, it is important to recall precautions when the infant is

younger than 10 days of life. For haemorrhage prevention, vitamin K administration is indicated (12), until the 10th day of life when the intestinal flora becomes established and starts to produce vitamin K. This is essential for production of prothrombin in the liver and necessary in the normal healing process (2,43). If the extraction can not be delayed, consultation with the paediatrician is necessary to investigate if the child has been medicated with vitamin K immediately after birth as prevention of haemorrhagic disease of the newborn. Vitamin K is administered intramuscularly (0,5-1,0mg) (33).

Another factors to consider are implantation and degree of mobility, interferences with feeding, possibility of traumatic injury and inconveniences of sucking (35). A case was reported where the breast-feeding was prematurely interrupted due to the presence of neonatal teeth (29). If the tooth is part of normal primary dentition the maintenance of it must be the first treatment option, unless this would cause injury to the baby or to mother (16,42).

One of the most common complications associated with natal and neonatal teeth is Riga-Fede Syndrome. Antonio Riga (37), Italian physician (1881), was the first who described this lesion. In 1890, F. Fede (1) published histological study of these lesions. In the late 1800s', this lesion was of particular concern in Italy because it was associated with malnourished infants and often resulted in death (5,37). This syndrome refers the trauma of the tip or ventral surface of the tongue in newborn and infants (39). The lesion starts as an ulcer and after repeated trauma, progresses to an enlarged, fibrous mass, which appears like an ulcerative granuloma. Pain is present and the infant suddenly starts to suffer from dehydration, feeding difficulties and failure thrive. When the patient has systemic complications the risk of potential infection is high (46).

According to some investigators, the detection of this lesion is an indication for tooth extraction (16,27,54). In some cases smoothing can relieve an acute incisal margin (29,30). Goho (19) reported the treatment of a natal tooth as covering the incisal portion of the tooth with composite resin.



Fig. 1: 1 month old baby with natal teeth.

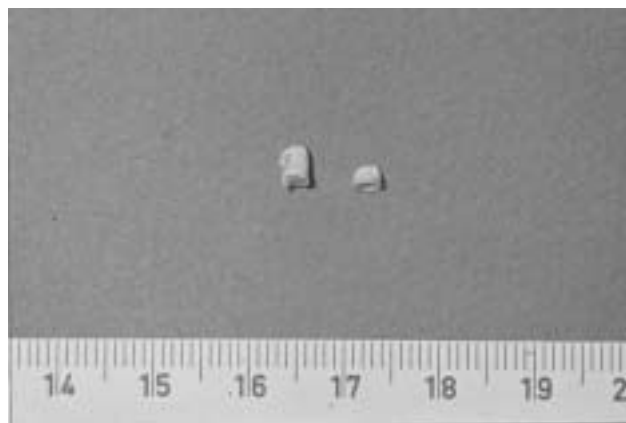


Fig. 2: Teeth after extraction.

Baghdadi (7) published a case of Riga-Fede disease in ten-days old male infant. The incisal edge was sharp and topical triamcinolone was applied, the ulcer resolved. Tomizawa (53) et al. reported seven cases of treatment of natal teeth by covering the incisal margin with resin, which aided rapid healing of the ulcers.

Stomahesive Wafers were used in some cases to cover the teeth and provide a smooth surface for the tongue to pass over during sucking, as in the cases published by Buchanan (15). He reported a case of four-week-old boy with a natal tooth and trauma of the tongue during sucking. The ulceration healed after four weeks using this conservative treatment. To relieve pain, treatment with an ointment such as Kenalog in Orabase is recommended (54).

Conclusions

Although natal and neonatal teeth do not appear frequently, proper evaluation and diagnosis are necessary for the best treatment option. Paediatricians are, usually, the first who find these teeth and early consultation with paediatric dentist can prevent complications.

Radiographic examination is the only way of revealing if the tooth is supernumerary or belongs to normal deciduous dentition. When teeth are supernumerary, they should be extracted. In this procedure, the clinician should first consider the well being of the patient and assess the risk of haemorrhage due to hypoprothrombinemia commonly present in newborns.

In most cases, natal and neonatal teeth belong to regular primary dentition and keeping these teeth in the mouth is the first choice of treatment. Alternatives such as smoothing the incisal edge or covering the edge with a composite resin are also recommended.

Periodic follow-up's by paediatric dentists are of fundamental importance, as are recommendations to the parents with respect to home dental hygiene and the use of fluoride.

References

- Abramson M: Sublingual granuloma in infancy. *J Pediatr* 1944;24:195-8.
- Allwright WC. Natal and neonatal teeth. *British Dent J* 1958;105:163-72.
- Almeida CM, Gomide MR, Nishiyama CK. Dente natal/neonatal. *Odontologia Clinica* 1997;7:43-5.
- Alvarez MP, Crespi PV, Shanska AL. Natal molars in Pfeiffer syndrome Type 3: A case report. *J Clinic Paediat Dent* 1993;18:21-4.
- Amberg S: Sublingual growth in infants. *Am J Med Sci* 1903;126:257-69.
- Anneroth G, Issacson AI, Linge G. Clinical, histological and micro-radiographic study of natal, neonatal and pre-erupted teeth. *J Dent Res* 1978;86:58-64.
- Baghdadi ZD. Riga-Fede disease: report of case and review. *J Clin Pediatr Dent* 2001;25(3):209-13.
- Bhaskar SN. Distúrbios de desenvolvimento dos maxilares, da denticao e dos dentes. In *Patologia Bucal*. Sao Paulo: Artes Médicas; 1976:151.
- Bigeard L, Hemmerle J, Sommermater JI. Clinical and ultrastructural study of the natal tooth: enamel and dentin assessments. *J Dent Child* 1996;63:23-31.
- Bjuggren G. Premature eruption in the primary dentition- a clinical and radiographical study. *Swed Dental J* 1973;66:343-55.
- Bodenhoff J. Natal and neonatal teeth. *Dental Abstr* 1960;5:485-88.
- Bodenhoff J, Gorlin RJ. Natal and neonatal teeth: folklore and fact. *Pediatr* 1963;32:1087-93.
- Bowden PE, Haley JL, Kansky A, Rothnagel JA, Jones DO, Turner RJ. Mutation of a type II keratin gene (K6a) in pachynochia congenital. *Nature Genetics* 1995;10:363-5.
- Brandt SK, Shapiro SD, Kittle PE. Immature primary molar in the newborn. *Pediatr Dent* 1983;5:210-13.
- Buchanan S, Jenkins C. Riga-Fedes syndrome: Natal or neonatal teeth associated with tongue ulceration. Case report. *Australian Dental Journal* 1997;42(4):225-7.
- Chow MH. Natal and neonatal teeth. *JADA* 1980;100:215-6.
- Fonseca MA, Mueller WA. Hallerman - Streiff syndrome: case report and recommendations for dental care. *J Dent Child* 1995;61:334-7.
- Friend GW, Mincer HH, Carruth KR, Jones JE. Natal primary molar: case report. *Pediatr Dent* 1983;5:210-3.
- Goho C. Neonatal sublingual traumatic ulceration (Riga-Fede disease): report of cases. *ASDC J Dent Child*. 1996;63(5):362-4.
- Gorlin RJ, Goldman HM, Thoma K. In: *Patologia Oral*. 4th Ed. Barcelona: Salvatores; 1973:pp.163-6.
- Gorlin RJ, Pinborg JJ, Cohen MM. Syndromes of the head and neck. New York: McGraw-Hill, 1976:82.
- Hals E. Natal and neonatal teeth: Histologic investigations in two brothers. *Oral Surg Oral Med Oral Pathol* 1957;10:509-21.
- Harila-Kaera V, Heikkinen T, Alvesalo L. The eruption of permanent incisors and first molars in prematurely born children. *Eur J Orthod* 2003;25(3):293-9.
- Hebling J, Zuanon ACC, Vianna DR. Dente Natal-A case of natal teeth. *Odontol Clin* 1997;7:37-40.
- Hooley JR. The infant's mouth. *J AM Dent Assoc* 1967;75:95-103.
- Jasmin JR, Guerithault SC. A scanning electron microscopic study of the enamel of neonatal teeth. *J Biol Buccale* 1991;19:309-14.
- Jasmin JR, Jonesco-Benaiche N, Muller-Giamarchi M. Natal and neonatal teeth. Management. *Ann Pediatr* 1993;40(10):640-1.
- Jefábková N, Kučera J. Natální a neonatální zuby. *Čs Pediatr* 1981;36:460-3.
- Kates GA, Needleman HL, Holmes LB. Natal and neonatal teeth: A clinical study. *J Am Dent Assoc* 1984;109:441-3.
- Kaur P, Sharminga A, Bhuller N. Conservative management of a complication of neonatal teeth: a case report. *J Indian Soc Pedod Prev Dent* 2003;21(1):27-9.
- Kominek J, Toman J, Rozková E. Dětská Stomatologie. Praha: Avicenum, 1980.
- Lautrou A. *Abreg d'anatomie Dentaire*. 2nd Ed., Paris: Masson, 1986:139-41.
- Leone RC, Araujo MCK. Doença hemorrágica do recém-nascido. In: *Pediatra básica*. 8a Ed. Sao Paulo: Sarvier, 1994:430-1.
- Leung AK. Natal teeth. *Am J Dis Child* 1986;140:249-51.
- Magitot E. Anomalies in the eruption of the teeth in the man. *Br J Dent Sc* 1983;26:640-1.
- Massler M, Savara BS. Natal and neonatal teeth. A review of twenty four cases reported in the literature. *J Pediatr* 1950;36:349-59.
- Matias, SR, Correa, MSNP. Radiologia em odontologia: Peimeira infancia. In: *Correa MSNP. Odontopediatria na Primeira infancia*. Sao Paulo: Santos; 1998: 209-19.
- Meryem U, Seval O, Hakan O, Hamdi C. Clinical and ultrastructural study of natal and neonatal teeth. *J Clin Pediatr Dent* 1999;23(3):173-7.
- Moncrieff A. Sublingual ulcer: with special reference to Riga's disease. *Br J Child Dis* 1933;30:268-74.
- N K-Hussein. Natal and neonatal teeth. *J Pedodont* 1990;14:110-2.
- Ooshima T, Mihara J, Saito T, Sobue S. Eruption of tooth-like like structure following the exfoliation of natal tooth: report of case. *J Dent Child* 1986;53:275-8.
- Roberts MW, Vann Jr, WF, Jewson, LG, Jacoway JR, Simon AR. Two natal maxillary molars. *Oral Surg Oral Med Oral Pathol* 1992;73:543-5.
- Rusmah M. Natal and neonatal teeth: a clinical and histological study. *J Clin Ped Dent* 1991;15:251-3.
- Ryba GE, Kramer IRM. Continued growth of human dentine papillae following removal of the crown of partly formed deciduous teeth. *Oral Surg Oral Med Oral Pathol* 1962;15:867-75.
- Shafer WG, Hine MK, Levy BM. *A Textbook of Oral Pathology*. 4th ed. Philadelphia, Pa: Saunders, 1983.
- Slayton R. Treatment alternatives for sublingual traumatic ulceration (Riga-Fede disease). *Pediatr Dent* 2000;22:5.
- Soni NN, Silberkweit M, Brown CH. Polarized light and microradiographic study of natal teeth. *J Dent Child* 1967;34:433-7.
- Southam JC. Retained dentine papillae in the newborn: a clinical and histopathological study. *Brit Dent J* 1968;125:534-9.
- Spouge JD, Feasby WH. Erupted teeth in the newborn. *Oral Surg Oral Med Oral Pathol* 1966;22:198-208.
- Stewart RE, Prescott GH. *Oral-facial genetics*. St. Louis, CV Mosby, 1976:142.
- Stoll C, Labay F, Geisert J, Alembik Y. Widemann-Rautenstrauch syndrome: a case report and review of the literature. *Genetic Counselling* 1998;9:119-24.
- Tay WM. Natal canine and molar in an infant. *Oral Surg Oral Med Oral Pathol* 1970;29:598-602.
- Tomizawa M, Yamada Y, Tonouchi K, Watanabe H, Noda T. Treatment of Riga-Fede's disease by resin-coverage of the incisal edges and seven cases of natal and neonatal teeth. *Shoni Shikagaku Zasshi*. 1982;27(1):182-90.
- Uzamis M, Turgut M, Olmez S. Neonatal sublingual traumatic ulceration (Riga-Fede disease): a case report. *Turk J Pediatr*. 1999;41(1):113-6.

53. Walter LRF, Ferelle A, Issao M. Necessidades odontológicas congênitas e de desenvolvimento. In: Odontologia Para o Bebe. Sao Paulo: Artes Médicas; 1996:145-51.

Submitted December 2003.

Accepted June 2004.

*Ana Lucía Seminario Antúnez de Mayolo, DDS, MDS,
University Hospital in Hradec Králové,
Department of Dentistry,
500 05 Hradec Králové,
Czech Republic.
e-mail: anase@hotmail.com*

SUBPENDYMAL ZONE: IMMUNOHISTOCHEMICALLY DISTINCT COMPARTMENT IN THE ADULT MAMMALIAN FOREBRAIN

Jaroslav Mokry¹, Dana Čížková¹, Jan Österreicher²

Charles University in Prague, Faculty of Medicine in Hradec Králové, Czech Republic: Department of Histology and Embryology¹; Purkyně Military Medical Academy in Hradec Králové, Czech Republic: Department of Radiobiology and Immunology²

Summary: The subependymal zone (SEZ) lining lateral walls of the lateral cerebral ventricles represents the site of active neurogenesis in the brain of adult mammals. Peroxidase immunohistochemistry performed in paraffin-embedded sections reveals that structural organization of the SEZ differs from other regions in the brain. The SEZ is devoid of synapses that are abundant in the adjacent striatal neuropil. Therefore immunostaining of synaptophysin detects sharp borders of the SEZ. Using immunophenotypization, we identified cell types constituting the SEZ in the intact rat forebrain. The presence of neural progenitor/stem cells was confirmed by finding of nestin-immunopositive cells. Detection of the astroglial marker GFAP confirmed that astrocytes represented major supporting elements responsible for creating a unique microenvironment of the SEZ. One type of the astroglia participated in covering surfaces of the blood vessels and boundaries of the SEZ. The second astroglial cell type formed branched elongated tubes that enwrapped other SEZ cell types with their cytoplasmic extensions. The interior of astrocytic channels was occupied with small densely aggregated NCAM-immunoreactive neuroblasts. Bipolar morphology indicated that these cells probably underwent migration. Immunodetection of other neuronal markers like β -III tubulin, MAP-2 and Pan neurofilaments identified positive cells in the neighbouring brain parenchyma but not in the SEZ. The rostral migratory stream (RMS) linked with the anterior SEZ had a similar structural arrangement. It contained a large amount of nestin⁺ and vimentin⁺ cells. The RMS consisted of GFAP⁺ astrocytic tubes ensheathing NCAM⁺ neuroblasts. On the contrary to the SEZ, the RMS neuroblasts expressed β -III tubulin. However, markers of postmitotic neurons MAP-2, Pan neurofilaments and synaptophysin were not expressed in the RMS. Our study describes a complex histological structure of the rat SEZ, identifies its individual cell types and demonstrates a usefulness of immunohistochemical detection of cell-specific markers in a study of microenvironment forming neurogenic zones in the mammalian brain.

Key words: Subependymal zone; Rostral migratory stream; Immunohistochemistry; Phenotypization; Rat forebrain

Introduction

Although for decades the brain had been considered as an organ incapable of regenerating the neuronal cells, nowadays it is generally accepted that neuronogenesis occurs within the adult mammalian central nervous system (CNS). A neural stem cell (NSC), a tissue-specific stem cell of the CNS, is responsible for generation of new neuronal and glial cells in situ. Its presence in the CNS has been confirmed by numerous studies based on incorporation of tritiated thymidine or bromodeoxyuridine (e.g. 1,29,37,38, 41), expression of nestin (which is considered to be a neural stem cell marker; 10) or cultivation of dissociated nervous tissue (6,35). The in vitro experiments gave the evidence that different regions of the adult CNS contained multipotent stem cells; so far NSCs have been isolated from the subependymal zone (SEZ; 3,6,9,30), rostral migratory stream

(RMS; 12), olfactory bulb (12,21), ependymal lining (15), hippocampus (3,30,32), other parts of the cerebral hemispheres (3,30,35), retina (2), spinal cord (16) etc. Of these, the SEZ represents the largest neurogenic region that continuously produces new neuronal and glial cells; the neuroblasts emigrate from the SEZ and incorporate in the target structures, e.g. in the olfactory bulb (via a specific pathway of the RMS) or neocortex (1,8,11,23). Following an injury to the adjacent brain parenchyma or exposure to growth factors, SEZ NSCs become activated and production of new cells in the SEZ rapidly increases (7,11,29,30,41), which documents functional participation of this region in the maintenance of brain tissue homeostasis.

In tissues, stem cells occupy specific microenvironments, the so-called niches, created by adjacent cells and extracellular structures that provide signals controlling the renewal of SCs and generation of their progeny. Due to

a large accumulation of NSCs along the SEZ, this zone structurally differs from the other brain regions. Whereas the white and gray matter of the brain contain nerve fibre tracts or interneuronal synapses making appropriate neuronal circuits, the SEZ is devoid of these structures. Permanent differentiated elements that likely play a key role in formation of the SEZ niche are represented by ependymal and astroglial cells. Doetsch et al. who analysed structure of the SEZ at the level of electron microscopy using serial sections identified two types of astroglial cells, the first one representing the element participating in delineation borders of this zone and the second type creating the tube-like channels ensheathing the immature SEZ cells (8). Similar astroglial tube-like structures were recognized in the RMS (34). These elongated channels delimitate pathway for neuroblasts emigrating from the SEZ to the olfactory bulb.

In the present study, we described a light microscopical architecture of the SEZ lining the lateral walls of lateral cerebral ventricles in paraffin-embedded sections of the intact rat forebrain. Using peroxidase immunohistochemistry, we identified precise boundaries of the SEZ and the cell types that coexist in the SEZ in a close relationship. Finally, we described expression of cell-specific markers in the RMS and compared its histological structure with the SEZ.

Materials and methods

Animals

Seven adult Wistar female rats (VELAZ, Prague, Czech Republic), approximately 3 months old and weighing 180–200 g, were used in this study. Experiments performed in this study were approved by the Ethical Committee supervising procedures on experimental animals at Charles University Medical Faculty in Hradec Králové.

Histology and Immunohistochemistry

Under deep anesthesia, rats were transcardially perfused with Carnoy's fixative. Brains were removed and immersed in the same fixative for at least three days, dehydrated in increasing concentrations of alcohols and embedded in paraffin. Serial seven-micrometre thick coronal sections were mounted on glass slides. Each 10th section was stained with haematoxylin and eosin, while other sections were processed for peroxidase immunohistochemistry.

Following deparaffinization, rehydration and microwave antigen retrieval, sections were incubated with the following primary antibodies for 45 min: anti-synaptophysin (SY38, 1:20, DAKO, Glostrup, Denmark), anti-GFAP (GA-5, 1:400, Sigma, Prague, Czech Republic), anti- β -III tubulin (TU-20, 1:200, Exbio, Prague, Czech Republic), anti-vimentin (V9, 1:40, Sigma), anti-MAP-2 (microtubule associated protein-2, HM-2, 1:500, Sigma), anti-PAN Neurofilament (clones DA2, FNP7 and RmdO20.11, 1:100, Zymed Laboratories Inc., San Francisco, CA), anti-NCAM

(neural cell adhesion molecule, 5B8, 1:4), anti-nestin (Rat 401, 1:4). Antibodies against NCAM and nestin were obtained from the DSHB, University of Iowa, Iowa City, IA, under contract N01-HD-6-2915 from the NICHD. After washing and incubation with the appropriate secondary antibody, streptavidin conjugated with horseradish peroxidase complex was applied for 45 min at room temperature. The intensity of faint immunoreactivity for synaptophysin was enhanced with the catalyzed signal amplification: after washing, the sections were incubated with 10 μ L biotin tyramine and 0.03% hydrogen peroxide for 10 min and then again incubated with streptavidin coupled with peroxidase. After rinsing, visualization was achieved by incubating with 3,3'-diaminobenzidine tetrachloride (Sigma) as the peroxidase substrate and hydrogen peroxide. The sections were then counterstained with methyl green.

Results

The subependymal zone

The SEZ is easily identifiable in lateral walls of the lateral cerebral ventricles (LCVs) between the ependyma and the striatum (Figs. 1, 2). The thickness of the SEZ varies according to its location; in the anterior SEZ, cells are arranged in several layers whereas posterior SEZ consists of an irregular layer of SEZ cells. Cellular density is larger in the SEZ than in the surrounding neuropil. Tightly packed cells of the SEZ are easily recognizable from the adjacent ependymal cell monolayer with characteristic round nuclei and distinct cilia that separates the SEZ from the ventricular cavity. The cells in the SEZ differ in their sizes, which indicate the presence of distinct cell types. Rich vascularization provides a proper nutrition to cells generated in the SEZ. Structure of the SEZ differs from all the other CNS regions because it is devoid of nerve fibre tracts or neuronal circuits formed by neuronal cells in other parts of the brain parenchyma. For that reason the SEZ lacks interneuronal synapses and it does not reveal immunoreactivity for glycoprotein of synaptic vesicles, synaptophysin. Due to small sizes of synaptic vesicles, a routine immunohistochemical detection of synaptophysin provides just a faint punctuate signal distributed throughout the mature brain parenchyma. Amplification of the specific signal using biotinylated tyramine results in an enormous increase of the intensity that allows to demarcate a sharp boundary between the immunopositive neuropil and immunonegative SEZ (Fig. 2).

Detection of glial fibrillary acidic protein (GFAP), a marker of astroglial cells that represent the main glial cell type of the CNS tissues, revealed that the SEZ contained a larger accumulation of macroglia than was typical for other brain regions (Fig. 2). Therefore astroglia represented a major supporting element responsible for creating a unique microenvironment of the SEZ. GFAP⁺ cells were adjacent to the ependymal lining where they extended many pro-

cesses; feltwork of processes formed a lamina underlying the ependyma. Only sporadic GFAP⁺ cells were inserted in the ependymal cell monolayer. Some astrocytic processes ensheathed the blood vessels by forming the perivascular limiting membrane. Other GFAP⁺ cells were localized at the interface with the striatal parenchyma. Immunohistochemistry visualized numerous cytoplasmic processes of astroglial cells due to the presence of bundles of intermediate filaments like GFAP, vimentin and nestin. In the SEZ, a dense meshwork of astrocytic processes formed tangentially oriented intercommunicating channels or glial tubes forming a characteristic complex system. Individual tubes ran nearly parallel to each other but they could branch and merge along the SEZ. Astrocytic meshwork forming the tubes enwrapped incompletely the aggregations of small basophilic cells.

Anti-NCAM (neural cell adhesion molecule) immunohistochemistry confirmed that these smallest cellular elements with a high nuclear/cytoplasmic ratio were neuroblasts. NCAM⁺ cells exhibited two main processes emerging from the opposite poles giving the cell an elongated and bi-

polar shape. Such morphology with tangentially oriented leading and trailing processes is characteristic for migrating neuroblasts (Fig. 2). Neuroblasts in the SEZ tended to cluster in elongated groups arranged in the form of numerous longitudinal chains parallel to the wall of the LCVs. These chains formed an extensive network that extended from the caudal to the rostral lateral wall of the LCVs. The continuous splitting and converging chains formed a characteristic structure of the SEZ. Networks of chains of migrating neuroblasts were ensheathed by astrocytes. Occasionally small clusters were visible in contact with blood vessels or in the adjacent neuropil.

Immunodetection of markers specific for fully differentiated neuronal cells like MAP-2, Pan NF and β -III tubulin revealed no positive cells in the SEZ. On the contrary, cells expressing markers specific for adult neuronal cells were scattered throughout the mature brain parenchyma, e.g. in the adjacent striatum (see Fig. 2). When stained for nestin, a marker of immature neural cells, immunopositive neural stem/progenitor cells were recognized in the SEZ where they were juxtaposed by clusters of neuroblasts. In other

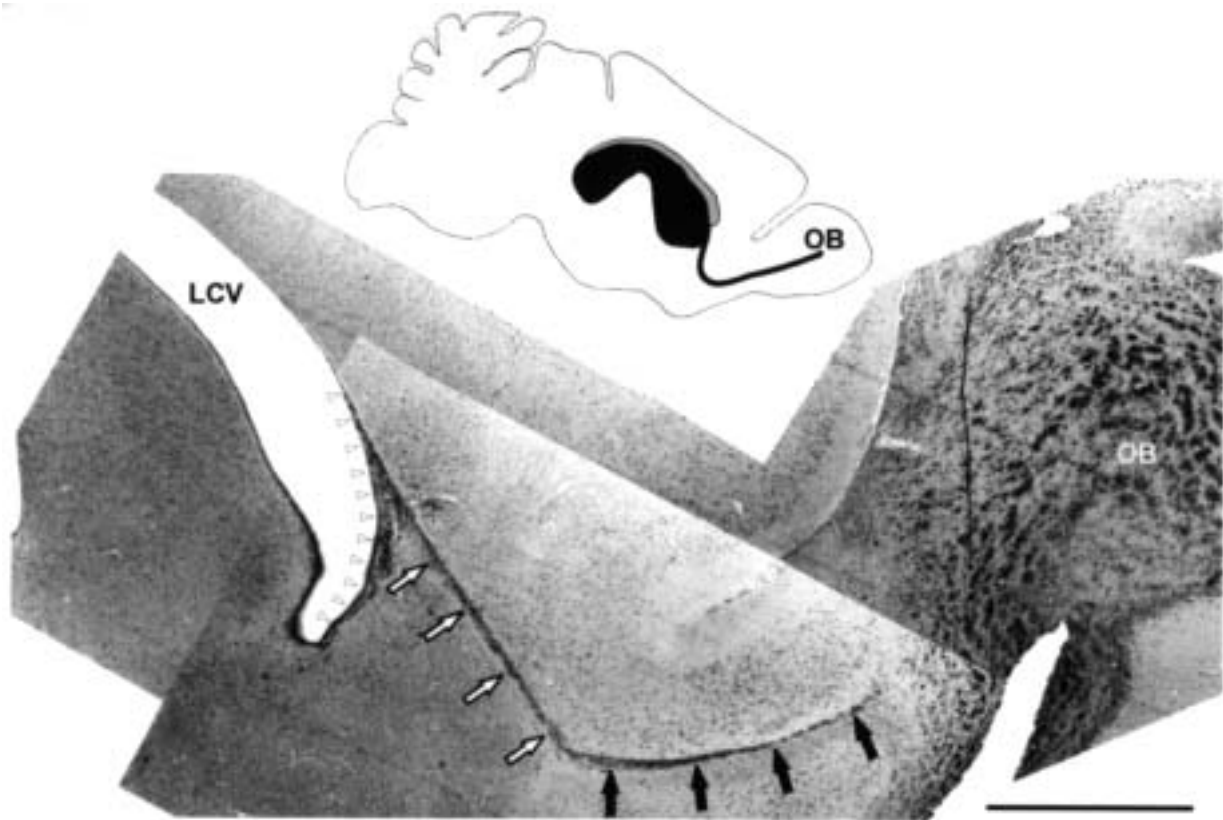


Fig. 1: A parasagittal section of the rat forebrain stained with haematoxylin and eosin reveals a variable thickness of the subependymal zone of lateral cerebral ventricles (LCV). In its anterior part, the SEZ reaches the largest thickness (arrowheads). At this site, the SEZ is associated with the rostral migratory stream (arrows) that serves to deliver immature cells to the olfactory bulb (OB). Vertical (white arrows) and horizontal limbs (black arrows) of the RMS are well visible. A schematic drawing of the corresponding parasagittal section through the rat brain depicts lateral cerebral ventricles lined by the SEZ and the RMS (black); the overlying corpus callosum is depicted in grey colour. Scale bar: 1 mm.

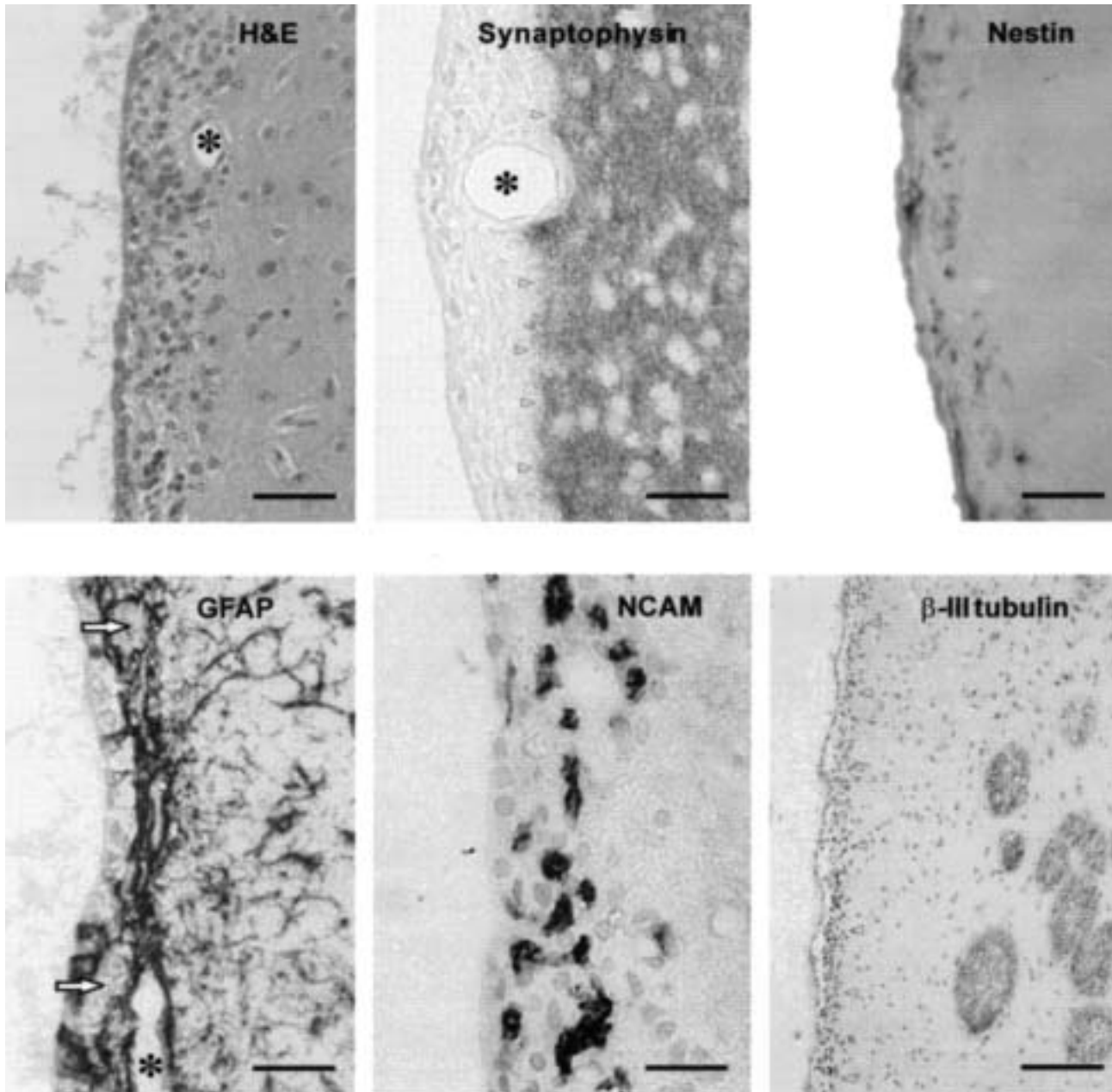


Fig. 2: Histological structure of the intact rat subependymal zone. Staining with haematoxylin and eosin shows a single layer of ciliated ependymal cells facing the cerebral ventricle and several layers of underlying basophilic SEZ cells. SEZ is characteristic by high cellular density due to a large accumulation of relatively small cells. Arrowheads indicate a boundary with the striatum; an asterisk marks a blood vessel inside the SEZ; scale bar: 25 μm . Synapses that normally occur in the brain neuropil are not found in the SEZ. Immunohistochemical detection and amplification of synaptophysin shows a sharp boundary between the SEZ and adjacent corpus striatum (arrowheads; scale bar: 25 μm). Anti-nestin staining reveals focal spots of neural stem and progenitor cells scattered throughout the SEZ; scale bar: 20 μm . GFAP⁺ astroglial cells inside the SEZ are densely packed and form longitudinal channels that contain clusters of small GFAP neuroblasts (arrows). Few GFAP⁺ cells are found in the ependymal monolayer. In the striatum, protoplasmic astrocytes are not so densely packed and they are visible as individual cells; scale bar: 20 μm . Detection of NCAM visualizes small and densely clustered neuroblasts forming elongated chains; occasionally, short processes of these bipolar cells are visible; scale bar: 20 μm . A marker of fully differentiated neuronal cells, β -III tubulin, is not found in the SEZ; it is expressed in the striatal nervous tissue; scale bar: 50 μm .

brain areas, anti-nestin immunostaining detected thick processes of astroglial cells rich for intermediate filaments, e.g. those forming superficial limiting membrane, and tanycytes that were abundant especially in the lining of the third cerebral ventricle.

Rostral migratory stream

The SEZ reaches its largest thickness in the site where the migrating neuroblasts enter the rostral migratory pathway (RMS). In parasagittal section of the rat brain (Fig. 1), it is well apparent that the RMS represents a thin strand of a tissue interconnecting the SEZ with the olfactory bulb (OB). Histological structure of the RMS mimics the SEZ

because it represents a continuation of the SEZ. There were no ependymal cells due to absence of ventricular system filled with the cerebrospinal fluid. Immunoperoxidase detection of synaptophysin identified the precise boundaries of the RMS because it was devoid of any synapses on the contrary to the adjacent neuropil (Fig. 3). GFAP was expressed in astroglial cells that formed a characteristic tubule-like structures ensheathing chains of small densely packed cells. These astroglial cells also expressed the intermediate filament vimentin. However, the anti-vimentin antibody did not allow to recognize these longitudinally oriented glial tubes because it provided an intense staining of all elements (i.e. mature glial cells and immature neural precursors) of the RMS. Immature cells migrating along the RMS could

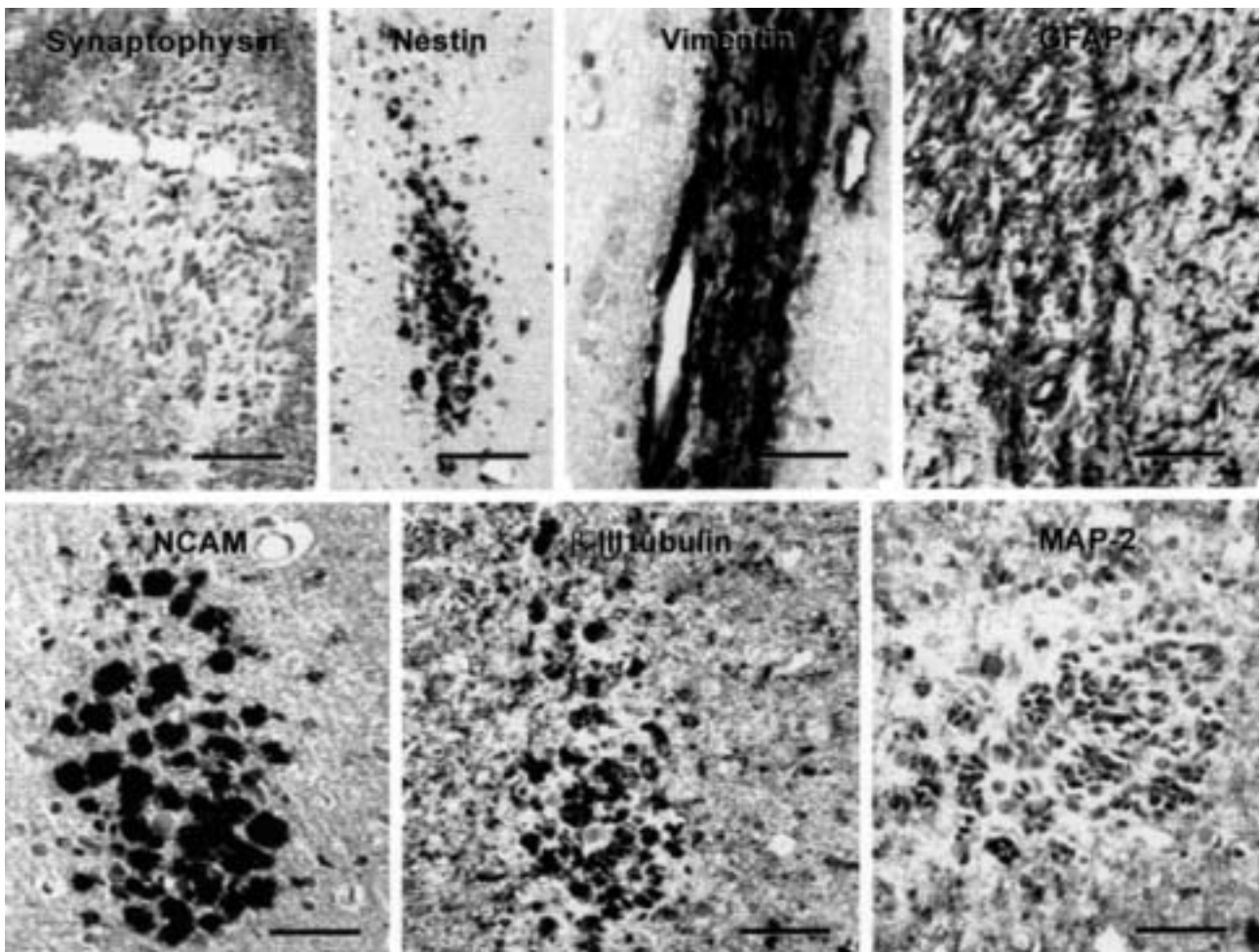


Fig. 3: Peroxidase immunohistochemistry defines antigenic profiles of cells in the rat rostral migratory stream. Synaptophysin is expressed only in the neuropil surrounding the RMS; scale bar: 20 μ m. The RMS cells express large levels of intermediate filament proteins nestin (scale bar: 30 μ m), vimentin (scale bar: 30 μ m) and GFAP. GFAP expressed in RMS astrocytes permits to identify channel-like structures that contain immunonegative neuroblasts. GFAP⁺ astrocytes outside the RMS do not form such channels; scale bar: 30 μ m. The RMS neuroblasts express high levels of NCAM (scale bar: 20 μ m) and moderate levels of β -III tubulin (scale bar: 30 μ m). A marker of dendrites of postmitotic neurons, MAP-2, is expressed only in the surrounding fully mature parenchyma (scale bar: 30 μ m). Sections were counterstained with haematoxylin to visualize nuclei of immunonegative cells.

be recognized with immunostaining of the nestin. Staining of markers specific for neuronal cells distinguished which cells belonged to a neuronal cell lineage. They expressed NCAM and β -III tubulin which identified migratory neuroblasts in the RMS. Detection of markers characteristic for postmitotic neurons did not reveal any immunoreactivity inside of the RMS; the only positive cells were located in the mature parenchyma outside the RMS.

Discussion

Immunohistochemical phenotypisation described in this study reveals a complex organisation of the subependymal zone (SEZ) of the intact rat forebrain. The major role of this specific CNS region is a production of new neural cell types, i.e. maintenance of neurogenesis. It is thought that this function is performed by primitive neural stem cells (NSCs) that reside inside the SEZ. Although their presence in the SEZ has been confirmed in numerous studies (see e.g. 6,8,18,29), the precise identity of the cell type responsible for neurogenesis remains still a matter of debate. Johansson et al. believe that ependymal cells lining the SEZ act as multipotent NSCs (15) whereas Doetsch et al. consider the SEZ astrocyte as the NSCs (9). However, both mentioned cell types share features of differentiated cells like tufts of beating cilia or elongated or flattened cellular processes. Tissue-specific stem cells in other organs show primitive morphology that lacks any signs of cellular differentiation and therefore we can expect that there is a similar primitive NSC inside the SEZ. The findings described by Johansson et al. and Doetsch et al. can be interpreted as an evidence that ependymal and astroglial cells or their precursors (which appear in the SEZ as well) can dedifferentiate under certain conditions and thus give rise to multipotent NSCs. Morphologically NSCs are identified *in situ* according to the expression of protein nestin. This intermediate filament is strongly expressed in endogenous adult NSCs and it can be detected reliably in formaldehyde-fixed, paraffin-embedded sections following microwave antigen retrieval (28). Nestin⁺ cells are found in focal clusters or as single cells scattered along the chains of migrating neuroblasts; these cells do not stain for neuronal or glial markers. It must be mentioned that nestin is also expressed in other cell types including astrocytes (reactive but also normal astrocytes), tanyocytes, endothelial cells, precursors of neural cells and few other cell types found in non-neural tissues (e.g. 27,28, Fig. 2) and therefore a finding of nestin-immunoreactive cells has to be carefully interpreted. Recently, other markers expressed by NSCs have been identified, e.g. mCD133 (39), CD34 (33), mCD24(5); their combination could be useful for confirmation of the NSC phenotype. After activation, e.g. in response to lesion of adjacent brain structures (11,29,41) or after activation with proliferative growth factors (7,17,30), NSCs start to divide and represent the major proliferating cell type. NSCs and their progenitors can be detected according to the expres-

sion of proliferation markers like PCNA or BrdU (29); however, it is important to realize that other SEZ cell types including B2 astrocytes and neuroblasts also undergo cellular divisions (8,25). NSCs represent a minor SEZ population; it is estimated that they form just 0.3% of all SEZ cells (36). High rates of cell proliferation are still observed in the SEZ during ageing and the number of SCs does not appear to change throughout life (38). The SEZ NSCs are multipotent. Their differential potential was confirmed *in vitro*; NSCs isolated from the SEZ give rise to progenitors differentiating into neuronal and glial cells (18,19,40). *In situ*, gliogenesis is stimulated by bone morphogenic protein. This stimulation can be suppressed by noggin produced by ependymal cells which subsequently results in production of neuroblasts (20). These regulatory pathways require a close relationship of different cell types that is necessary to create a SEZ niche.

Astroglial cell represents another cellular element participating in formation of the SEZ niche. Astroglial cell endfeet cover the boundaries of the SEZ against the mature nervous tissue and ependyma, they are coupled with each other by gap junctions and are in an intimate contact with all the other SEZ cell types including neuroblasts, stem cells and blood vessels. They can detect alterations in neuronal and precursor number, translate signals from the vasculature and other cells and provide rapid propagation of signalling within the neurogenic niche. Moreover, astroglial cells can secrete factors supporting neurogenesis and therefore they are the key elements creating a neurogenic microenvironment in the SEZ (19). Astroglial cells in the SEZ contain glycogen particles and express markers of mature astroglial cells GFAP, vimentin and S100 protein (14,29). They form a lacunar system that incompletely enwrap small basophilic cells and compartmentalise the SEZ into longitudinally oriented tubes that run nearly parallel to each other. Detection of NCAM reveals spindle-shaped neuroblasts aggregated in elongated clusters arranged in network of interconnected chains. Bipolar morphology of NCAM⁺ cells (leading and tail processes) is characteristic for migrating cells. The neuroblasts emigrate from the SEZ as they travel along the glial tubes and they divide giving rise to new neuroblasts. Although the above mentioned cell types are the most characteristic for the adult mammalian SEZ, other elements present here include small percentage of tanyocytes within the ependymal layer, sporadic microglial cells and endothelial cells (8). The latter cell type participates in nutrition of other SEZ cells and also in formation of a unique neurogenic milieu (26). BDNF released by endothelial cells acts as a survival factor of newly generated neurons (24) and neurogenesis occurs in foci closely associated with blood vessels (31). A specialised basal lamina extends from blood vessels, contacts all SEZ cell types and terminates in small bulbs adjacent to the ependymal cells (26). This basal lamina and associated extracellular matrix plays an important role in cell tethering and ligand binding and forms an essential part of the SEZ stem cell niche.

Histological structure of the rostral migratory stream (RMS) closely resembles the forebrain SEZ. The reason is that the RMS also develops from the periventricular area. While the SEZ develops from the ventricular zone of the lateral cerebral ventricles, the RMS arises from the ventricular zone of the olfactory cerebral ventricle. At later developmental stages the olfactory ventricle obliterates and does not generate ependymal cells but its subventricular zone remains to be associated with a corresponding area of the LCVs. The RMS consists of two distinct cellular compartments corresponding to its two main cell types: longitudinally arranged GFAP⁺ astroglial tubes and chains of fusiform NCAM⁺ neuroblasts, which are contained within these fields (Fig. 3). As the neuroblasts travel inside of glial tubes they proliferate (22). Their migration and division are regulated by different beta1 integrins (13). The newly generated neural precursors start to express another neuronal marker, β -III tubulin. After reaching the olfactory bulb, the neuroblasts differentiate into GABAergic granule cells and dopaminergic periglomerular interneurons (4,22). A strong immunoreactivity for nestin in the RMS indicates the presence of immature cells including neural precursor and stem cells. Despite the ongoing differentiation of neuroblasts migrating throughout the RMS, several recent studies confirmed, that the RMS still contains a large amount of multipotent NSCs (12).

Immunohistochemical analysis of the RMS and SEZ permits to identify cell types constituting both areas and to study their intercellular relationship. Both areas represent a heterogeneous constellation of cells with differentiated and undifferentiated phenotypes. The mature cell compartment is represented by tangentially oriented intercommunicating glial channels forming a complex system enwrapping the immature neuroblasts and NSCs. Such structural arrangement is necessary for creation of specialized niches supporting neurogenesis and represents a histological feature unique to these CNS areas.

Acknowledgement

The authors thank to Mrs. Helena Růckerová and Mrs. Hana Hollerová for their skilful technical assistance. The work was supported by a project No. 304/03/1515 from Grant Agency of the Czech Republic.

References

- Altman J. Autoradiographic and histological studies of postnatal neurogenesis. IV. Cell proliferation and migration in the anterior forebrain, with special reference to persisting neurogenesis in the olfactory bulb. *J Comp Neurol* 1969;137:433-58.
- Anchan RM, Reh TA, Angello J, Balliet A, Walker M. EGF and TGF- α stimulate retinal neuroepithelial cell proliferation in vitro. *Neuron* 1991;6:923-36.
- Arsenijevic Y, Villemure JG, Brunet JF et al. Isolation of multipotent neural precursors residing in the cortex of the adult human brain. *Exp Neurol* 2001;170:48-62.
- Betarbet R, Zigova T, Bakay RAE, Luskin MB. Dopaminergic and gabaregic interneurons of the olfactory bulb are derived from the neonatal subventricular zone. *Int J Devl Neurosci* 1996;14:921-30.
- Calaora V, Chazal G, Nielsen PJ, Rougon G, Moreau H. mCD24 expression in the developing mouse brain and in zones of secondary neurogenesis in the adult. *Neuroscience* 1996;73:581-94.
- Chiasson BJ, Tropepe V, Morshead CM, van der Kooy D. Adult mammalian forebrain ependymal and subependymal cells demonstrate proliferative potential, but only subependymal cells have neural stem cell characteristics. *J Neurosci* 1999;19:4462-71.
- Craig CG, Tropepe V, Morshead CM, Reynolds BA, Weiss S, van der Kooy D. In vivo growth factor expansion of endogenous subependymal neural precursor cell populations in the adult mouse brain. *J Neurosci* 1996;16:2649-58.
- Doetsch F, Garcia-Verdugo JM, Alvarez-Buylla A. Cellular composition and three-dimensional organization of the subventricular germinal zone in the adult mammalian brain. *J Neurosci* 1997;17:5046-61.
- Doetsch F, Caillé I, Lim DA, Garcia-Verdugo JM, Alvarez-Buylla A. Subventricular astrocytes are neural stem cells in the adult mammalian brain. *Cell* 1999;97:703-16.
- Frederiksen K, McKay RDG. Proliferation and differentiation of rat neuroepithelial precursor cells in vivo. *J Neurosci* 1988;8:1144-51.
- Gould E, Reeves AJ, Graziano MSA, Gross CG. Neurogenesis in the neocortex of adult primates. *Science* 1999;286:548-52.
- Gritti A, Bonfanti L, Doetsch F et al. Multipotent neural stem cells reside into the rostral extension and olfactory bulb of adult rodents. *J Neurosci* 2002;22:437-45.
- Jacques TS, Relvas JB, Nishimura S et al. Neural precursor cell chain migration and division are regulated through different beta1 integrins. *Development* 1998;125:3167-77.
- Jankowski A, Sotelo C: Subventricular zone-olfactory bulb migratory pathway in the adult mouse: Cellular composition and specificity as determined by heterochronic and heterotopic transplantation. *J Comp Neurol* 1996;371:376-96.
- Johansson CB, Momma S, Clarke DL, Risling M, Lendahl U, Frisén, J. Identification of a neural stem cell in the adult mammalian central nervous system. *Cell* 1999;96:25-34.
- Kalyani AJ, Mujtaba T, Rao MS. Expression of EGF receptor and FGF receptor isoforms during neuroepithelial stem cell differentiation. *J Neurobiol* 1999;38:207-24.
- Kuhn H, Winkler J, Kempermann G, Thal LJ, Gage FG. Epidermal growth factor and fibroblast growth factor-2 have different effects on neural progenitors in the adult rat brain. *J Neurosci* 1997;17:5820-9.
- Kukekov VG, Laywell ED, Suslov O et al. Multipotent stem/progenitor cells with similar properties arise from two neurogenic regions of adult human brain. *Exp Neurol* 1999;156:333-44.
- Lim DA, Alvarez-Buylla A. Interaction between astrocytes and adult subventricular zone precursors stimulates neurogenesis. *Proc Natl Acad Sci USA* 1999;96:7526-31.
- Lim DA, Tramontin AD, Trevejo JM, Herrera DG, Garcia-Verdugo JM, Alvarez-Buylla A. Noggin antagonized BMP signaling to create a niche for adult neurogenesis. *Neuron* 2000;28:713-26.
- Liu Z, Martin LJ. Olfactory bulb core is a rich source of neural progenitor and stem cells in adult rodent and human. *J Comp Neurol* 2003;459:368-91.
- Lois C, Alvarez-Buylla A. Long-distance neuronal migration in the adult mammalian brain. *Science* 1994;264:1145-48.
- Lois C, Garcia-Verdugo J-M, Alvarez-Buylla A. Chain migration of neuronal precursors. *Science* 1996;271:978-81.
- Louissaint A Jr, Rao S, Leventhal C, Goldman SA. Coordinated interaction of neurogenesis and angiogenesis in the adult songbird brain. *Neuron* 2002;34:945-960.
- Menezes JRL, Smith CM, Nelson KC, Luskin MB. The division of neuronal progenitor cells during migration in the neonatal mammalian forebrain. *Mol Cell Neurosci* 1995;6:496-508.
- Mercier F, Kitasako JT, Hatton GI. Anatomy of the brain neurogenic zones revisited: fractones and the fibroblast/macrophage network. *J Comp Neurol* 2002;451:170-88.
- Mokry J, Nemeček S. Angiogenesis of extra- and intraembryonic blood vessels is associated with expression of nestin in endothelial cells. *Folia Biol (Prague)* 1998;44:155-61.
- Mokry J, Nemeček S. Immunohistochemical detection of intermediate filament nestin. *Acta Med (Hradec Králové)* 1998;41:73-80.
- Mokry J, Karbanová J, Österreicher J. Experimental brain injury induces activation of neural stem cells in the forebrain subependyma. *Applied Immunohistochemistry and Molecular Morphology* 2003;11:161-7.
- Palmer TD, Markakis EA, Willhoite AR, Safar F, Gage FH. Fibroblast growth factor-2 activates a latent neurogenic program in neural stem cells from diverse regions of the adult CNS. *J Neurosci* 1999;19:8487-97.
- Palmer TD, Willhoite AR, Gage FH. Vascular niche for adult hippocampal neurogenesis. *J Comp Neurol* 2000;425:479-94.
- Palmer TD, Takahashi J, Gage FH. The adult rat hippocampus contains primordial neural stem cells. *Mol Cell Neurosci* 1996;8:389-404.
- Parati EA, Bez A, Ponti D et al. Human neural stem cells express extra-neural markers. *Brain Res* 2002;925:213-21.
- Peretto P, Merighi A, Fasolo A, Bonfanti L. Glial tubes in the rostral migratory stream of the adult rat. *Brain Res Bull* 1997;42:9-21.

35. Reynolds BA, Weiss S. Generation of neurons and astrocytes from isolated cells of the adult mammalian central nervous system. *Science* 1992;255:1707-10.
36. Rietze LR, Valcanis H, Brooker G, Thomas T, Voss AK, Bartlett PF. Purification of a pluripotent neural stem cell from the adult mouse brain. *Nature* 2001;412:736-9.
37. Smart I. The subependymal layer of the mouse brain and its cell production as shown by autoradiography after thymidine-H3 injection. *J Comp Neurol* 1961; 116:325-38.
38. Tropepe V, Craig CG, Morshead CM, van der Kooy D. Transforming growth factor- α null and senescent mice show decreased neural progenitor cell proliferation in the forebrain subependyma. *J Neurosci* 1997;15:7850-9.
39. Uchida N, Buck DW, He D et al. Direct isolation of human central nervous system stem cells. *Proc Natl Acad Sci USA* 2000;97:14720-5.
40. Whittemore SR, Morassutti DJ, Walters WM, Liu R-H, Magnuson DSK. Mitogen and substrate differentially affect the lineage restriction of adult rat subventricular zone neural precursor cell populations. *Exp Cell Res* 1999;252:75-95.
41. Zhang RL, Zhang ZG, Zhang L, Chopp M. Proliferation and differentiation of progenitor cells in the cortex and the subventricular zone in the adult rat after focal cerebral ischemia. *Neuroscience* 2001;105:33-41.

Submitted January 2004.

Accepted September 2004.

*Doc. MUDr. Jaroslav Mokry, Ph.D.,
Charles University in Prague,
Faculty of Medicine in Hradec Králové,
Department of Histology and Embryology,
Šimkova 870, P. O. Box 38,
500 38 Hradec Králové, Czech Republic.
e-mail: mokry@lfhk.cuni.cz*

PASSIVATION OF DENTAL AMALGAMS AND MERCURY RELEASE

Luděk Joska¹, Miroslav Marek²

Institute of Chemical Technology, Prague, Czech Republic: Department of Metals and Corrosion Engineering¹; Georgia Institute of Technology, Atlanta, U. S. A.: GTRI/EOEML²

Summary: Objectives: In this study the rate of dissolution of mercury from two dental amalgams with different compositions and structures was determined *in vitro* under different oxidation and abrasion conditions, and the results were correlated with the electrochemical characteristics. **Methods:** A spherical high copper and a lathe-cut very high-copper amalgam were tested in aerated and deaerated artificial saliva. The electrochemical characteristics were determined by potential-time, anodic polarization, polarization resistance and cathodic stripping measurements. Mercury release tests were performed after either stabilization in the solution, or abrasion using SiC papers or rotary toothbrush, with or without toothpaste. Dissolved mercury was determined by atomic absorption spectrophotometry. **Results:** Both amalgams exhibited passivation, the amalgam with the higher copper content passivating spontaneously even when the oxygen content in the solution was minimized. At a higher oxygen content in the solution the rate of mercury release from the amalgams was lower than when the oxygen content was minimized, and decreased further after a pre-exposure. Brushing generally increased the release. **Significance:** The results show the importance of the oxidation conditions and passivation characteristics of dental amalgams for mercury release, especially in the transient state after abrasion by chewing or tooth brushing.

Key words: Dental amalgam; Passivation; Abrasion

Introduction

The release of mercury from dental amalgam restorations remains a matter of public and scientific interest. Numerous studies have been reported regarding the mechanism and rate of mercury release *in vivo* and *in vitro* and using a variety of experimental techniques. Several critical reviews of the literature on mercury release *in vivo* have been published (2,8,10,11,12,25,26).

There is evidence that the mercury release rate is primarily affected by the presence or absence of a tin oxide film on the γ_1 (Ag-Hg-Sn) phase, which is the matrix of the dental amalgam structure and is richest in mercury (15,16, 28). Correlations between the tin content in the γ_1 phase and mercury evaporation and dissolution have been reported (6,7,13,14,15). Models of mercury release and of the tin oxide formation and its effect on mercury release have been proposed (14,16).

If the tin oxide film serves as an effective barrier to the mercury release, its thinning or removal would result in an increase in the mercury release rate. Gum chewing, mastication or tooth brushing may cause such a degradation of the oxide film. Berglund (2) measured the intra-oral mercury vapor release and reported spikes corresponding to chewing and brushing. Mercury release has been reported to be significantly increased by chewing gum (3). An arti-

cial mouth has been used to study the effect of chewing and brushing on mercury release *in vitro* (1).

Since the oxide film barrier on the γ_1 phase forms electrochemically by reaction of the dissolved tin with the electrolyte, it reforms spontaneously following thinning or removal by mechanical abrasion. The amount of mercury released during a time period involving abrasion then depends on the kinetics of the film growth. This kinetics may be affected by chemical and electrochemical conditions, such as acidity and oxidation power of the electrolyte, as well as by the properties of the amalgam. In this study the mercury release was examined for two high-copper amalgams of different composition and structure and for several oxidation and abrasion conditions, and the results were correlated with the electrochemical behavior of the amalgams.

Materials and methods

Two commercial high-copper, single alloy composition amalgams were examined. The nominal compositions, provided by the manufacturers, and alloy/mercury ratios are presented in Table 1 (volume fractions of the γ_1 phase were determined by image analysis). Tytin is a typical spherical high-copper amalgam alloy with 60% Ag and sufficient copper content (12%) to eliminate the γ_2 phase. ANA 2000 is a low-silver (43%), very high-copper (~ 25%) amalgam alloy,

lathe-cut, containing some mercury (2%) and used with a higher mercury/alloy ratio than Tytin. The amalgams were selected on the basis of an earlier study, which showed substantial difference in the electrochemical behavior (9).

The alloys were mixed according to manufacturers' instructions, and standard specimens 4 mm dia. were prepared according to ISO 1559. Samples for testing were prepared by attaching four specimens of the same amalgam to a brass stud using conductive glue, and casting the assembly in epoxy resin. The epoxy casting was machined to expose the cross-sections of the four specimens (exposed area 0,5 cm²) and to a conical shape serving as a plug for a weighing bottle with a standard ground glass taper. In addition to the amalgams, specimens of pure copper (purity 99,995 wt %, VUK, Czech Republic) and Sn (purity 99,999 wt %, VUK, Czech Republic) were prepared for the polarization tests.

All electrochemical and dissolution measurements were performed using artificial saliva of the following composition and conditions: KCl: 20,1 mmol/l; NaHCO₃: 17,9 mmol/l; NaH₂PO₄: 3,6 mmol/l; KSCN: 5,1 mmol/l; lactic acid: 0,10 mmol/l, pH 6,8, temperature 37±0.5°C. The atmosphere was controlled by bubbling through the solution before the test a mixture of either N₂/10% CO₂ for 2 h (deaerated, oxygen content minimized), or air/10% CO₂ for 1 h (aerated, oxygen content similar to the conditions in the oral cavity).

The electrochemical tests were performed using a standard 3-electrode glass test cell with a jacket for temperature control by a flow of water from a constant-temperature circulator. The electrochemical system was a model PC4/Fas (Gamry, U.S.A). The tests consisted of potential-time, anodic polarization, polarization resistance and galvanostatic measurements. The open-circuit potentials were measured in both aerated and deaerated electrolytes after wet-grinding the specimens on FEPA P2400 SiC papers. The potentials were measured with respect to a Ag/AgCl/3mol/L KCl reference electrode, and the values were converted to the Standard Hydrogen Electrode (SHE) scale. Before the exposure in the deaerated electrolyte the surface oxides were stripped by cathodic reduction for 60 s at -0.82 V/SHE. The potentials were recorded for 2 h. For the potentiodynamic polarization measurements the electrolyte was deaerated, the specimens were wet-ground on FEPA P2400 SiC papers, and the surface oxides were stripped before the scan initiation by cathodic reduction for 60 s at -0.82 V/SHE. The polarization curves were recorded at a potential scanning rate of 1 mV/s from a potential 0.1 V below the open circuit potential to 0.4 V/SHE. The polarization resistance R_p was measured as a function of time for ANA 2000 in aerated and deaerated solutions by scanning the potential at a rate

of 0.5 mV/s in the range of ± 15 mV from the open circuit potential and determining R_p as the slope of the potential vs. current density line at the open-circuit potential.

A qualitative determination of the presence or absence of a reducible oxide was obtained by galvanostatic reduction in a deaerated electrolyte at -0.4 A/m² for Tytin and -0.9 A/m² for ANA 2000. The presence of a plateau on the potential-time curve at about -0.6 V/SHE was taken as evidence of the presence of tin oxide on the surface. Specimens were tested after a 2-h exposure to either aerated or deaerated synthetic saliva at 37°C.

The mercury dissolution tests were performed using standard 12 ml glass weighing bottles with a ground-glass neck, into which the specimens could be inserted. The bottles were filled with aerated or deaerated artificial saliva, which was pre-warmed to 37°C. After specimen insertion the bottles were placed in an incubator and maintained at 37°C for 2 h. The solution from each bottle was then stabilized by addition of 10 ml of a solution of 1g/l of K₂Cr₂O₇ in 30% HNO₃, and analyzed for mercury using an atomic absorption spectrophotometer with a cold-vapor generation accessory (Models SpectraAA-300 and VGA-76, respectively, Varian Techtron Pty, Australia). The detection limit was 0.1 ppb. Four to eight analyses were performed for each solution sample, as well as for appropriate standards. The results of four replicate tests were averaged to obtain the mean values and standard deviations; the means were compared using student's t-test at p=0,05.

Before the mercury dissolution exposures the surfaces of the specimens were prepared using one of the following procedures:

- Wet-grinding using FEPA P2400 SiC paper.
- Wet-grinding using FEPA P2400 SiC paper and an open-circuit pre-exposure in the aerated electrolyte for 2 h.
- Brushing without toothpaste using a rotary toothbrush (Sunbeam Model 4209, Sunbeam-Oster Household Products, U.S.A.) at a frequency of 2750 min⁻¹, for 20s in the aerated electrolyte at 37°C.
- Brushing with toothpaste in air using the same rotary toothbrush for 20s, followed by rinsing with aerated electrolyte at 37°C. A common commercial toothpaste, Colgate Cavity Protection (Colgate-Palmolive Co., U.S.A.), pH = 7,3, E_{redox} = 0,300 V/SHE, was used in this procedure.

Results

The results of the open circuit potential measurements for the two amalgams in both aerated and deaerated electro-

Tab. 1: Materials tested.

Amalgam	Ag [wt.%]	Cu [wt.%]	Sn [wt.%]	Hg in alloy [wt.%]	Alloy to Hg ratio	γ ¹ volume fraction	Manufacturer
ANA 2000	43.0	25.4	29.6	2.0	1:1	0,54 (SD=0,05)	Nordiska Dental AB, Sweden
Tytin	60.0	12.0	28.0	-	1:0,74	0,36 (SD=0,07)	Kerr, U.S.A.

lytes as a function of the exposure time are presented in Fig. 1. The potential of ANA 2000 increased with time for both conditions and stabilized at a potential about 100 mV higher in the solution saturated with a gas mixture containing 10% oxygen (aerated) than in the solution, in which dissolved oxygen was minimized (deaerated). The potential of Tytin showed an initial fast increase and stabilization in the deaerated solution at a potential about 400 mV more negative than ANA 2000 under the same conditions. In the

Tab. 2: Evidence of tin oxide after 2-h exposure.

	Deaerated electrolyte	Aerated electrolyte
Tytin	no	yes
ANA 2000	yes	yes

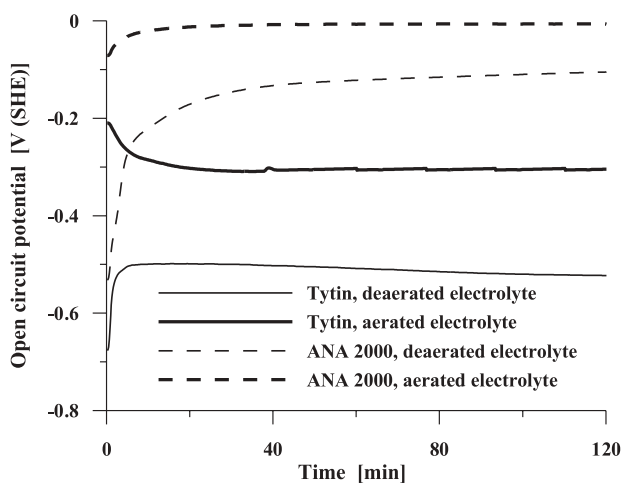


Fig. 1: Open circuit potentials of Tytin and ANA 2000 amalgams as a function of exposure time in aerated and deaerated artificial saliva at 37°C.

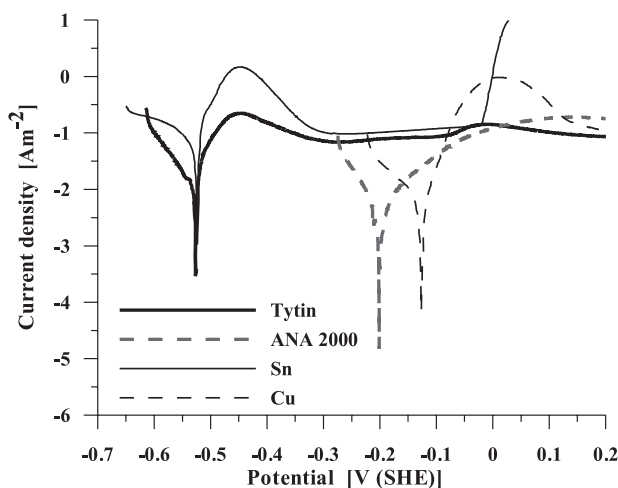


Fig. 2: Polarization curves for Tytin and ANA 2000 amalgams, Sn and Cu in deaerated artificial saliva at 37°C.

aerated solution the potential initially decreased and stabilized a value about 200 mV higher than in the deaerated solution, but about 300 mV more negative than the potential of ANA 2000 under the same conditions.

The polarization curves for both amalgams, as well as those for pure tin and copper in the deaerated solution are presented in Fig. 2. The curves for both Tytin and Sn showed a primary passivation peak at about -0,45 V/SHE, while the curve for ANA 2000 exhibited only passive behavior in

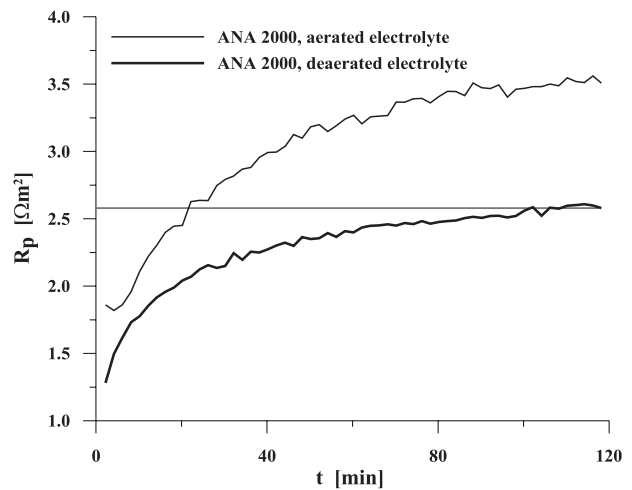


Fig. 3: Polarization resistance of ANA 2000 amalgam as a function of exposure time in aerated and deaerated artificial saliva at 37°C.

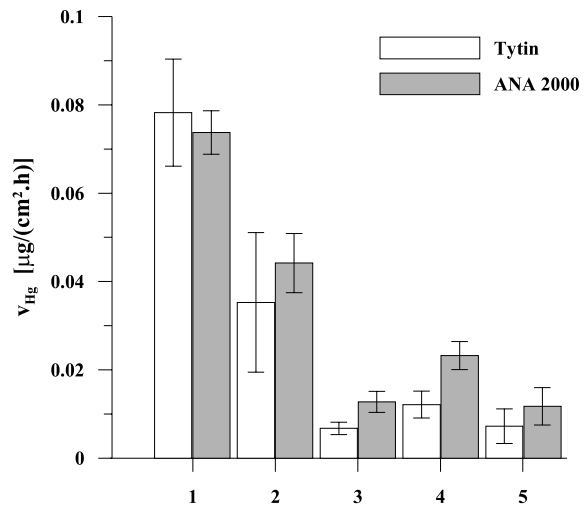


Fig. 4: Average dissolution rates for 2-h exposures of Tytin and ANA 2000 amalgams in artificial saliva at 37°C. (1) Wet-ground, deaerated electrolyte. (2) Wet-ground, aerated electrolyte. (3) 2-h pre-exposure in aerated electrolyte. (4) Brushed with a rotary toothbrush without toothpaste, aerated electrolyte. (5) Brushed with Colgate toothpaste, aerated electrolyte. Bars show means of at least 4 replicate tests; error bars show \pm standard deviation.

the range of potentials examined. The polarization results for copper showed a broad peak at about 0 V/SHE, at which potential a small peak on the curve for Tytin also was observed. A sharp increase in current, indicating breakdown of passivity was observed for tin at about 0 V/SHE, but not for either of the amalgams.

Results of the galvanostatic tests are summarized in Table 2. Evidence of the presence of a surface oxide was found for ANA 2000 under both oxygenated and deoxygenated conditions, for Tytin only in the oxygenated solution. The polarization resistance R_p , which is inversely proportional to the rate of electrochemical reaction, as a function of the exposure time in aerated and deaerated solutions for ANA 2000 is presented in Fig. 3.

The results of the mercury release measurements are summarized in Fig. 4. For exposure in the deaerated electrolyte immediately following wet-grinding there was no significant difference between the amalgams in the 2-h release rate. In the presence of oxygen (aerated solution) the means were significantly lower than in the deaerated solution ($p=0,05$).

When the release rate was measured in the aerated solution after a 2 h pre-exposure, the means were significantly lower than during the first two hours, and lower for Tytin than for ANA 2000 ($p=0,05$). Brushing without toothpaste increased the mercury release rate, and the rate was significantly higher for ANA 2000 than for Tytin ($p=0,05$). Brushing with toothpaste, however, did not significantly affect the mercury release rate.

Discussion and conclusions

The release of mercury from dental amalgam and the electrochemical behavior of the amalgam are related because electrochemical reactions in the oral environment change the state of the surface, through which mercury evaporates or dissolves. The two amalgams examined in this study exhibited substantially different electrochemical potentials in synthetic saliva, as shown in Fig. 1. The open circuit potential of the amalgam is a mixed potential, affected by the anodic and cathodic reactions on all the exposed phases of the microstructure. The open circuit potential of Tytin in deaerated electrolyte, after reduction of the surface oxide has stabilized at $E = -0,51$ V/SHE. This value is close to the equilibrium potential of the $\text{Sn}(\text{OH})_2/\text{Sn}$ couple ($E = -0,492$ V/SHE at the pH and temperature of the electrolyte) (4). Since a shift in the potential in the positive direction would require oxidation of the tin in the tin-containing phases, the open circuit potential in a solution of low oxidation power remained close to the equilibrium potential.

In a solution containing air the potential of Tytin was more positive by about 0,2 V than in the deaerated electrolyte, and was in the passive region (see Fig. 2) due to the increased oxidizing power of the electrolyte resulting in increased cathodic reaction rate. The open circuit potential of the amalgam remained well below the potential for dis-

solution of copper (standard equilibrium potential for Cu^{2+}/Cu $E^\circ = 0,340$ V) or the potential for oxidation of copper to cuprous oxide Cu_2O ($E = 0,053$ V (SHE) at the pH and temperature of the electrolyte) (5).

The stabilized open circuit potential of ANA 2000 was more positive by about 0,3 to 0,5 V than the potential of Tytin and was in the region of passivity in both the aerated and deaerated electrolytes (Figs. 1 and 2). This means that ANA 2000 passivates spontaneously even in the absence of oxygen in the electrolyte by electrochemical reaction with water resulting in oxidation of tin. The difference between the open circuit potentials of the two amalgams can be attributed to the substantially higher copper content in ANA 2000. The potential is near to the theoretical potential of the $\text{Cu}/\text{Cu}_2\text{O}$ equilibrium, oxidation of copper may be expected because of the destabilizing effect of mercury on the oxide films on η' (24).

The qualitative results of the galvanostatic stripping tests for the presence or absence of tin oxide following different exposure conditions, presented in Table 2, were consistent with the interpretation of the potential and polarization data. No oxide was detected on Tytin after a 2-h exposure in deaerated electrolyte, provided that the initial, air-formed oxide was cathodically stripped. Under the same exposure conditions, however, oxide was found on ANA 2000. Oxide was found on both amalgams after exposure to the aerated electrolyte, in agreement with the potential and polarization data showing that both amalgams in the presence of dissolved oxygen passivated spontaneously.

The results presented in Fig. 4 show that there was no statistically significant difference ($p \leq 0,05$) between the two amalgams in the mercury release when they were tested after wet-grinding in either aerated or deaerated electrolyte. In the aerated electrolyte the average release was significantly lower than in the absence of dissolved oxygen for both amalgams, confirming that an oxide barrier to the mercury release was formed on the γ_1 phase in the solution of higher oxidation power.

The key difference between the two amalgams in the mercury release was shown by the results for an aerated electrolyte after a 2-hour pre-exposure. According to the electrochemical results both amalgams were in a passive state under this condition, but significantly more mercury was dissolved from ANA 2000 than from Tytin. The rate of mercury release is primarily affected by the area of the mercury-rich γ_1 phase and the tin content in this phase (15), because the tin oxide surface film that forms by oxidation of tin in the γ_1 phase is a barrier to the mercury release. Although the amount of tin in the γ_1 phase of ANA 2000 was not found in the literature, it is likely to be similar to the amount in Tytin (1,25 wt.%), based on the data for similar alloys (15). The higher rate of mercury release from ANA 2000 thus can be attributed mainly to a higher volume and surface area ratio of the γ_1 phase.

When the oxygen content in the solution was minimized, the oxide barrier on the γ_1 phase in Tytin was mini-

mal while ANA 2000 still passivated spontaneously, and there was not significant difference in the mercury release rate between the two amalgams. Since the mercury release was measured during a 2-h exposure immediately following wet-grinding and cathodic stripping of the oxide, the result is an average for a period, in which substantial changes in the surface condition occur by formation or growth of an oxide film barrier on the γ_1 phase. The increase in the polarization resistance with time, presented in Fig. 3 for ANA 2000, shows that it takes more than two hours for the amalgam to reach a relatively stabilized surface condition and that the kinetics of passivation depends on oxygen concentration in electrolyte. This may explain why the release rate from ANA 2000 was not more dramatically lower than from Tytin, in spite of the larger source of mercury. For the aerated solution, there was again no statistically significant difference in mercury release during the first two hours of exposure, as both amalgams developed the oxide film barrier on the γ_1 phase, which reduced the mercury release. The mercury release rate dropped significantly more for Tytin than for ANA 2000 compared with the release under the condition of deaeration. This difference is consistent with the electrochemical evidence that aeration caused a change for Tytin from incipient passivation to a fully passive state, while ANA 2000 was passive under both conditions. The potential increase thus made a larger difference for Tytin, on which it allowed an effective oxide film to form, than for ANA, on which the oxide film only thickened.

Abrasion due to brushing is expected to thin the surface oxide on the γ_1 phase and thus increase the mercury release rate. Berglund (2) reported increased mercury emission as a result of toothbrushing under clinical conditions. The simulated *in vitro* brushing used in this study after a 2-h pre-exposure in aerated electrolyte increased mercury dissolution for brushing without a tooth paste but not for brushing with tooth paste, possibly due to a lubricating effect of the toothpaste or formation of corrosion products by reaction with the components of the toothpaste. The increase was, however, relatively small compared with the complete removal of the surface oxide by wet-grinding on a SiC paper.

The results of this study show that the oxidation conditions in the environment and passivation characteristics of the amalgam both play an important role in the mercury release, especially under transient conditions, such as after an abrasion event. While the tin content and volume fraction of the γ_1 phase have primary effects on the formation of the oxide diffusion barrier, other phases of the microstructure affect the passivation process by their effect on the actual electrochemical potential and kinetics of the reactions. The mercury release is further affected by the presence of other substances during and after abrasion by chewing or toothbrushing through variation in the oxidation power, chemistry and abrasiveness of the environment.

The article deals with the effect of the interaction of dental amalgam with a simulated oral environment on mer-

cury release, presenting one of the possible views of the subject. An extensive and exhaustive collection of review articles assessing various aspects of the use of dental amalgams has been published by Novak et al. (17-23,27).

In high-copper amalgams, mercury is released practically solely from phase γ_1 . The „wetter“ amalgam is prepared, i.e. the more mercury is used for amalgamation, the larger mercury source area is created. From this, and not only this, point of view it is clearly desirable to use amalgams dosed by the manufacturer and amalgams with a mercury content below 50 percent by weight. A broad range of materials of different composition are available at present. From the practical point of view we may state that the choice of a high-copper amalgam from among materials with a higher tin content provides for a higher level of phase γ_1 alloying with this element, and consequently for a lower extent of the patient's burdening with mercury. As shown by this study on amalgams with largely different electrochemical properties, the kinetics of the formation of a layer based on tin oxide affects the rate of mercury release. However, the differences found during the study were never extreme.

Acknowledgements

This investigation was supported by research project MSM 223100002 from the Ministry of Education, Youth and Sports (Czech Republic).

References

- Berdouses E, Vaidyanathan TK, Dastane A, Weisel C, Houpt M, Shey Z. Mercury release from dental amalgams: an *in vitro* study under controlled chewing and brushing in an artificial mouth. *J Dent Res* 1995;74:1185-93.
- Berglund A. Estimation by a 24-hour study of the daily dose of intra-oral mercury vapor inhaled after release from dental amalgam. *J Dent Res* 1990;69:1646-51.
- Bjorkman L, Lind B. Factors influencing mercury evaporation rate from dental amalgam fillings. *Scand J Dent Res* 1992;100:354-60.
- Deltombe E, De Zoubov N, Vanleughenaghe C, Pourbaix M. Tin. In: Pourbaix M, ed. *Atlas of Electrochemical Equilibria in Aqueous Solutions*, Houston: NACE, 1974:475-84.
- De Zoubov N, Vanleughenaghe C, Pourbaix M. Copper. In: Pourbaix M, ed. *Atlas of Electrochemical Equilibria in Aqueous Solutions*, Houston: NACE, 1974: 384-92.
- Feracane JL, Adey JD, Nakajima H, Okabe T. Mercury vaporization from amalgams with varied alloy compositions. *J Dent Res* 1995;74:1414-7.
- Feracane JL, Hanawa T, Okabe T. Effectiveness of oxide films in reducing mercury release from amalgam. *J Dent Res* 1992;71:1151-5.
- Chen KI, Ju CP, Lin JH. Effect of particle configuration on structure and properties of dispersed Pd-containing dental amalgam. *Biomaterials* 1999;20: 1851-66.
- Joska L, Bystrianský J, Novák P. The effect of the alloy powder preparation on the corrosion behaviour of dental amalgams. In: *Proceedings of the 13th ICC*, Granada, Spain 2002.
- Krone CA, Ely JTA, Thoresen J. Method for measuring mercury release from dental amalgam. *Bull Environ Contam Toxicol* 2002;68:180-6.
- Mackert JR, Berglund A. Mercury exposure from dental amalgam fillings: absorbed dose and the potential for adverse health effects. *Crit Rev Oral Biol Med* 1997;8:410-36.
- Mackert JR. Factors affecting estimation of dental mercury exposure from measurements of mercury vapor levels in intra-oral and expired air. *J Dent Res* 1987;66:1775-80.
- Mahler DB, Adey JD, Fleming MA. Hg emission from dental amalgam as related to the amount of Sn in the Ag-Hg (γ_1) phase. *J Dent Res* 1994;73: 1663-8.
- Marek M. The effect of tin in the Ag-Hg phase of dental amalgam on dissolution of mercury. *Dent Mat* 1997;13:353-9.
- Marek M. The effect of tin on the corrosion behavior of the Ag-Hg phase of dental amalgam and dissolution of mercury. *J Dent Res* 1990;69:1786-90.

16. Marek M. The release of mercury from dental amalgam: The mechanism and in vitro testing. *J Dent Res* 1990;69:1167-74.
17. Novák L, Půža V, Červinka M, Kolářová J. Problematika amalgámových výplní. I. Historie a současnost amalgámu. *Čes stomatol* 1996;96:80-4.
18. Novák L, Půža V, Červinka M, Kolářová J. Problematika amalgámových výplní. II. Druhá amalgámová válka. *Čes stomatol* 1996;96:115-9.
19. Novák L, Půža V, Červinka M, Kolářová J. Problematika amalgámových výplní. III. Rtuť a její sloučeniny v životním prostředí. *Čes stomatol* 1996;96:156-61.
20. Novák L, Půža V, Červinka M, Kolářová J. Problematika amalgámových výplní. IV. Uvolňování par rtuti z amalgámových výplní. *Čes stomatol* 1996;96:196-203.
21. Novák L, Půža V, Červinka M, Kolářová J. Problematika amalgámových výplní. V. Zatížení ošetřujících a pacientů rtutí. *Čes stomatol* 1997;97:7-15.
22. Novák L, Půža V, Červinka M, Kolářová J. Problematika amalgámových výplní. VI. Amalgámová výplň jako příčina závažných onemocnění. *Čes stomatol* 1997;97:61-5.
23. Novák L, Půža V, Červinka M, Kolářová J. Problematika amalgámových výplní. VIII. Alternativní výplňové materiály za amalgám a závěr souboru prací zabývajících se problematikou amalgámových výplní. *Čes stomatol* 1997;97:157-62.
24. Ogletree RH, Marek M. Effect of mercury on corrosion of η' Cu-Sn phase in dental amalgams. *Dent Mat* 1995;11:332-6.
25. Okabe T, Elezbak B, Carrasco L, Ferracane JL. Mercury release from dental amalgams into continuously replenished liquids. *Dent Mat* 2003;19:38-45.
26. Olsson S, Bergman M. Daily dose calculations from measurements of intra-oral mercury vapor. *J Dent Res* 1992;71:414-23.
27. Půža V, Červinka M, Novák L, Chmelařová V, Kolářová J. Problematika amalgámových výplní. VII. Experimentální sledování cytotoxicity amalgámů a jejich výluhů. *Čes stomatol* 1997;97:112-25.
28. Uo M, Berglund A, Cardenas J, Pohl L. Surface analysis of dental amalgams by X-ray photoelectron spectroscopy and X-ray diffraction. *Dent Mat* 2003;19:639-44.

Submitted June 2004.

Accepted October 2004.

*Ing. Luděk Joska, CSc.,
Institute of Chemical Technology,
Department of Metals and Corrosion Engineering,
Technická 5, 166 28 Praha 6,
Czech Republic.
e-mail: Ludek.Joska@vscht.cz*

THERAPEUTIC EFFICACY OF DIFFERENT ANTIDOTAL MIXTURES AGAINST POISONING WITH GF-AGENT IN MICE

Lucie Bartošová, Gabriela Kunešová, Kamil Kuča, Josef Vachek

Purkyně Military Medical Academy in Hradec Králové, Czech Republic: Department of Toxicology

Summary: The toxicity of cyclohexyl methylphosphonofluoridate (GF-agent; cyclosarin) and therapeutic efficacy of four oximes (trimedoxime, methoxime, obidoxime and HI-6) in combination with atropine or benactyzine (BNZ) was studied in mice. The oxime therapy combined with anticholinergic drug was administered intramuscularly (i.m.) 1 or 2 min after i.m. GF-agent challenge. All the drugs were applied in dose of 20% of LD₅₀. Obidoxime and trimedoxime that were combined with atropine were less effective than methoxime and HI-6 in combination with BNZ when applied 2 minutes after GF-agent poisoning. When the drugs were administered 1 min after GF-agent challenge already, in case of methoxime, the faster application of therapy resulted in significantly higher protective ratio, while for obidoxime the therapeutic effectivity did not depend significantly on the seasonableness of therapeutic intervention. The present findings show that all four combinations of oxime with anticholinergic drug decrease the GF-agent toxicity more than twofold regardless of the time of treatment administration.

Key words: *GF-agent; Cyclosarin; Methoxime; Obidoxime; Trimedoxime; HI-6; Atropine; Benactyzine; Acute Toxicity; Mice*

Introduction

GF-agent (cyclosarin; cyclohexyl methylphosphonofluoridate) is a highly toxic organophosphorus acetylcholinesterase (AChE, EC 3.1.1.7) inhibitor, known since the end of World War II, which has the potential for being used as a chemical warfare agent. This potential increased during Operation Desert Shield and Desert Storm with the possibility (later confirmed by the UN special commission) that GF-agent constituted of the Iraqi chemical agent inventory (11).

A combined regimen of therapy is now generally considered as the most effective medical approach for the treatment of nerve agent poisoning of military personnel (4). In the event of poisoning, immediate therapeutic treatment with an anticholinergic drug, such as atropine sulfate, antagonizes the effects of excess acetylcholine (ACh) at muscarinic receptor sites, and an oxime, such as pyridinium-2-aldoxime methylchloride (2-PAM), is used for the reactivation of any unaged inhibited enzyme (16).

Clinical experiences have indicated that oximes are not always very efficient reactivators of AChE depending on the type of nerve agent intoxication. Therefore, none of these oximes can be regarded as a broad spectrum antidote, i.e. effective against all nerve agents (5). Two oximes, obidoxime and 2-PAM, that are presently commercially available, are considered to be of insufficient efficacy against certain nerve agents, e.g. soman and GF-agent (19), while

in case of sarin poisoning this combination is quite effective. The inhibitory potency of GF-agent against AChE (rabbit brain) is similar to that of soman (6). The *in vivo* toxicity of GF-agent is similar to that of tabun in mice and rats and to sarin in rabbits and approximately twofold lower than to soman in rats (2). In guinea-pigs the GF-agent is two-threefold less toxic than soman (11). For GF-agent inhibited enzyme, aging should not be the major cause of its refractory property toward the oxime, since its half-time of aging is more than 4 h, a rate comparable with sarin-inhibited enzyme (12).

The purpose of this study was to compare the therapeutic efficacy of various oximes in combination with anticholinergic drug both administered 2 or 1 minute after challenge of GF-agent.

Material and Methods

Animals

Female mice, weighing 21–27 g, from Velaz Prague (Czech Republic) were kept in an air-conditioned room with light from 07:00 to 19:00 h and had free access to standard chow and tap water. The mice were divided into groups of six animals each. Handling of experimental animals was under the supervision of the Ethics Committee of the Purkyně Military Medical Academy and the Medical Faculty of Charles University (Hradec Králové, Czech Republic).

Material

GF-agent (cyclohexyl methylphosphonofluoridate; cyclosarin) of 99.9% purity was obtained from Military Technical Institute in Zemianské Kostolany (Slovak Republic). Its purity was determined by acidimetric titration. The oximes of at least 98.0 % purity were synthesized earlier in the Department of Toxicology of Purkyne Military Medical Academy in Hradec Králové (Czech Republic). All other chemicals and drugs of analytical grade were obtained commercially and used without further purification.

Animal experiment

In our experiment, methoxime (1,1-bis(pyridinium-4-aldoxime)methane dichloride), trimedoxime (1,3-bis(pyridinium-4-aldoxime)propane dichloride), obidoxime (1,3-bis(pyridinium-4-aldoxime)-2-oxapropane dichloride) or HI-6 (1-(pyridinium-2-aldoxime)-3-(pyridinium-4-carbamoyl)-2-oxapropane dichloride) in combination with atropine or benactyzine (BNZ) were used for treatment of GF-poisoned mice. This oxime therapy combined with anticholinergic drug was administered intramuscularly (i.m.) 1 or 2 min after i.m. GF-agent challenge. The dose of 20% of LD₅₀ for all drugs applied for treatment was chosen in order to evaluate the protective ratio for the maximum applicable therapeutic dose.

Data analysis

GF-agent-induced toxicity was evaluated by the assessment of LD₅₀ values and their 95% confidence limits within 1 week after administration of GF-agent at five different doses with six mice per dose (18). The efficacy of tested treatment was expressed as a protective ratio (LD₅₀ value of GF-agent in treated mice/ LD₅₀ value of GF-agent in non-treated mice). The differences between LD₅₀ values were considered to be significant when P < 0.05 (13).

Results

The therapeutic efficacy and protective ratio of antidotal treatment administered 2 min following GF-agent challenge are summarized in Table 1. Obidoxime and trimedoxime that were combined with atropine were less effective than methoxime and HI-6 in combination with BNZ. Methoxime in combination with BNZ appeared to be the most effective antidotal treatment of GF-agent intoxication in mice from those tested. Therapeutic efficacy of obidoxime and methoxime was further tested when applied already 1 min after GF-agent challenge and the results are presented in Table 2. These oximes were proved in more detail because as medicines they are components of Czech Army antidotal means against nerve agents. In case of methoxime the faster application of therapy resulted in significantly higher protective ratio, while for obidoxime the

therapeutic effectivity did not depend significantly on the seasonableness of therapeutic intervention.

Tab. 1: The therapeutic effect of different antidotal mixtures administered 2 min following GF-agent challenge.

Treatment	LD ₅₀ (µg/kg) with 95% confidence limits	Protective ratio
-	170 (151-190)	-
Trimedoxime, Atropine	465 (374-578)*	2.74
Methoxime, Benactyzine	645 (584-714)*	3.79
Obidoxime, Atropine	369 (291-466)*	2.17
HI-6, Benactyzine	594 (536-658)*	3.49

*significantly different from the untreated group at the level of P < 0.05

Tab. 2: The therapeutic effect of different antidotal mixtures administered 1 min following GF-agent challenge.

Treatment	LD ₅₀ (µg/kg) with 95% confidence limits	Protective ratio
-	170 (151-190)	-
Methoxime, Benactyzine	982 (912-1056)*	5.78
Obidoxime, Atropine	424 (388-464)	2.49

*significantly different from the group treated 2 min following GF-agent challenge at the level of P < 0.05

Discussion

The present findings show that all four combinations of oxime with anticholinergic drug decrease the GF-agent toxicity more than 2-fold. In earlier studies it was shown that the reactivating efficacy of methoxime *in vitro* is higher than that of pralidoxime, obidoxime, HI-6 or HLö7 in the case of GF-agent inhibited AChE. The reactivating efficacy of oximes *in vitro* usually corresponds to their therapeutic efficacy *in vivo* (9). In our *in vivo* study the therapeutic regimen consisting of methoxime and BNZ resulted in the highest protective ratio from all the oximes tested in both time schemes of application. *In vivo* the effectiveness of oximes against the toxic effects of nerve agents including GF is usually tested in combination with atropine (1,3). Although, some other anticholinergic drugs (e.g. benactyzine, biperiden) should be more advantageous than atropine for the elimination of toxic effects of nerve agents because of their central antimuscarinic effects. It was confirmed that the anticholinergic drug selection is not as important for the survival as the choice of AChE reactivator (7, 14). However, selection of cholinergic drug in treatment regimen of nerve agent poisoning plays a key role in reduction of epileptiform seizures that are in a strong relationship with acute lethal and neurotoxic effects of nerve agents. Atropine sulfate, the drug used almost universally as an

antidote for anticholinesterase poisoning, is less potent anticholinergic drug than biperiden or trihexyphenidyle for control of nerve agent-induced seizures (15). Although in both therapeutic regimens with the highest protective ratios BNZ as the anticholinergic drug was used, the importance of the choice of anticholinergics needs to be further verified. In our study the oximes were applied in dose of 20% LD₅₀, while usually maximum permissible dose of oxime for treatment of nerve agent poisoning is 10% of LD₅₀ (10, 17). Our results show, when compared to data available in literature that the protective ratio in case of obidoxime and atropine is almost 1.5 fold higher when 20% of LD₅₀ of oxime was applied (2.49) than for 16% of LD₅₀ of obidoxime (1.7) (8). This increase in protective ratio is rather considerable, but another increase of oxime dosing would probably resulted in organism damage by own oxime toxicity.

In conclusion, the presented data indicate that HI-6 and methoxime in combination with BNZ were significantly more effective than obidoxime and trimedoxime in combination with atropine in treatment of GF-agent intoxication.

Acknowledgement

The authors express their appreciation to Mrs. E. Vodáková for her excellent technical assistance and to Mr. V. Bláha for his help with the statistical evaluation. The study was supported by the Grant of Ministry of Defense no. ONVLAJEP20031.

References

- Clement JG. Efficacy of various oximes against GF (cyclohexyl methylphosphonofluoridate) poisoning in mice. *Arch Toxicol* 1992;66(2):143-4.
- Coleman IW, Patton GE, Bannard RA. Cholinolytics in the treatment of anticholinesterase poisoning. V. The effectiveness of Parpanit with oximes in the treatment of organophosphorus poisoning. *Can J Physiol Pharmacol* 1968; 46(1):109-17.
- Dawson RM. Review of oximes available for treatment of nerve agent poisoning. *J Appl Toxicol* 1994;14(5):317-31.
- Dunn MA, Sidell FR. Progress in medical defense against nerve agents. *JAMA* 1989;262(5):649-52.
- Eyer P, Hagedorn I, Klimmek R et al. HL6-7 dimethansulfonate, a potent bispyridinium-dioxime against anticholinesterases. *Arch Toxicol* 1992;66(9):603-21.
- Gray PJ, Dawson RM. Kinetic constants for the inhibition of eel and rabbit brain acetylcholinesterase by some organophosphates and carbamates of military significance. *Toxicol Appl Pharmacol* 1987;91(1):140-4.
- Kassa J. The influence of anticholinergic drug selection on the effectiveness of oximes against soman-induced supralethal poisoning in mice. *Acta Med (Hradec Králové)* 2001;44(2):77-9.
- Kassa J, Bajgar J. Therapeutic efficacy of obidoxime or HI-6 with atropine against intoxication with some nerve agents in mice. *Acta Med (Hradec Králové)* 1996;39(3):27-30.
- Kassa J, Cabal J. A comparison of the efficacy of acetylcholinesterase reactivators against cyclohexyl methylphosphonofluoridate (GF agent) by *in vitro* and *in vivo* methods. *Pharmacol Toxicol* 1999;84(1):41-5.
- Kassa J, Vachek J. A comparison of the efficacy of pyridostigmine alone and the combination of pyridostigmine with anticholinergic drugs as pharmacological pretreatment of tabun-poisoned rats and mice. *Toxicology* 2002;177(2-3): 179-85.
- Koplovitz I, Gresham VC, Dochterman LW, et al. Evaluation of the toxicity, pathology, and treatment of cyclohexylmethylphosphonofluoridate (CMPPF) poisoning in rhesus monkeys. *Arch Toxicol* 1992;66(9):622-8.
- Luo C, Liang J. Evaluation of combined toxic effects of GB/GF and efficacy of Jielin Injection against combined poisoning in mice. *Toxicol Lett* 1997;92(3): 195-200.
- Roth Z, Josifko M, Tréka V. Statistické metody v experimentální medicíně. Praha: Státní zdravotnické nakladatelství, 1962:405-13.
- Sevelová L, Vachek J. Effect of methoxime combined with anticholinergic, anti-convulsant or anti-HCN drugs in tabun-poisoned mice. *Acta Med (Hradec Králové)* 2003;46(3):109-12.
- Shih TM, Duniho SM, McDonough JH. Control of nerve agent-induced seizures is critical for neuroprotection and survival. *Toxicol Appl Pharmacol* 2003; 188(2):69-80.
- Shih TM, McDonough JH. Efficacy of biperiden and atropine as anticonvulsant treatment for organophosphorus nerve agent intoxication. *Arch Toxicol* 2000; 74(3):165-72.
- Shih TM, McDonough JH. Organophosphorus nerve agents-induced seizures and efficacy of atropine sulfate as anticonvulsant treatment. *Pharmacol Biochem Behav* 1999;64(1):147-53.
- Tallarida R, Murray R. Manual of pharmacological calculation with computer programs. New York: Springer Verlag, 1987:145.
- Worek F, Widmann R, Knopff O et al. Reactivating potency of obidoxime, pralidoxime, HI 6 an HL6-7 in human erythrocyte acetylcholinesterase inhibited by highly toxic organophosphorus compounds. *Arch Toxicol* 1998;72(4):237-43.

Submitted February 2004.

Accepted June 2004.

Mgr. Lucie Bartošová,
P.O.Box 35/T,
Purkyně Military Medical Academy,
500 01 Hradec Králové,
Czech Republic.
e-mail: sevelova@pmfhk.cz

WHAT ARE THE REACTIVITIES OF CORONARY ARTERIES HARVESTED FROM THE HEARTS EXPOSED TO COLD ISCHEMIC PRESERVATION?

Caner Arslan¹, Sibel Özyazgan², Kazım Beşirli¹, Emir Cantürk¹, Gökçe Şirin¹, Kürşat Bozkurt¹, Gökhan Akkan²

University of Istanbul, Cerrahpaşa Medical Faculty, Turkey: Department of Cardiovascular Surgery¹, Department of Pharmacology²

Summary: This study was designed to determine the effects of pretransplant ischemic hypothermic period on reactivities of major coronary arteries. Eleven pigs were used. Right, left anterior descending and circumflex coronary arteries harvested from 6 pigs following single dose of cardioplegia and cardiectomy. The same procedures were performed in 5 pigs after 6 hours static 4 °C hypothermic preservation of the hearts. Strips prepared from these 3 coronary arteries were placed in organ chambers and contractions with acetylcholine and histamine and KCL and dilatations with noradrenaline following submaximal contractions with acetylcholine and histamine were documented. There was no statistically significant difference between results taken from both groups. The pretransplant period (until 6 hours) does not cause important differences on the reactivities of coronary arteries.

Key words: Porcine coronary artery; Transplantation.

Introduction

Today heart transplantation is one of the frequently performed surgical procedures. Donor shortage, pretransplant ischemic time and after transplantation immune reactions, heart failure, coronary vasculopathy are the major drawbacks of this procedure. Here, we focused on how pretransplant ischemic period effects reactivities of coronary arteries.

Material and Methods

In this study, 11 home pigs were used. Their weights were ranging from 12 to 16 kg. Feeding was ceased 12 hours before the operation. The pigs were sedatized by intramuscular injection of 2 mg/kg xylazine hydrochloride and 0.5 mg/kg midazolam 15 minutes before operation. Then full sedation was made by intramuscular 20 mg/kg ketamine hydrochloride injection. After insertion of 22 no silastic venous cannula, deep anesthesia was made by intravenous injection of half of the initial doses of xylazine and ketamine⁽³⁾. Then the pigs were intubated 4.5 no tube and ventilated 12 times in a minute and tidal volume was 10–15 ml/kg at 40 % FiO₂. Median sternotomy was made and pericardium was opened. After 400 unite/kg heparine was given from the right atrium, superior vena cava (SVC) and inferior vena cava (IVC) were occluded. After 4 cardiac cycle, ascending aorta was clamped and 10 ml/kg crystalloid

cardioplegia solution (Plegisol) at 4 °C was infused into the aortic root at the pressure of 150 mmHg. At the same time, right superior pulmonary vein partially excised to decompress the heart chambers and cold isotonic at 4 °C was poured into the pericardium for topical cooling. The heart was extirpated from the pericardial cavity just after cardioplegia and heart stop. Proximal 1.5 cm part of the left anterior descending coronary (LAD), circumflex (CX) and right coronary arteries (RCA) were harvested from the heart. This procedure was made just after the hearts were extracted from the pericardium in 6 pigs, in other 5 pigs after 6-hour cold ischemic preservation at 4 °C.

Coronary artery segments were put into Krebs-ringer solution, after cleaning from soft tissues. Rings 3 mm in width were prepared from those arteries and they were opened and longitudinal arterial strips were obtained. These strips were inserted into the organ chambers filled with Krebs-ringer solution aerated with carbojen (95 % O₂ and 5 % CO₂) at 37 °C and their one end were connected to isometric force displacement transducer of TDA 97 polygraph.

During first 90 minutes, 5 gr stress was applied to the strips for balance and every 20 minutes solution was changed. At the end of the experiment, wet weight (w.w.) of every strip was measured. Contractions and relaxations of coronary artery strips were calculated as mg stress per mg w.w. by the soft ware of TDA 97 polygraph at computer connected to the organ chamber and simultaneous contractions and relaxation graphics were drawn. From these

graphics, pD_2 (- Log EC50) values (sensitivity) which is the negative logarithm of half value maximum reaction and also maximum contraction and maximum relaxation values were calculated. Concentration-contraction graphics were obtained from cumulative addition of acetylcholine (Ach) (10^{-9} , 3×10^{-9} , 10^{-8} , 3×10^{-8} , 10^{-7} , 3×10^{-7} , 10^{-6} , 3×10^{-6} , 10^{-5} , 3×10^{-5} , 10^{-4} mM) and histamine (His) (6×10^{-6} , 3×10^{-6} , 10^{-6} , 6×10^{-5} , 3×10^{-5} , 10^{-5} , 6×10^{-4} , 3×10^{-4} , 10^{-4} mM) and KCL (20, 40, 60, 80 mM) until the maximum reaction was taken after balance period. The second dose of drug was not given before contraction reached a plateau from the first dose of drug. Relaxation graphics were obtained from the arterial strips contracted with submaximal (EC 90) Ach and His by cumulative addition of noradrenalin (NA) (10^{-9} , 3×10^{-9} , 10^{-8} , 3×10^{-8} , 10^{-7} , 3×10^{-7} , 10^{-6} , 3×10^{-6} , 10^{-5} , 3×10^{-5} , 10^{-4} mM). From these graphics percent inhibition of relaxation for NA and pD_2 values were calculated. Again the second dose of drug was not given before relaxation caused by previous one had reached a plateau. Before every medication, 45 minutes rest periods were taken and during these times strips were washed in every 15 minutes.

For statistical analysis between groups, one way ANOVA and post hoc Tukey-Kramer HSD tests were used and $p < 0.05$ was set for significance.

Results

There is no statistically significant difference between two groups in pD_2 values of contraction reactions to cumulative Ach, His and KCL of LAD, CX and RCAs taken from the 6 pigs in the first group and 5 pigs in the second group (Tab. 1).

Tab. 1: Mean and standard deviations of pD_2 values of Ach, His and KCL contraction reactions of RCA, CX and LAD from 6 pigs in the first group and 5 pigs in the second group.

	RCA	CX	LAD
1 st group Ach	6.23±0.09	6.15±0.17	6.36±0.25
2 nd group Ach	6.21±0.11	6.30±0.13	5.99±0.08
1 st group His	3.40±0.32	3.70±0.16	3.62±0.10
2 nd group His	3.71±0.07	3.62±0.16	3.49±0.14
1 st group KCL	1.58±0.03	1.66±0.08	1.73±0.04
2 nd group KCL	1.44±0.10	1.47±0.04	1.55±0.03

Tab. 2: Mean and standard deviations of pD_2 values of Ach, His submaximal contraction and NA relaxation reactions of RCA, CX and LAD from 6 pigs in the first group and 5 pigs in the second group.

	RCA	CX	LAD
1 st group Ach	7.20±0.31	7.54±0.33	7.15±0.33
2 nd group Ach-NA	6.95±0.42	6.60±0.26	6.73±0.17
1 st group His-NA	7.20±0.10	7.50±0.27	7.36±0.29
2 nd group His-NA	6.78±0.08	6.73±0.08	6.47±0.11

There is also no statistically significant difference between two groups in pD_2 values of Ach, His contraction-NA relaxation reactions (Tab. 2).

Statistically significant difference is not determined between maximum contractions of LAD, CX and RCAs in the both groups to Ach, His and KCL, except maximum contractions of RCAs in two groups to Ach. The maximum contraction value of RCAs in the first group 357 ± 180 mg/mg w.w. in contrast to 656 ± 127 mg/mg w.w. in the second group.

Discussion

In this study, we used single dose cardioplegia and static hypothermic preservation. LAD, CX and RCAs were harvested immediately after cardioplegia in one group and 6 hours later which is the maximum safe period for static hypothermic preservation in the heart transplantation in the other group. We didn't compose additional groups by making endothelial injury in the coronary artery strips because we were interested in the effects of pretransplant time loss.

A prominent decrease was determined in nitric oxide synthase activity in endothelial cell culture of porcine coronary arteries preserved in 4 °C University of Wisconsin solution (UWS) for 6 hours in contrast to ones preserved in 37 °C UWS. This is a damage to the heart caused by long term hypothermic preservation (5). In contrast to this, it is shown that vascular smooth muscle and endothelium-dependent relaxations were preserved in canine coronary arteries after 24-hour hypothermic (4 °C) storage in UWS in another study (6). Maximum contraction to Ach, His and KCL is related smooth muscle cell and endothelial function (4, 5). In our experiment, there was no meaningful difference between maximum contractions of coronary arteries in both groups except RCAs.

There was no meaningful difference between sensitivity (pD_2) values of contraction reactions to Ach, His and KCL and relaxation reactions to NA of contracted coronary arteries by Ach and His in both groups. It is seen that there is no serious difference in functions of endothelium and smooth muscle of coronary arteries taken from the hearts immediately after harvesting and the hearts preserved for 6 hours at static hypothermia (4 °C).

It can be said that pretransplant static hypothermic preservation time does not effect posttransplant myocardial performance by effecting coronary arteries. Regression of endothelial dysfunction occurring early after transplantation shows episodic nature of immune injury (1). Endothelial dysfunction is common in the early period after transplantation. Early constrictor response of coronary arteries to acetylcholine can be accepted as a sign of intimal injury. By intracoronary ultrasonography, one year after transplantation, a significant increase is found in the intimal thickness of coronary artery segments which con-

tracts to early posttransplant intracoronary injection of acetylcholine (2).

Here, significant difference between sensitivity (pD_2) values of contraction reactions of coronary arteries to Ach in both groups is not determined. This supports that length pretransplant ischemic hypothermic period is not effective in the etiology of posttransplant intimal thickness and atherosclerosis.

Conclusions

Absence of meaningful differences in reactivities of coronary arteries in both groups points that endothelial and smooth muscle cell injury originates from delivery of cardioplegia not from the static hypothermic preservation period. We can also conclude that pretransplant period until 6 hours cannot play any role in the development of post-transplant vasculopathy.

Acknowledgements

This study was financially supported by Istanbul University Research Foundation. We are grateful to Professor Tuncay Altug who is the chief of Research Animal Laboratory in Cerrahpaşa Medical Faculty and Dr. Nurten Öcalan from the same institution for their great help.

References

1. Anderson TJ, Meredith IT, Uehata A, Mudge GH, Selwyn AP, Ganz P et al. Functional significance of intimal thickening as detected by intravascular ultrasound early and late cardiac transplantation. *Circulation* 1993;88: 1093-100.
2. Davis SF, Yeung AC, Meredith IT et al. Early coronary dysfunction predicts the development of transplant coronary artery disease at 1 year posttransplant. *Circulation* 1996;93:457-62.
3. Harvey RC, Walber J. Special considerations for anesthesia and Analgesia in research animals. In: Short CE ed. *Principles and Practice of Veterinary Anesthesia*. Edinburg: Williams and Wilkins, 1987:380-92.
4. Lin PJ, Chang CH, Yao PC, Liu HP, Hsieh HC, Tsai KT. Enhancement of endothelium dependent contraction of the canine coronary artery by UW solution. *Transplantation* 1994;58:1323-8.
5. Redondo J, Manso MA, Pacheco ME, Hernandez L, Salaires M, Marin J. Hypothermic storage of coronary endothelial cells reduces nitric oxide synthase activity. *Cryobiology* 2000;4:292-300.
6. Sorajja P, Cable DG, Schaff HV. Hypothermic storage with University of Wisconsin solution preserves endothelial and vascular smooth muscle cell function. *Circulation* 1997;96(suppl 9):297-303.

Submitted February 2004.

Accepted July 2004.

Dr. Caner Arslan,
TDV, 29 Mayıs Hastanesi,
Kalp ve Damar Cerrahisi Kliniği,
Emniyet müdürlüğü yanı,
Vatan cd. Kanlı çıkmazı sk. 34250,
Fatih/ İstanbul - Turkey.
e-mail: canerkvc@yahoo.com

GAINS AND LOSSES OF HLA CLASS II (DR) AND CD4 IN ATYPICAL HYPERPLASIA, CARCINOMA IN SITU AND INFILTRATING DUCTAL CARCINOMA OF THE BREAST

Demetrio Tamiolakis¹, Ioannis Venizelos², Maria Lambropoulou⁴, Theodoros Jivannakis⁴, Evagelia Seliniotaki¹, Panagiotis Tsikouras⁵, Vasilios Limberis⁵, Angelos Tsalkidis³, Nikolas Papadopoulos³

General Hospital of Chania: Department of Cytology¹; Ippokration Hospital of Salonica: Department of Pathology²; Democritus University of Thrace: Department of Histology – Embryology³; Department of Obstetrics and Gynecology⁵; General Hospital of Drama: Department of Pathology⁴

Summary: Aim: Breast cancer is a frequent cause of death among women with gynaecologic malignancies despite the introduction of combination chemotherapy. There is therefore a need for new therapeutic strategies for patients with breast cancer, such as cellular immunotherapy. In this immunohistochemical study we analyzed the epithelial expression of major histocompatibility complex (MHC) class II (HLA-DR) on atypical and malignant primary mammary epithelial cells, as well as the magnitude of the stromal T lymphocytes (T4 subset) at the tumor site. Experimental design: The study was carried out retrospectively in tumor tissue from 82 patients with mammary lesions (31 cases of atypical ductal hyperplasia -ADH-, 12 cases of ductal carcinoma in situ -DCIS- and 39 cases of infiltrating ductal carcinoma not otherwise specified -IDC-NOS). Medullary carcinomas were not included in our investigation. Material used had been formalin fixed and paraffin embedded. Results: HLA class II (DR) was expressed in 20 of 31 ADHs (64.5%), in 4 of 12 DCISs (33.3%), and in 10 of 39 IDC-NOSs (25.6%). CD4 was expressed in 9 of 31 ADHs (29%), in 5 of 12 DCISs (42%), and in 26 of 39 IDC-NOSs (67%). Conclusions: The results showed decreased epithelial expression of HLA class II (DR) and increased stromal expression of CD4, as the lesion progressed to malignancy. Gradual loss of epithelial HLA class II expression might be a manifestation of cellular differentiation from the atypical form versus the malignant one, signaling simultaneously a selective effect on the response capacity of the immune system.

Key words: HLA class II (DR); CD4; Atypical ductal hyperplasia of the breast; Breast cancer

Introduction

Studies of the relation between the tumour and host immune systems have shown that major histocompatibility class (MHC)-I antigen expression, normally present in all nucleated cells, is reduced in malignancies (11,20,21,26, 41). This feature was related to tumour progression in experimental tumour systems (18,43,46). Furthermore, human leukocyte antigen (HLA)-DR, a class II MHC antigen, which is normally expressed only in antigen presenting cells of the immune system (24), shows variable expression in malignancies (16,30).

The examination of MHC antigen expression in breast carcinoma in particular has been prompted by the observation that lymphocytic infiltrates occur in two thirds of these malignancies (22), suggesting that the immune system may be active in the modulation of tumour behavior. MHC-I expression in breast cancer was found to be hetero-

geneous, but usually decreased (29,47,48,49). In some studies prominent MHC-I expression was related to better tumour differentiation (47,49), and a favorable prognosis (5), whereas in other no such correlations were found (6,31,37,44). Regarding HLA class II (DR) expression in breast cancer, most studies report intermediate values (1,4,25,29,31,32,49,50), but the findings are variable (3,22). HLA class II (DR) expression may also be related to tumour grade; two studies reported that none of the carcinomas that were negative or only focally positive were well differentiated (4,50). However, several other studies failed to support this finding (25,31,49). The link between HLA class II (DR) expression and prognosis also remains unclear (29,37,48)

Increasing evidence of a critical role for the T helper cell in initiating, regulating, and maintaining antitumour immune responses (40) justifies more investigation of HLA class II. HLA-DR (class II) expression by primary breast

cancers is positively correlated with the differentiation state of the tumour and the expression of progesterone receptors (both associated with good prognosis). Furthermore, in medullary carcinoma of the breast (generally associated with a good prognosis and a florid T lymphocyte response) the HLA class II (DR) expression was 74.5% in primary tumours and 67.3% in nodal metastases, compared to 17.7% and 7% in ductal carcinomas (27). It is not hard to imagine how loss of HLA class I expression may aid escape from immune surveillance but HLA class II antigens (which are normally presented to T lymphocytes by professional antigen-presenting cells, not tumour cells) may not be subject to such easy down-regulation by the tumour itself and therefore specific MHC class II molecules may be more likely to confer variability in cancer susceptibility than MHC class I molecules (19).

The current study determined the HLA class II (DR) expression of atypical ductal hyperplasia, ductal carcinoma in situ and infiltrating ductal carcinoma of the breast with quantification of stromal infiltration by CD4+ T lymphocytes, with aim to allow future assessment of whether HLA class II expression has an impact on clinical outcome.

Materials and methods

Tumor samples were obtained from 82 patients ranging in age from 35–85 years. The mean (SD) age of our patients was 57.8 years, and mean tumor size in the cases of IDC-NOS was 2.4 cm (range 0.9 to 6.5 cm). All our selected cases were recovered from routine histological files. 15 patients were premenopausal. The 82 tumours studied included 31 cases of atypical ductal hyperplasia (ADH), 12 cases of ductal carcinoma in situ (DCIS) micropapillary pattern, and 39 cases of infiltrating ductal carcinoma not otherwise specified (IDC-NOS) of the breast. Our material included cases with an abundant stromal lymphocytic infiltrate. The 31 cases of ADH and 12 cases of DCIS were an accidental finding in patients which had been operated for fibrocystic changes of the breast. Stage of disease at presentation (in the cases of IDC-NOS) was known in 23 patients; most (70%) had stage II disease, and the remainder were divided equally between stage I and stage III. Fifteen patients had lymph node metastases. The specimens had been fixed in 10% formal-saline and processed routinely through absolute alcohol and xylene before embedding to paraffin wax. Conventional histological stains included hematoxylin and eosin. Regional Committees of Ethics approved the study. Written informed consent was obtained from all patients, and the procedures followed were in accordance with the institutional guidelines.

Immunohistology

Additional slides were stained with several monoclonal antibodies that are reactive in paraffin sections for immunohistochemical studies. An antigen-retrieval method

using a pressure cooker was performed before immunohistochemical staining (34). The staining consisted of a first-stage incubation with the following primary monoclonal antibodies: HLA class II (DR) (TAL.1B5); CD20 (L26); CD4 (1F6); CD8 (C8-144). Bound antibodies were visualized employing the alkaline phosphatase anti-alkaline phosphatase (APAAP) method (9) and Fast Red for development. Negative controls were omission of primary antibody. Positive controls for anti-HLA II (DR) and anti-CD4 antibody were the staining of stromal cells and the tissue of tonsils respectively. We focus our attention on HLA class II (DR), and CD4 antibodies since the others antigens were beyond the scope of our study.

The immunostained sections were examined with an X 40 objective and the distribution of HLA class II (DR) and CD4 within the cell was recorded. To count the number of cells with HLA II (DR) and CD4 staining, a 10 X 10 square calibrated grid was inserted into the eyepiece of an Olympus BX40 binocular microscope.

Five-to-ten fields were examined for each section, and at least 1000 cells were scored, depending on cellularity. The percentage of positive cells was recorded as the HLA class II (DR) and CD4 indices.

$$\text{HLA-II (DR) index} = \frac{\text{No of positive cells}}{\text{No total (positive+negative cells)}}$$

$$\text{CD4 index} = \frac{\text{No of positive cells}}{\text{No total (positive+negative cells)}}$$

The indices ranged from 0–100%, with a mean of 18%. The mean index was evaluated in three ranges: low index (under 18%), grade I; moderate index (from 18 to 50%), grade II; and high index (from 51 to 100%), grade III.

For all cases both the percentage and intensity of HLA class II (DR) staining were numerically scored as in Table 1. Particular emphasis was given on the total percentage of epithelium stained, the intensity of staining and uniformity. Intensity was derived by comparison of epithelial staining with stromal cell reactivity.

Tab. 1: Scoring system for HLA class II (DR) expression.

Percentage of cell expression	score
0	0
18	1
50	2
100	3
Intensity of HLA class II (DR) expression	score
Negative	0
Very weak, just detectable	1
Readily detectable	2
Just less intense than stromal cells	3
Strong intensity, equal to stromal cells	4

Results

The sections were examined independently by two observers, and positive cellular staining for HLA class II (DR) and CD4 antigens were manifested as fine red cytoplasmic expression.

HLA class II (DR) was expressed in 20 of 31 of atypical ductal hyperplasias (ADH) (64,5%) (Fig. 1), in 4 of 12 ductal carcinomas in situ (DCIS) (33.3%) (Fig. 2), and in 10 of 39 infiltrating ductal carcinomas not otherwise specified (IDC-NOS) (25,6%) (Fig. 3). CD4 was expressed in 9 of 31 ADHs (29%) (Fig. 4), in 5 of 12 DCISs (42%), and in 26 of 39 IDC-NOS (67%) (Fig. 5). There was a variable reduction of the intensity and proportion of epithelial staining from ADH towards IDC-NOS. On the contrary, there was a variable increase in the numbers of CD4 positive stromal infiltrates from ADH towards IDC-NOS. HLA class II (DR) expression by malignant epithelium showed the greatest change from that seen in ADH. In 10 cases of

IDC-NOS, 3 cases exhibited epithelial HLA class II (DR) expression in a manner similar to that seen in ADH, and 7 cases showed variable reduction of the intensity and numbers of epithelial cells stained. From the 4 cases of DCIS 2 cases showed HLA class II (DR) expression as in ADH and 2 exhibited variable expression.

Lymphocytes - Stromal cells identified with CD20, CD4, and CD8 were morphologically lymphocytes. Lymphocytes were predominantly in periductal and intralobular connective tissue in benign ADH. Both B and T lymphocytes were identified in a ratio of approximately 1: 3.5, and with slightly more CD4 than CD8 positive cells. Interepithelial cells were also present, the vast majority of which were T lymphocytes, mainly CD4. In DCIS and IDC-NOS, lymphocytes were predominantly in stroma around tumour cell islands, with only occasional single cells adjacent to tumour cells. B and T lymphocytes were present in a ratio of approximately 1: 2, again with a predominance of CD4 cells being found.

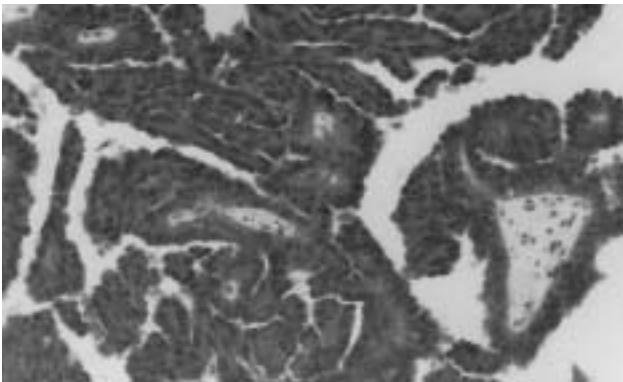


Fig. 1: HLA class II (DR) expression in atypical ductal hyperplasia (ADH) with micropapillary pattern. Immunostaining using APAAP technique (red labeled cells). Original magnification X200.

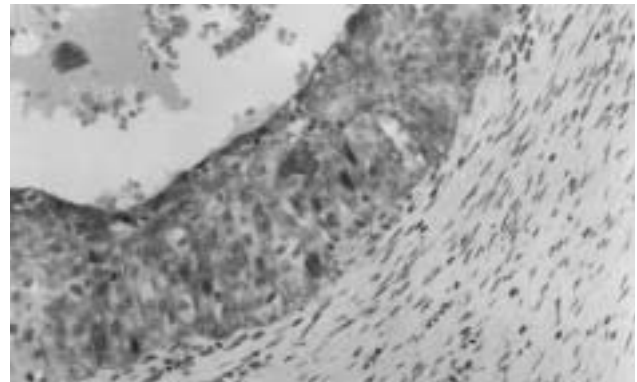


Fig. 2: HLA class II (DR) expression in comedo ductal carcinoma in situ (DCIS). Immunostaining using APAAP technique (red labeled cells). Original magnification X200.

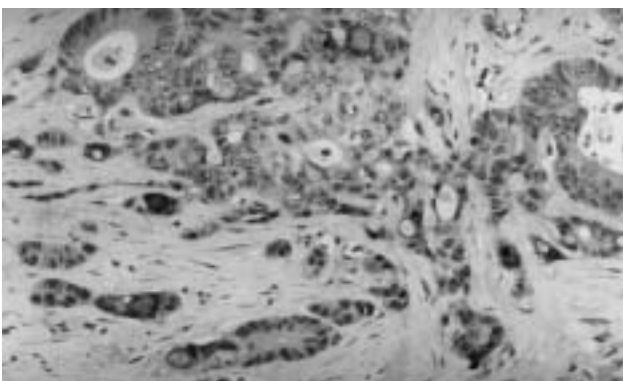


Fig. 3: HLA class II (DR) expression in infiltrating ductal carcinoma (IDC-NOS). Immunostaining using APAAP technique (red labeled cells). Original magnification X200.

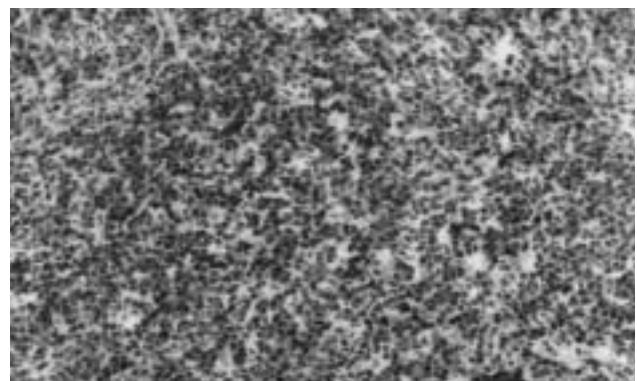


Fig. 4: Atypical ductal hyperplasia (ADH): Stromal T lymphocytes positive for the immunohistochemical stain directed against the CD4 antigen (stain, alkaline phosphatase antialkaline phosphatase; original magnification, X200).

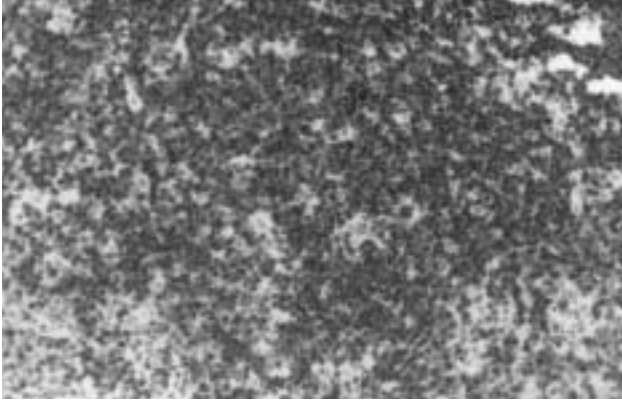


Fig. 5: Infiltrating ductal carcinoma (IDC-NOS): Stromal T lymphocytes positive for the immunohistochemical stain directed against the CD4 antigen (stain, alkaline phosphatase antialkaline phosphatase; original magnification, X200).

Tab. 2:

Average numbers of HLA class II (DR)+ mammary epithelial cells in ADH, DCIS, and IDC-NOS per high power field (range in brackets).

	ADH	DCIS	IDC-NOS
HLA II (DR) antibody	30.7 (4.7-142)	26.6 (0.3-60)	2.85 (0.3-11.1)

Average numbers of CD4+ mammary stromal cells in ADH, DCIS, and IDC-NOS per HPF (range in brackets)

	ADH	DCIS	IDC-NOS
CD4 antibody	3.3 (0.2-9.7)	22.9 (0.5-74)	41 (4.7-89)

Quantification - Stromal lymphocytes identified by each monoclonal antibody were present in far greater numbers in DCIS and IDC-NOS as compared with ADH ($p < 0.001$).

Epithelial Staining - It was observed that all monoclonal antibodies directed against lymphocytes also reacted with both non-malignant and malignant epithelium in a substantial number of cases. However, intensity of staining was generally weak and did not interfere with the recognition and quantification of infiltration of lymphocytes.

Interrelationship of epithelial HLA class II (DR) antigens and stromal infiltrate - DCIS and IDC-NOS with greater HLA class II (DR) expression had more intense stromal infiltration by total T lymphocytes, this being reflected by the CD4 subsets in both instances. Carcinomas with loss of HLA II (DR) expression had slightly fewer CD4 positive cells.

Table 2 shows the average numbers of HLA class II (DR)+ and CD4+ cells in atypical ductal hyperplasia, ductal carcinoma in situ, and infiltrating ductal carcinoma of the breast, respectively.

Discussion

In the present study, we clearly demonstrated a loss of HLA class II (DR) expression from atypical ductal hyperplasia towards invasive carcinoma.

It is well known that HLA class II antigens are usually expressed on such immune cells as macrophages, B cells and activated T cells and that they are also involved in antigen presentation as well as in the regulation of the helper T cell function. A number of studies have also revealed the expression of class II antigens by both various non-immune normal and malignant cells (1,2,4,14,33,38,48,45), although the biological significance of the class II expression of such cells remains unclear.

The presence of epithelial hyperplasia is the most important risk factor for subsequent malignancy. Fibrocystic changes increase progressively in women through the child-bearing years, reach a peak during the perimenopausal period, and regress after menopause (2). Although the various components of fibrocystic change are usually found together, it has become increasingly clear that this is a heterogeneous group of lesions that should be diagnosed separately (17). The extent and type of epithelial proliferation found in these biopsy specimens is a major predictor for the subsequent development of mammary carcinoma, whereas the other components are of little significance in that regard (13). In addition, epidemiological similarities to breast cancer apply most consistently to the subset of patients with significant epithelial atypia (36).

Atypical ductal hyperplasia (ADH) accounts for less than 3% of all breast lesions found at biopsy. This is probably an underestimate of its incidence because it lacks distinctive features that would bring it to medical attention. It is most common in postmenopausal women. Several studies have shown that women with diagnosed ADH have a relative risk of 4.0 to 5.0 for the subsequent development of invasive carcinoma (12,13, 28).

A common criticism is that the reproducibility of diagnosing ADH is low, and this has been attributed to a lack of consensus regarding its histologic criteria (39). Recent studies have taken an empirical approach to defining ADH that is based on evaluating the association between worrisome proliferative lesions (irrespective of traditional concepts of dysplasia) and the clinical outcome (12,13). Reproducible diagnostic criteria have been defined (42), and these have been used repeatedly to validate ADH as a strong risk factor for breast cancer (12,13).

There is a controversy regarding whether ADH is merely a risk factor, or also a precursor lesion for breast cancer. Some authors have suggested that ADH is a small non-invasive carcinoma, basing their speculation on the close histologic resemblance between them. However, noninvasive carcinoma has a twofold to threefold stronger association than ADH does with the subsequent development of invasive carcinoma, and this risk is ipsilateral for non-invasive carcinoma (35), but bilateral for ADH (12,28).

Noninvasive carcinoma is also often seen in continuity with concurrent invasive disease, whereas ADH is not. These data and observations indicate that noninvasive carcinoma may be both a risk factor and a non obligatory precursor for invasive carcinoma, though ADH may be a marker of increased risk (8). However, this issue is far from settled, and is likely to remain so until more is known about the biology of breast cancer evolution.

On the other hand, in view of immunological aspects, the class II expression of tumor cells has been reported to correlate with the local infiltration of lymphocytes (10,23). There have been reported studies examining antigen presentation by epithelial cells from the human breast (7,15).

In the present study, expression of HLA class II (DR) by epithelial neoplastic cells was possibly mediated by stromal T helper lymphocytes as lymphoid cell infiltrates were observed to all biopsy specimens containing HLA class II (DR) positive neoplastic cells. The increased aberrant expression of HLA II in tumor cells has been viewed as an important feature to escape tumor recognition by immune cells, and correlates with high grade malignancy and enhanced metastatic potential. In our series of breast lesions, there was a decreased expression of HLA II as the neoplastic process progressed to malignancy and a subsequent increased immune response, providing new insights for a better understanding of the tumorhost relationships in this form of neoplasia.

MHC tumor expression before, during, or after immunotherapy may be a necessary step in tumor response to treatment (15). Breast cancer has low activity of tumor infiltrating lymphocytes, and immunotherapy has not shown any advantage. Studies have shown that malignancies that respond to interleukin (IL)-2 treatment express HLA-DR before treatment, whereas non-responding tumors do not, either before or after treatment. Likewise, malignant melanomas transfected with MHC-I genes showed better responses to IL-2 treatment, and MHC-I induction in a highly tumorigenic adenovirus-2 transformed cell line resulted in the complete loss of oncogenicity. Therefore, we suggest that immunotherapy with a cocktail of cytokines known to induce MHC-II expression may induce breast tumor cells to express MHC-II antigens. This could increase their immunogenicity and susceptibility to cytotoxic and helper T cells, respectively, and activate lymphocytic infiltrates to proliferate in situ.

Acknowledgment

We thank Irene Apostolou for her excellent technical assistance in the immunohistochemical studies.

References

- Bartek J, Petrek M, Vogtesek B et al. HLA-DR antigens on differentiating human mammary gland epithelium and breast tumors. *Br J Cancer* 1987;56:727-33.
- Bartow SA, Pathak DR, Black WC, Key CR, Teaf SR. Prevalence of benign, atypical and malignant breast lesions in populations at different risk for breast cancer: a forensic autopsy study. *Cancer* 1987;60:2751-60.
- Bernard D, Maurizis JC, Ruse F et al. Presence of HLA-D/DR antigens on the membrane of breast tumor cells. *Clin Exp Immunol* 1984;56:215-21.
- Brunner CA, Gokel JM, Riethmiller G et al. Expression of HLA-D subloci DR and DQ by breast carcinomas is correlated with distinct parameters of favorable prognosis. *Eur J Cancer* 1991 ;27:411-6.
- Concha A, Esteban F, Cabrera T et al. Tumor aggressiveness and MHC class I and II antigens in laryngeal and breast cancer. *Semin Cancer Biol* 1991;2:47-54.
- Concha A, Cabrera T, Ruiz-Cabello P et al. Can the HLA phenotype be used as a prognostic factor in breast carcinomas? *Int J Cancer* 1991;6(suppl):146-54.
- Concha A, Ruiz-Cabello F, Cabrera T, Nogales F, Collado A, Garrido F. Different patterns of HLA-DR antigen expression in normal epithelium, hyperplastic and neoplastic malignant lesions of the breast. *Eur J Immunogenet* 1995;22(4):299-310.
- Connolly JL, Schnitt SJ. Benign breast disease: resolved and unresolved issues. *Cancer* 1993;71:1187-9.
- Cordell JL, Falini B, Erber WN et al. Immunoenzymatic labeling of monoclonal antibodies using immune complexes of alkaline phosphatase and monoclonal anti-alkaline phosphatase (APAAP complexes). *J Histochem Cytochem* 1984; 32:219-29.
- Dammrich J, Buchwald J, Papadopoulos T, Muller-Hermelink HK. Special subtypes of pulmonary adenocarcinomas indicated by different tumor cell HLA-expression and stromal infiltrates. *Virchows Arch B Cell Pathol* 1991;61:9-18.
- Doyle A, Martin WJ, Funa K. Markedly decreased expression of class I histocompatibility antigens protein, and mRNA in human small cell lung cancer. *J Exp Med* 1985;161:1135-51.
- Dupont WD, Page DL. Risk factors for breast cancer in women with proliferative breast disease. *N Engl J Med* 1985;312:146-51.
- Dupont WD, Parl FF, Hartmann WH et al. Breast cancer risk associated with proliferative breast disease and atypical hyperplasia. *Cancer* 1993;71:1258-68.
- Esteban F, Concha A, Huelin C et al. Histocompatibility antigens in primary and metastatic squamous cell carcinoma of the larynx. *Int J Cancer* 1989;43:436-42.
- Feinmesser M, Sulkes A, Morgenstern S, Sulkes J, Stern S, Okon E. HLA-DR and beta 2 microglobulin expression in medullary and atypical medullary carcinoma of the breast: histopathologically similar but biologically distinct entities. *J Clin Pathol* 2000;53(4):286-91.
- Ghosh AK, Moore M, Street AJ et al. Expression of HLA-D sub-region products on human colorectal carcinomas. *Int J Cancer* 1986;38:459-64.
- Godfrey SE. Is fibrocystic disease of the breast precancerous? *Arch Pathol Lab Med* 1986;110(11):991.
- Goodenow RS, Vogel JM, Linsk RL et al. Histocompatibility antigens on murine tumors. *Science* 1985;230:777-83.
- Gourley C, Thornton C, Massie C et al. Is there a relationship between HLA type and prognostic factors in breast cancer? *Anticancer Research* 2003;23:633-8.
- Hämmerling G, Maschek U, Sturmhöfel K et al. Regulation and functional role of MHC expression on tumors. In: Melchers F, Albert ED, Von Boehmer AH et al, eds. *Progress in immunology*, vol 7. Berlin: Springer-Verlag, 1989:pp1071-8.
- Holden CA, Sanderson AR, MucDonald DM. Absence of human leukocyte antigen molecules in skin tumors and some cutaneous appendages: evidence using monoclonal antibodies. *J Am Acad Dermatol* 1983;9:567-71.
- Hurlimann J, Saraga P. Mononuclear cells infiltrating human mammary carcinomas: Immunohistochemical analysis with monoclonal antibodies. *Int J Cancer* 1985;35:753-62.
- Kamma H, Yazawa T, Ogata T, Horiguchi H, Iijima T. Expression of MHC class II antigens in human lung cancer cells. *Virchows Arch B Cell Pathol* 1991;60: 407-12.
- Kaufman JF, Auffray C, Korman AJ et al. The class II molecules of the human and murine major histocompatibility complex. *Cell* 1984;36:1-13.
- Koretz K, Moldenhauer G, Majdic O et al. Correlation of HLA-D/II antigen expression in breast carcinoma with local lymphohistiocytic infiltration reveals considerable dysregulation in a subset of tumors. *Int J Cancer* 1989;44:816-23.
- Lampson LA, Fisher CA, Whelan JP. Striking paucity of HLA-A, B, C and beta-2-microglobulin on human neuroblastoma cell lines. *J Immunol* 1983;130: 2471-8.
- Lazaro B, Anderson A, Kajdacsy-Balla A, Hessner M. Antigenic characterisation of medullary carcinoma of the breast: HLA-DR expression in lymph node positive cases. *Appl Immunohistochem Molecul Morphol* 2001;9:234-41.
- London SJ, Connolly JL, Schnitt SJ, Colditz GA. A prospective study of benign breast disease and the risk of breast cancer. *JAMA* 1992;267:941-4.
- Lucin K, Iternicka Z, Jonjic N. Prognostic significance of T-cell infiltrates, expression of 2-microglobulin and HLA-DR antigens in breast carcinoma. *Pathol Res Pract* 1984;190:1134-40.
- Müller C, Ziegler A, Müller C et al. Divergent expression of HLA-DC/MB, -DR and -SB region products on normal and pathological tissues as detected by monoclonal antibodies. *Immunobiology* 1985;169:228-49.
- Moller P, Mattfeldt T, Gross C et al. Expression of HLA-A, -B, -C, -DR, -DQ, and of HLA-D-associated invariant chain (Ii) in non-neoplastic mammary epithelium, fibroadenoma, adenoma and carcinoma of the breast. *Am J Pathol* 1989;135: 73-83.

32. Natali PG, Giacomini P, Bigotti A et al. Heterogeneity in the expression of HLA and tumor-associated antigens by surgically removed and cultured breast carcinoma cells. *Cancer Res* 1983;43:660-8.
33. Natali P, Bigotti A, Cavalieri R et al. Gene products of the HLA-D region in normal and malignant tissues of nonlymphoid origin. *Hum Immunol* 1986;15:220-33.
34. Norton AJ, Jordan S, Yeomans P. Brief, high-temperature heat denaturation (pressure cooking): a simple and effective method of antigen retrieval for routinely processed tissues. *J Pathol* 1994;173:371-9.
35. Page DL, Dupont WD, Rogers LW, Landenberger M: Intraductal carcinoma of the breast: follow up after biopsy only. *Cancer* 1982;49:751-8.
36. Parazzini F, La Vecchia C, Franceschi S et al. Risk factors for pathologically confirmed benign breast disease. *Am J Epidemiol* 1984;120:115-22.
37. Perez M, Cabrera T, Lopez Nevot MA et al. Heterogeneity of the expression of class I and II HLA antigens in human breast carcinoma. *J Immunogenet* 1986;13:247-53.
38. Redondo M, Concha A, Oldiviola R et al. Expression of HLA class I and II antigens in bronchogenic carcinomas: its relationship to cellular DNA content and clinical-pathological parameters. *Cancer Res* 1991;51:4948-54.
39. Rosai J. Borderline epithelial lesions of the breast. *Am J Surg Pathol* 1991; 15:209-21.
40. Rosenberg SA. Progress in human tumour immunology and immunotherapy. *Nature* 2001;411:380-4.
41. Rubin JT, Elwood LJ, Rusenberg SA et al. Immunohistochemical correlates of response to recombinant interleukin-2-based immunotherapy in humans. *Cancer Res* 1989;49:7086-92.
42. Schnitt SJ, Connolly JL, Tavassoli FA et al. Interobserver reproducibility in the diagnosis of ductal proliferative breast lesions using standardized criteria. *Am J Surg Pathol* 1992;16:1133-43.
43. Schrier PI, Bernards R, Vaessen RT et al. Expression of class I major histocompatibility antigens switched off by highly oncogenic adenovirus 12 in transformed rat cells. *Nature* 1983;305:771-5.
44. Tsuda H, Hirohashi S, Higuchi K et al. Beta-2-microglobulin expression in relation to amplification of oncogenes and prognosis in breast carcinoma. *Histopathology* 1990;16:600-2.
45. van Duinen SG, Ruiter DJ, Broecker EB et al. Level of HLA antigens in locoregional metastases and clinical course of the disease in patients with melanoma. *Cancer Res* 1988;48:1019-25.
46. Vogel J, Tanaka K, Hoekzema GS et al. Experimental strategies for modification of histocompatibility antigen in tumor cell. *Cancer Metastasis Rev* 1987;6: 677-93.
47. Weiss MA, Michael JG, Pesce AJ et al. Heterogeneity of 2-microglobulin in human breast carcinoma. *Lab Invest* 1981;45:46-57.
48. Wintzer HO, Benzing M, von Kleist S. Lacking prognostic significance of 2-microglobulin, MHC class I and class II antigen expression in breast carcinomas. *Br J Cancer* 1990;62:289-95.
49. Zuk JA, Walker RA. Immunohistochemical analysis of HLA antigens and mononuclear infiltrates of benign and malignant breast. *J Pathol* 1987;152:275-85.
50. Zuk JA, Walker RA. HLA class II sublocus expression in benign and malignant breast epithelium. *J Pathol* 1988;155:301-9.

Submitted May 2004.

Accepted July 2004.

*Nikolas Papadopoulos,
Assoc. Prof. in Histology-Embryology,
Democritus University of Thrace,
Dragana, 68 100 Alexandroupolis,
Greece.
e-mail: npapad@med.duth.gr*

CORRELATION OF SERUM MAGNESIUM WITH DYSLIPIDEMIA IN MAINTENANCE HEMODIALYSIS PATIENTS

Hamid Nasri¹, Azar Baradaran²

Shahrekord University of Medical Sciences, Shahrekord, Iran: Hajar Medical, Educational and Therapeutic Center, Section of Hemodialysis¹; Hospital Bou-Ali, Damavand St.Tehran, Iran: Center of Research and Reference Laboratory of Iran²

Summary: One of the factors involved in accelerated atherosclerosis in hemodialysis patients is dyslipidemia. In this study we considered factors involved in intensification of dyslipidemia in hemodialysis patients. This study was done on 36 maintenance hemodialysis patients. Serum lipoprotein (a), Triglyceride, Cholesterol, HDL-C, LDL-C and also serum Intact parathormone (iPTH), Calcium, Phosphorus, Magnesium were measured. In statistical analysis there was not any correlation between serum lipids and iPTH. There was not correlation between serum calcium with serum lipids ($p > 0.05$). There was not correlation between CaxP product with serum lipids ($p > 0.05$). There was a positive correlation between serum Magnesium and Lipoprotein(a) ($P < 0.05$) and also positive correlation between serum magnesium with triglyceride level ($P < 0.05$) was seen too. Magnesium doesn't increase the lipoprotein synthesis. It may involve in the regulation of some enzymes responsible for lipoprotein synthesis. Correlation of serum magnesium with serum triglycerides can be due to changes in hepatic triglyceride metabolism. Lipoprotein(a) is a non traditional factor of premature atherosclerosis, its association with serum magnesium needs more attention in hemodialysis patients.

Key words: Magnesium; Hemodialysis, Dyslipidemia; Parathormone

Introduction

Hemodialysis patients are characterized by a number of biochemical abnormalities including hyperlipidemia. The importance of cardiovascular illness as the cause of death in hemodialysis patients, make it imperative to consider the risk factors involved (2). Hyperlipidemia has been incriminated as a risk factor of atherosclerotic vascular disease in dialyzed patients (6). Hemodialysis is associated with hypertriglyceridemia without cholesterol accumulation. The principle other dyslipidemias consisting of high serum lipoprotein (a) levels and low serum high density lipoprotein, whereas plasma low density lipoprotein (LDL) cholesterol is usually not elevated (2,6,7). The cause of hypertriglyceridemia is an increased production of Apo B protein and a marked decrease in the metabolism of VLDL, Primarily as a result of decreased endothelial cell delipidation of VLDL (6). Magnesium (Mg) retention can be a problem in patients on maintenance hemodialysis. Magnesium deficiency has a possible role in the perturbation of lipid metabolism in the non-uremic population. Furthermore other data showed that there is a correlation between dyslipidemia and high magnesium level in hemodialysis patients (11), but data are scanty and we therefore

sought to consider the association of serum Magnesium and the lipid profiles in patients under maintenance hemodialysis treatment due to end-stage renal failure disease.

Materials and methods

This study is descriptive-analytic that was carried-out on thirty-six patients under regular hemodialysis due to end-stage renal failure. Since 3 years ago all of the patients hemodialyzed with polysulfone membrane hollow fibers. Patients undergoing thrice or twice weekly hemodialysis. The duration of each hemodialysis session is four hour. The magnesium concentration in the dialysate fluid is 1 mmol/L. Factors serves as exclusion criteria were antilipid drug taking and active or chronic infection. For patients' plasma cholesterol (Chol) Triglyceride (Tg), High-density lipoprotein-cholesterol (HDL-C), Lipoprotein (a) [Lp(a)] and Intact parathormon (iPTH), serum Magnesium (Mg), Calcium (Ca), Phosphorus (P) were measured. Low-density lipoprotein-cholesterol (LDL-C) was calculated by Friedewald's formula (3). Lipoprotein (a) measured by enzyme immunoassay (ELISA) with Immuno-biological laboratories (IBL) kit of Germany, other lipids were measured by standard kits, iPTH was measured by RIA with DSL-8000

Tab. 1: The results of laboratory data.

Variable	Maximum	Minimum	Mean \pm SD
LP(a) μ mol/L	3.4	0.32	1.3 \pm 0.70
Tg mmol/L	3.4	0.45	1.53 \pm 0.75
Chol mmol/L	5.8	2.6	3.98 \pm 0.8
HDL-C mmol/L	1.3	0.47	0.74 \pm 0.26
LDL-C mmol/L	4.14	0.26	2.3 \pm 1
iPTH ng/L	2234	25	439.4 \pm 433.3
Mg mmol/L	1.65	0.29	0.6 \pm 0.3
CaXP	95	30	54.2 \pm 16.6

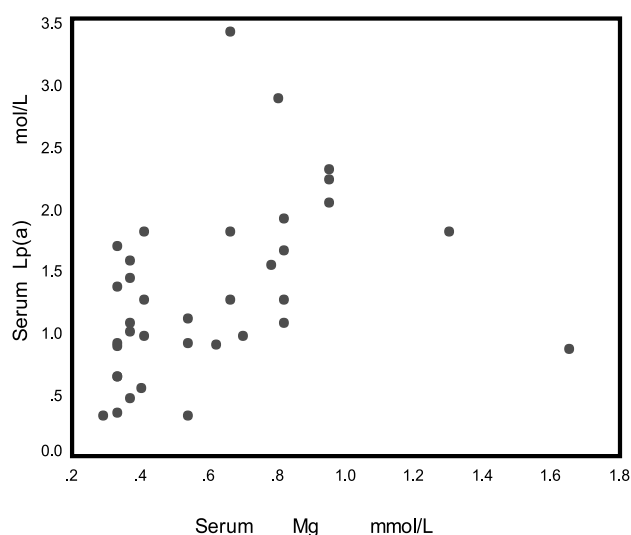


Fig. 1: Correlation of serum Magnesium with serum Lp(a) values ($r=0.541$, $p<0.01$).

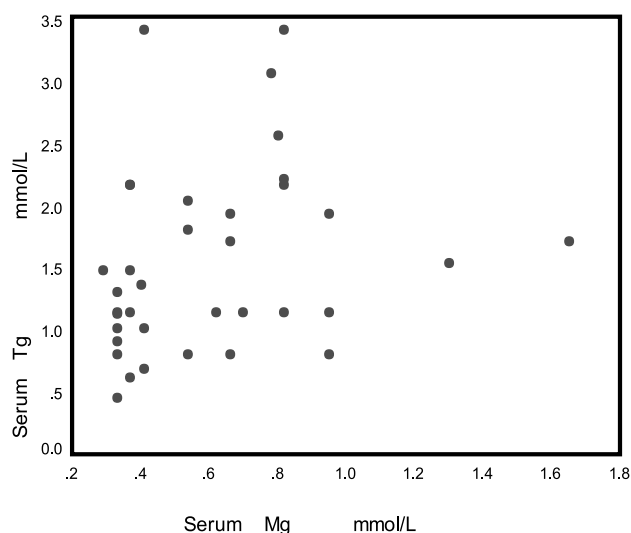


Fig. 2: Correlation of serum Magnesium with serum Triglyceride values ($r=0.368$, $p=0.014$).

kit of USA. Magnesium was measured by calorimetric method. Data are expressed as the Mean \pm SD. For correlations Spearman rho test was used and P value less than 0.05 was considered significant.

Results

The total patients were thirty-six (F=16 M=20). The mean \pm SD of age of patients were 47.5 ± 16.6 years. The length of the time patients have been on hemodialysis were 25 ± 24.4 months. Table one shows patients data. In this study, there was a significant positive correlation between serum Magnesium and Lipoprotein(a) ($r=0.541$, $p<0.01$) (Fig. 1). Significant positive correlation between serum Magnesium with Triglyceride level ($r=0.368$, $p=0.014$) was observed too, (Fig. 2). There were not significant correlation between serum Magnesium with Cholesterol, HDL-C, and LDL-C ($p>0.05$). There were not any positive correlation between serum Calcium, iPTH and Ca x P product with serum lipids ($P>0.05$).

Discussion

In this study there was a positive correlation between serum Mg levels and serum Lp(a) also significant positive correlation of serum Mg levels with Tg was seen too, means high serum Mg in hemodialysis patients might be associated with some types of dyslipidemia seen in hemodialysis patients. Uremic patients undergoing hemodialysis had dyslipidemia consisting of high serum Tg and Lp(a) levels without cholesterol increment, while High-density lipoprotein-cholesterol has generally been found to be decreased (1,2,6). There is well documented that this lipid profile specially high serum Lp(a) and low HDL-C are highly atherogenic and are one of factors that accelerate atherosclerosis seen in these patients (1,2,3,6,7,11) and needs more attention to find the etiology and treatment of this dyslipidemia. It has been suggested that Mg deficiency is related to alteration in lipid metabolism (11). Some animal studies showed that Mg-deficient diet is associated with high serum Tg or Cholesterol levels. Rayssiguier et al. showed that in Mg-deficient non-uremic rats, no changes in serum cholesterol were found (9,10). In this way Inagaki et al. found in uremic rats, Magnesium deficiency increased Tg levels and decreased HDL-chol levels (4). In contrast Itoh et al. utilized magnesium hydroxide (548 mg/dl to males and 411 mg/dl for females) for 4 weeks and noted a significant improvement in blood pressure, additionally, the HDL : LDL ratio and total cholesterol improved with the magnesium treatment (5). Recently Robles et al. in a study on twenty-five hemodialysis patients found a positive significant correlation between serum magnesium levels and total cholesterol, and a nearly significant correlation between serum Tg and serum Triglycerids (11). In contrast to this study we found no positive correlation between serum cholesterol with magnesium levels. We found a positive correlation between

serum magnesium and triglyceride too. Lipoprotein(a) is an independent risk factor for atherosclerotic cardiovascular disease (CVD) in general population and dialysis patients (7). In this study we found a significant correlation between serum Magnesium and LP(a) levels. Serum Lp (a) elevation in hemodialysis patients can be due to uremia that could influence Lp(a) metabolism. The kidneys may play a role in Lp(a) catabolism and the end-stage renal disease might result in elevated Lp(a) levels (1,6,8,12). Based on recent observations, showing significant correlations between serum lipoprotein (a), IL-6 and TNF- α . Levels, it is hypothesized that an activated acute phase reaction may be the underlying cause for high levels of lipoprotein (a) found in patients receiving chronic hemodialysis (5,11). Magnesium does not seem to increase lipoprotein synthesis. It may be involved in the regulation of some enzymes responsible for lipoprotein synthesis (11). While there were a trend toward an increase of triglycerid levels with increasing Magnesium levels it could be due to changes in hepatic triglycerid metabolism induced by Magnesium(11). In the meantime, further clinical study into this important aspect of hemodialysis patients is needed.

References

1. Bairaktari E, Elisaf M, Tsolos O, Siamopoulos KC. Serum LP(a) levels in patients with moderate renal failure. *Nephron* 1998;79:367-80.
2. De Gomez NT, Giammona AM, Touceda LA, Raimondi C. Lipid abnormalities in chronic renal failure Patients undergoing hemodialysis. *Medicina (Buenos Aires)* 2001;61:142-6.
3. Friedewald WT, Levy R, Fredrickson DS. Estimation of the concentration of Low-density lipoprotein cholesterol in plasma without use of the preparative ultracentrifuge. *Clin Chem* 1972;18:799-502.
4. Inagaki O, Shono T, Nakagawa K, Gomikawa S, Mori H, Fujita Y. Effects of magnesium deficiency on lipid metabolism in uremic rats. *Nephron* 1990;55:176-80.
5. Itoh K, Kawasaki T, Nakamura M. The effects of high oral magnesium supplementation on blood pressure, serum lipids and related variables in apparently healthy Japanese subjects. *Br J Nutr* 1997;78:737-50.
6. Keane WF, Oda H. Lipid abnormalities in end stage renal disease *Nephrol Dial Transplant* 1998;13(suppl 1):45-9.
7. Quashing T, Krane V, Metzger T, Warner C. Abnormalities in Uremia lipoprotein metabolism and its impact on Cardiovascular disease. *Am J Kid Dis* 2001; 138(suppl 1):S14-S9.
8. Rabin T, Donaski N, Finder L et al. Renal handling of human apolipoprotein (a) and its fragments in the rat. *Am J Kid Dis* 2001;138(3):619-30.
9. Rayssiguier Y, Gueux E, Bussiere L, Durlach J, Mazur A. Dietary Magnesium affects susceptibility of lipoproteins and tissues to per oxidation in rats. *J Am College Nut* 1993;12(2):133-4.
10. Rayssiguier Y, Gueux E, Weiser D. Effects of magnesium deficiency on lipid metabolism in rats fed a high carbohydrate diet. *J Nutr* 1981;111:1877-83.
11. Robles NR, Escola JM, Albarran L, Espada R, Cruz A. Correlation of serum magnesium and serum lipid levels in hemodialysis patients. *Dial Transplant* 1998;27(10):644-8.
12. Zimmermann J, Herrlinger S, Pruy A, Wanner C. Mechanism of high serum lipoprotein (a) in hemo dialysis patients. *JCI* 1993;91:397.

Submitted March 2004.

Accepted November 2004.

*Hamid Nasri, M.D.,
Shahrekord university of Medical sciences,
Hajar Medical, Educational and Therapeutic Center,
Section of Hemodialysis,
Shahrekord, Iran.
e-mail: hamidnasri@skums.ac.ir*

OUR EXPERIENCE WITH DIAGNOSTICS OF CONGENITAL DISORDERS OF GLYCOSYLATION

Albahri Ziad¹, Marklová Eliška¹, Vaníček Hubert¹, Minxová Lenka¹, Dědek Petr¹, Skálová Sylva¹, Talábová Marika², Vávrová Jaroslava³ and Rencová Eva⁴

Charles University in Prague, Faculty of Medicine in Hradec Králové, Czech Republic: Department of Paediatrics¹, Department of Neurology², Department of Clinical Chemistry³, Department of Ophthalmology⁴

Summary: The aim of this study is to report our 3years experience with the screening of congenital disorders of glycosylation. A common isoelectric focusing method with immunofixation was used for analysis of serum transferrin and α_1 -antitrypsin, apart from several other procedures. A group of about 1000 individuals, both healthy controls and patients, mostly with signs of a metabolic disease were examined. Here we present an overview of 1) hypoglycosylation findings, 2) distribution of protein variants, 3) misguiding rare Tf variants found in our set, and 4) association of some phenotypes with various diseases.

Key words: *Glycoproteins; Hypoglycosylation; Inborn errors; Screening; Methods*

Introduction

Glycosylation of proteins and lipids mainly takes place in endoplasmic reticulum and the Golgi apparatus of various cells, primarily of the liver. Congenital disorders of glycosylation (CDG) make a new group of inherited metabolic diseases (IMD) with autosomal recessive pattern of inheritance. Pathogenesis of CDG is a consequence of impaired building or processing of glycoproteins caused by various enzymes or transport defects, thus resulting in hypoglycosylation. Two main types (CDG I and CDG II) and an ever-increasing number of subtypes can be differentiated (CDG type Ia-l and CDG type IIa-d, so far).

CDG affect all organs and particularly the CNS, with the exception of CDG types Ib and Ih, where hepatic-intestinal signs prevail. The most frequent type Ia presents differently in various life periods. Clinical signs are dominated by psychomotor retardation and blood coagulation defects, presenting as thrombosis, bleeding, or stroke-like episodes, but many other symptoms occur, e.g. cerebellar hypoplasia, ophthalmologic abnormalities, dysmorphic features, and neuropathy. The CDG type II is rare, but usually has a more severe clinical course compared to CDG type I (9,11,20).

Various screening methods are available, the most common one being isoelectric focusing (IEF) of serum transferrin (Tf), apart from other procedures (combined commercial chromatographic assays, capillary- or agarose gel electrophoresis, or HPLC), and other glycoproteins, e.g.

thyroxin-binding globulin (TBG) and antithrombin III (AT III), suitable for the first step of diagnostics. However, this approach cannot identify all defects, so that other investigations, such as thorough analysis of glycans, and especially enzyme assays and mutations identification must follow.

The aim of our effort was to introduce a screening procedure for this recently recognized group of inherited metabolic disorders, in our country not diagnosed before. Here we present results of our 3-years experience, involving only one, rather small region of Czech Republic.

Materials and methods

About 1000 serum samples of both healthy controls (n=100; blood donors, surgery-patients, friends, and relatives) and patients with various clinical, mostly IMD-suspicious symptoms of various ages (1 months - 62 years) were screened. Serum of premature newborns, alcohol abusers and patients with hepatopathy served as pathological reference samples (due to secondary defects of glycosylation as consequence). Also CDG-positive samples obtained from other laboratories have been checked out. Only surplus material was used for analyses.

Besides serum and plasma, also dry spots with blood or other type of material are suitable for analysis: 4 mm circle was punched out and eluted with 60 μ l distilled water for 24 h at +4 °C, and about 40 μ l of the eluate was removed, after centrifugation ready for IEF (29). Cerebrospinal fluid (CSF) was either concentrated (15-times in vacuum) and

further processed in the same way as the serum, or a native sample was used, and finally stained with more sensitive silver nitrate (see later) because of comparatively lower levels of Tf in this material. Urine is suitable for analysis of oligosaccharides, useful in CDG type IIb diagnosis.

All chemicals were of analytical grade, supplied by Pharmacia, Merck, Sigma, or Bio-Rad. Use of double-distilled water for all analytical steps is essential.

Tf isoforms by IEF. IEF of Tf is a simple and rapid technique, which allows quantitative determination of all the Tf isoforms. Tf is a glycosylated iron-transporting protein, synthesized mainly by the liver. Serum Tf generally occurs in sialylated form: five sialic acid residues contribute to the acidic pI of Tf, and their loss causes a basic shift within the pI of 5.2–5.9. Current methods use IEF combined either by Western blotting, or immunofixation with Coomassie Brilliant Blue/silver nitrate staining. The latter variant, which was employed in our study is basically that used in Nijmegen laboratories (see Acknowledgment) (23) with minor modifications. For comparison of results, other procedures have also been tested.

Iron saturation of Tf. Serum Tf has two iron-binding sites, but normally only about one-third of Tf is fully saturated. Differences in the ferrous ion content lead to different IEF patterns, and thus in vitro iron saturation is generally necessary. It is achieved by mixing 50 μ l serum (dry-spot eluate or other material) with 15 μ l freshly prepared mixture of ferric citrate (10 mmol/l) and NaHCO_3 (0.5 mol/l), 2:1. After 1 h incubation at room temperature, the samples (except the concentrated CSF) were diluted 6-times with water, thus ready for application (6,16).

Gel hydration. Dry IEF gels with immobilized pH gradient, ranging from pH 4.0–7.0 (Immobiline DryPlate, 240 x 110 x 0.5 mm, Pharmacia) were rehydrated (in vertical position of cassette with U-frame, previously touched with Repel-Silane, Pharmacia) in glycerol (2.2 mol/l, about 25 ml) for 2 h at room temperature. The gel can be then stored up to one week at +4 °C (12).

IEF separation. LKB Multiphor 2217 and Power Supply 2103 was used. After the rehydrated gel was installed (by use of paraffin oil drops, without air-bubbles) on the cooling plate, both cathodal and anodal electrode strips, soaked with ampholine solutions pH 6.0–8.0 and 3.5–5.0, resp. (codes 80–1125–93 and 80–1125–89, Amersham), were placed on the appropriate gel margins. The gel was then pre-focused for 10 min at 1000 V, 4 mA, 4 watt, and then for 20 min at 2000 V, 4 mA, 8 watt. After 1.5 μ l of saturated serum/plasma sample (or 3 μ l CSF, and 5 μ l of a dry-spot eluate) were applied to the gel, IEF continues for 30 min at 1000 V, 4 mA, 4 watt, and finally for 4 h at 2000, 4 mA, 8 watt, constantly at +10 °C.

Immunofixation. Immediately after IEF, the gels were covered with 900 μ l of polyclonal IgG antibodies to Tf (Dako, code A 0061), and incubated in a moist chamber for 45 min. Unprecipitated (non-Tf) proteins were overnight washed out from the gel by saline. Next day the gel was kept

in distilled water for 1 h by reason of salts elimination, and Tf isoforms were then fixed to the gel by trichloroacetic acid (20 g/100 ml, 10 min washing).

Staining. Gel was stained for 10 min by continuous shaking in freshly prepared mixture of Coomassie Blue stock solution (Pharmacia, prepared according to producer instructions), and acetic acid (3,6 mol/l), 1:1. Alternatively, a silver nitrate was used for low Tf levels in CSF (26). Destaining was done with a mixture of methanol-acetic acid-water, 3:1:6, until colorless background. The gel was then dried by air, and evaluated by densitometry (DS2D, μ LaAp, SR, with MS ScanSlide and ICR software).

Interpretation. IEF in a pH gradient of 4.0–7.0 reveals eight Tf isoforms: the tetra- and pentasialo-Tf prevail in healthy controls, while the CDG patient's serum shows a marked elevation of hyposialylated forms (such as disialo-, monosialo-, and asialo-Tf, called carbohydrate deficient Tf, CDT). IEF CDG type I pattern shows decreased tetrasialo-Tf and a marked elevation of disialo-Tf, while the asialo-, monosialo-, and disialo-Tf typically increase in CDG type IIa and IIc, although the both patterns may diverge (9, 15,20).

Detection of polymorphism in Tf glycoprotein. An extended polymorphism of TF is well known, some of the variants being difficult to distinguish from a CDG pattern, so that a special attention must be paid to their recognition and differentiation. Most common C (with C1–C16 subtypes), and several subtypes of the rare B and D (both shifting, compared to C) variants are distinguished (1,9).

Neuraminidase (sialidase; EC.3.2.1.18) is an enzyme that selectively splits the terminal sialic acid residues on the glycan chain, thus converting all Tf isoforms to the asialo-form. Serum of controls at IEF shows one band only, in contrast to protein variants, which retain their shifted or double-banded positions. The freeze-dried powder of enzyme (Sigma, code N-2876) was dissolved (1 mg/ml) in Tris - HCl buffer pH 7 (0.1 mol/l), and incubated with iron-saturated serum in a ratio 2:1 at room temperature overnight (16,33). A control sample with saline was prepared for comparison. After a 40-time dilution with saline, the 4- μ l volume was ready for IEF application.

For better interpretation of Tf D (possibly also Tf B) variant, gel of higher pH range (3.5–9.0) is used (18), while gel pH 5–6 is more suitable for precise discrimination of Tf C subtypes (8).

It is widely recommended to confirm generalized defect of glycosylation by analysis of more than just one glycoprotein.

IEF of thyroxin-binding globulin (TBG). The TBG type C (common) physiologically exhibits mainly the octasialo-isoform. The CDG patients show an increase of hyposialylated tetra- and pentasialo-TBG. Our experience with the method (19,28) is limited, as the TBG antibody for immunodetection is commercially no more (hoping temporarily) available.

IEF of α_1 -antitrypsin (aAT). The optimum for the most common variant aAT M (86–99 %) lies between pH 4–5,

nevertheless for practical reasons we tested at first the conditions similar to those used for Tf (gels of pH range 4–7). Sample pretreatment with cystein (to prevent anomalous patterns resulting from aged sera) (12), use of specific antibody (anti-aAT, Dako, code Q 0363), and skipping the iron-saturation step, are the minor variation of the method used for Tf analysis. The hexasialo-isoform is prominent in the healthy, whereas higher tetrasialo-aAT is pathognomic for CDG. The rare S, Z, and F genetic variants should be properly identified for reliable interpretation of results (28).

Other screening methods have been checked for comparison of result reliability and economic criteria.

Tf isoforms by electrophoresis on agarose with Western blotting. Proteins are separated by electrophoresis on agarose and then passively transferred onto a nitrocellulose membrane. The immobilized isoforms of Tf are detected immunochemically using a double antibody system, consisting of rabbit anti-human Tf, followed by HRP-conjugated donkey anti-rabbit serum (15).

Gels were prepared from medium-osmotic agarose and electrophoresis veronal buffer pH 8.6, I=0.085 (1 g agarose 100 ml, dissolved by heating for 15 min), placed on a plastic supporter (Pharmacia), and dried with filter paper. Then 2- μ l volume of serum samples, diluted 50-times with saline were applied, and electrophoresis was carried-out (LKB Multiphor) at 100 mA and 400 V for 4 hours. The gel was dried with filter paper, and the separated proteins were blotted on nitrocellulose sheet (Pharmacia), using a 1 kg weight-press for 2 h. Two antibodies, namely rabbit anti-human Tf serum (Dako), and donkey anti-rabbit HRP (Amersham), as well as 4-chloro-1-naphthol as a color developer, were used. For other details of Western blotting see (2,27).

Sometimes it is helpful to purify Tf from serum prior to carrying out further studies (e.g. HPLC), although this is not essential for routine IEF testing; methodical details on Tf pretreatment by affinity chromatography and HPLC will be described elsewhere.

Enzyme assays. Diagnosis of the most frequent type CDG Ia is completed by measurement of cellular phosphomannomutase (PMM; EC 5.4.2.8) activity; the enzyme

converts mannose-6-phosphate to mannose-1-phosphate. Similar enzyme assay for checking phosphomannoisomerase (PMI; EC.5.3.1.8) activity is required for CDG type Ib diagnosis.

Blood samples were obtained from 12 healthy individuals, age range 3 m – 60 y. A two-step procedure has been adopted for isolation of peripheral blood leukocytes: it starts with the heating of whole EDTA-blood (6–10 ml, 37°C, 40 min) and centrifuging the separated supernatant. The pellet was then washed by NaCl solutions in a stepwise manner, using concentrations 0.2, 3.6, and 0.9/100 ml with centrifugation in between (5). The cells disintegration was achieved mechanically by numerous passing (30-times) of leukocyte pellets, previously dissolved in 50 μ l HEPES buffer pH 7.1, 0.05 mol/l, through a syringe needle (Luer, 0.5 x 25) (3), one freeze/thaw cycle, and finally, centrifugation at 500 g for 10 min. The resulting extract was ready for the enzymatic assay and protein determination.

The traditional assay for both enzymes is based on the reduction of NADP(+) to NADPH. A method of van Schaftingen (30) with slight modification (7) was used for both enzyme assays. EDTA-plasma is preferred, giving statistically higher results, when compared to the samples with heparin (3). A volume of the cell supernatant, containing 0.8 mg of protein (100–150 μ l) was used; the incubates (1 ml) comprise glucose-1,6-biphosphate (22) instead of the originally recommended mannose-1,6-biphosphate. To detect enzyme activity, spectrophotometer Unicam UV 2, and for protein quantification, Cobas Mira were used.

Results

The reference values of Tf isoforms distribution in our set of controls have been established (Table 1).

Abnormalities of glycosylation, detected in about 6.7 % of our patients group have been associated with e.g. Hashimoto thyroiditis, Budd-Chiari syndrome, systemic lupus erythematosus, and epilepsy (in two infants, treated with Phenaemalthen), apart from liver disease, rheumatoid arthritis, and some patients with cystic fibrosis. No correlation with total serum levels of Tf and aAT was found.

Tab. 1: Tf isoforms by IEF in controls and various patients showing increased CDT (the values exceeding a reference range are *in italics*). Distribution in %; Tf isoforms 0–7: asialo- – heptasialo-Tf; V: our CDG patient, N: C1/D4–5 Tf variant, S: hepatitis C, K: lupus erythematosus, H: antiepileptics in therapy, B: newborn.

Tf isoforms	Controls		Patients						
	Mean	SD	CDG Ia	V	N	S	K	H	B
0	0.4	0.4	<i>12.4</i>	<i>1.9</i>	<i>11.7</i>	<i>3.3</i>	0.0	<i>2.7</i>	<i>1.8</i>
1	1.3	0.9	2.4	0.0	<i>4.5</i>	<i>3.7</i>	<i>4.4</i>	0.0	<i>5.4</i>
2	6.5	2.2	<i>28.5</i>	<i>19.2</i>	4.9	<i>12.0</i>	7.6	3.6	<i>9.2</i>
3	13.2	7.3	8.8	8.7	2.0	19.8	10.3	12.2	9.4
4	51.2	11.0	<i>39.8</i>	51.0	60.4	<i>40.0</i>	50.8	<i>44.7</i>	<i>59.1</i>
5	18.8	8.1	8.1	11.5	6.3	12.5	15.1	24.8	9.5
6	6.3	3.4	0	7.8	7.2	7.7	7.0	9.2	5.6
7	2.3	2.5	0	0	3.0	1.0	4.6	2.8	0

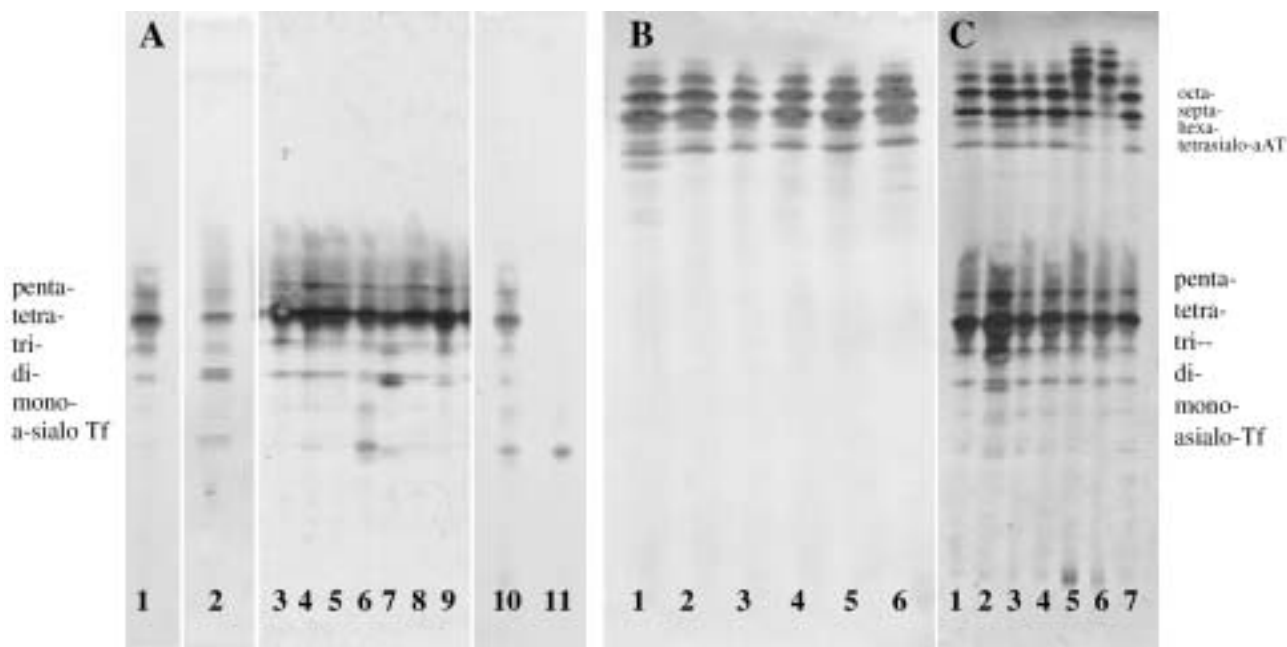


Fig. 1: IEF of Tf and aAT on Immobiline DryPlate gel at pH range 4-7.

A) Tf: Lane 1, 3, 4, 5, 8, 9: healthy controls, Lane 2: a CDG type Ia patient (Tf C1/C2), Lane 6: Tf C1/D4-5 variant, Lane 10: the same variant in the father, Lane 11: as in the Lane 10 after neuraminidase treatment, Lane 7: our CDG patient (Tf C1/C2); note increase disialo-Tf when compared to controls.

B) aAT: Lane 1: our CDG patient, Lane 2, 3: father and mother of the CDG patient, Lane 4, 5, 6: healthy controls; note the extra band of our CDG patient when compared to the controls.

C) Tf and aAT on the same gel, Lane 1, 3, 4, 7: healthy controls, Lane 2: secondary increase CDT (Tf C1/C2), while aAT is normal, Lane 5, 6: normal Tf, but aAT polymorphism.

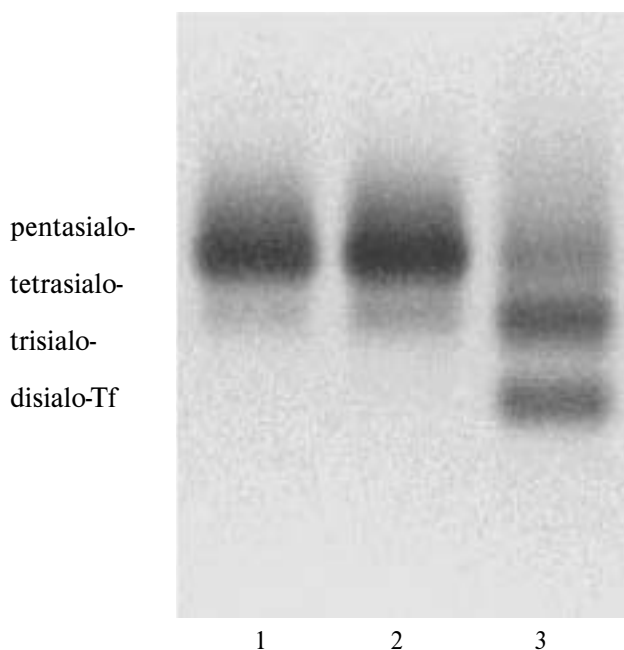


Fig. 2: Agarose electrophoresis pattern of Tf isoforms; Lanes 1, 2: controls, Lane 3: patient with CDG type Ia.

The clinical feature of a 5-year-old mentally retarded boy with various nonspecific symptoms raised suspicion of CDG. IEF showed an increase of disialo-Tf (Table 1) compared with normal mean values. Also aAT analysis revealed abnormal IEF-profile in this child (Fig. 1), as well as a result of electrophoretic separation of Tf isoforms on agarose gel (Fig. 2). The patient is a carrier of the C1/C2 (double bands) genetic variant. Further analysis of serum TF disclosed that this TF variant was inherited from patient's mother, otherwise healthy. PMM assay showed only slight decrease of enzyme activity in leukocytes; mutation analysis is pending.

In our set of subjects besides the most common C1-Tf variant (84 % in controls and 79 % in the patient group), we have found also the heterozygous C1/C2 form with a significantly higher frequency in the Crohn's disease (30 %) and the cystic fibrosis (27 %) patient subgroups, compared to controls (16 %) and the total patients group (20 %). Other rare phenotypes C2, C1/C3, C1/B and C1/D (in 0.48, 0.32, 0.24 and 0.24 %, resp.), were also recognized (Albahri, in press).

To demonstrate a risk of the possible misinterpretation we report on a methotrexate treated adolescent boy, followed for potential long-therapy-effects on the Tf-glycoforms

ratio. His IEF pattern showed isolated increase of asialo-Tf (Fig. 1). Further investigation based on the neuraminidase test, analysis of serum aAT, and a search for a polymorphism type in the family confirmed the suspected rare C1/D4-5 genetic variant, thus falsely simulating a CDG.

No gender differences from the viewpoint of both aspects, hypoglycosylation and distribution of genetic variants, have been found in our set of patients and controls.

Possibility of simultaneous analysis of Tf and aAT in the same gel was tested with good results; as the position of individual isoforms doesn't overlap, both specific antibody solutions can be applied on the appropriate parts of gel surface for selective detection. Having been inspired by Artuch et al (2), we used also an antibody cocktail for detection of both glycoproteins in one run (Fig. 1).

Discussion

Screening of serum Tf by IEF proved to be reliable at the first stage of CDG diagnostics. IEF conditions similar to those described for Tf are also suitable for aAT analysis, so that glycosylation level of both glycoproteins, greatly significant for CDG diagnostics, may be followed by one IEF run.

The IEF screening of CDG is unreliable in neonates in the first 3 weeks of life, when a significant proportion of circulating Tf is still derived from the mother source.

Some other conditions should be first excluded from the possible differentials before a diagnosis of CDG is made, such as pregnancy, galactosemia, fructosuria, alcohol abuse, severe liver diseases, chronic obstructive lung disease, iron-deficient anemia, and possibly the use of antiepileptic medication.

Also changes in the amino acid sequence of the polypeptide chain of Tf (namely the D genetic variants) should be always considered; test with neuraminidase gives an unambiguous result. The knowledge of Tf microheterogeneity is fundamental for correct analysis and interpretation of IEF results; at least 36 Tf protein variants are known, showing a distinct variability.

The distribution and frequency of genetic variants in our set roughly correspond to those reported for the European population (homozygous variant C in 98 %, B and D are rare; subtypes: C1 in 70-80 %, C2-C16 in 2 %; heterozygous variants: C1/C2 in 10 %, C1/C3 and B/C in 0.7 %, and C/D in 0.2 %) (13).

An association of certain genetic diseases with some pathological conditions was reported, e.g. higher frequency of Tf C2 variant with spontaneous abortion, prematurity, rheumatoid arthritis (25), Alzheimer's disease (21), and lower Fe-binding capacity (31). Tf C3 is suggested to show certain protection against some smoking-derived types of lung-carcinoma (4). On the other hand, comparably lower occurrence of Tf C1/C2 is reported in patients with cystic fibrosis (24). Our finding of increased frequency of the heterozygous C1/C2 variant in children rather contradicts

(cystic fibrosis) and further extends (Crohn's disease) these observations.

The algorithm of CDG investigation begins with physician's suspicion, based on clinical symptoms and/or biochemical findings (low level of various serum glycoproteins). CDG screening usually starts with IEF of serum Tf isoforms, but other methods (17), and also other glycoproteins, such as aAT, TBG, AT III, α_1 -antichymotrypsin, ferritin, α_2 -antiplasmin, haptoglobin, orosomucoid, vitamin D-binding protein, retinal-binding protein, α_2 -HS-glycoprotein (fetuin), plasminogen, or Zn- α_2 -glycoprotein (28,34) and hexosaminidase (10) are convenient for CDG screening. However, possible protein polymorphism must always be considered.

When excluding all possible secondary causes (young age, severe liver afflictions, galactosemia and fructosuria, or rare Tf variants), positive IEF results usually reliably lead to diagnosis of CDG type I, which is further proved by enzyme assays and mutation analysis.

However, negative IEF result doesn't exclude rarer CDG types IIb and IIc, so that the structure of either lipid-linked or protein-linked glycan, possibly membrane antigens (such as Bombay, or Lewis-X) in leukocytes, or lectin binding ability, should be followed. Glycophorin A and the band III in erythrocyte membrane may be pathognomic for HEMPAS and CDG type Ig, resp., and some other subtypes, not clearly classified so far (CDG-x) (20).

Moreover, electrophoretic analysis of serum apolipoproteins C-III and apo-E (32), as well as α -dystroglycan in skeletal muscle (14) may be helpful for detection of O-glycosylation defects, which possibly constitute a new CDG subgroup.

Since CDG is an autosomal recessive congenital disorder, it has important consequences for the family, and thus a genetic counseling should be offered.

The disease probably remains largely underdiagnosed. Following the frequent reports on diversity of clinical signs in CDG patients, the screening criteria should be very wide. Thus the CDG diagnosis is to be considered in all cases with psychomotor retardation, ophthalmologic abnormalities, seizures, multiorgan failure, and liver and clotting abnormalities, at least.

Acknowledgment

Thanks are due to K. Huyben, Univ. Klinisch-Genetisch Centrum, Nijmegen, Netherlands, to G. Keir, Department of Neuroimmunology, National Hospital for Neurology and Neurosurgery, London, UK and to J Pribišová, Fac Hosp, Hradec Králové, CR for advice and laboratory manuals.

The study was supported by Grant No 85/2001/C/LFHK and partly by Grant No 1770/G3/FRVS from Charles University, Czech Republic.

References

1. Arndt T. Carbohydrate-deficient transferrin as a marker of chronic alcohol abuse: a critical review of preanalysis, analysis, and interpretation. *Clin Chem* 2001; 47(1):13-27.

2. Artuch R, Ferrer I, Pineda J et al. Western blotting with diaminobenzidine detection for the diagnosis of congenital disorders of glycosylation. *J Neurosci Methods* 2003;125:167-71.
3. Barnier A, Dupré T, Cuer M, Vuillaume-Barrot S, Durand G, Seta N. Leukocyte phosphomannomutase activity in diagnosis of congenital disorder of glycosylation Ia. *Clin Chem* 2002;48:934-6.
4. Beckman LE, Van Landeghem GF, Sikstrom C, Lundgren R, Beckman L. Protective effect of transferrin C3 in lung cancer? *Oncology* 1999;56(4):328-31.
5. Beutler E, Kuhl W. The diagnosis of the adult type of Gaucher's disease and its carrier state by demonstration of deficiency of beta-glucosidase activity in peripheral blood leukocytes. *J Lab Clin Med* 1970;76:747-55.
6. de Jong G, van Noort WL, Feelders RA, de Jeu-Jaspars CM, van Eijk HG. Adaptation of transferrin protein and glycan synthesis. *Clin Chim Acta* 1992; 212(1-2):27-45.
7. de Koning TJ, Dorland L, van Diggelen OP et al. A novel disorder of N-glycosylation due to phosphomannose isomerase deficiency. *Biochem Biophys Res Commun* 1998;245(1):38-42.
8. Gorg A, Weser J, Westermeyer R et al. Isoelectric focusing with immobilized pH gradients for the analysis of transferrin (Tf) subtypes and variants. *Hum Genet* 1983; 64(3):222-6.
9. Grünewald S, Matthijs G, Jaeken J. Congenital disorders of glycosylation: a review. *Pediatr Res* 2002;52:618-24.
10. Jaeken J, Kint J, Spaepen L. Serum lysosomal enzyme abnormalities in galactosaemia. *Lancet* 1992;340(8833):1472-3.
11. Jaeken J. Komrower Lecture. Congenital disorders of glycosylation (CDG): it's all in it! *J Inher Metab Dis* 2003;26:99-118.
12. Jeppsson JO, Franzen B. Typing of genetic variants of alpha 1-antitrypsin by electrofocusing. *Clin Chem* 1982;28(1):219-25.
13. Kamboh MI, Ferrell RE. Human transferrin polymorphism (review). *Hum Hered* 1987;37:65-81.
14. Kano H, Kobayashi K, Herrmann R et al. Deficiency of alpha-dystroglycan in muscle-eye-brain disease. *Biochem Biophys Res Commun* 2002;291:1283-86.
15. Keir G, Winchester BG, Clayton P. Carbohydrate-deficient glycoprotein syndromes: inborn errors of protein glycosylation. *Ann Clin Biochem* 1999;36:20-36.
16. Kim S, Westphal V, Srikrishna G et al. Dolichol phosphate mannose synthase (DPM1) mutations define congenital disorder of glycosylation Ia (CDG-Ia). *J Clin Invest* 2000;105(2):191-8.
17. Kleinert P, Kuster T, Durka S et al. Mass spectrometric analysis of human transferrin in different body fluids. *Clin Chem Lab Med* 2003;41(12):1580-8.
18. Kühnl P, Spielmann W. A third common allele in the transferrin system, TfC3, detected by isoelectric focusing. *Hum Genet* 1979;50(2):193-8.
19. Macchia PE, Harrison HH, Scherberg NH, Sunthornthepvarakul T, Jaeken J, Refetoff S. Thyroid function tests and characterization of thyroxine-binding globulin in the carbohydrate-deficient glycoprotein syndrome type I. *J Clin Endocrinol Metab* 1995;80:3744-9.
20. Marquardt T, Denecke J. Congenital disorders of glycosylation: review of their molecular bases, clinical presentations and specific therapies. *Eur J Pediatr* 2003; 162:359-79.
21. Namekata K, Imagawa M, Terashi A, Ohta S, Oyama F, Ihara Y. Association of transferrin C2 allele with late-onset Alzheimer's disease. *Hum Genet* 1997; 101(2):126-9.
22. Niehues R, Hasilik M, Alton G et al. Carbohydrate-deficient glycoprotein syndrome type Ib. Phosphomannose isomerase deficiency and mannose therapy. *J Clin Invest* 1998;101:1414-20.
23. Noort WL van, Jong G de, Eijk HG van. Ideale scheidings kwantificering van sialo transferrine fracties in humaan serum. *Tijdschr NVKC* 1993;18:43-45.
24. Pascali VL, Bravo E, Auconi P et al. Transferrin subtypes in cystic fibrosis. *Eur J Pediatr* 1984;143(2):133-4.
25. Petré S, Vesterberg O. Separation of different forms of transferrin by isoelectric focusing to detect effects on the liver caused by xenobiotics. *Electrophoresis* 1989;10(8-9):600-4.
26. Roelandse FWC, van der Zwart N, Didden JH, van Loon J, Souverein JHM. Detection of CSF leakage by isoelectric focusing on polyacrylamide gel, direct immunofixation of transferrins, and silver staining. *Clin Chem* 1998;44:351-3.
27. Seta N, Barnier A, Hochedes F, Besnard MA, Durand G. Diagnostic value of Western blotting in carbohydrate deficient glycoprotein syndrome. *Clin Chim Acta* 1996;254:131-40.
28. Stibler H, Holzpach U, Kristiansson B. Isoforms and levels of transferrin, anti-thrombin, alpha₂-antitrypsin and thyroxine-binding globulin in 48 patients with carbohydrate-deficient glycoprotein syndrome type I. *Scand J Clin Lab Invest* 1998; 58:55-62.
29. Stibler H, Jaeken J, Kristiansson B. Biochemical characteristics and diagnosis of the carbohydrate-deficient glycoprotein syndrome. *Acta Paediatr Scand* 1991;375 (Suppl 375):21-31.
30. Van Schaftingen E, Jaeken J. Phosphomannomutase deficiency is a cause of carbohydrate-deficient glycoprotein syndrome type I. *FEBS Lett* 1995;377:318-20.
31. Wong CT, Saha N. Effects of transferrin genetic phenotypes on total iron-binding capacity. *Acta Haematol* 1986;75(4):215-8.
32. Wopereis S, Grünewald S, Morava E et al. Apolipoprotein C-III Isofocusing in the diagnosis of genetic defects in O-glycan biosynthesis. *Clin Chem* 2003; 49:1839-45.
33. Wuyts B, Delanghe J R, Kasvosve I. Determination of carbohydrate-deficient transferrin using capillary zone electrophoresis. *Clin Chim* 2001;47:247-255.
34. Yuasa I, Ohno K, Hashimoto K, Iijima K, Yamashita K, Takeshita K. Carbohydrate deficient glycoprotein syndrome: electrophoretic study of multiple serum glycoproteins. *Brain Dev* 1995;17:13-9.

Submitted March 2004.

Accepted July 2004.

**MUDr. Eliška Marklová, Ph.D.,
Charles University in Prague,
Department of Pediatrics,
Laboratory of Inherited Metabolic Diseases,
500 05 Hradec Králové,
Czech Republic.
e-mail: marklova@lfhk.cuni.cz**

THE IMPAIRMENT OF GASTRODUODENAL MUCOSAL BARRIER BY COFFEE

Eubica Cibičková, Norbert Cibiček, Petr Ždánský¹, Pavel Kohout²

students of Charles University in Prague, Faculty of Medicine in Hradec Králové, Czech Republic; University Hospital in Hradec Králové: Department of Gerontology and Metabolism¹; Thomayer's University Hospital: Department of Internal Medicine²

Summary: Background: Even though coffee is not considered to be responsible for development of peptic ulcer, it may, however, prolong its healing by increasing acidity of gastric content. In our former work we observed a profound increase in sucrose permeability (above normal values) in healthy volunteers regularly drinking coffee for years. In literature, many factors affecting sucrose permeability have been described so far. None of them, however, studied the effect of coffee. Subjects, materials and methods: 10 young asymptomatic habitual coffee drinkers were included in the study. The probands underwent SaLM test twice – first time without coffee restriction and second time after 48-hour coffee abstinence. The ingested SaLM solution comprised sucrose (25.0 g), lactulose (10.0 g), mannitol (2.0 g), xylose (2.0 g) and water (up to 100 ml). Urine was collected for five hours and the samples were analysed using gas chromatography. Results were compared with those of 8 young healthy volunteers not drinking coffee. Permeability for sucrose was significantly higher in the group of habitual coffee drinkers in comparison with non-coffee drinkers ($p < 0.01$). After 48-hour coffee abstinence sucrose excretion decreased significantly ($p < 0.05$) to a level not differing from that of non-coffee drinkers ($p = 0.54$). Conclusions: Our results indicate that coffee may damage gastroduodenal mucosa in habitual coffee drinkers. In a time period of 48 hours the gastroduodenal mucosa is capable of a significant regeneration.

Key words: *Gastrointestinal permeability, Sucrose, Coffee*

Introduction

Even though coffee is not considered to be responsible for development of peptic ulcer, it may prolong its healing by increasing acidity of gastric contents (4). Coffee stimulates gastrin release and gastric acid secretion. However, no association between coffee and dyspepsia has been found. On the other hand, the most frequently reported symptom after coffee drinking is heartburn, which is in accordance with the finding that coffee promotes gastro-oesophageal reflux (1).

Sucrose permeability is established non-invasive means for evaluation of upper gastrointestinal tract impairment (13). In our former work (3) we observed a profound increase in sucrose permeability (above normal values) in healthy volunteers regularly drinking coffee for longer time.

Factors described in literature which have an effect on sucrose permeability include life-style factors (e.g. cigarette smoking (6)), drugs (e.g. NSAIDs (12) and corticosteroids (9)) and bacteria (e.g. *Lactobacillus* (7), *Helicobacter* (2)). Effects of coffee on functional integrity of upper gastrointestinal tract barrier have not been studied yet.

Subjects, materials and methods

10 young asymptomatic habitual coffee drinkers (2 males and 8 females, age 22.7 ± 1.1 , range 21–24), students of medicine, were included in the study. Each individual drank minimum 1 cup of coffee (0.25 litre) daily for at least 1 year (2.2 cups, range 1–4, for 4.3 years, range 1–8). All provided written, informed consent. Since this study was methodically similar to our previous studies, which gained approval of the Ethics Committee, in this case it was not asked to approve the protocol. Subjects who smoked cigarettes, had antecedents of gastroduodenal diseases and history of NSAIDs (within last 10 years) were not included.

The habitual coffee drinkers underwent SaLM test twice – first time without coffee restriction and second time after 48-hour coffee abstinence. After night fasting the probands provided a urine sample from the second morning urine, since the first morning urine might contain adulterants capable of interfering with disaccharides during laboratory investigations. This urine was considered a control sample. After that the probands ingested SaLM solution of composition as follows: sucrose (25.0 g), lactulose (10.0 g), man-

nitrol (2.0 g), xylose (2.0 g) and water (up to 100 ml). After the ingestion, they fasted for 2 hours without intake of fluids. During the next three hours the probands excluded meals and drinks containing sugar. In this 5-hour period, urine was collected into a container (two drops of 1% thiomersal were added as a conservant). Samples of this urine were compared with control samples and were analysed using gas chromatography. The samples were either processed immediately after delivery, or were kept frozen at -20°C . After centrifugation, 50 μl with addition of internal standard (sorbos) and reference material (inositol) were evaporated to dryness under nitrogen. The residue was derivatised using hydroxylamine hydrochloride to produce oximes, which were then silylated with N,O-bis-(trimethylsilyl)-trifluoroacetamide (BSTFA) to produce trimethylsilyl-ethers. These products were determined using capillary gas chromatograph (Hewlett-Packard 5890 II, series II with a flame ionisation detector and integrator HP 3396A, capillary column HP-5). The obtained data were analysed using CSW 32 software (Data Apex).

The results were compared with 8 young healthy non-smokers not drinking coffee (5 males and 3 females, age 22.1 ± 1.8 , range 19–25). This group was considered a control group. They underwent the SaLM test once as described above.

Results

The mean sucrose permeability in the control group was $0.059 \% \pm 0.025$ as opposed to habitual coffee drinkers without coffee restriction with mean sucrose permeability equal to $0.203 \% \pm 0.112$ (see Fig. 1). The sucrose permeability was significantly higher in the latter group in comparison with the former group ($p < 0.01$, two-sample test).

In habitual coffee drinkers after 48-hour coffee abstinence, sucrose excretion decreased significantly ($p < 0.05$, paired T-Test) to $0.107 \% \pm 0.088$. The reached level of sucrose permeability was not differing from that of non-coffee drinkers ($p = 0.54$, Kolmogorov-Smirnov test).

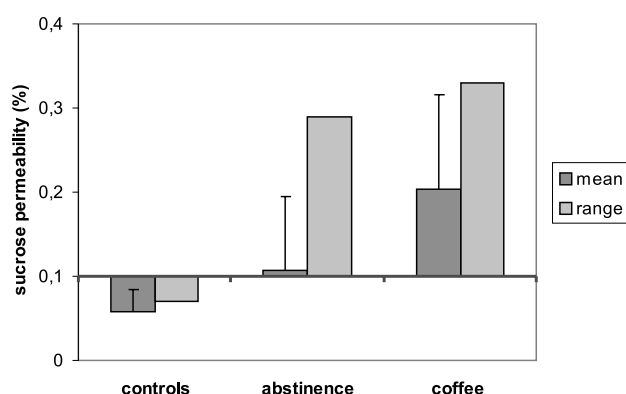


Fig. 1: Permeability for sucrose in unrestricted coffee drinkers and after abstinence.

Discussion

The normal value obtained from healthy probands not drinking coffee by adding two standard deviations to mean (less than 0.11 %) supports the value found by ROC (Receiver operating characteristic) analysis (less than 0.10 % with 95 % sensitivity and 33 % specificity) using volunteers with no respect to habitual coffee drinking (3).

We are aware of some limitations as to the interpretation of our results. Firstly, and not surprisingly, we found standard deviation and range of sucrose permeabilities to be substantially high, especially in the group of coffee drinkers. This finding is consistent with permeability tests in general, and makes them problematic with respect to recommendations for clinical utilisation. This variability may, to some extent, be explained on one hand by known and described factors (starting with complete ingestion of testing solution and ending up with accuracy of laboratory analysis) and on the other hand by differences in quantity and quality of mucosal damage, as seen in the trends of standard deviation. However, the range indicates (in compliance with the concrete values), that the value of sucrose permeability depends quite considerably on an individual, even though the importance and in our case also significance of the mean is indisputable (see Fig. 1). As for clinical praxis, in the light of these conclusions further specifications ought to be included into sucrose permeability protocols (not excluding the use of alcoholic beverages, cigarette smoking etc.).

Secondly, neither of our groups of volunteers was examined endoscopically. Therefore, an asymptomatic organic damage to the upper gastrointestinal tract mucosa could not be excluded. Nevertheless, with regard to healthy probands, we do not intend to minimize this limitation (in order to keep the convenience of the study).

Thirdly, some authors have shown that the gastroduodenal mucosal barrier is altered by *Helicobacter pylori* infection (2, 5, 14). Other studies, however, did not support this finding (8, 11, 15). Bearing this controversy in mind, we cannot tell for sure that our groups of probands are comparable. Therefore, we find it beneficial to include a non-invasive *Helicobacter pylori* test (e.g. a breath test) in future.

Fourthly, some authors suggest, that caffeine might slow gastric emptying (1). It might hence increase the exposure of gastric mucosa to sucrose. Be that the case, it would be for us problematic to determine the extent of its damaging effect in this area, since transit time also affects the results of permeability tests in general. In our study, it could therefore possibly be co-responsible for the increase of sucrose in urine. Since other studies (1, 10) indicate that coffee does not affect gastric emptying or small bowel transit, we considered this questionable effect of caffeine negligible. Lastly, our study uses a small group of volunteers. To obtain solid results for clinical praxis a much larger group ought to be studied.

Conclusions

Our results indicate that coffee may damage gastroduodenal mucosa in habitual coffee drinkers. In a time period of 48 hours the gastroduodenal mucosa is capable of a significant regeneration.

Hence, our findings will modify the protocols for sucrose permeability tests. The patients undergoing these tests should not drink coffee at least for 2 days before the test. Otherwise habitual coffee drinking ought to be taken into consideration and the results should be interpreted adequately.

Acknowledgements

The authors would like to thank the working team of the Laboratory of the Department of Gerontology and Metabolism, University Hospital in Hradec Králové, Czech Republic, and RNDr. E. Čermáková for her kind help with statistics.

References

1. Boekema PJ, Samsom M, van Berge Henegouwen GP, Smout AJ. Coffee and gastrointestinal function: facts and fiction. A review. *Scand J Gastroenterol Suppl* 1999;230:35-9.
2. Borch K, Sjøstedt C, Hannevad U, Soderholm JD, Franzen L, Mardh S. Asymptomatic *Helicobacter pylori* gastritis is associated with increased sucrose permeability. *Dig Dis Sci* 1998;43:749-53.
3. Cibiček N, Cibičková E, Kohout P, Žďánský P. Využití testu propustnosti pro sacharózu (SaLM) v detekci postižení sliznic horní části trávicí trubice u pacientů s horním dyspeptickým syndromem - pilotní studie. *Acta Medica (Hradec Králové) Suppl* 2004;47(1):23-28.
4. Fixa B. Peptický vřed In: Bureš J et al. *Základy vnitřního lékařství*, Praha: Galén 2003:280.
5. Fukuda Y, Bamba H, Okui M et al. *Helicobacter pylori* infection increases mucosal permeability of the stomach and intestine. *Digestion* 2001;63 (Suppl 1):93-96.
6. Gotteland M, Cruchet S, Frau V et al. Effect of acute cigarette smoking, alone or with alcohol, on gastric barrier function in healthy volunteers. *Dig Liver Dis* 2002; 34(10):702-6.
7. Gotteland M, Cruchet S, Verbeke S. Effect of *Lactobacillus* ingestion on the gastrointestinal mucosal barrier alterations induced by indometacin in humans. *Aliment Pharmacol Ther* 2001;15:11-7.
8. Graham DY. Pathogenesis of increased sucrose permeability in *H. pylori* gastritis. *Dig Dis Sci* 2000;45:889.
9. Kisiltas S, Imeryuz N, Gurcan T et al. Corticosteroid therapy augments gastroduodenal permeability to sucrose. *Am Coll of Gastroenterology* 1998;93: 2420-4.
10. Nieuwenhoven MA, Brummer RJM, Brouns F. Gastrointestinal function during exercise: comparison of water, sports drink, and sports drink with caffeine. *J Appl Physiol* 2000;89:1079-85.
11. Rabassa AA, Goodgame R, Sutton FM, Ou CN, Rogenerud C, Graham DY. Effects of aspirin and *Helicobacter pylori* on the gastroduodenal mucosal permeability to sucrose. *Gut* 1996;39:159-63.
12. Smecuol E, Bai JC, Vazquez H. Acute gastrointestinal permeability responses to different non-steroidal anti-inflammatory drugs. *Gut* 2001;49(5):650-5.
13. Sutherland LR, Verhoef M, Wallace JL, Van Rosendaal G, Crutcher R, Meddings JB. A simple, non-invasive marker of gastric damage: sucrose permeability. *Lancet* 1994;343:998-1000.
14. Suzuki K, Yasuo K, Sawada N et al. SS1 *Helicobacter pylori* disrupts the paracellular barrier of the gastric mucosa and leads to neutrophilic gastritis in mice. *Virchows Arch* 2002;440:318-24.
15. Vera JF, Gotteland M, Chavez E, Vial MT, Kakariek E, Brunser O. Sucrose Permeability in children with gastric damage and *Helicobacter pylori* infection. *J Pediatr Gastroenterol Nutr* 1997;24:506-11.

Submitted April 2004.

Accepted September 2004.

**Lubica Cibičková,
Velká 156, 753 01 Hranice,
Czech Republic.
e-mail: cibickova@seznam.cz**

CALCIPHYLAXIS INVOLVING BOTH THE UPPER AND LOWER EXTREMITIES

Tulay Ozer¹, Ali Borazan², Mubin Hosnuter³, Eksal Kargi³, Ahmet Savranlar¹, Ahmet Yilmaz⁴

Karaelmas University School of Medicine, Turkey: Department of Radiology¹, Department of Internal Medicine², Department of Plastic and Reconstructive Surgery³; Kocaeli University School of Medicine, Turkey: Department of Nephrology⁴

Summary: Calciphylaxis is an uncommon complication of end stage renal disease (ESRD) and secondary hyperparathyroidism. It is characterized by cutaneous necrosis with mural calcifications and thrombosis in the small vessels of dermis. It is important to diagnose and treat, because the mortality rate from calciphylaxis is very high. We present the case of a patient with ESRD and type II diabetes mellitus developing calciphylaxis of the both upper and lower extremities with a normal corrected calcium-phosphate product level. After amputation, necrosis was shown to progress rapidly resulting in death in one month.

Key words: *Calciphylaxis*

Introduction

Calciphylaxis is a rare, life threatening and debilitating condition found in patients with end stage renal disease (ESRD). Usually there is an elevated phosphate level and secondary hyperparathyroidism, ensuing increased calcium-phosphate product. This causes deposition of calcium phosphate in tissues and in both small and intermediate dermal vessels. Less commonly, cutaneous calcification in this disease can occur with normal serum calcium and phosphate levels (12). Although exact pathogenesis is not known, certain trigger factors, such as trauma, albumin, sepsis, iron supplementation, and corticosteroid therapy can precipitate the calcium deposition in vulnerable patients (17). Patients are usually admitted or referred to surgical clinics suffering from painful, red to purple livedoid plaques that may involve the full thickness of the skin, and subcutaneous tissue. In a few days, these areas become necrotic, eventually leading to extensive ulcerations. The lesions most commonly occur at lower extremities. This article reports of a rare case, who presented with calciphylactic skin necrosis on both upper and lower extremity with normal serum corrected calcium-phosphate product level.

Case report

A 48 year-old man with a 4-year history of peritoneal dialysis caused by diabetic nephropathy was referred to our clinic because of full thickness painful skin necrosis on the

feet and hands. He had been diagnosed with type II diabetes mellitus 12 years earlier but discontinued regular treatment. Besides, he had a long-standing history of hypertension and ischemic heart disease. His medications included erythropoietin, iron preparations, doksazosin, amlodipin, and valsartan. Patient stated that the lesions had begun as a purple discoloration resembling purpura. Eventually, these lesions extended peripherally and progressed to full-thickness skin necrosis and scar, indicating deep necrosis of the subcutaneous fat to the level of the investing muscular fascia. The patient especially complained of intense pain and itching at the wound sites. Physical examination revealed pale conjunctivas and the skin, cyanotic-painful fingers on extremities, and the cutaneous necrosis areas on the feet and hands (Fig. 1). Laboratory findings were as follows: Na, 133 mmol/L (137-145 mmol/L); K, 3.2 mmol/L; albumin, 17 g/L (35-50 g/L); sedimentation rate 70 mm/h; calcium (Ca), 2.45 mmol/L (2.1-2.6 mmol/L); corrected Ca for hypoalbuminemia, 2.9 mmol/L; ionized Ca, 1.3 mmol/L (0.8-1.2 mmol/L); phosphate, 1.49 mmol/L (0.8-1.45 mmol/L); corrected calcium-phosphate, 53.36 mg²/dL². He was found to have a significant degree of hyperparathyroidism, with parathyroid hormone (PTH) level: 658 ng/L (15-65 ng/L). Markedly elevated serum urea: 45.3 mmol/L (3.5-17 mmol/L) and creatinine: 804.4 μmol/L (70-106 μmol/L) levels were identified due to chronic state of uremia.

Bilateral plain roentgenograms of the extremities revealed extensive calcification in the arteries and the sub-



Fig. 1: The appearance of the extremities of this patient. Established necrotic areas on the fingers are seen (a). The toe of the left foot had been amputated (b).



Fig. 2: Plain radiographs of both upper and lower extremities of the patient with calciphylaxis. Extensive calcifications can be seen in digital arteries of both hand (a) and small and large vessels of the thigh (b).

cutaneous tissue (Fig. 2). Arterial Doppler ultrasonography of lower extremities showed non-pulsating peripheral vessels because of massive calcified plaques in wall of the vessels. Angiography showed occlusion at the level of two thirds distal of the anterior tibialis vessel. On echocardiography, degenerative changes of the aorta and mitral valves, left ventricular hypertrophy, and left atrium enlargement were found. Microscopic examination of biopsy specimens taken from lesions demonstrated fat necrosis with extensive calcifications of small vessel's media and intimal hyperplasia. All findings were consistent with calciphylaxis with no evidence of vasculitis. This case was diagnosed as calciphylaxis according to his biochemical, clinical and histopathological features. The patient received hemodialysis for the treatment of uremia during hospitalization and ray-

amputation was done for his left foot's first finger. Unfortunately, the necrosis showed rapid progression after amputation and the patient expired within a month as a result of sepsis and multiple organ failure.

Discussion

The most severe complication of the abnormal calcium and phosphate metabolism of ESRD is calciphylaxis. This disorder was first reported by Bryant in 1899 (3) and then subsequent studies named it as either calciphylaxis or uremic gangrene syndrome (17,19). Affected patients are characteristically dialysis dependent and suffer from secondary or tertiary hyperparathyroidism with high level of serum calcium-phosphate product ($>70 \text{ mg}^2/\text{dL}^2$) [12]. In

the case reported here, the level of the serum corrected calcium-phosphate were normal. The pathogenesis remains unexplained, but the term calciphylaxis is often used because of the similarity of findings with those occurring in rats in experiments by Selye who induced hypercalcaemia in the human. Uremia and hyperphosphataemia are often more obvious than hypercalcaemia. The high calcium-phosphate product level ($>70 \text{ mg}^2/\text{dL}^2$) is the most important determinant, but some patients with normal calcium and phosphate level do develop calciphylaxis (17,19).

The media of blood vessels in the involved tissue is usually calcified. The affected vessels may show intravascular thrombosis, without inflammation. Firstly, calciphylaxis appears as reticulated, violaceous, mottled patches, soon after progressing to ecchymosis, cordlike nodules, livedo reticularis, or necrosis (5,8,12). Gangrene and self amputation of digits or extremities has been reported (4,18). The lesions most commonly occur below the knees, and if restricted to below midcalf and to the fingers (distal type), the prognosis is good, with a 70% survival rate. Extensive lesions in proximal type usually affect the buttocks, thighs, shoulders and trunk are very bad prognosis, with a mortality rate of more than 85% in some series (14). Necrosis may involve other sites, such as the penis, tongue, breast, muscle or bowel (2,6,11,15).

The pathogenic mechanism is related to predisposing conditions that create a conducive environment for calcium precipitation in sensitized patients. Calcification occurs when an appropriate challenging factor is then introduced. Identified sensitizers include vitamin D compounds, parathyroid hormone, phosphates, and calcium salts, as well as infections, particularly granulomatous disorders, and cryofibrinogenemia. Challenging agents include metallic salts, local trauma, certain organic compounds (albumin and egg yolk), corticosteroids, intramuscular iron dextran complex, calcium heparinate, and intramuscular tobramycin. The sensitizing event and the challenging insult don't have to occur at the same time to cause disease (10,17). Patients with diabetes and chronic renal failure have a much higher risk of developing acral gangrene (16). The reported case is a good example of this condition. Poorly compensated diabetes, underdialysis, high ionized calcium (with high total calcium when corrected to low albumin level) may be the other factors that precipitating the calciphylaxis in our patient. The differential diagnosis includes pyoderma gangrenosum, necrotizing vasculitis, purpura fulminans, autoimmune vasculitis, peripheral vascular diseases, cryoglobulinemia, diabetes, warfarin-induced skin necrosis, disseminated intravascular coagulation, and bacterial endocarditis (5,12,18).

Treatment of calciphylaxis is difficult. Prevention is the best option, if possible, by management of the elevated phosphate levels with binding agents. Once lesions begin to appear, parathyroidectomy may be considered. Patients with parathyroid disease have the best prognosis after parathyroidectomy with autotransplantation of parathyroid

tissue (9). The parathyroid glands are removed totally but small piece of gland is buried in to muscle. If the disease process continues, the transplanted gland is also removed. Uremia and hypercalcemia should be corrected. Hyperbaric oxygen therapy and administration of prednisone, cimetidine, and systemic corticosteroids have been suggested as medical management (1,7,10). Intensive wound care, administration of antibiotics, debridement of necrotic tissue, corrections of electrolytes are most important factors in preventing sepsis (10,12,18). Death is usually caused by uncontrollable sepsis after infection of the chronic ulcerations.

References

1. Basile C, Montanaro A, Masi M et al. Hyperbaric oxygen therapy for calcific uremic arteriolopathy: a case series. *J Nephrol* 2002;15:676-80.
2. Bedoya RM, Gutierrez JL, Mayorga F. Calciphylaxis causing localized tongue necrosis: a case report. *J Oral Maxillofac Surg* 1997;55:193-6.
3. Bryant JH, White WH. A case of calcification of the arteries and obliterative endarteritis associated with hydronephrosis in a child aged six months. *Guys Hosp Rep* 1899;55:17-9.
4. Duh QY, Lim RC, Clark OH. Calciphylaxis in secondary hyperparathyroidism: diagnosis and parathyroidectomy. *Arch Surg* 1991;126:1213-9.
5. Edwards RB, Jaffe W, Arrowsmith J et al. Calciphylaxis: a rare limb and life threatening cause of ischemic skin necrosis and ulceration. *Br J Plast Surg* 2000;53:253-5.
6. Flanigan KM, Bromberg MB, Gregory M et al. Calciphylaxis mimicking dermatomyositis: ischemic myopathy complicating renal failure. *Neurology* 1998;51:1634-40.
7. Gilson RT, Milum E. Calciphylaxis: case report and treatment review. *Cutis* 1999; 63:149-53.
8. Gipstein RM, Coburn JM, Adams DA et al. Calciphylaxis in man: a syndrom of tissue necrosis and vascular calcification in 11 patients with chronic renal failure. *Arch Intern Med* 1976;136:1273-80.
9. Giroto JA, Harmon JW, Ratner LE et al. Parathyroidectomy promotes wound healing and prolongs survival in patients with calciphylaxis from secondary hyperparathyroidism. *Surgery* 2001;130:645-50.
10. Howe SC, Murray JD, Reeves RT et al. Calciphylaxis, a poorly understood clinical syndrome: three case reports and a review of the literature. *Ann Vasc Surg* 2001;15:470-3.
11. Jacobsohn HA, Jenkins PG, Jacobsohn KM. Penile calciphylaxis. *Urology* 2002; 60:344-7.
12. Kane WJ, Petty PM, Sterioff S et al. The uremic gangrene syndrome: improved healing in spontaneously forming wounds following subtotal parathyroidectomy. *Plast Reconstr Surg* 1996;98:671-8.
13. Mehta RL, Scott G, Sload JA et al. Skin necrosis associated with acquired protein C deficiency in patients with renal failure and calciphylaxis. *Am J Med* 1990;88:252-7.
14. Odom RB, James WD, Berger TG. *Andrew's Diseases of The Skin; in Errors in Metabolism*. Philadelphia: W.B. Saunders Comp, 2000:660.
15. Patetsios P, Bernstein M, Kim S et al. Severe necrotizing mastopathy caused by calciphylaxis alleviated by total parathyroidectomy. *Am Surg* 2000;66:1056-8.
16. Scheinman PL, Helm KF, Fairley JA. Acral necrosis in a patient with chronic renal failure. *Calciphylaxis*. *Arch Dermatol* 1991;127:248-9.
17. Selye H, Gabbiani G, Strebel R. Sensitization of calciphylaxis by endogenous parathyroid hormone. *Endocrinology*. 1962;71:554-8.
18. Senturk S, Hosnuter M, Tosun Z et al. Calciphylaxis: Cutaneous necrosis in chronic renal failure. *Ann Plast Surg* 2002;48:104-5.
19. Torok L, Kozepessy L. Uraemic gangrene syndrome. *Acta Dermatol Venereol* 1991;71:455-7.

Submitted June 2004.

Accepted September 2004.

Tulay Ozer, MD,
Zonguldak Karaelmas Üniversitesi Tıp
Fakültesi Hastanesi Radyoloji A.D.
67600, Kozlu, Zonguldak-Turkey.
e-mail: tulayozertnn.net

ACUTE STOMACH VOLVULUS - CASE REPORT

Pavel Hladík¹, Robert Čáp², Tomáš Holeček¹

Charles University in Prague, Faculty of Medicine and University Hospital in Hradec Králové, Czech Republic: Department of Surgery¹; Purkyně Medical Military Academy in Hradec Králové, Czech Republic: Department of War Surgery²

Summary: Stomach volvulus in its acute form is a serious sudden disorder in the abdominal cavity. The case of stomach volvulus, that had been successfully surgically solved, is described in the presented paper. Even though the volvulus was not caused by the hiatus hernia, the antireflux fundoplication according to Nissen-Rossetti was performed besides the frontal gastropexy.

Key words: *Stomach volvulus; Antireflux surgery*

Introduction

The stomach volvulus is a rotation for more than 180°. It causes the stomach obstruction. The vessel compression may lead to stomach wall necrosis. This disorder was first described by Ambrosie Pare in 1579 as a complication of strangulated diaphragmatic hernia after a cut injury. In 1866 Berti described the acute stomach volvulus in a 66-year-old woman who died of the high ileus. In 1896 Berg performed the first successful operation after previous percutaneous decompression with trocar and canulla. The frequency of appearance of this disease is not high, but on the other hand, the chronic form of the disease is more frequent than it was supposed in the past (3,5,6).

From the anatomic point of view there are three types of volvulus - organoaxial, mesenterioaxial, and the combined form. From the clinical point of view we can observe the acute and the chronic volvulus; according to the etiology the volvulus can be either primary or secondary. Anamneses show that painful epigastrium and feelings of full stomach and vomiting are typical. Borchartd-Lenormontov's trias is a typical symptom in the acute stadium of the disease: sudden appearance of severe pain in abdominal cavity with vomiting, nausea, and impossibility of introduction of the stomach probe. Diagnosis of stomach volvulus is clearly confirmed by the contrast X-ray examination of the stomach (12).

Derotation of the stomach and control of possible ischemic changes on its wall are the principles of the surgical treatment. The identification of the volvulus cause and its removal follow. The operation is finished by prevention of the rotation recurrence - the various types of gastropexy.

Therapeutically, it is important to leave the stomach probe until the full stomach motility has been restored (7,8,11).

Chronic stomach volvulus is manifested more by non-specific symptoms that lead to suspicion of other disorder of gastroduodenum or cholecystopathy (1).

Case report

A 30-year-old woman was admitted to the surgical department. She suffered from an acute pain of abdomen and feeling of flatulence in epigastrium. She had a very strong nausea; before the admission she had vomited once. Even after the introduction of a nasogastric tube there was no sign of desuflation of the stomach. The contrast X-ray examination of the stomach diagnosed stomach volvulus (Fig. 1 and 2). The ultrasound of the abdomen showed epigastric flatulence and gallbladder and biliary ducts free of any pathologic changes.

It was very important to find that the patient had suffered from similar difficulties (though not so strong) intermittently for several years.

The operation from upper-middle laparotomy was performed immediately. The whole epigastrium was filled with dilated stomach. Derotation of the combined type of volvulus was performed under uneasy conditions. The stomach tube was manually placed into the correct position, because before the operation it had reached only to the level of cardia. Fundus of the stomach was fixed by distal surface adhesion to the abdominal wall. After dissecting the adhesions it was possible to put the stomach to the normal anatomic position. After that there was a clearly visible gap between the arms of esophageal hiatus. That defect was re-



Fig. 1: Contrast X-ray without introduced stomach tube. The image shows distally convoluted stomach fundus, and under the left diaphragm there is dilated stomach body.



Fig. 2: Contrast X-ray after introduction of the stomach tube. The tube reaches to the level of cardia. The contrast medium has moved into distal part of the stomach.

duced by two sutures. Also the abdominal part of the esophagus was free; the Hiss's angle was straightened. Therefore the antireflux fundoplication according to Nissen-Rosseti was performed. The remaining part of the stomach fundus and the stomach body were fixed to the diaphragm and to anterior abdomen wall by sutures as frontal gastropexy. The stomach tube remained in the stomach until the peristalsis was restored (i.e. the third day after operation).

The postoperative course was without complications, the incision was healed p.p.i., control stomach X-ray was normal, without any symptoms of gastroesophageal reflux. The usual diet regime followed after the patient's dismissal. During the control (5 weeks after the operation) she did not mention any dyspeptic difficulties. X-ray of stomach was without any pathologic changes.

Discussion

The surgical revision is indicated for the treatment of the acute stomach volvulus. In cases presented in the case-histories in literature there was mentioned that after the operation the hiatus hernia was proved (8). Therefore the antireflux surgical operation is necessary to be performed (3).

In some cases presented in literature the disorder is solved only by derotation of the stomach and damage of the perigastric adhesion only, without the following gastropexy (10). Because of possible recurrence of the volvulus the various kinds of gastropexy (Tanner, Maingot, Opolzer, etc.) are being recommended (5,11,12).

In case the secondary type of volvulus is concerned, the surgical solution is aimed to eliminate the cause. According to the literature (1) it is possible to solve the stomach volvulus by endoscopy. But usually it is not possible to reach the final solution and the volvulus recurrence is very common. Endoscopy can be connected with parallel laparoscopy.

In our case the situation was complicated by big dilatation of the stomach and it was very difficult to perform the exact antireflux plastics and gastropexy. In the presented case we derotated and desufflated the stomach and we freed it from the adhesion.

Then we reduced the size of esophageal hiatus and we performed the antireflux fundoplication according to Nissen-Rossetti. The operation was finished by frontal gastropexy. Performance of antireflux plastics in gastroesophageal junction has been mentioned by other authors,

too (4,6). This method should be performed especially during the operation when it is clear that the patients may possibly have problems with hiatal hernia or gastroesophageal reflux in the future.

References

1. Bhasin DK, Nagi B, Kochhar R et al. Endoscopic management of chronic organoaxial volvulus of the stomach. *Am J Gastroenterol* 1990;85:1486-8.
2. Ejstrud P, Jensen F. Kronisk ventrikelvolvulus. *Ugeskr Leger* 1995;157:55-6.
3. Eren R, Nasehi P, Walser F. Der Magenvolvulus. *Chirurg* 1983;54:818-20.
4. Eyskens E, Van der Stighelen Y. Volvulus van de maag. *Acta Chir Belg* 1984;84:209-18.
5. Gosin S, Ballinger WF. Recurrent volvulus of the stomach. *Am J Surg* 1965;109:642-6.
6. Johnson JA, Thompson AR. Gastric volvulus and upside-down stomach. *Am J Surg* 1968;115:505-15.
7. Niederle B, Šebek V. Operace náhlých příhod břišních. Praha: Státní zdravotnické nakladatelství, 1962:182-3.
8. Novák M, Mrázová M, Leypold J, Jurka M. Volvulus žaludku. *Bratisl Lek Listy* 1990;91:383-5.
9. Patel NM. Chronic gastric volvulus: Report of a case and review of literature. *Am J Gastroenterol* 1985;80:170-3.
10. Růžička P, Pešková M, Šváb J. Chronický volvulus žaludku. *Rozhl Chir* 1989;68:100-2.
11. Senapati MK, Tapase VG. Chronic volvulus of the stomach: to operate? *Tropical Doctor* 1997;27:41-3.
12. Tanner NC. Chronic and recurrent volvulus of the stomach. *A J Surg* 1968;115:505-15.

Submitted June 2004.

Accepted July 2004.

MUDr. Pavel Hladík, Ph.D.,
Školská 36, 500 11 Hradec Králové 11,
Czech Republic.
e-mail: hladikp@lfhk.cuni.cz

IRON DEPOSITION IN THE BRAIN FOLLOWING THE ISCHEMIA IN A RAT MODEL OF ISCHEMIC TOLERANCE

Viera Danielisová, Miroslava Némethová, Jozef Burda

Slovak Academy of Sciences, Institute of Neurobiology, Košice, Slovak Republic: Department of Neurochemistry

Summary: Preconditioning of the brain by short-term ischemia increases brain tolerance to the subsequent severer ischemia. In this study, we investigated iron deposition in the cerebral cortex and the ischemic tolerance in a rat model of cerebral ischemia. Forebrain ischemia was induced by four-vessel occlusion for 5 min as ischemic preconditioning. Two days after preconditioning or after the sham-operation, the second ischemia was induced for 20 min. Changes in the cerebral cortex were examined after 1 to 8 weeks of recirculation following 20 min ischemia with or without preconditioning using the iron histochemistry. Granular deposits of the iron were found in the cytoplasm of the pyramidal cells in the layers III and V of the frontal cortex after 1 week of recirculation. When the rats were exposed to 5 min ischemia 2 days before 20 min lasting ischemia, the deposition of iron in the cytoplasm of the pyramidal cells in layers III and V of the frontal cortex was significantly lower during all periods of reperfusion. Preconditioning 5 min ischemia followed by 2 days of reperfusion before 20 min ischemia also prevented degeneration of the pyramidal neurons in layers III and V of the frontal cortex.

Key words: Cerebral ischemia; Ischemic tolerance; Iron; Frontal cortex

Introduction

Short periods of preconditioning by the ischemia can confer protection against injury which results from longer periods of focal or global ischemia in the central nervous system. Since preconditioning harnesses robust endogenous protective potential of the tissue, elucidation of the mechanisms responsible for the induction of ischemic tolerance may have practical value in the search for effective means of therapeutic intervention in stroke.

Iron is necessary for normal neural function but it must be stringently regulated to avoid iron-induced oxidative injury (1). The recirculation of blood after transient ischemia causes an increase in low molecular weight species of iron, and free radicals formation initiated by iron leads to the brain damage by lipid peroxidation (11). Iron-induced hydroxyl radicals, lipid peroxidation and apoptotic cell death can be blocked by both, endogenously generated and exogenously administered nitric oxide. The ischemic preconditioning induces expression of stress proteins such as hemeoxygenase-1, neuronal nitric oxide synthase, redox factor-1 and inhibits p66^{shc}, as well as hypothermia therapy suppresses the generation of toxic reactive oxygen, lipids and thiol species evoked by bioactive iron complexes in the brain (4).

Free iron, more than any other transition metal, has been implicated in redox transitions and consequential ge-

neration of oxygen free radicals. The iron regulatory proteins, which control other Fe-binding proteins and thus the regulation of cellular iron metabolism also play a role in decreasing the reactive oxygen species generating capacity of Fe (2).

There were many studies dealing with the role of iron in neuronal damage during early stages of cerebral ischemia (6), but abnormal iron deposition at a late stage after transient cerebral ischemia has not been reported except in the histochemical studies of the spatial and temporal distributions of the iron (5), ferritin, and transferrin (as iron binding proteins), and of the astroglial and microglial reactions at 1–24 weeks after transient forebrain ischemia (8).

In the present study, we investigated postischemic neuronal damage in the layer V of the cerebral cortex. We examined abnormal iron deposition in the brain during the chronic phase after ischemia, using the intensification of Perl's histochemical reaction for ferric iron by 3,3'-diaminobenzidine (DAB). We also assessed the effectiveness of ischemic tolerance induced by preconditioning with respect to the cell damage and iron deposition.

Materials and Methods

The experiments were done in agreement with the Slovak Law of Animal Protection No. 115/1995 and under the supervision of the Institutional Ethical Committee for ani-

mal research. 8- to 10-weeks-old male rats of the Wistar strain were used. The rats' weight was 250–300 g at the beginning of the experiment. They were placed on a deprivation schedule to maintain their weights at approximately 80% of the free-feeding level. The rats were housed in groups of four per cage under the constant temperature ($23 \pm 2^\circ\text{C}$) and a 12-h light/dark cycle (light period: 07.00–19.00 h), with water freely available. Transient forebrain ischemia was induced by the four vessel occlusion method (4-VO) described by Pulsinelli and Brierley (9) with modifications (10). Briefly, the rats were anaesthetised i.p. by ketamine (100 mg/kg body wt) and xylozine (15 mg/kg body wt). Vertebral arteries were electrocauterized through the alar foramen of the first cervical vertebra. Both common carotid arteries were exposed through a ventral midline cervical incision and ligatures were placed loosely around each artery without interrupting the carotid blood flow. Next day, under light fluothane anaesthesia both common carotid arteries were reexposed and occluded with aneurysmal clips to induce forebrain ischemia. The arteries were occluded for 5 min (ischemic preconditioning) and 2

days later the carotid arteries were occluded for 20 min again. At the end of 20 min lasting bilateral carotid occlusion, blood flow was restored by releasing the clips. The rats which became unresponsive and lost the righting reflex during bilateral carotid artery occlusion, and did not reveal seizures during and after the ischemia were retained in the experiment. Only such animals can be considered to fulfil the criteria of adequate ischemia. Criteria of forebrain ischemia were the following: the bilateral loss of the righting reflex, paw extension, and the mydriasis. Sham-operated animals ($n=4$ in each group) were treated in a same manner but without the occlusion of the common carotid arteries. Rectal temperature of animals was maintained at 37°C during the surgery and following ischemia by the heating pad and lamp. The animals were sacrificed at 1, 4 and 8 weeks after the preconditioning ischemia or after the second ischemia.

At 1, 4 and 8 weeks of recirculation, the animals ($n=6$ in each group) were deeply anaesthetised i.p. by the above mentioned mixture of ketamine and xylozine and then perfused transcardially with saline, followed by 4% parafor-

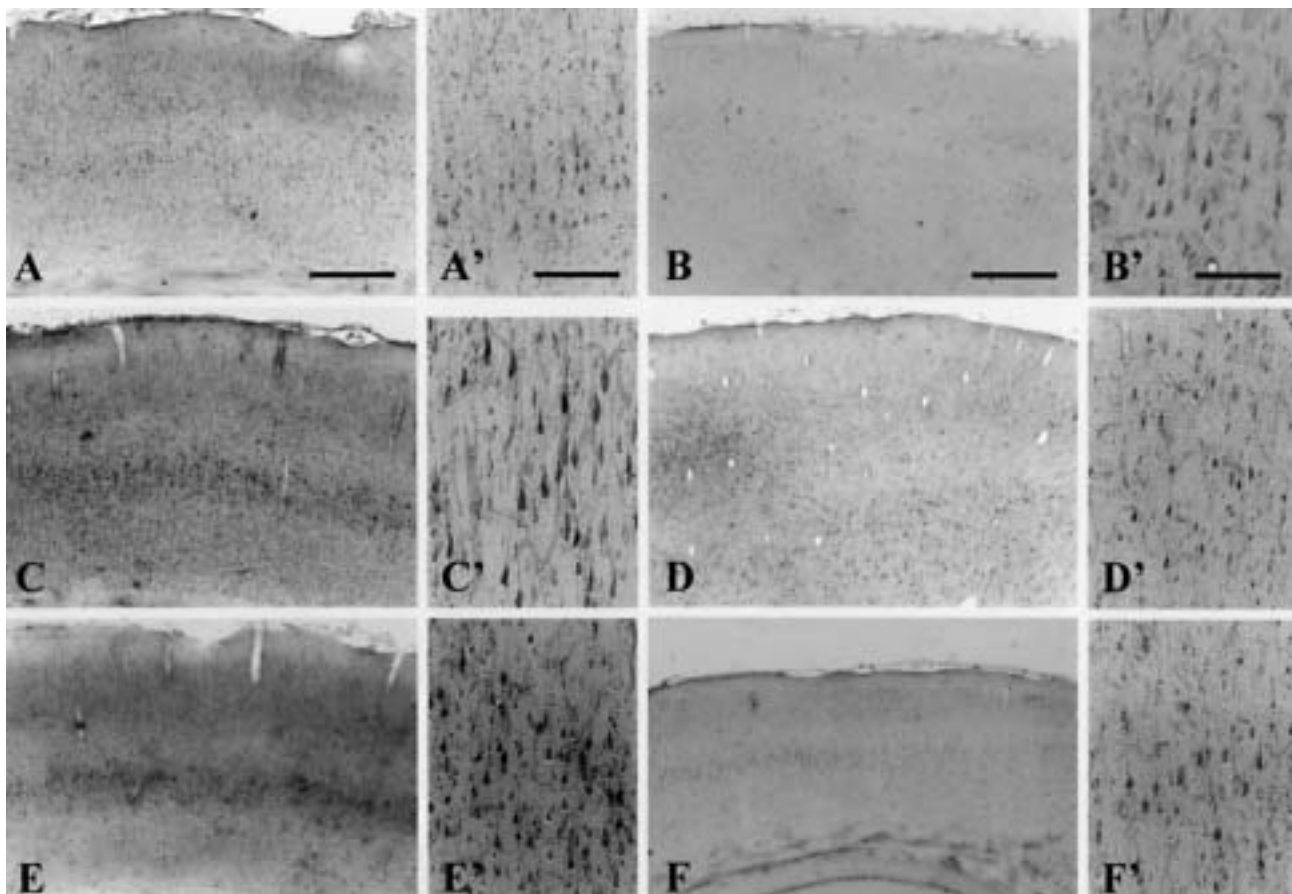


Fig. 1: Photomicrographs of Perl's reaction at a level of frontal cortex without preconditioning after 1 week (A and A'), 4 weeks (C and C'), 8 weeks (E and E') of reperfusion, and with preconditioning after 1 week (B and B'), 4 weeks (D and D'), 8 weeks (F and F') of reperfusion. Scale bar: 400 μm (A, B, C, D, E, F) and 40 μm (A', B', C', D', E', F').

maldehyde solution with 0.1 M phosphate buffer (PB; pH 7.4). The brains were removed from the skull, and postfixed for 3 h in the same fixative. The brains were cut coronally on a vibratome to 30 μm . The sections were stained with hematoxylin-eosin and by Perl's reaction with or without 3,3'-diaminobenzidine (DAB) intensification (7). Sections were well washed with deionized water for at least 30 min, incubated in Perl's solution (1% potassium ferrocyanide/1% HCl) at the room temperature for 30 min followed by washing with deionized water for 30 min. Sections without DAB intensification were counterstained with neutral red and mounted. For the intensification of Perl's reaction, the sections were incubated for 20 min in 0.5% DAB in 0.1 M PB and for 15 min in the same medium with 0.005% H_2O_2 . The reaction was finished by washing with deionized water for 30 min. Some sections were counterstained with methyl green. Control slides were amplified with DAB but without the preincubation with Perl's solution. No positive staining was found in any of control slides.

Statistical significance of differences between the groups was analysed using one-way ANOVA test followed by post-hoc Duncan's test. The result $p < 0.05$ was considered to be significant.

Results

Ischemic changes in neurons induced by transient forebrain ischemia were evaluated on sections of the frontal cortex stained with hematoxylin and eosin. In this model, neuronal damage was observed only in the layers III-V of the cerebral cortex. The effect of preconditioning was visible already after 1 week of recirculation.

In sham-operated control rats, the iron was occasionally present in the perikarya and neuronal processes of some

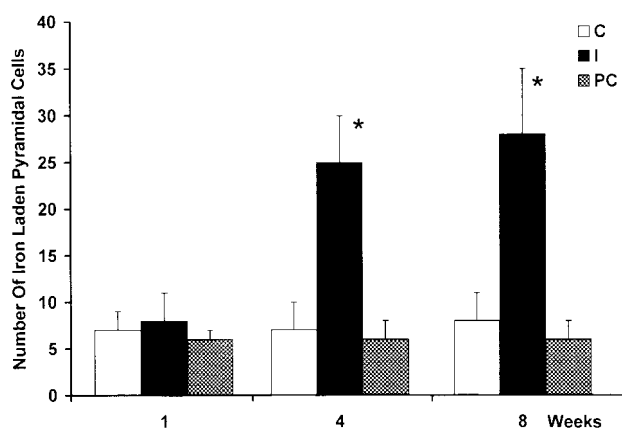


Fig. 2: Number of iron-positive pyramidal neurons in layer V of frontal cortex. Neurons were counted using a light microscope at a 50-fold original magnification. An area of $3.0 \times 10^4 \mu\text{m}^2$ ($460 \times 650 \mu\text{m}$) was counted. Values are means \pm SD. * $p < 0.05$ compared to ischemic rats without preconditioning.

pyramidal neurons in the layer V and in a part of the layer III of the frontal cortex in the form of fine granular deposits. The number of iron-containing pyramidal cells in the layer V of the frontal cortex increased in 1 week and reached maximal values after 8 weeks of recirculation (Figs. 1A, A'; C, C'; E, E'). The injured cellular layer was strongly iron stained (Figs. 1E, E'). The protective effect of 5 min ischemia 2 days before 20 min severe ischemia was visible in layer V of the frontal cortex (Figs. 1B, B'; D, D'; F, F').

Granular iron deposits in pyramidal neurons of the frontocortical layer V showed significant increase at 4 and 8 weeks compared to ischemic rats without preconditioning (Fig. 2)

Discussion

The iron deposition in cerebral cortex in a rat model of cerebral ischemia and possible increase of ischemic tolerance of the brain was investigated. We examined the iron deposition in the rat brain during the chronic phase following transient forebrain ischemia with and without preconditioning. The iron began to accumulate after the first week of recirculation in the cytoplasm of the pyramidal cells in the layer V of the frontal cortex. Conspicuous iron deposition was seen in the mentioned cells after 8 weeks. Preconditioning with 5 min ischemia 2 days before 20 min ischemia preserved the pyramidal cell layer V of the frontal cortex and produced only a minimal number of iron-containing cells during recirculation.

Abnormally high levels of iron deposition as well as oxidative stress have been demonstrated in a number of neurodegenerative disorders including Alzheimer's disease and those characterised by nigral degeneration such as Parkinson's disease, multiple system atrophy, and progressive supranuclear palsy. Microglia cells are the major sites of iron bound in ferritin and are thought to be partly responsible for oxidative damage in neurodegenerative disorders. Microglia stimulated *in vivo* with phorbol ester shows increased lipid peroxidation resulting from a superoxide-dependent release of iron from ferritin (12). The interaction of oxidative stress with control of iron metabolism in the brain is confirmed by finding of abnormal iron deposition associated with lipid peroxidation in a transgenic mouse model (with the expression of interleukin IL-6 in astrocytes) of the blood-brain barrier defect associated with progressive neurodegeneration (3).

Preconditioning induction of genes and proteins, capable to prevent or repair the oxidative damage caused by reactive oxygen species, peroxy lipid radicals and reactive peptidyl thiol radicals could enhance the recovery and repair of partially damaged neurons in the brain. Neuroprotection against cerebral ischemia can be realised if the brain is preconditioned by previous exposure to a brief period of ischemia. Preconditioning of the rat brain by short-term cerebral ischemia induces resistance to subsequent severe ischemia.

Conclusions

This study indicates that preconditioning of the brain by 5 min ischemia 2 days before 20 min ischemia prevented neuronal damage by the reduction or limitation of iron accumulation in the layer V of the frontal cortex. It has been suggested that short ischemic attacks might provide the preconditioning necessary to protect the brain from later, more severe insults. Our data confirm that this indeed might be the case of postischemic iron metabolism.

Acknowledgement

This study was supported by the Slovak Grant Agency for Science SK-VEGA 2/3219/23.

References

1. Benkovic SA, Connor JR. Ferritin, transferrin, and iron in selected regions of the adult and aged rat brain. *J Comp Neurol* 1993;338:97-113.
2. Campbell A, Smith MA, Sayre LM, et al. Mechanisms by which metals promote events connected to neurodegenerative diseases. *Brain Res Bull* 2001;55:125-32.
3. Castelnau PA, Garrett RS, Palinski W, Witztum JL, Campbell II, Powell HC. Abnormal iron deposition associated with lipid peroxidation in transgenic mice expressing interleukin-6 in the brain. *J Neuropathol Exp Neurol* 1998;57:268-82.
4. Chiueh CC. Iron overload, oxidative stress, and axonal dystrophy in brain disorders. *Pediatr Neurol* 2001;25:138-47.
5. Danielisová V, Gottlieb M, Burda J. Iron deposition after transient forebrain ischemia in rat brain. *Neurochem Res* 2002;27:237-42.
6. Davalos A, Real JMF, Soler SS, Molins A, Planas E, Genis D. Iron-related damage in acute ischemic stroke. *Stroke* 1994;25:1543-6.
7. Hill JM, Switzer RC. The regional distribution and cellular localisation of iron in the rat brain. *Neuroscience* 1984;11:595-603.
8. Kondo Y, Ogawa N, Asanuma M, Ota Z, Mori A. Regional differences in late-onset iron deposition, ferritin, transferrin, astrocyte proliferation, and microglial activation after transient forebrain ischemia in rat brain. *J Cereb Blood Flow Metab* 1995;15:216-26.
9. Pulsinelli WA, Brierley JB. A new model of bilateral hemispheric ischemia in the unanesthetized rat. *Stroke* 1979;10:267-72.
10. Schmidt-Kastner R, Paschen W, Ophoff BG, Hossmann K-A. A modified four-vessel occlusion model for including incomplete forebrain ischemia in rats. *Stroke* 1989;20: 938-46.
11. Siesjo BK. Mechanisms of ischemic brain damage. *Crit Care Med* 1988;16: 954-63.
12. Yoshida T, Tanaka M, Sotomatsu A, Hirai S, Okamoto K. Activated microglia cause iron-dependent lipid peroxidation in the presence of ferritin. *Neuroreport* 1998;9:1929-33.

Submitted March 2004.

Accepted November 2004.

***MVDr. Viera Danielisová, CSc., PhD.,
Department of Neurochemistry,
Institute of Neurobiology,
Slovak Academy of Sciences,
Šoltésovej 6, 040 01 Košice,
Slovak Republic.
e-mail: danielis@saske.sk***

THEORETICAL BASIS OF NEW METHODOLOGY OF MATHEMATICAL-STATISTICAL DECISION MAKING WITH THE HELP OF BIOMARKERS FROM MASS SPECTRA

Jiří Knížek

Charles University in Prague, Faculty of Medicine in Hradec Králové, Czech Republic: Department of Medical Biophysics

Key words: *Biomarker; Decision Making; Mass Spectra; Proteom*

There are at disposal N_S mass spectra for the group of N_S provably *sick* patients, N_H mass spectra for the group of N_H provably *healthy* patients and finally N_E mass spectra for patient whose state of health is being *examined*. With this quite general data a doctor in clinic should make decision about null hypothesis

H_0 : *patient is healthy*

(against *alternative that patient is not healthy*) as correctly as possible. In addition this doctor should make decision about miscellaneous null hypotheses

H_0 : *patient is healthy in*

$$\langle x_{j_1}; x_{j_2} \rangle \cup \langle x_{j_3}; x_{j_4} \rangle \cup \dots \cup \langle x_{j_{2m-1}}; x_{j_{2m}} \rangle$$

where $\langle x_{j_1}; x_{j_2} \rangle \cup \langle x_{j_3}; x_{j_4} \rangle \cup \dots \cup \langle x_{j_{2m-1}}; x_{j_{2m}} \rangle$ is unified set of m intervals on the whole spectral range respecting single biomarkers, or respecting (certain biologically autonomous) groups of biomarkers. The proposed *Theoretical basis of new methodology of mathematical-statistical decision making with the help of biomarkers from mass spectra* enables to solve these thorny problems. The *new methodology*, as opposed to the methods (1,2) used so far, solves the problems universally.

Nowadays this proposal is discussed in detail through e-mail with firms Geneva Bioinformatics S.A. (Prof. Ron D. Appel, Ph.D. and Dr. Frdrique Lisacek, Ph.D.) and Bruker Daltonik GmbH in Bremen (Dr. Wolfgang Pusch, Ph.D.).

References

1. Tibshirani R, Hastie T, Narasimhan B, Soltys S, Shi G, Koong A, Le QT: Sample classification from protein mass spectrometry by "peak probability contrasts", *Bioinformatics - Bioinformatics Advance Access*, Oxford University Press 2004; 1-34.
2. Wu B, Abbott T, Fishman D, McMurray W, Mor G, Stone K, Ward D, Williams K, Zhao H: Comparison of statistical methods for classification of ovarian cancer using mass spectrometry data, *Bioinformatics* 2003;19:13:1636-43.

Submitted October 2004.

Accepted December 2004.

Dipl. Ing. Jiří Knížek, Ph.D.,
Charles University in Prague,
Faculty of Medicine in Hradec Králové,
Department of Medical Biophysics,
500 38 Hradec Králové,
Czech Republic.
e-mail: knizekj@lfhk.cuni.cz



The issue of ACTA MEDICA you have in your hands contains papers that were at the root of lectures given at “27th Days of Medical Biophysics”. These Days originated 26 years ago, when medical physics changed into medical biophysics.

That change meant a shift in emphasis – from applications of classical physics, to new branches of science such as molecular biology, informatics, and modelling (simulation). It also enlarged the sphere of subjects fostered at medical schools, which in turn diversified the problems the faculties of medical biophysics must solve. And it diversified their field of collaborators outside of higher education.

This issue of ACTA MEDICA contains papers that are evidence of the changes that have occurred in the last 26 years.

I believe a perusal of the abstracts will indicate at least some articles you will want to read in full. And I hope that reading the papers will make you want to attend the next “Biophysical Days”, and personally meet the Czech and Slovak biophysicists.

Prof. Pravoslav Stránský

A CONTRIBUTION TO SONOGRAPH IMAGE QUALITY ESTIMATION USING POINT SPREAD FUNCTION

Ladislav Doležal, Jan Hálek

Palacky University Olomouc, Faculty of Medicine, Czech Republic: Institute of Medical Biophysics

Summary: In medical sonography, sonograph image quality is an essential aspect for the safety of both patient and doctor. Its evaluation therefore requires an accurate and objective method for measurement. In this regard, a number of methods are in current use. Most of these are based on tissue mimicking phantom imaging. In contrast, we have used another principle based on Point Spread Function (PSF) analysis which is a product of the measuring system we have developed. In this case, the measured sonograph scans a small metallic ball target that moves in a water bath on a specified trajectory. The Region Of Interest (ROI) of the sonogram containing the ball target picture is digitised and the amplitude of the pixels analysed. The result is the PSF from which we calculate the lateral resolution (LR). For this purpose, we use our own original software. Using this method, we have to date been able to plot LR characteristics over the scanning plane. The method allows us to differentiate separate scanning lines and even multiple focal areas for dynamic focussing systems. It can detect malfunctions in dynamic focussing, size of aperture, time gain compensation function and/or transducer element failure. The procedure itself is not as easy or as fast to use as tissue mimicking phantoms or 3D signal to noise ratio evaluation, but it provides accurate and objective numeric parameters corresponding to the quality of image at any specified point over the whole scanning area. It is also a very powerful tool when used in combination with the other methods mentioned above.

Key words: *Sonography; Quality; Resolution; Point spread function; Measurement*

Introduction

Problems related to the safety of ultrasound application, judged from the point of view of patients, nursing and examining personnel, ultrasound biological effects have dominated the more than 50 years of ultrasound use in medicine; the direct effects of ultrasound energy on living tissue have been intensively focussed on for a considerable time. On the other hand, the dangers inherent in incorrect treatment resulting from erroneous diagnosis based on misinterpretation of the sonogram has only been taken into consideration in the last decade. Such misinterpretation has a number of sources. Firstly, artefacts. When evaluating the risks of image artefacts, it is necessary to differentiate objective and subjective factors.

a) Objective risk factors include:

- physical imaging artifacts,
- inadequate quality of imaging equipment caused by low technical standard, poor maintenance or age of the equipment.

b) Subjective factors relate to the skills of the *examiner*. These include:

- unfamiliarity with the physical mechanisms of ultrasound image creation, lack of skills in operating the

equipment and hence inability to set the optimal working parameters,

- lack of knowledge of the topographic anatomy necessary for correct image interpretation,
- inborn characteristics of the observer, such as spatial imagination and the ability to abstract what is seen.

Physical artifacts here are based on the physical properties of ultrasound waves and the environment in which they are propagated. As such they are unequivocally definable according to laws of physics and to eliminate them, it is necessary to apply appropriate procedures and imaging methods. If these do not exist, the laws of physics must be accepted and taken into consideration. In this case eliminating the risks is totally dependent on the experience of the examiner and the above mentioned subjective characteristics.

On the other hand, the sonograph imaging quality is a factor completely dependent on the technical parameters of the equipment. In order to increase the imaging quality or eliminate imaging defects and thus reduce the risks, it is necessary to create a system for determining and objectively evaluating the relevant qualitative parameters (1).

This is very difficult and requires definition of the parameters of sonographic imaging quality, development of

suitable measuring methods, procedures for their evaluation and creation of a graded system of sonograph quality criteria.

At present, commercial testing objects for B-mode (for example ATS 520, RMI 403 GS, CIRS etc.) are being produced. These contain defined non-homogeneities whose image is analyzed by subjective observation (5). To fulfill all important physical criteria for correct mimicking of the tissue (4), the construction has to be rather sophisticated, although there are back up programs for their easier application and processing of the results - for example the Canadian UltraQ (2). This testing method is fast and relatively inexpensive, but is, however, burdened with a large error resulting from subjective assessment of image quality, even with the use of computer technology.

Another very interesting method (7), utilizes spatial analysis of the signal/noise ratio in a three-dimensional image of a special testing object to create the image characterization for signals with small amplitude. This method is suitable for fast orientation measurement and is substantially more objective than the ones mentioned earlier. Its only disadvantage is that it shows an integral parameter which is dependent on the depth and cannot therefore determine the lateral details of the image defect. Second, analysis of spatial image distortion and characterization of the system for high amplitude reflected signals is not possible. Both of these methods are primarily suitable for in situ screening studies which are not time consuming given the equipment workload. They do not, however, produce detailed objective information. Another simple and fast testing method is the control of homogeneity of the transducer field by common plane reflector, developed by the Sonora Co. (3) and called FirstCall 2000. This is suitable for fast detection of a defective spot on the electronic probe, but it is not, however, able to measure specific physical parameters such as, for example, resolution.

Another type of measurement that can be used for analyzing sonograph qualitative parameters is measurement of the characteristics of the radiated ultrasound field. This method, however, does not evaluate the image quality. It only determines the parameters of the transmitting ultrasound signal and is suitable mainly for controlling the radiated ultrasound intensity, or, possibly, its space and time distribution, which is significant for maintaining the allowed limits and for assessment of the effects of ultrasound energy in various types of tissue boundary. These are not the only measuring methods available. There are also mathematical models of the ultrasound field radiated by certain types of probes (6) and its temperature effects.

In short, quantitative and accurate evaluation of the image quality is very problematic and there exist few institutions world wide dealing with this issue using the methods mentioned above.

Our contribution is a new system of evaluating parameters for sonograph quality imaging in various imaging modes and methodical procedures for their quantitative,

objective and accurate imaging. For this purpose, we evaluated the characteristics of the Point Spread Function (PSF) of the point reflector was carried out and the results were used for measuring spatial resolution using the newly developed measuring equipment.

Methods

We used a principle based on the PSF analysis, which is a product of the measuring system we have developed. The measured sonograph scans a small metallic ball target that moves in a water bath on a specified trajectory. The bath is filled with degassed water and the walls are fitted with absorbant material. The positioning system has a ball target holder, designed according to instructions given in the IEC. The ball target consists of a small steel sphere, a laser welded to a tiny platinum wire which is fixed in a holder. The shape of the wire ensures that the sphere is oriented in front of the transducer in the scanned plane with the welding point in the distal position. The platinum wire is strong enough to eliminate any movement of the ball target during displacement in the water bath due to hydrodynamic forces. 3D positioning is arranged using three stepper motors connected to precise support screws. The motors are driven by a computer controlled power unit. The video signal from the test US scanner is driven to Frame Grabber NI PCI-1411 (National Instruments), digitalized and Region Of Interest (ROI) is stored after on-line evaluation. The system selects the video frame containing the peak amplitude for each measurement point in the scanning plane to derive the PSF function in a lateral direction centered in the pixel with the maximum amplitude. The PSF in the axial direction is obtained by the same procedure. A different method is used to record the transverse resolution. The distribution of maximum echo pixels in ROI during vertical movement of the reflection ball is recorded from each frame.

To calculate the Lateral Resolution (LR) we analyse the PSF in the lateral direction. As LR we take the width of the amplitude peak in one half of the amplitude and recalibrate for the actual amplitude level.

Values $A_{+LR}(x_+)$ and $A_{-LR}(x_-)$ are found for the following conditions:

$$x_+ > 0 \text{ and } x_- < 0$$

$$A_{\pm LR} = \frac{A_{MAX} + A_{MIN}}{2} \quad [1/255]$$

We can then express the LR corrected for difference between measured maximal amplitude A_{MAX} and maximal possible amplitude 255 digitalisation units

$$LR = (x_+ - x_-) * \frac{255}{A_{MAX}} \quad [mm]$$

A_{MAX} is a peak amplitude in PSF

A_{MIN} is minimal signal amplitude level in PSF (background noise level).

To date we have been able to plot the LR characteristic over the scanning plane. This can differentiate separate scanning lines and even multiple focal areas for dynamic focussing systems. Currently we are working on accurate side lobe estimation. Our measuring system can detect malfunctions in dynamic focussing, size of aperture, time gain compensation function and/or transducer element failure.

The method itself is not as easy or as fast to use as tissue mimicking phantoms or 3D signal to noise ratio evaluation, but it provides accurate and objective numeric parameters corresponding to the quality of image at any specified point over the whole scanning area. It is also a very powerful tool when used in combination with the other methods mentioned above.

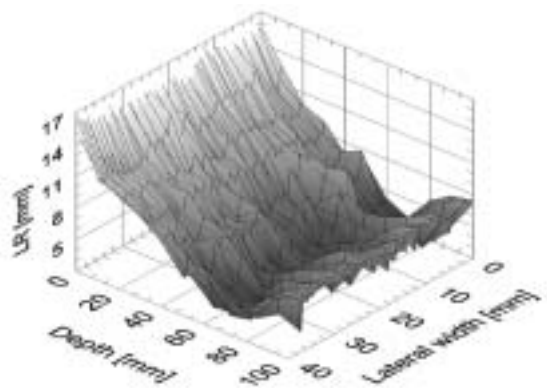


Fig. 1: LR characteristics of linear array transducer 3.5 MHz, one focal point used in depth 80 mm.

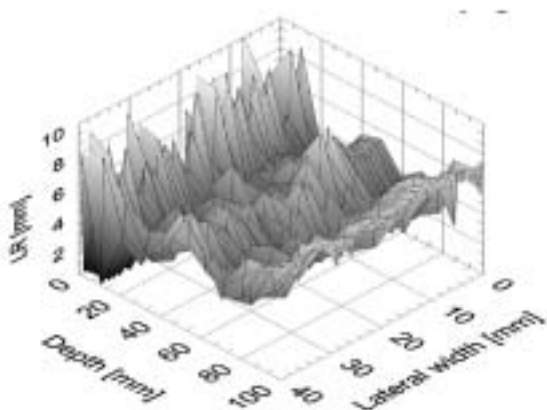


Fig. 2: LR characteristics of linear array transducer 3.5 MHz, two focal points used in depth 30 mm and 80 mm.

Results

We are able to display the shape of 2D LR distribution in the scan area of linear, convex and/or sector transducers in different working modes. The LR characteristics enable the measuring to detect analysis malfunction in dynamic focussing and size of aperture, time gain compensation function and its nonuniformity and/or transducer element(s) failure.

A sample of dynamic focussing effectivity comparison for use of one or two focal points is shown in Figs. 1 and 2. The transducer used: linear array 3.5 MHz, total imaging area of the transducer is 100 mm by 180 mm, measured area 40 mm width and 100 mm depth.

Conclusions

A number of different sonographs using various transducers have been evaluated to date with promising results. Once the accuracy and reproducibility of this system are confirmed, it will be combined together with existing methods to create a method for measuring parameters of sonograph image quality and generate a databank of qualitative parameters of sonographs of various types and from different manufacturers.

The measuring system is protected by patent application PV 2003-3425.

Our work is supported by grant KONTAKT No.: 1P2004 ME720.

References

1. Alasaarela, E., Koivukangas, J.: Evaluation of image quality of ultrasound scanners in medical diagnostics. *J Ultrasound Med* 1990;1(9):23-34.
2. Available on Internet: < <http://www.ramssoft.biz/products/ultraiq/index.htm> >
3. Available on Internet: < <http://www.4sonora.com/test/firstcall.asp> >
4. Kollmann Ch, Bergmann H, Trabold T, Zotz R. Ein Testobjekt zur Qualitätssicherung von 3D-Ultraschalgeräten. *Z Med Phys* 2001;1(11):45-52.
5. Rownd JJ, Madsen EL. Phantoms and automated system for testing the resolution of ultrasound scanners. *Ultrasound Med Biol* 1997;23(2):245-60.
6. Rozman J, Orel D, Václavík V et al. Modelová studie vyzařování ultrazvukových sond. Výsledky řešení projektu Grantové agentury ČR č. 102/00/0936, VUT v Brně, 2002. ISBN 80-214-2289-0.
7. Satrapa J, Doblhoff G. Automated quality control of diagnostic ultrasound appliances. *Ultraschall Med* 2002;23(2):123-8.

*Ing. Ladislav Doležal, CSc.,
Palacky University Olomouc,
Faculty of Medicine, Institute of Medical Biophysics,
Hněvotínská 3, 775 15 Olomouc,
Czech Republic.
e-mail: ladol@tunw.upol.cz*

NON-LINEAR MECHANICAL BEHAVIOR OF VISCO-ELASTIC BIOLOGICAL STRUCTURES - MEASUREMENTS AND MODELS

Stanislav Ďoubal, Petr Klemra, Vladimír Semecký, Jiří Lamka, Monika Kuchařová

Charles University in Prague, Faculty of Pharmacy in Hradec Králové, Czech Republic: Department of Biophysics and Physical Chemistry

Summary: Mechanical properties of biological structures affect functional ability of organism. Current knowledge is prevalently concentrated on static characteristics. The present work analyzed dynamic mechanical responses of various biological materials. Following biological structures were measured: samples of aorta walls of human origin and from model organisms, human body surface, and samples of bones of various types and origin. Linear approximation leads in case of aortas and bones to simple Voight's model. Modules of elasticity (in tensile loading) of aortas were from 10^2 kPa to 10^3 kPa. Module of elasticity of bones were from 10^6 Pa to 10^{10} Pa. Viscous coefficients of aortas were from 10^2 Pa.s to 10^3 Pa.s. Viscous coefficients of bones were from 10^0 Pa.s to 10^2 Pa.s. Nonlinearities: We found that following types of nonlinearities are significant: strain-stress relationship, time-dependent changes in elastic as well as viscose bodies. Strain and stress is well approximated by quadratic function $\sigma = a \varepsilon^2 + b \varepsilon + c$ with parameters $a = 1833$, $b = 135$, $c = 20.0$ (porcine aorta). Time-dependence in elastic coefficient: At the beginning of responses the elastic coefficient was of 42% lower then at 0.02 s of duration of the response (porcine aortas). Analogical results follow also from experiments on other structures (skin, bones).

Key words: *Biomechanics; Non-linear models; Dynamic toughness; Elasticity; Visco-elasticity; Veins; Bones; Skin*

Introduction

Mechanical properties of biological structures affect functional ability of organism. Changes in biomechanics are connected with the process of aging as well as with numerous diseases. Knowledge of mechanical behaviour of biological materials is further crucial for assessment of mechanical compatibility of artificial materials that are in mechanical contact with organism.

From the phenomenological point of view, the interrelations between mechanical stresses and corresponding deformations are used as fundamental characteristics of mechanical behaviour. An extensive bibliography exists in this field (1,9,10,13,14). Nevertheless, the works are prevalently concentrated on static mechanical characteristics of materials, namely on static deformation responses on loading or on elastic module.

The dynamics of mechanical responses is researched considerably less, in spite of the fact that biological materials (veins, bones and others) are loaded dynamically in physiological conditions. The problem is (among others) in availability of convenient experimental methodology. The currently applied apparatuses for measurement of dynamics of visco-elastic materials are, as a rule, primarily designed for measurement of industrial plastics, the appliances are

expensive and (more or less) unfit to the measurement of biological materials. The unavailability of convenient instruments results also in unsatisfactory knowledge of non-linear behavior of biological structures in static regime and in virtually no knowledge of dynamic nonlinearities.

With regard to this fact, the dynamic biological elastometer was designed and tested in our laboratories. The apparatus enables measurement of static as well as dynamic deformation responses of biological materials, including veins, in tensile, pressure, or torsion loadings. The appliance is based on innovated version that is described in our previous papers (3,6,7). The application scope of the device includes also identification of linear dynamic models and further also determination of non-linear character of parameters of biological mechanical systems.

In our previous research, the mechanical parameters of following biological structures were measured: samples of aorta walls of human origin and from model organisms (4), human body surface (skin) *in vivo* (2,5) and samples of bones of various types and origin.

In physiological range of loadings, the structure of rheological models of aorta walls and bones corresponds to simple Voight's model (Fig. 1). Modules of elasticity of Hooke's (H) bodies of aorta walls were of order from 10^2 kPa to 10^3 kPa and viscous coefficients of Newton's bodies

(N) were of order from 10^2 Pa.s to 10^3 Pa.s, in case of linear approximation. Modules of elasticity of bones were of order from 10^6 Pa to 10^9 Pa, viscous coefficients of bones were of order from 10^0 Pa.s to 10^2 Pa.s, also in case of linear approximation.

The structure of rheological model of human skin consists of combination of two Voight's structures (Fig. 2). Time constant of dominant structure (corresponding to about 90% of static deformation) was in interval from 10^{-2} s to 10^{-1} s, time constant of secondary structure was of two orders slower.

Mechanical behavior of biological structures is generally non-linear. The nonlinearities of type hysteresis, non-sensitivity, saturation, Bingham's liquid, St. Venant's body etc. are mentioned in theory of visco-elasticity. Nevertheless, in our experiments we found that only following three types of nonlinearities influence the mechanical behavior of structures under study: strain-stress relationship (mainly in aorta walls), time-dependent changes in elastic as well as viscous bodies during mechanical dynamic response.

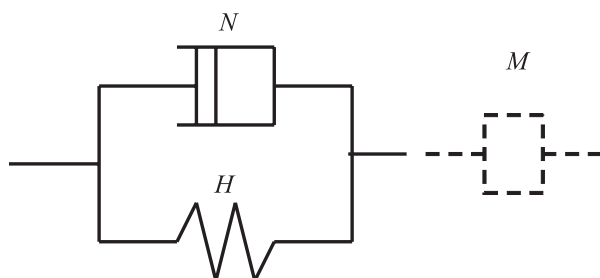


Fig. 1: Structure of linear rheological model of aorta walls and bones (full line). Inertial body (dotted line) represents the aggregate mass of moving part of mechanical system.

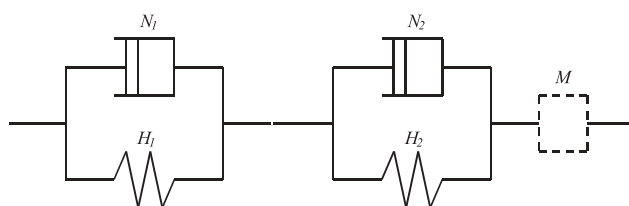


Fig. 2: Structure of linear rheological model of human body surface.

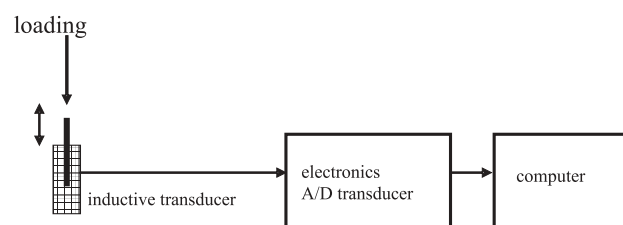


Fig. 3: Block diagram of the appliance.

As the non-linear nature of mechanical behavior of biological structures (notably veins) is often crucial for many aspects, and virtually unknown, we will further deal with this topic in more detail.

Methods

Measuring appliance

Applied version of the apparatus (Fig. 3) enables measurement of samples of material (length 5–50 mm, width 1–10 mm) in tensile stress. In pressure and torsion loadings it is possible to measure samples of length in range from 10 mm to 50 mm, the cross section area of samples is of range from 1 mm^2 to 100 mm^2 . Samples are fixed and connected with gauge (mass of gauge is 12.6 g). Changes of deformation are detected by means of inductive transducer (coil with moving ferromagnetic rod inside). The weight of gauge represents the minimal initial loading of samples (Figs 1 and 2, element *M*). The deformation force is produced by inserting weights on a pan on the top of the gauge (electronically or manually) or, in case of impulse characteristic, is generated by quick “knock” on the gauge. The signal from transducer is processed by electronics, amplified, transformed to digital form by A/D transducer and processed in computer. The time constant of electronics is 1.25 ms. Minimal detectable change of deformation is about $2 \text{ }\mu\text{m}$, it depends on the level of interfering random errors (mainly due to vibrations and electromagnetic disturbances).

Material

a) Aorta walls

Samples of walls of porcine *aorta thoracica* obtained from young 18 pigs (6 months, male, *Sus scrofa f. domestica*) in transversal (circumferential) direction were measured in two successive series. The aim of first series (10 aortas) was to verify methodology. In the second series, 8 aortas were examined using standard procedure. In the following text, the results of second series are described.

Further, samples of walls of human aorta (*pars thoracica*, 5 men, 8 women, age from 37 to 78 years) and samples of walls of aorta of 8 young pheasants (*Phasianus spp.*, hen, age 3 months) were measured, also in transversal direction.

b) Bones

Samples of bones (*caput femoris, substantia compacta*, human cadavers, 2 men, 7 women, age from 52 to 79 years) maintained for several weeks in conservation solution were measured. Measurements were performed on grindings ($35 \times 8 \times 8 \text{ mm}$) in flexion and torsion strains.

Further samples of pheasant scapula (*Phasianus spp.*, hen, age 3 months) were measured immediately after sacrificing animals. Whole bones were measured in flexion strains.

c) Humen skin *in vivo*

Two groups consisting of 15 men and 27 women (age range from 20 to 58 years) were used in experiment. The deformation response was measured on the left palm (above the middle of *abductor pollicis brevis*) in pressure strain.

Results

a) Non-linearity in static regime

The results of experiments on human aortas proved to be close to analogical results on pigs. Consequently, the porcine aortas seem to be good model of mechanical behavior of human veins. Above it, in case of pigs, we used more extensive and more homogenous set. Therefore, the results obtained on the basis of measurement of porcine aortas are presented in following text.

The relationships between strain and stress (Fig. 4) was derived on the basis of steady state levels of transient characteristics. Nonlinearity of the relation was proved by statistical test of sequential differences (s.l. = 0.05). For the data shown, the relation is well approximated by quadratic function $\sigma = a \varepsilon^2 + b \varepsilon + c$ with parameters $a = 1833 \pm 449$, $b = 135 \pm 75$, $c = 20.0 \pm 2.6$.

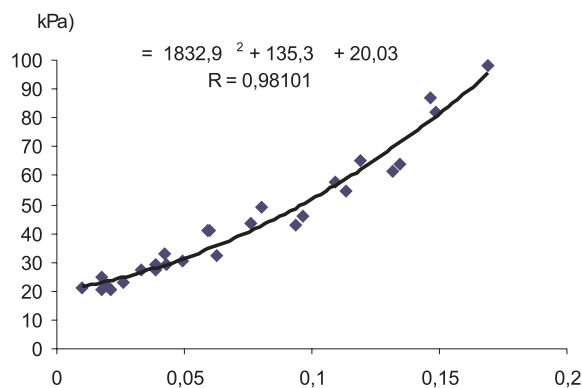


Fig. 4: Relationships between deformation and loading in transversal (circumferential) direction in pig aortas (pigs 6 months, males). The grey area indicates interval of loadings corresponding to physiological range of pressures inside aorta.

b) Non-linearity in dynamic regime - dependency of elastic element on time during deformation response.

At the beginning of responses the value of the elastic coefficient (Fig. 1, element H) was, in average, of 42% lower than at 0.02 s of duration of the response (in case of porcine aortas). The difference is statistically significant for s.l. = 0.01 (proved by Student's t-test). The lower interval estimate of the difference of means assures the minimum change 20 % ($p = 0.95$). It seems to be probable that the magnitude of elastic coefficient is asymptotically increasing with time to the level in steady state. Analogical results follow also from experiments on human and pheasant aortas.

Similar tendency was found in case of elastic element of pheasant scapula (increase 10%) and human skin (increase 60 %). On the contrary, elastic element of samples of bones (*caput femoris*) maintained in conservation solution was constant during dynamic response.

c) Non-linear behaviour of viscose element

Analysis of dynamic responses indicates non-linear behavior of viscose elements in all experiments, with exception of human bones maintained in conservation solution. Preliminary results suggest the decrease of the value of viscose element with the increasing strain and probably also with duration of the response.

Discussion

The aim of presented work is to contribute to better understanding of mechanical behavior of biological materials. Especially, we focused on non-linear dynamics of mechanical responses.

In static regime, we found that the strain-stress curves of aorta walls may be approximated by quadratic function. In other words, we found that differential elastic module decreases linearly with stress. The toughness increases distinctly if the pressure inside aorta exceeds physiological levels. Albeit the non-linear nature of static response of is known and in some extent described, we elucidate this phenomenon in more details. This finding is important, among others, for the study of hypertension.

We believe that the time-dependent character of mechanical parameters of biological materials has not been described till now. This phenomenon, consisting in growing toughness during dynamic response, may be important for biomechanics in general and especially for understanding of principles of biophysics of circulatory system.

Obviously, the more detailed study is necessary in future. Also the elucidation of structural and molecular background of this phenomenon remains to be found.

Conclusion

The appliance for dynamic measurements of biological materials enables to obtain more detailed information on biomechanics and thus contribute to progress in this field.

Study was supported by grant J13/98MSM111600002.

References

1. Collins R, Hu CL. Dynamic Deformation Experiments on Aorta Tissues. *J Biomechanics* 1972;5:333-5. 5
2. Doubal S, Klemra P, Procházková M. Viskoelastické parametry lidské kůže - měření a perspektivní aplikace v gerontologii a kosmetice. *Lékař Technika* 2003;34(4):137-44. 11
3. Doubal S, Klemra P. Aparatura pro měření křivek toku viskoelastických materiálů. *Lékař Technika* 2001;32(4):95-9. 8
4. Doubal S et al. Dynamika deformační reakce cévních stěn na mechanické zatížení. *Lékař Technika*, zasláno do tisku 2004. 9
5. Doubal S, Klemra P. Visco-elastic response of human skin and aging. *J Amer Aging Assoc* 2002;25(3):115-7.10

6. Ďoubal S. Identifikace rheologických parametrů viskoelastických těles, Čs Farmacie 2000;49(3):124–30. 7
7. Ďoubal S. Rheologické modely biologických materiálů - identifikace a výpočet parametrů. Lékař Technika 200;31(2):50–4. 6
8. Eykhoff P. System identification, parameter and state estimation. New York: John Willey and Sons, 1974:242–54. 14
9. Holzapfel GA, Gasser TC, Ogden RW. A new constitutive framework for arterial wall mechanics and a comparative study of material models. J Elasticity 2000;61:1–48. 3
10. Komárek P. Mechanical properties of tissues of the cardiovascular system. In: Biomechanics (Ed.:Valenta J.), Praha: Academia, 1993:142–79. 1
11. Kubík S, Kotek Z, Šalamon M. Teorie regulace II. Praha: SNTL, Praha, 1969: 77–199. 13
12. Kubík S, Kotek Z, Šalamon M. Teorie regulace I. Praha: SNTL, 1968:22–39. 12
13. Monos E. Venous biomechanics: Physiology and measurement. J Cardiovascular Diagnosis Procedures 1972;13(2):147–154. 2
14. Steinman DA, Vorp DA, Ethier CR. Computational modeling of arterial biomechanics: Insights into pathogenesis and treatment of vascular disease. J Vasc Surg 2003;37(5):1118–28. 4

***Prof. RNDr. Ing. Stanislav Ďoubal, CSc.,
Charles University in Prague,
Faculty of Pharmacy in Hradec Králové,
Department of Biophysics and Physical Chemistry,
Heyrovského 1203, 500 05 Hradec Králové,
Czech Republic.
e-mail: doubal@faf.cuni.cz***

MECHANICAL PROPERTIES OF SELFEXPANDABLE STENTS

Josef Hanuš, Jiří Záhora

Charles University in Prague, Faculty of Medicine in Hradec Králové, Czech Republic: Department of Medical Biophysics

Summary: The stents or stentgrafts (covered stents) are the medical instruments used in invasive radiology for miniinvasive treatment of stenosis and aneurysms especially in the blood circulation system. We measured and compared the mechanical parameters of different selfexpandable Nitinol stents, which differed in the geometry (radius and length), in the type of construction (number of branches and rising of winding) and in the diameter of the used wire. The results of measurements confirmed the theoretical assumptions that just the diameter of the Nitinol wire significantly influences the rigidity and the level of compressibility of the stent as well. The compromise must be found between the required rigidity of the stent and the minimal size of the delivery system. The exact description of the relation between the mechanical properties and geometry and construction of the stents enables us to design the stent to fit the patient's needs. The results of measurement are also necessary for the design and identification of the parameters of the models of the stents.

Key words: *Stent; Mechanical parameters; Strain-stress curve*

Introduction

The miniinvasive implantation of stents or stentgrafts for various indications is a very quickly developed sophisticated trend in medicine (1,2). These methods are used for correction of aneurysms or stenosis in the cardiovascular system, for correction of limited passage in the digestive system, in the urinary tract or in the biliary duct. The minimal traumatization of the patient, the improvement of the life comfort, shorten of the patient's stay in the hospital are the typical advantages of these methods. But on the opposite side also some disadvantages can occur, typically the leakage or the shift of stent, limited chemical resistance of the materials of the stents. We suppose that the main reason of these problems is that the mechanical properties, dimension and the dynamical properties of the stent do not correspond to the properties of the vessel or generally of tissue where this stent is implanted. That is the reason, why we want to identify and to describe these relations between the mechanical properties of stents and tissues. Our originally developed device for measurement of mechanical properties of stents or vessels and results of measurements of selfexpandable Nitinol stents and short reference to their chemical resistance are described in this paper.

Chemical resistance

The stents are designed for the long time implantation so that the chemical interaction with the inner environment

of the human body is expected. This long time interaction (at least 10 years) is substituted by experiments that simulate the expected corrosion in the real time. The electrochemical degradation tests (according to ISO/DIS 10993-15/2000) were applied for the evaluation of the resistance of Nitinol and steel wires, the typical material for the construction of stents. The special solution of electrolytes simulates the inner environment of the body, in our case the blood plasma+oxygen, but also the artificial saliva can be used. The level of corrosion of different material is given in the figures 1 (laboratories of Technical University of Ostrava). There are many parameters that characterize the chemical resistance of materials but the pictures are the most illustrative for the first information. Results show the different corrosion level of tested material that depends not only



Fig. 1: Wire in the artificial plasma (exposition 160 min.).

on the chemical composition and the surface protection but also on the technology of processing that can be different according to the producer.

Measuring system

The developed original measuring system allows measurement of mechanical properties of stents, measurement of strain-stress curves or simulation of radial and axial deformation. We designed two arrangements of measuring systems, the measurement of the stent response to the axial and to the radial deformation. In case of radial deformation the device consists of hermetically closed plastic glass vessel in which the stent is placed in the distilled water or in the air. The stent is joined to the system of the tubes with the valves. The temperature of water can be held on constant value or its course can be defined by using the accurate thermostat with cooling for fast response. The tubes can be closed or opened by the valves so that the defined pressure of peristaltic pump affects the wall of stent. The expansion and the compression of the stent can be simulated in this way. Pressure course and corresponding change of stent radius are on-line measured by the probes connected to the computer. The original contactless method of measurement of the stent radius is based on the on-line processing of the digitalized image from the video camera (Topica TP 606D/3) by using the NI program. The axial prolongation of the stent is measured by the accurate linear potentiometer (position sensor) that is directly bounded with the screw of the positioning system that is used for longitudinal deformation. The axial force for longitudinal deformation is measured by the dynamometer that is connected directly to the positioning device. All measurements are on line controlled and processed by the LabVIEW software and hardware platform. The schematic diagrams of the measuring system in the arrangement for the measurement of radial forces, dynamic measurement and simula-

tion and in the arrangement for axial (longitudinal) forces measurement are given in the figures 2.

Method of measurement

The mechanical response of selfexpandable spiral Nitinol stents of the same design and different geometry was compared. The spiral stents are knitted from one Nitinol wire and can be described as a set of horizontally and vertically shifted spirals (springs). Measured stents differ in the diameter of Nitinol wire and in the rising of the winding. Number of single left and right spirals (number of the left and the right arms of stent) is common. We measured and compared stents, which differed only in one from above mentioned two parameters. From the practical point of view it is technically simpler to generate the axial force for deformation of stent instead of the radial force. It is very important from this reason to know the relation between the effect of radial and axial forces. We suppose for measurement that the result deformation doesn't depend on the type of functioning force (axial or radial) or that the relation between radial and axial forces effect is exactly given. This assumption we can verify experimentally by measurement of both arrangements of measuring device (see figure 2). All parameters of stents (diameter, length, temperature, axial force) are measured on-line simultaneously and repeatedly with given sampling frequency (typically 1 s). Nitinol stent follows some properties, which correspond with the exclusive behavior of Nitinol, especially its superelasticity (3). Nitinol can exist in two phases, soft martensite for the lower temperature and hard austenite for the higher temperature. The temperature of transformation is given not only by the composition but also by the stress of stent. We must also study the relation between the strain-stress curves course and temperature from these reasons. All measurements were done for the laboratory and the body temperature.

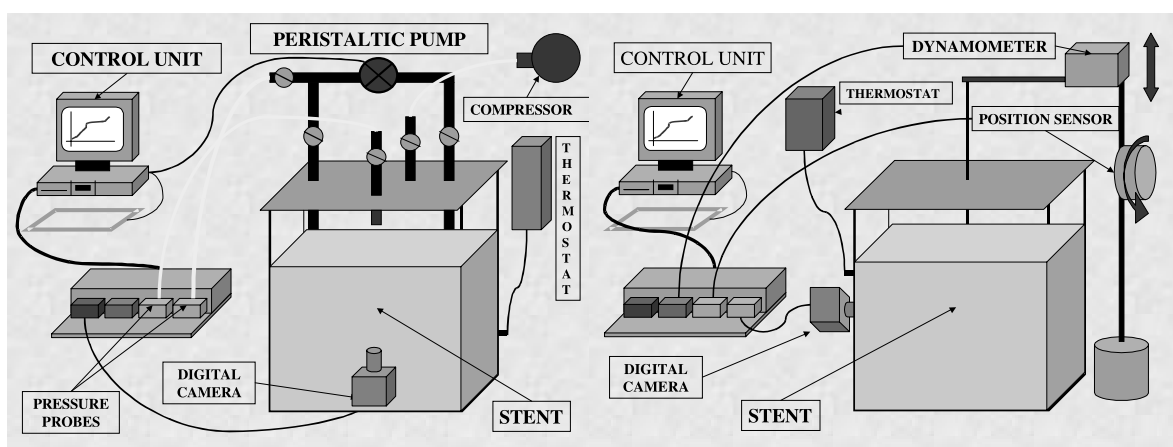


Fig. 2: Measuring system (a - arrangement for measurement of deformation by radial force, b - arrangement for measurement of deformation by axial force).

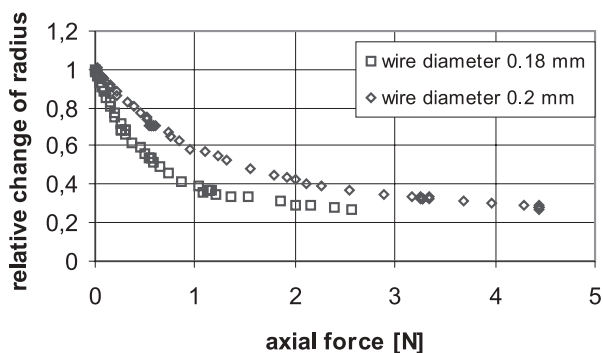


Fig. 3: Strain-stress curves of Nitinol stent for different wire diameter. The effect of axial force to radial deformation is illustrated.

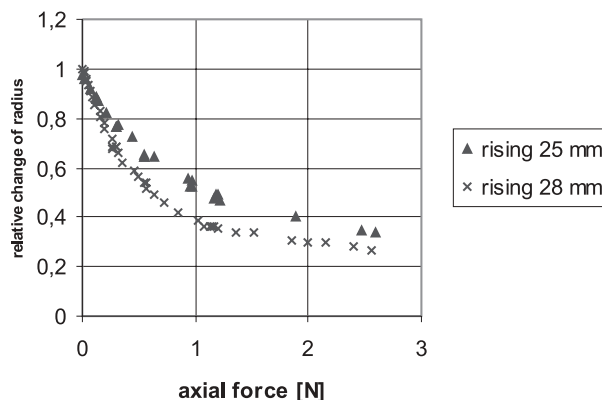


Fig. 4: Strain-stress curves of Nitinol wire for different rising of windings. The effect of axial force to radial deformation is illustrated.

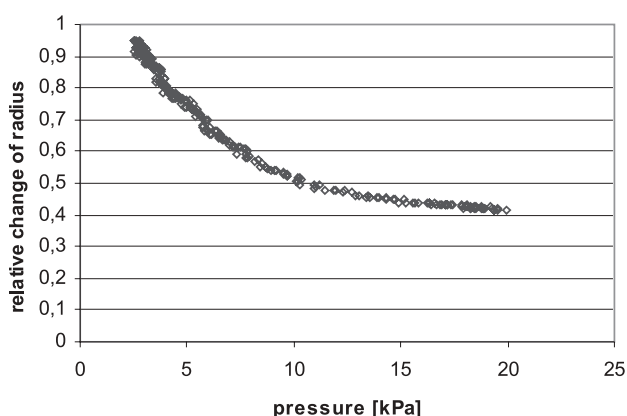


Fig. 5: Strain-stress curve of Nitinol stent. Effect of radial force (pressure) to radial deformation is illustrated.

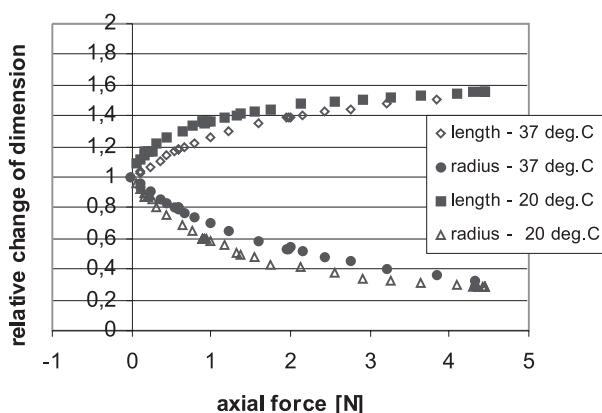


Fig. 6: Strain-stress curve of Nitinol stent. Effect of the temperature to the radial and axial deformation is illustrated.

Results of measurement

We compared the results of measurement of Nitinol stents with these parameters:

Diameter of Nitinol wire: 0.2 and 0.18 mm

Number of left and right arms of stents: 12 left arms + 12 right arms (arm = single spiral)

Rising of winding: 25 mm and 28 mm (distance between successive coils of the single spring)

Geometry of stents: diameter 16 mm, length 72 mm or diameter 12 mm, length 77 mm

Temperature of environment: laboratory temperature (approx. 20 °C) and body temperature 37 °C

We combined for measurements pairs of stents that differ only in one parameter, in diameter of Nitinol wire or in the rising of windings. Absolute value of diameter and length of the stents are not important because the deformation of the stent can be expressed as the relative change of the original size. The figure 3 illustrates the effect of axial force to the radial deformation of the stents with different diameter of Nitinol wire. The figure 4 illustrates the same type of de-

formation for two stents with different rising of windings. The figure 5 illustrates the relative radial deformation of the stent caused by the radial force (outside pressure) and at last the figure 6 describes the influence of the temperature to the radial and axial deformation of stent.

Conclusion

The originally developed measuring system and methodology were successfully tested for measurement of mechanical properties of Nitinol selfexpandable stents. System allows according to its arrangement the generation of defined course of axial and radial forces functioning to the stent or biological system. The set of sensors and probes allows the accurate contactless measurement of strain; it means the radial and the axial deformation of stressed system. The experiments cleared some mechanical characteristics of tested stents and also confirmed the theoretical assumptions concerning the relation between the geometry and the construction of stent and its mechanical performance. For instance the relation between the radius and

length changes enables us to estimate exactly the real length of stent after its pushing out from the delivery system and its expansion into the vessel. The measurements also confirmed theoretical assumption (4,5) that the suitable choice of the diameter of wire is the best way of setting of required rigidity of the stent because the spring stiffness is directly proportional to fourth power of the diameter of the wire. It is necessary to accent on the opposite side that the diameter of the wire limits minimal size of the delivery system.

References

1. Duda SH. Physical properties of Endovascular Stents: An Experimental Comparison. *J Vasc Intervent Radiol* 2000 ;**11**:645-54.
2. Dyet JF, Watts WG, Ettles DF. Mechanical properties of metallic stents: How do these properties influence the choice of stent for specific lesions? *CardioVasc Intervent Radiol* 2000;**23**:47-54.
3. Shabalovskaya SA. On the nature of the biocompatibility and on medical applications of NiTi shape memory and superelastic alloys. *Biomed Mater Eng* 199;**6**(4):267-89.
4. www.efunda.com/designstandards/springs/
5. physics.uwstout.edu/statStr/Strength/Columns/cols75

*Doc. Ing. Josef Hanuš, CSc.,
Charles University in Prague,
Faculty of Medicine in Hradec Králové,
Department of Medical Biophysics,
Šimkova 870, 500 38 Hradec Králové,
Czech Republic.
e-mail: Hanus@lfhk.cuni.cz*

STANDARDISATION IN ULTRASONOGRAPHY: PRINCIPLE AND DIAGNOSTIC SIGNIFICANCE

Zuzana Hlinomazová¹, Ivo Hrazdira²

Masaryk University of Brno, Faculty of Medicine, Czech Republic: University Hospital Bohunice, Eye Clinic¹; St. Anna University Hospital, Clinic of Imaging Methods²

Summary: Disadvantage of ultrasonography is its dependence on subjective assessment of displayed images. The way how to minimize both intraobserver and interobserver differences is creation of standard conditions for examination including a quantitative approach to evaluation of tissue reflectivity. The oldest mode of standardisation is standardised A- scan, used in ophthalmology. It enables differentiation of echoes, reflected from different ocular structures and is helpful in assessment of extraocular muscle thickness. Standardisation of B- scan depends on the type of diagnostic device and is based on quantification of image echogenicity. In our study reference values of grey-level histogram were established for some thyroid diseases using standard setting of imaging parameters. Results indicate that both standardised A- and B- scan should be helpful in differential diagnostics.

Key words: Standardised echography; Ultrasonography; A- scan; B- scan; Echogenicity

Introduction

Evaluation of sonograms is based on subjective assessment of displayed image. Unequal values of image parameters (brightness, contrast, structure, homogeneity) may lead to intraobserver and mainly interobserver differences in image interpretation. Many attempts struggled to overcome this disadvantage by standardising the conditions of examination. Standardisation allows every examiner to obtain the same echogram when examining the same type of tissue and to achieve repeatable and comparable results. Standardisation is relatively easy in one-dimensional A- scan, depending mainly on the form of tissue-echo amplification. The standardised A- scan is hitherto used in ophthalmology. Standardisation of B- scan is more complicated, because the image quality depends on numerous parameters. The aim of this study was to accentuate the parameters of ultrasound image standardisation and assess its clinical significance.

Standardised A- scan

This mode is used in ophthalmology only. Eye tissues in comparison to other human tissues have relative low attenuation. This enables application of high frequencies (10–20MHz) and achievement of higher axial and lateral resolution. Besides of 2D and 3D imaging ophthalmology as a single medical branch exploits also A scan, firstly in

the standardised form. This consists in usage of a special „S“shaped amplification curve enabling the optimal displaying of tissue echo. The optimal dynamic range for imaging of eye structures is 65 dB. Increasing this value by 6 dB is necessary for imaging of very tiny opacities in aqueous humour. Lowering this value by 24 dB enables to imagine very low echoic structures (3). The term of standardised A- scan have been introduced in ophthalmologic examination by Ossoinig (10,11). „S“amplification is for displaying of ocular echoes more advantageous than linear or logarithmic ones. Examination in standardised A- scan involves a special ultrasound device. The first ultrasound machine for standardised A- scan was 7200MA (Kretztechnik) with an 8MHz transducer, one of its successor is Ophtascan S (Biophysics Medical) using a 10MHz probe. Actually the standardised A- scan is combined with the B- scan. The two-dimensional B- scan renders synoptic images of the eye and orbit and determines planes for detailed examination (1,3). Standardised A- scan is used preferably for reflectivity assessment enabling differentiation of various ocular lesions (retinal detachment, tumour, foreign body). Particularly useful is standardized A- scan in examination of extraocular muscles (2,9,12) and of optic nerve (5). In evaluation of extraocular muscles results of measurement with ultrasound are comparable to those with MRI (2).

Figure 1 shows standardised A- scan of a physiological internal direct muscle. Fig. 2 represents a standardised A- scan of a malignant melanoma of uvea. Figures 3 and 4

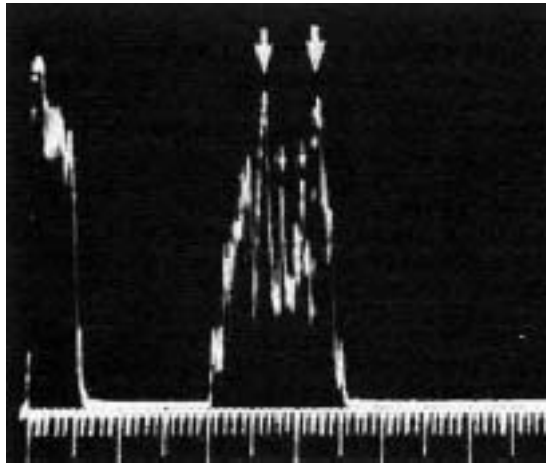


Fig. 1: Standardised A-scan of an oculomotor muscle (great arrows). Small arrows denote the reflectivity of real muscular tissue – physiological state.

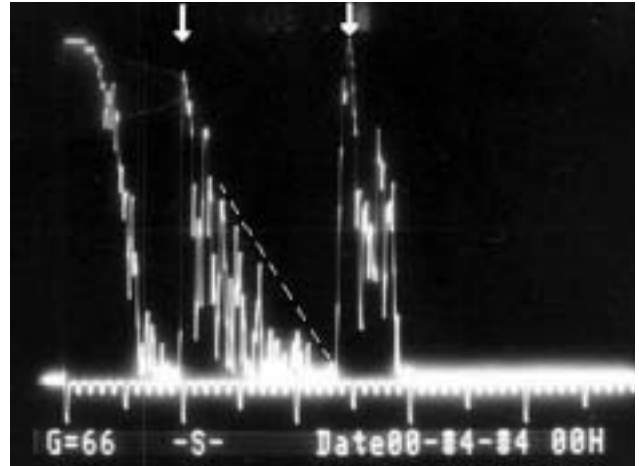


Fig. 2: Standardised A-scan of a malignant melanoma of uvea (arrows). Middle reflectivity with pronounced attenuation (---).

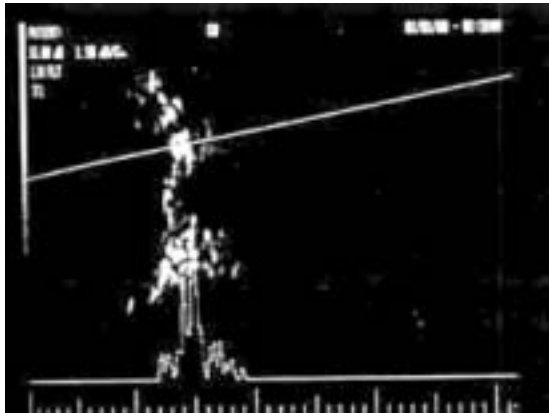


Fig. 3: A- and B-scan of a normal orbit.

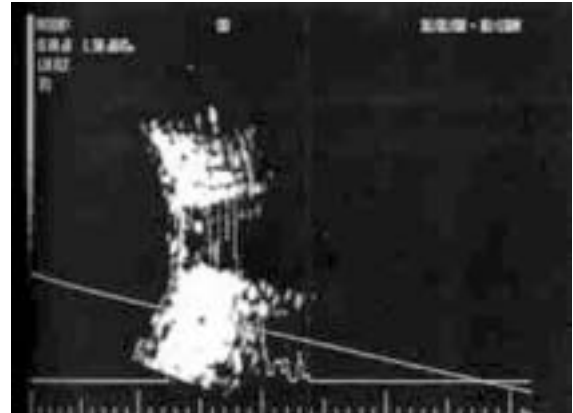


Fig. 4: A- and B-scan of an orbit with higher reflective orbital fat.

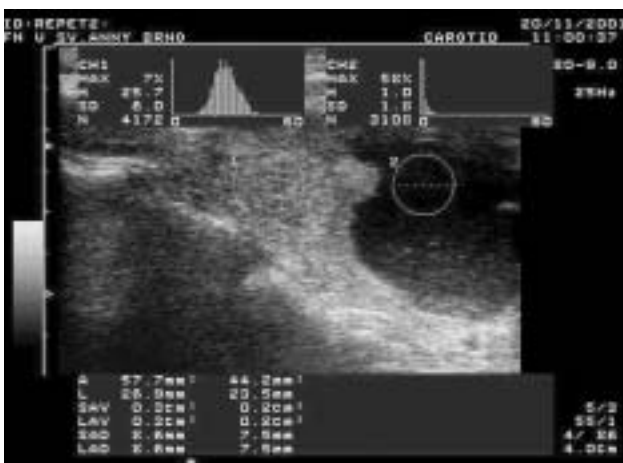


Fig. 5: Grey-level histogram of a thyroid cyst in comparison to a normal thyroid tissue.

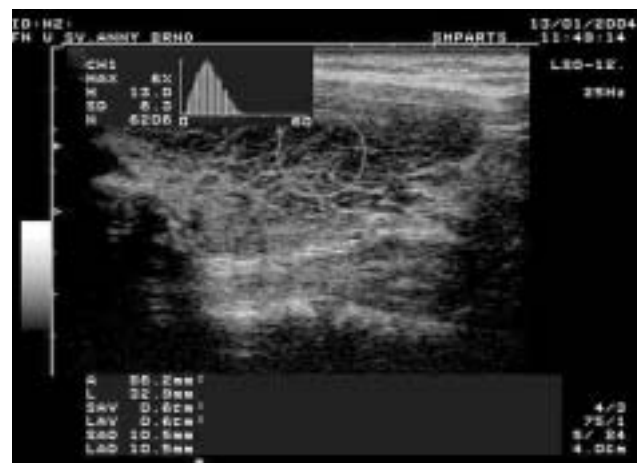


Fig. 6: Grey-level histogram of Hashimoto's thyroiditis.

demonstrate superposed A- and B- scan of the orbit with normal and increased reflectivity of orbital fat.

Standardised B- scan

B- scan is actually used as a common imaging method for examination in many branches of medicine, including ophthalmology. Its advantage is a rapid topographic and structural orientation in the examined region. In distinction to standardised A- scan based on a single echo imaging, the B- scan image is formed by summation of multiple echoes in the given plane and standardization covers several parameters such as brightness, contrast, structure and homogeneity. For standardisation purpose the application of statistical methods is essential. The quantitative approach is based on texture analysis. A simple, but most frequently used method is the assessment of echogram by means of grey-level histograms. The echogram texture is characterised by mean grey value of calculated pixels, its standard deviation and graphical representation of grey level. However, these techniques do not offer the possibility of assessing the relationship between neighbouring pixels. The method is appropriate especially for distinguishing regions with different echogenicity and homogeneity, and was applied mainly in examination of thyroid (4,8). Fig. 5 represents grey-scale histograms of 2 regions of the thyroid gland with different echogenicity and fig. 6 echogram of the same organ with completely inhomogeneous structure.

Clinical benefit

Together with the technical development of ultrasound diagnostic devices their resolving acuity improves. New machines exploiting computer technology are equipped with new imaging modalities enabling better imaging of tissue echoes.

All attempts for standardisation in ultrasonography are connected with several problems:

1. Adjustment of standard conditions is limited to device used.
2. Standardisation requires great examiner's experience.
3. Setting up of reference values needs application of statistical methods.

The main clinical significance of standardised A- scan consists in differential diagnostics of ocular and orbital tumours, retinal detachment and foreign bodies' identification. However, the correct assessment of A- scan images involves great experience, and therefore the A- scan in the last time should be replaced by new modalities of B- scan with special transducers operating at high frequencies.

The standardised B- scan is based on statistical processing of ultrasound image texture. As an example of this procedure the application of grey-level histogram for echogenicity assessment of thyroid lesions may serve. For this study the ultrasound machine Toshiba Powervision 6000 with a linear 12 MHz transducer at a dynamic range of 84

dB was used. Results of statistical analysis of 200 grey-level histograms of 80 patients are presented in table 1.

Differences in echogenicity between normal thyroid tissue and various thyroid lesions were highly statistically significant ($p > 0.01$). However, we do not confirm literature data indicating that grey-level histograms may be helpful in differentiation between benign and malignant lesions. (6). In our group of patients these differences were not statistically significant. Distinguishing between benign and malignant lesions requires application of more sophisticated statistical methods. We do not agree with the findings that the level of echogenicity may influence the width of histogram (7). In our opinion the width of histogram is function of tissue homogeneity.

Tab. 1: Standardised grey-level values for different thyroid diseases.

Normal thyroid (25)	
Mean grey-level	22.6 (18.5–26.7)
SD	4.2
Adenoma (20)	
Mean grey-level	18.5 (15.4–19.8)
SD	5.3
Carcinoma (15)	
Mean grey-level	17.3 (13.6–20.1)
SD	5.2
Hashimoto (20)	
Mean grey-level	13.3 (9.3–16.4)
SD	5.6

Conclusion

Standardisation of A- and B- scan ultrasonography helps in establishing constant parameters for examination. This leads to reduction of subjective differences in image assessment and thus to improvement of diagnostic accuracy.

References

1. Byrne SF. Standardized echography of the eye and orbit. *Neuroradiology* 1986;28:618–40.
2. Demer JL, Kerman BM. Comparison of standardized echography with magnetic resonance imaging to measure extraocular muscle size. *Am J Ophthalmol* 1994;118:351–61.
3. Hlinomazová Z. Místo a význam ultrasonografie v diagnostice endokrinních orbitopatií. Dissertation. Faculty of Medicine, Hradec Králové, 1999:108pp.
4. Hrazdira I. Mohou histogramy sedí přispět k přesnější interpretaci ultrazvukových obrazů? *Čes Radiol* 2003;57:72–4.
5. Haritoglou C, Herzum H, Ehrh O, Ossoinig KC, Kampik A. Echographic differential diagnosis of optic nerve widening. *Ophthalmologie* 2002;99:559–65.
6. Kitaoka F, Sakai H, Kurda Y et al. Internal echo histogram examination has a role in diagnosing malignant tumors from benign masses in the breast. *Clin Imaging* 2001;25:151–3.
7. Maeda K, Utsu M, Kihai PE. Quantification of sonographic echogenicity with grey-level histogram width: a clinical tissue characterization. *Ultrasound Med Biol* 1998;24:225–34.
8. Mazziotti G, Sorvillo F, Iorio S et al. Grey-scale analysis allows a quantitative evaluation of thyroid echogenicity in the patients with Hashimoto's thyroiditis. *Clin Endocrinol* 2003;59:223–9.
9. Pierro L, Zaganelli E, Tavola A, Muraglia M. Extraocular muscle size comparison between normal and myopic eyes using standardized A scan echography. *Ophthalmologica* 1998;212(suppl 1):22–4.

10. Ossoinig K. Ein neues Gerät für die klinische Echo-Ophthalmographie. In M. Masin and J. Poujol (Eds.) Diagnostica Ultrasonica in Ophthalmologia. Paris: Proceedings of SIDUO IV, 1971:131-7.
11. Ossoinig KC. A new echographic sign for the reliable diagnosis of Graves's disease (in German). Klin Monatsbl Augenheilkd 1982;180:189-97.
12. Sacca S, Polizzi A, Macri A, Patrone G, Rolando M. Echographic study of extraocular muscle thickness in children and adults. Eye 2000;14:765-9.

***MUDr. Zuzana Hlinomazová, Ph.D.,
Křídlovická 16a, 603 00 Brno,
Czech Republic.
e-mail: zhlinom@fnbrno.cz***

SPECTRAL CHARACTERISTICS OF THE SUPRAMOLECULAR COMPLEXES OF POLYPYRROLIC SENSITIZERS AND CYCLODEXTRIN CARRIERS: USAGE IN PHOTODYNAMIC THERAPY OF TUMORS

Martin Huf¹, Hana Kolářová¹, Robert Bajgar¹, Jaroslav Maceček¹, Marek Tomečka¹, Pavla Nevřelová¹, Jiří Mosinger², Pavel Tomek³, Miroslav Strnad⁴

Palacky University Olomouc, Faculty of Medicine, Czech Republic: Institute of Medical Biophysics¹; Charles University in Prague, Faculty of Science, Czech Republic: Institute of Inorganic Chemistry²; Palacky University Olomouc, Faculty of Science, Czech Republic: Institute of Experimental Physics³, Laboratory of Growth Regulators⁴

Summary: The objective of our work was to describe the photophysical properties (absorption and fluorescence) of the sensitizers TPPS₄, ZnTPPS₄ a PdTPPS₄ and above all the complexes of these sensitizers with cyclodextrin carriers HP- α -CD, HP- β -CD and HP- γ -CD (2-hydroxypropyl- α , β , γ -cyclodextrin) in a suitable environment for the cultivation of cancerous cell lines, and to determine the optimal radioactive conditions for maximizing photodynamic effects in cancerous cells.

Key words: Polypyrrolic sensitizer; Cyclodextrin carrier; PDT; Absorption spectrum; Fluorescence spectrum

Introduction

Photodynamic therapy (PDT) has lately been involved in the treatment of oncological, cardiovascular, skin and eye diseases. PDT is founded on the use of sensitizers, which have a longer retention time in cancerous cells. During the photoactivity of sensitizers, using visible radiation of suitable wavelength, the generation of cytotoxic material is occurred which leads to irreversible damage in cancerous cells. In contrast to conventional treatment methods (surgery, radiotherapy and chemotherapy) PDT allows selective removal of cancerous cells without damaging the surrounding healthy tissue (1,2,7,8).

Today the quite often used sensitizer is Photofrin II. This sensitizer is one of the so-called „first generation sensitizers“, which sets the standard for its class. Above all it's selectivity is too narrow. Furthermore, thanks to it's narrow extinction coefficient it is necessary to use a large amount of the sensitizer to achieve a photodynamic reaction.

The above mentioned problems lead to the creation so-called „second generation sensitizers“. This includes porphyrin, phtalocyanines, naphthalocyanines, chlorins, and also polypyrrolic sensitizers TPPS₄, ZnTPPS₄ a PdTPPS₄. „Second generation sensitizers“ are considerably more selective which enhances the effectivity of PDT (3,5,6). Naturally they are hydrophobic, so they dissolve poorly in water. This problem can be solved by the use of a suitable

sensitizer carrier (polymer particles, liposomes, antibodies, etc.).

Cyclodextrins (CD) are currently under intensive study as one of the suitable carriers for this entire class of medicine, and also of photodynamically active materials. Cyclodextrins are cyclic oligosacharades, compounded of 6, 7 a 8 (α , β α γ) a - 1, 4-D - glucopyranose units. Photodynamically active materials are bound in the cyclodextrin cavity with the help of hydrophobic and van der Waals forces. This binding with the CD allows a hydrophobic sensitizer to be transported in a water based medium. CD also has a significant monomerization effect, which inhibits the aggregation of sensitizers and increases the quantum yield and life span of the excited state of the sensitizer (4).

Material and methods

The absorption spectra of the cultivation medium (DMEM), the selected solution of porphyrin sensitizers TPPS₄, ZnTPPS₄ and PdTPPS₄ and these sensitizers with cyclodextrin carriers HP- α -CD, HP- β -CD and HP- γ -CD were measured with spectrophotometer UNICAM UV 550. Fluorescent spectra were obtained with the use of spectrofluorometer HITACHI F4500. The cultivation medium was used as the solvent. The concentration of the sensitizer was 10 μ M, cyclodextrin carrier was 1 mM, thus cyclodextrin was compared with the sensitizers in hundredfold concentration excess.

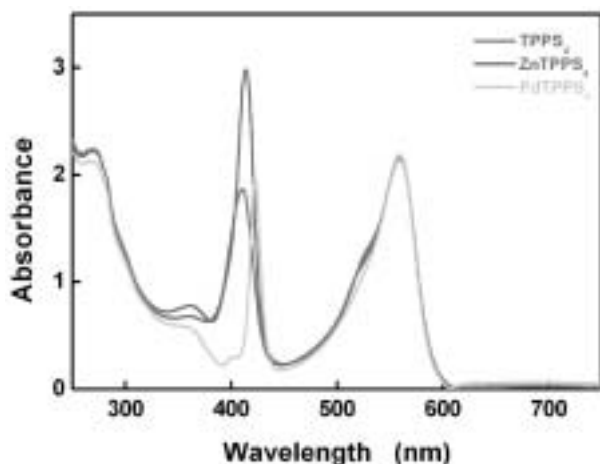


Fig. 1: Absorption spectra of 10 μM sensitizers.

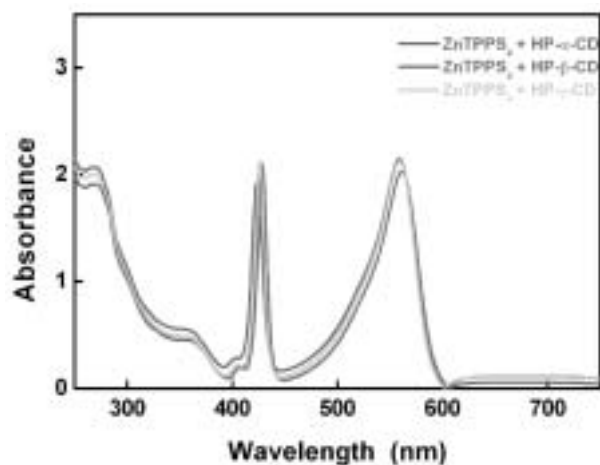


Fig. 2: Absorption spectra of 10 μM ZnTPPS₄ bound to 1 mM cyclodextrin carriers.

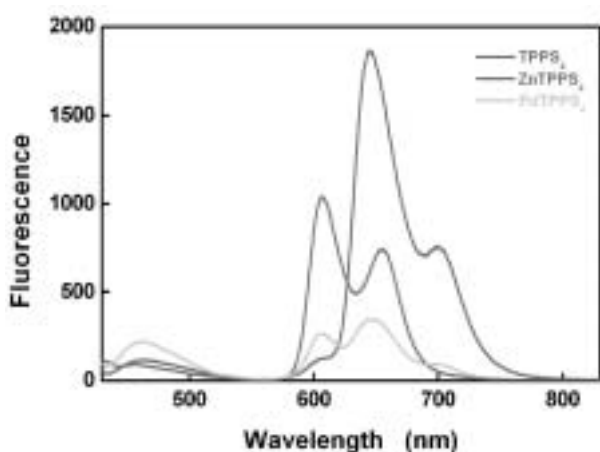


Fig. 3: Fluorescence emission spectra of 10 μM sensitizers. Exciting wavelengths are the same like wavelengths of absorption maxima of sensitizers in the Soret region.

Results

Fig. 1 shows the absorption spectrum of the polypyrr-olic sensitizer solution. The wavelength absorption maximum for sensitizer TPPS₄ is 415 nm. The sensitizer ZnTPPS₄ expresses a shift in absorption maximum to the short wavelength of 2 nm, thus the level of 413 nm. The absorption maximum of sensitizer PdTPPS₄ is near the wavelength 423 nm. Fig. 2 shows the absorption spectra of the sensitizer ZnTPPS₄ in combination with the cyclodextrin carriers, which demonstrates that the type of used carrier only slightly affects the form of the spectrum.

In Fig. 3 the fluorescent emission spectra are obtained near the wavelength which corresponds to the sensitizer absorption maximum in the Soret region. The spectra illustrate a strong difference in the location of the maxima and the fluorescence intensity, where as with all of sensitizers there emerges two distinct fluorescent bands. TPPS₄ shows the highest fluorescence. The fluorescence intensity is near that of other sensitizers, after which sensitizers ZnTPPS₄ a PdTPPS₄ diminish along with it, such that it highlights the longer wavelength maximum with regard to the maximum short wavelength. Sensitizer PdTPPS₄ gains a long wavelength band with a higher intensity of fluorescence. Individual sensitizers also differ in the position of their fluorescent maxima. Fluorescent emission spectra of the sensitizer ZnTPPS₄ in combination with the cyclodextrin carriers, which demonstrates that the type of used carrier only slightly affects the form of the spectrum. We found similar behavior in the recordings of the spectra for sensitizers TPPS₄ a PdTPPS₄.

Discussion

The absorption spectra were measured in conditions parallel to that of the cultivated tumor cells. The spectra were measured in the cultivation medium; its character can influence the resulting exposure parameters because a portion of active radiation will likely be absorbed by the cultivation medium itself. The absorption spectra of the sensitizer solutions differ in absorption spectra of the cultivation media only in the region of short wavelength of light. Minor differences in the spectra of different sensitizers in this area fit their individual chemical structure (Fig. 1). The absorption of the sensitizer solutions in the ultraviolet area of the electromagnetic spectrum and the area around the wavelength 560 nm pertains to its cultivation medium, which was used as the solvent. The cyclodextrin carrier caused a shift in the absorption maxima of individual sensitizer solutions (Fig. 1 and 2). If we take a sensitizer in a cyclodextrin carrier then the absorption spectra of these complexes will not differ from the type of carrier used (Fig. 2). The fluorescent spectra of the sensitizers differ in their fluorescent intensity, in the long wavelength maxima (Fig. 3). These differences are attributed to their individual chemical structure.

Conclusion

The study of photophysical properties allows the establishment of irradiation parameters and conditions of the cultivation of cancer cells for combined studies of the cytotoxicity and phototoxicity of sensitizers bound in cyclodextrin carriers *in vitro* methods.

Special thanks

This work was supported by a grant from the Palacky University (grant no. 11101101), the GAČR grant no. 203/02/1483, and research plan MŠMT no. 153100008.

References

1. Jori G. In vivo transport and pharmacokinetic behavior of tumour photosensitizers. *Ciba Found Symp* 1989;146:78–86.
2. Konan YN, Gurny R, Allemann E. State of the art in the delivery of photosensitizers for photodynamic therapy. *J Photochem Photobiol B.* 2002;66(2): 89–106.
3. Leach MW, Higgins RJ, Autry SA, Boggan JE, Lee SJ, Smith KM. In vitro photodynamic effects of lysyl chlorin p6: cell survival, localization and ultrastructural changes. *Photochem Photobiol* 1993;58(5):653–60.
4. Moan J. Properties for optimal PDT sensitizers. *J Photochem Photobiol B.* 1990;5(3–4):521–4.
5. Mosinger J, Kliment V Jr, Sejbál J, Kubat P, Lang K. Host – guest complexes of anionic porphyrin sensitizers with cyclodextrins. *J Porphyrins Phthalocyanines* 2002;6:513–23.
6. Ochsner M. Photodynamic therapy: the clinical perspective. Review on applications for control of diverse tumorous and non-tumorous diseases. *Arzneimittelforschung* 1997;47(11):1185–94.
7. Strauss WS, Gschwend MH, Sailer R, Schneckenburger H, Steiner R, Ruck A. Intracellular fluorescence behaviour of meso – tetra (4-sulphonatophenyl) porphyrin during photodynamic treatment at various growth phases of cultured cells. *J Photochem Photobiol B.* 1995;28:155–61.
8. Wood SR, Holroyd JA, Brown SB. The subcellular localization of Zn (II) phthalocyanines and their redistribution on exposure to light. *Photochem Photobiol* 1997;65:397–402.

Mgr. Martin Huf,
Palacky University Olomouc, Faculty of Medicine,
Institute of Medical Biophysics,
Hněvotínská 3, 775 15 Olomouc,
Czech Republic.
e-mail: m.huf@seznam.cz

THE CELLULAR UPTAKE OF SENSITIZERS BOUND TO CYCLODEXTRIN CARRIERS

Hana Kolářová¹, Martin Huf¹, Jaroslav Maceček¹, Pavla Nevřelová¹, Marek Tomečka¹, Robert Bajgar¹, Jiří Mosinger², Miroslav Strnad¹

Palacky University Olomouc, Faculty of Medicine, Czech Republic: Department of Biophysics, Laboratory of Growth Regulators¹; Charles University in Prague, Faculty of Science, Czech Republic: Department of Inorganic Chemistry²

Summary: Photodynamic therapy of cancer uses the interaction of sensitizers and light to destroy cancer cells. In this study we tested the cellular uptake of *meso*-tetrakis(4-sulfonatophenyl)porphine (TPPS4) and its complex PdTPPS4 in the presence or absence of 2-hydroxypropyl-cyclodextrins (hpCDs) on G361 human melanoma cells. Self-fluorescence in G361 cells were measured by Perkin-Elmer LS50B luminometer equipped with well plate reader accessory. Morphological changes in cells have been evaluated using inversion fluorescent microscope Olympus IX 70 and image analysis. The uptake of the sensitizer PdTPPS4 at the given time interval from 1 to 48 hours is markedly higher than the uptake of TPPS4. The highest uptake was found for sensitizer PdTPPS4 in combination with hp β CD. TPPS4 and PdTPPS4 especially in the supramolecular complex with nontoxic cyclodextrin carriers represent efficient sensitizers for photodynamic therapy in vitro on G361 cells.

Key words: Sensitizers; Uptake; G361 human melanoma cells

Introduction

Photodynamic therapy (PDT) is a treatment for neoplastic disease that involves the selective destruction of tumors using light-activated sensitizer compounds that preferentially accumulate in target tissue areas (1,4,8). The photochemical interactions of the sensitizer, light, and molecular oxygen produce cytotoxic singlet oxygen and other forms of active oxygen, such as peroxide, hydroxyl radical and superoxide ion resulting in damage of organelles within malignant cells and leads to tumor ablation (2,9). The major sites of PDT damage are membranous organelles, such as mitochondria, lysosomes and plasma membrane. The efficiency of sensitizers in situ is most likely to be dependent on their local accumulation and specific cellular uptake in the tumor site, stimulating research toward the development of water soluble and efficient in vivo sensitizer – delivery system with a high potential to target specific organs. In the present study we used *meso*-tetrakis(4-sulphonatophenyl)porphine (TPPS4) and paladium complex of TPPS4 (PdTPPS4) as model sensitizers (6,7). We report here the uptake of a sensitizer into G361 human melanoma cells in the presence or absence of 2-hydroxypropyl- β -cyclodextrin (hp β CD).

Material and methods

Cellular uptake: The G361 cells (ATTC, USA) were divided in the amount of 10^4 to each well (Dynatech plates 8 x 12, flat bottom) and filled in DMEM with 10% FCS. The sensitizer was added into the holes in concentrations of 0; 0.1; 0.3; 1; 3; 10; 30 and 100 μ M in the absence or presence of hpCDs in a 100-fold concentration excess compared to the sensitizer. The cells were incubated in a thermobox (37°C, 5 %CO₂). After 1; 3; 6; 10; 16; 24 and 48 hours of incubation, the medium above the adhering cells was removed. Each emptied hole was 2x washed with 120 μ l of DMEM. After washing 100 μ l of DMEM was added into each hole and self-fluorescence (TPPS4 excitation at 415nm, emission at 645nm, PdTPPS4 excitation at 423nm, emission at 645nm) in G361 cells were measured with respect to individual sensitizer by Perkin-Elmer LS50B luminometer equipped with well plate reader accessory (Perkin-Elmer Corp., Norwalk, CT). The whole plate was read once with a read time of 0.2 s for each well. We found these settings optimal, increasing the read time per well and/or adjusting slit widths did not improve the signal to background ratio. Subsequently, from each of the holes 10 μ l of medium was withdrawn and the volume was replaced by

the same one of 20 % SDS. The holes were mildly shaken and incubated for 5 minutes; then their fluorescence was measured again.

Self-fluorescence of sensitizers in G361 cells: Twice washed trypsinated G361 cells were divided in the amount of 10^4 to each well and filled in DMEM with 10% FCS in a total volume of 80 μ l. After 24 hours of cultivation at 37°C in 5% CO₂ the 20 μ l of sensitizer was added. Cells were cultivated with sensitizers at concentrations ranging from 0.1 to 125 μ g/ml. The total volume of 100 μ l (cells with additives) were cultivated for 24 hours. Cell uptake and morphological changes in cells have been evaluated using inversion fluorescent microscope Olympus IX 70 and image analysis.

Results

Fig. 1 shows that the uptake of the sensitizer PdTPPS4 at the given time interval is markedly higher than the uptake of TPPS4. The presence of the hpCD carrier did not affect the accumulation of TPPS4, but significantly affect uptake of PdTPPS4. The highest uptake was found for sensitizer PdTPPS4 in combination with hp β CD.

The presence of the hpCD significantly increases the level of an accumulation of PdTPPS4 in cells after a long-time period of incubation and gives no saturation character even after 48 hours of incubation. This is in contrary of free PdTPPS4 that reaches saturation after 24 hours (Fig. 2).

Self fluorescence of sensitizers in cells was evaluated by inversion fluorescent microscope Olympus IX 70 and image analysis. The major sites of cell uptake are plasma membrane, mitochondria and lysosomes (Fig. 3).

Discussion

Efficiency of PDT is affected by various factors including photophysical properties of a sensitizer, wavelength of the activation light, depth of the light penetration in the biological tissue, tissue response on singlet oxygen, etc. (3,5,10). The wavelength of used light that activates the sensitizer dictates the proper absorption spectrum of a sensitizer as well as the depth of the treatment effect. Uptake of a sensitizer into tumor cells may vary depending on the metabolic state of individual cells. The measurement of the uptake of sensitizers into the G361 cells shows the difference between the free sensitizers and bound to hpCD carriers. The kinetic of PdTPPS4 uptake is higher than for TPPS4. While the presence of hpCDs does not notably affect the uptake of TPPS4, in the case of PdTPPS4 cyclodextrin carriers hp β CD cause a significant magnification in accumulation of the sensitizer. The most effect on the level of distribution of the sensitizers in G361 cells was found for PdTPPS4 in combination with hp β CD. G361 cells are sensitive to photodynamic damage by sensitizers in the presence or absence of hpCDs (3). In conclusion, PdTPPS4 and TPPS4 especially in the supramolecular complexes with hpCDs carriers represent efficient sensitizers.

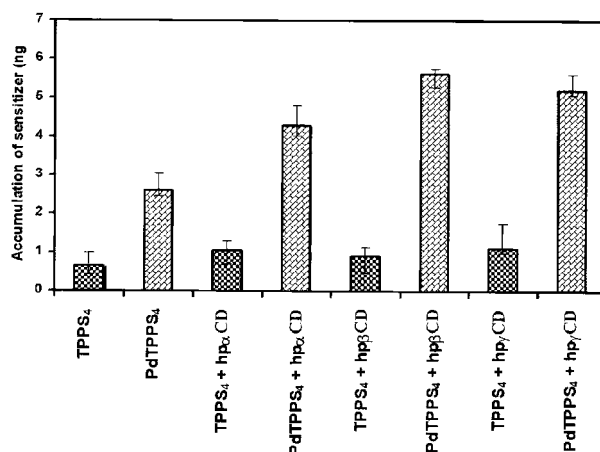


Fig. 1: The uptake of TPPS4 (3 μ M) and PdTPPS4 (3 μ M) sensitizers in the absence or presence of 100 fold molar excess of hpCDs into G361 cells (10^4) after 24 hours of incubation in DMEM with 10% FCS.

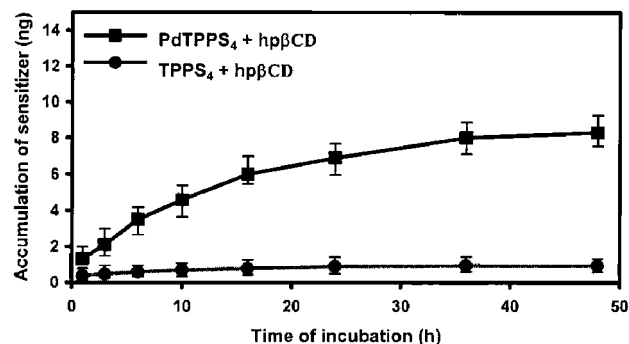


Fig. 2: Time dependent uptake of TPPS4 and PdTPPS4 sensitizers (3 μ M sensitizer, 10^4 G361 cells in DMEM with 10% FCS) bound to hp β cd.

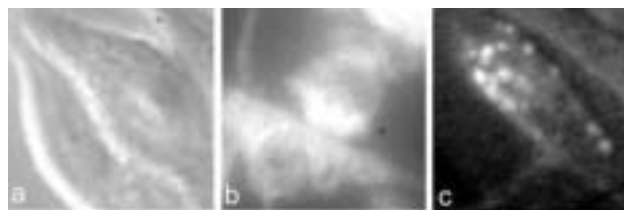


Fig. 3: Self fluorescence of PdTPPS4 sensitizer (12 μ g/ml) bound to hp β cd after 24 hours of cultivation in DMEM with 10% FCS in G361 cells. Excitation wavelength - 420 nm. (3a: transmitted light, 3b: accumulation of sensitizer on plasma membrane and mitochondria, 3c: accumulation of sensitizer on lysosomes).

Acknowledgements

The authors thank Olina Hustakova for assistance with tissue cultures. This work was supported by the grant project of Grant Agency No. 203/02/1483 and Ministry of Education MSM No. 153100008.

References

1. Brown SB, Brown JE, Veron DI. Photosensitising drugs - their potential in oncology. *Expert Opin Invest Drugs* 1999;8(12):1967-79.
2. Dahle J, Steen HB, Moan J. The mode of cells death induced by photodynamic treatment depends on cell density. *J Photochem Photobiol B: Biology* 1999; 70(3):363-7.
3. Kolářová H, Mosinger J, Lenobel R, Kejlová K, Jirová D, Strnad M. In vitro toxicity testing of supramolecular sensitizers for photodynamic therapy. *Toxicol in Vitro* 2003;17(5-6):775-8.
4. Lui H, Anderson RR. Photodynamic therapy in dermatology: Recent developments. *Dermatol Clin* 1993;11:1-13.
5. Moor ACE. Signaling pathways in cell death and survival after photodynamic therapy. *J Photochem Photobiol B: Biology* 2000;57:1-13.
6. Mosinger J, Deumié M, Lang J, Kubát P, Wagnerová DM. Supramolecular sensitizer: complexation of meso tetrakis (4 sulfonatophenyl) porphyrin with 2-hydroxypropyl - cyclodextrins. *J Photochem Photobiol A: Chemistry* 2000;130:13-20.
7. Mosinger J, Mička Z. Quantum yields of singlet oxygen of metal complexes of meso tetrakis (4 sulfonatophenyl) porphyrin. *J Photochem Photobiol A: Chemistry* 1997;107:77-82.
8. Sibata Ch, Conluzzi VC, Oleinick NL, Kinsella TJ. Photodynamic therapy in oncology. *Expert Opin Pharmacother* 2001;2(6):917-27.
9. West CM. Size-dependent resistance of human tumour spheroids to photodynamic treatment. *Br J Cancer* 1989;59:510-4.
10. Zaidi SL, Oleinick NL, Zaim MT, Mukhthar H. Apoptosis during photodynamic therapy -induced ablation of RIF-1 tumors in C3H mice: electron microscopic histopathologic and biochemical evidence. *J Photochem Photobiol B: Biology* 1994;58:771-6.

*Doc. RNDr. Hana Kolářová, CSc.,
Palacky University Olomouc, Faculty of Medicine,
Department of Biophysics,
Laboratory of Growth Regulators,
Hněvotínská 3, 775 15 Olomouc,
Czech Republic.
e-mail kol@tunw.upol.cz*

AGE AND SEX VARIABILITY OF INITIAL PARTS OF THE QRS COMPLEX DISPLAYED IN ISOINTEGRAL MAPS OF YOUNG PEOPLE

Katarína Kozlíková, Juraj Martinka

Comenius University, Faculty of Medicine, Bratislava, Slovak Republic: Institute of Medical Physics and Biophysics

Summary: Although body surface electrocardiographic mapping is used also in clinical practice, there are only a few papers concerning the isointegral maps (IIMs) in children. We constructed IIMs of 169 healthy young people during the initial parts of the QRS complex: the first 20 ms (QRS₂₀), 30 ms (QRS₃₀), 40 ms (QRS₄₀), and from 20 ms to 40 ms (QRS₂₀₋₄₀). Subjects were divided into 6 groups: 9-10 y (F1, M1), 13-14 y (F2, M2), 18-19 y (F3; M3). We analysed the extreme values of each time integral. We found maxima and peak-to-peak values decreasing with age, while minima tended to increase (became less negative). Most age differences were found in IIM QRS₂₀₋₄₀ and between peak-to-peak values. Least differences were between minima. Maxima and peak-to-peak values were higher in males than in females. No significant differences were found in any extreme value between groups F1 and M1 except for IIM QRS₂₀ maxima. Significant sex differences increased with age. The only significant difference found in minima was between F2 and M2. Most sex differences were found in IIM QRS₂₀. We assume that our findings can be explained (at least in part) by the influence of heart - chest geometry.

Key words: *Body surface mapping; Isointegral map; QRS complex; Children; Statistical analysis*

Introduction

Physiologic values of electrocardiographic parameters are important to be known before stating the diagnosis. Individual characteristics of isointegral maps (IIMs) are influenced by different factors such as age or sex. They may contribute to relatively high variability among measured parameters of patients or control subjects. Although it is important to know how these factors may affect used IIM characteristics, isointegral mapping of controls in different age and sex groups is very rare (8,9,10,11). Only a very little is known about IIM parameters in children (1,3,4,5,6,8,9). In our study we tried to fill in this gap with amplitude analysis of IIMs of initial parts of the QRS complex in children and young adults.

Patients and Methods

We recorded and analysed IIMs of 169 young healthy people (90 females and 79 males). They were chosen from over 200 records of young people from which subjects revealing any electrocardiographic abnormality or any technical problem of the record were excluded. Remaining subjects were distributed into six groups after their age and sex: 9-10 years (group F1: 17 girls; group M1: 15 boys), 13-14 years (F2: 25 girls; M2: 23 boys), and 18-19 years

(F3: 48 women; M3: 41 men). None of measured subjects suffered by any cardiovascular disease or had any abnormality found neither on 12-lead standard electrocardiograms or M-mode echocardiograms.

We used the limited 24-lead system after Barr implanted in the mapping system ProCardio (2,12) for the recording of the electric heart field and data processing. During each examination a record of one second duration was registered (a single heartbeat) in supine position. Linear baseline was taken through T-P segments. The onset and offset of the QRS complex was established manually from the root mean square signal (7).

We compared extreme values of IIMs (maximum, minimum, and peak-to-peak value = maximum - minimum) (7). For construction of IIMs we used following integration intervals: the first 20 ms (IIM QRS₂₀), the first 30 ms (IIM QRS₃₀), and the first 40 ms of QRS complex (IIM QRS₄₀), and the interval from 20 ms to 40 ms of QRS complex (IIM QRS₂₀₋₄₀).

Statistical analysis was performed in following way using the program Statgraphics 3 plus (13). All data were tested for normal distributions using skewness and kurtosis. If they were found normal, variance check was done using Bartlett's test (age differences). If variances were found to be the same, analysis of variance was used with Fisher's least significant differences. If any of previous conditions

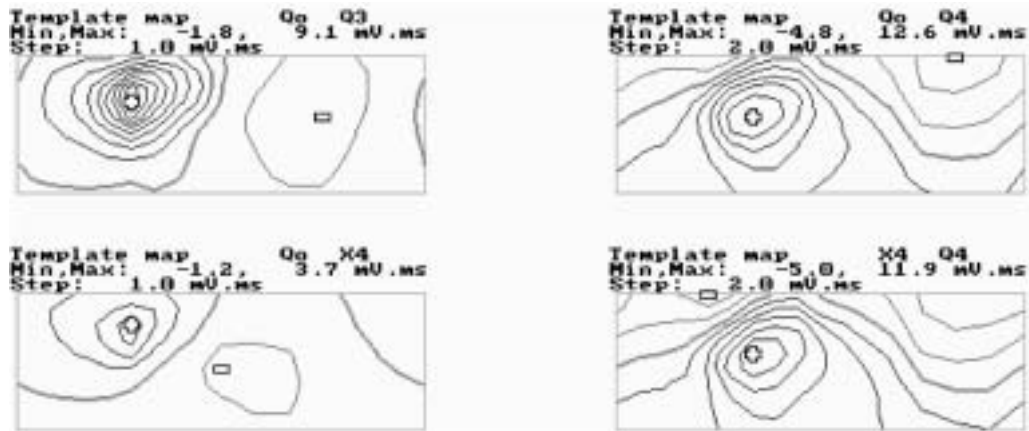


Fig. 1: Mean IIMs of group F3. Each rectangle displays chest surface with the anterior chest on the right and back on the left. Maximal and minimal values are marked by plus and minus signs, respectively, and displayed above each map. Step concerns the difference between two successive isointegral lines. Template (group) maps are marked as QoQ3 (IIM QRS₃₀), QoQ4 (IIM QRS₄₀), QoX4 (IIM QRS₂₀), and X4Q4 (IIM QRS₂₀₋₄₀).

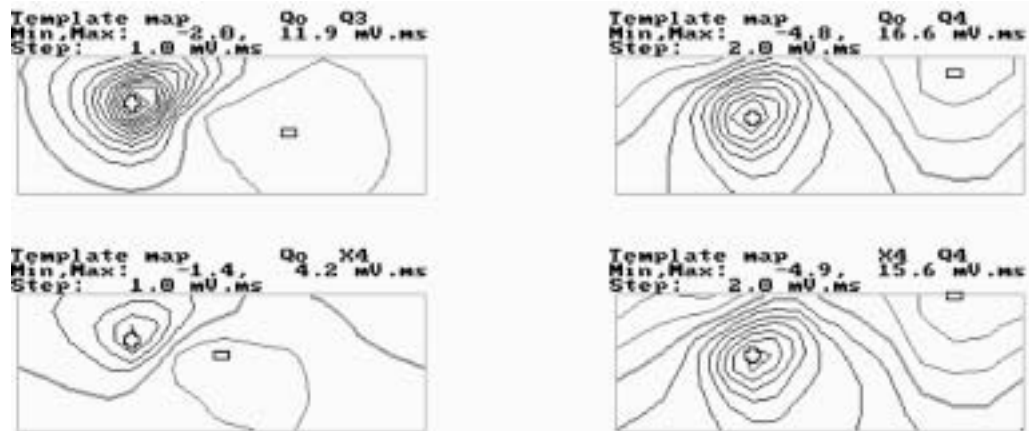


Fig. 2: Mean IIMs of group M3. Next description as in Figure 1.

Tab. 1: Values of maxima in isointegral maps in all studied groups and differences between sexes of the same age.

Group IIM	F1 (n=17)	F2 (n=25)	F3 (n=48)	M1 (n=15)	M2 (n=23)	M3 (n=41)
QRS ₂₀	5.1 ± 1.8 (5.4) < 2.2; 8.6>	4.1 ± 1.4 (3.7) < 1.7; 6.9>	3.8 ± 1.3 # (3.8) < 1.3; 9.3>	6.7 ± 2.5 * (6.5) < 3.0; 12.0>	5.0 ± 1.5 * (4.9) < 2.1; 7.6>	4.6 ± 1.4 (4.4) & < 2.6; 8.5>
QRS ₃₀	12.9 ± 4.0 (12.0) < 5.7; 21.7>	11.2 ± 4.0 (10.4) < 5.7; 19.3>	9.9 ± 3.0 # (9.8) < 3.7; 20.2>	16.7 ± 6.7 (15.7) < 6.8; 29.7>	14.0 ± 4.1 * (13.6) < 6.7; 19.6>	12.8 ± 4.1 (12.9) && < 6.6; 21.8>
QRS ₄₀	23.4 ± 8.0 (21.6) < 11.7; 42.2>	18.8 ± 6.9 # (16.8) < 7.0; 37.6>	14.6 ± 5.2 # (14.1) < 6.3; 32.7>	23.3 ± 7.0 (23.0) < 12.6; 36.0>	23.1 ± 6.7 (22.5) < 14.5; 38.3>	20.7 ± 6.8 (21.2) &&& < 9.2; 43.1>
QRS ₂₀₋₄₀	24.4 ± 7.1 (22.9) < 12.6; 39.8>	17.9 ± 6.2 # (15.9) < 7.4; 35.4>	13.5 ± 4.8 # (12.1) < 6.0; 30.2>	23.0 ± 5.7 (21.7) < 14.8; 30.8>	22.6 ± 6.5 # (21.1) ** < 14.6; 38.5>	18.9 ± 6.5 # (19.5) &&& < 7.1; 42.5>

Values were not distributed normally. Statistical significance: * p < 0.05; &p < 0.01; ** p < 0.005; &&p < 0.001; &&&p < 0.0001.

was not fulfilled, Kruskal-Wallis test and Mann-Whitney test for medians were used. Sex differences were compared between corresponding age groups in pairs. For normal data Student's t-test was used considering equal or non-equal variances after Fisher's test. Else Mann-Whitney test for medians was used. Statistically significant differences were assumed for $p < 0.05$ or less.

Results

Mean IIMs of each group revealed smooth dipolar distributions with one maximum and one minimum. The only exception was in the IIM QRS₄₀ where an indication of second minimum was found at the right upper back in women (group F3, Figure 1) and in the right clavicular area in men (group M3, Figure 2).

Group extreme values of isointegral maps are given in Tables 1-3 with statistically significant differences found between corresponding sex groups. Values are given in form

of mean \pm standard deviation, median in parentheses, range is given below them in form of closed interval. Statistically significant differences concerning the age are given in Tables 4-6. If the comparison is not given, it was not significant.

We found mean maxima and mean peak-to-peak values decreasing with age in all evaluated groups of both sexes (Tables 1 and 3). This trend was valid also for their medians. Minima behaved in a different way (Table 2). In most cases there were the lowest (deep) minima in the youngest children except for IIM QRS₄₀ and IIM QRS₂₀₋₄₀ in group M2. The highest (shallow) minima tended to be in the oldest groups except for IIM QRS₃₀ in males where it was found in group M2. Most age differences were found in IIM QRS₂₀₋₄₀, which displayed the activation comprising the middle of the QRS complex, and between peak-to-peak values. Least differences were between minima. As more than one third of data sets were not distributed normally, we have taken medians to perform these comparisons.

Tab. 2: Values of minimum in isointegral maps in all studied groups and differences between sexes of the same age.

Group IIM	F1 (n=17)	F2 (n=25)	F3 (n=48)	M1 (n=15)	M2 (n=23)	M3 (n=41)
QRS ₂₀	-3.6 \pm 4.6 # (-2.4) < -21.0; -1.0 >	-1.6 \pm 0.6 (-1.5) < -3.0; -0.8 >	-1.6 \pm 0.4 (-1.6) < -2.5; -0.9 >	-2.8 \pm 1.1 (-2.5) < -5.3; -1.4 >	-2.2 \pm 0.6 ** (-2.2) ** < -3.5; -0.8 >	-1.8 \pm 0.6 # (-1.8) < -3.7; -0.8 >
QRS ₃₀	-2.7 \pm 0.6 (-2.6) < -4.0; -1.8 >	-2.6 \pm 1.1 # (-2.3) < -5.4; -0.7 >	-2.7 \pm 0.8 (-2.7) < -4.4; -0.9 >	3.4 \pm 1.2 (-3.1) < -5.7; -1.3 >	-2.9 \pm 1.0 (-2.8) < -4.8; -0.6 >	-3.0 \pm 1.2 # (-2.7) < -8.0; -1.3 >
QRS ₄₀	-6.6 \pm 3.0 # (-6.3) < -14.7; -2.3 >	-6.4 \pm 2.4 (-5.6) < -12.9; -2.4 >	-5.3 \pm 2.5 # (-4.6) < -13.1; -1.6 >	-6.3 \pm 2.3 (-6.0) < -12.2; -2.9 >	-6.9 \pm 3.0 # (-6.1) < -17.4; -3.3 >	-5.4 \pm 2.2 # (-4.9) < -12.5; -2.5 >
QRS ₂₀₋₄₀	-8.0 \pm 3.7 # (-7.1) < -18.3; -3.0 >	-7.6 \pm 2.5 (-6.6) < -12.9; -4.9 >	-5.9 \pm 2.8 # (-5.0) < -15.1; -2.3 >	-7.6 \pm 3.0 # (-6.9) < -16.6; -4.0 >	-7.7 \pm 3.4 (-6.4) < -18.0; -3.3 >	-6.0 \pm 3.3 # (-5.2) < -18.6; -2.1 >

Values were not distributed normally. Statistical significance: ** $p < 0.005$.

Tab. 3: Values of peak-to-peak in isointegral maps in all studied groups and differences between sexes of the same age.

Group IIM	F1 (n=17)	F2 (n=25)	F3 (n=48)	M1 (n=15)	M2 (n=23)	M3 (n=41)
QRS ₂₀	8.7 \pm 4.9 # (7.3) < 5.0; 26.0 >	5.7 \pm 1.5 (5.7) < 3.5; 8.8 >	5.4 \pm 1.4 # (5.5) < 2.2; 10.7 >	9.5 \pm 2.6 (9.5) < 5.3; 15.3 >	7.2 \pm 1.8 ** (7.3) & < 3.6; 9.8 >	6.4 \pm 1.7 (6.2) *** < 3.6; 10.4 >
QRS ₃₀	15.6 \pm 4.2 (14.4) < 8.2; 25.5 >	13.7 \pm 4.7 (12.7) < 7.2; 23.1 >	12.6 \pm 3.5 # (12.2) < 4.6; 24.5 >	20.1 \pm 7.4 (18.5) < 8.1; 35.4 >	16.9 \pm 4.6 * (16.3) * < 8.9; 22.6 >	15.8 \pm 4.8 (15.8) ** < 8.5; 26.2 >
QRS ₄₀	29.9 \pm 9.9 (26.5) < 14.0; 53.6 >	25.3 \pm 8.8 # (23.2) < 9.4; 47.8 >	19.9 \pm 7.1 # (18.4) < 7.9; 43.8 >	29.6 \pm 8.3 (29.6) < 16.7; 43.7 >	30.0 \pm 7.8 (28.0) * < 19.5; 47.1 >	26.1 \pm 8.4 (27.6) *** < 12.0; 53.2 >
QRS ₂₀₋₄₀	32.4 \pm 9.4 (30.0) < 15.6; 52.2 >	25.4 \pm 7.9 # (22.1) < 14.0; 46.2 >	19.4 \pm 7.1 # (17.7) < 8.5; 43.0 >	30.6 \pm 7.2 (30.5) < 18.8; 39.9 >	30.3 \pm 8.3 # (28.3) * < 19.9; 51.9 >	24.9 \pm 9.1 # (23.6) && < 9.2; 56.6 >

Values were not distributed normally. Statistical significance: * $p < 0.05$; ** $p < 0.005$; && $p < 0.001$; *** $p < 0.0005$.

Tab. 4: Significant age differences between medians of groups for maxima.

IIM	F1-F2	F2-F3	F1-F3	M1-M2	M1-M3
QRS ₂₀	NS	NS	p < 0.01	p < 0.05	p < 0.005
QRS ₃₀	NS	NS	p < 0.01	NS	NS
QRS ₄₀	p < 0.05	p < 0.01	p < 0.0001	NS	NS
QRS ₂₀₋₄₀	p < 0.005	p < 0.005	p < 0.0001	NS	p < 0.05

NS: not significant

Tab. 5: Significant age differences between medians of groups for minima.

IIM	F1-F2	F2-F3	F1-F3	M2-M3	M1-M3
QRS ₂₀	p < 0.005	NS	p < 0.0001	NS	p < 0.001
QRS ₄₀	NS	p < 0.05	NS	p < 0.05	NS
QRS ₂₀₋₄₀	NS	p < 0.005	p < 0.05	p < 0.05	p < 0.05

NS: not significant

Tab. 6: Significant age differences between medians of groups for peak-to-peak values.

IIM	F1-F2	F2-F3	F1-F3	M1-M2	M2-M3	M1-M3
QRS ₂₀	p < 0.01	NS	p < 0.001	p < 0.01	NS	p < 0.0005
QRS ₃₀	NS	NS	p < 0.01	NS	NS	NS
QRS ₄₀	NS	p < 0.005	p < 0.0005	NS	NS	NS
QRS ₂₀₋₄₀	p < 0.01	p < 0.0005	p < 0.0001	NS	p < 0.05	p < 0.05

NS: not significant

Mean maxima and mean peak-to-peak values were higher in males than in corresponding females except for groups F1 and M1 in IIM QRS₄₀ and IIM QRS₂₀₋₄₀ (Tables 1 and 3). This was also valid for medians. No significant differences were found in any extreme value when comparing the youngest girls and boys except for maxima in IIM QRS₂₀. The number of significant sex differences increased with increasing age. The only significant difference found in sex minima comparison was between groups F2 and M2 (Table 2). Most sex differences were found at the very beginning of the QRS complex (IIM QRS₂₀).

Discussion and Conclusions

We did not find published results of IIMs during the initial parts of QRS complex in children. Similar sex differences were found in two published papers. In the first one, Q-zone maps (from the beginning of the QRS complex to its middle, comparable with our IIM QRS₄₀) were analysed in adults (20–46 years old) (10). Forty male subjects had significantly higher maxima than 15 females. Differences between minima were not significant. Published maps were recorded with 117 chest leads. In the second paper, QR maps (comparable with our IIM QRS₄₀) were analysed in 18 men and 25 women (18–19 years old) (11). Higher extreme values were found in men.

Age differences were analysed in 2 papers. In both, significantly higher values of maxima in younger children (9–10 years) and deeper minima in older children (13–14

years) were found in IIMs during the whole QRS complex and corresponded with our findings (8,9). These maps were recorded in sitting position using 80 chest electrodes.

When looking at these findings, there still remains the question why we found decreasing values with increasing age in young people. One possible answer is the influence of heart geometry, as well as the geometry heart – chest. Or are the changes during puberty responsible for the differences?

References

- Asano Y, Izumida N, Kiyohara K et al. Diagnosis of right ventricular overload by body surface QRST isointegral maps in children with postoperative right bundle branch block. *J Electrocardiol* 1995;28(3):209–21.
- Barr RC, Spach MS, Herman-Giddens GS. Selection of the number and positions of measuring locations for electrocardiography. *IEEE Trans Biomed Eng* 1971; 18(2):125–38.
- Izumida N, Asano Y, Kiyohara K et al. QRST isointegral map reflects the sudden reduction of right ventricular pressure after balloon pulmonary valvuloplasty. *J Electrocardiol* 1995;28(3):223–9
- Izumida N, Asano Y, Kiyohara K et al. Precordial leads QRST time integrals for evaluation of right ventricular overload in children with congenital heart diseases. *J Electrocardiol* 1997;30(3):257–64.
- Izumida N, Asano Y, Wakimoto H et al. Analysis of T wave changes by activation recovery interval in patients with atrial septal defect. *Int J Cardiol* 2000; 74(2–3):115–24.
- Izumida N, Kiyohara K, Asano Y et al. The body surface QRST isointegral maps in infants with right ventricular overload. *Jpn Circulat J* 1993;57(2): 123–30.
- Kozliková K. Body surface integral maps, their characteristics and methods of quantitative analysis. (in Slovak) *Bratisl Med J* 1990;91(11):815–23.
- Kozliková K, Turzová M, Tyšler M et al. Body surface integral mapping of ventricular activation in boys during puberty. (in Slovak) *Bratisl Med J* 1988; 89(9):694–705.

9. Kozlíková K, Maco M, Sabolová K, Popperová E. Absolute extrema of body surface integral maps in normal children. In: Antalóczy Z, Préda I, eds. *Advances in Electrocardiology*. Amsterdam: Excerpta Medica, 1990:161-4.
10. Montague JM, Smith ER, Cameron DA et al. Isointegral analysis of body surface maps: Surface distribution and temporal variability in normal subjects. *Circulation* 1981;63(5):1166-72.
11. Popperová E, Sabolová K, Maco M, Kozlíková K, Tyšler M, Turzová M. Isointegral analysis of ventricular activation in young people. In: Janoušek V, Špála M, eds. *Current trends in pathophysiology*. (in Slovak) Praha: Univerzita Karlova, 1989:325-6.
12. Rosík V, Tyšler M, Turzová M. Portable Device for ECG Mapping. In: Frollo I, Plačková A, eds. *Measurement'97. Proceedings, International Conference of Measurement*. Bratislava: SAS, 1997:367-70.
13. Statgraphics® PLUS, version 3 for Windows. User manual. Rockville: Manugistics, Inc., 1997:738pp.

***Doc. RNDr. Katarína Kozlíková, Ph.D.,
Comenius University, Faculty of Medicine,
Institute of Medical Physics and Biophysics,
Sasinkova 2, SK 813 72 Bratislava,
Slovak Republic.
e-mail: katarina.kozlikova@fmed.uniba.sk***

INFLUENCE OF D-GLUCOSE ON LIPID SOLID SUPPORT MEMBRANE SYSTEM AS ATTEMPT FOR BIOSENSING OF MEDICALLY RELEVANT MOLECULES

Galina Laputková, Michal Legiš, Ján Sabo

P. J. Šafárik University, Faculty of Medicine, Slovak Republic: Department of Medical Biophysics

Summary: The influence of D-glucose on a lipid solid support system with the aid of impedance spectroscopy as a preliminary attempt for the biosensing of medical relevant molecules was studied. In spite of some shortcomings, s-BLM's proved to be an appropriate model for the study of lipid membrane - D-glucose interactions. The shortcomings were the roughness of the metal support, and the lack of homogeneity in the monolayer or multilayer lipid structures.

Key words: *Supported lipid membrane; Biosensor; Glucose*

Introduction

In recent years, so-called supported lipid membranes (s-BLM's), representing functional interfaces between biomaterial and the electrically conductive support - freshly cut tip of stainless steel, silver or platinum wire - have become a focus of intensive investigation and a frequently used model of cell membrane. S-BLM's, i.e. freely suspended lipid membranes on a hydrophilic support, have been developed by Tien and Salamon (10). The system overcomes some of the drawbacks of planar black lipid membranes. It is also noted for its long term stability and its ease of preparation in a reproducible way. Supported lipid membranes have been used in fundamental studies of lipid assemblies, in studies of membrane structure and membrane dynamics, and in studies of the electrochemical properties of membranes (1,8). However, the primary attraction of s-BLM's is their possible application to the field of biosensing. Their applications include providing the means to observe changes in the properties of a deposited lipid layer induced by the layer's surroundings (3). The unique features of s-BLM's are the prerequisite for incorporation of various biological molecules, such as poreforming peptides, channel proteins, and receptors. Such molecules retain their native functions after incorporation, thus allowing the interactions of incorporated molecules with external ligands (9).

The topic of this paper is to establish the influence of D-glucose on s-BLM with the aid of impedance spectroscopy as a preliminary attempt for the biosensing of medical relevant molecules. The choice of D-glucose was influenced especially by the fact that D-glucose changes the electrical properties of s-BLM modified with anthraquinone-2-sul-

phonic acid as we demonstrated with cyclic voltammetry in our previous work (5).

Materials

1,2-Diacyl-*sn*-glycero-3-phosphocholine (DPPC) from egg yolk was purchased from Sigma. N-dodecane (Sigma), D-glucose, and all chemical compounds were of analytical grade and were used without further purification. The solutions of inorganic salts were prepared in freshly distilled and deionized water obtained from a Millipore filter system. Deionized water had a resistivity of ~ 18.2 MΩ cm.

Formation of supported lipid bilayers

The simplest suitable technique for the formation of s-BLM's has proven to be the deposition of a lipid membrane on a freshly created metallic surface (10). The formation of s-BLM is based on the interaction of amphiphilic lipid molecule with a nascent metal surface. Prior to the self-assembling of the lipid bilayer on the platinum support, a Teflon coated platinum wire (0.5 mm diameter) was immersed in a lipid forming solution, and, while still immersed, the wire was cut so as to provide a sufficiently reproducible section of the wire. The membrane forming solution used in the experiments was prepared by mixing the ethanol-lipid solution with n-dodecane to attain a final lipid concentration of 5 %. A drop of the solution will adhere to the electrode tip, because of the great affinity between the lipid molecules and the freshly cut metal surface. The electrode tip, with the drop of lipid solution adhered to it, was then immersed into the aqueous electrolyte bath, which preferably consists of 100 mmol.l⁻¹ KCl at a pH of 5.5.

Impedance measurements

The electrochemical properties of the platinum surface were studied by impedance spectroscopy. The electrical impedance $Z(\omega)$ is complex, and determined by the following formula:

$$Z(\omega) = \frac{U(\omega)}{I(\omega)} = |Z(\omega)| \cdot e^{i\varphi(\omega)}$$

where $U(\omega)$ is the voltage applied to the system, $I(\omega)$ is the measured current response, and ω is the angular frequency.

For data representation, we used the polar coordinates of $Z(\omega)$, the absolute value $|Z(\omega)|$, and the phase $\varphi(\omega)$.

For the impedance spectroscopy experiments, we used the commercially available electrochemical analyzer Zahner Elektrik IM6e (Zahner Meßtechnik, GmbH, Germany), and controlled it with a personal computer. The measuring cell contained the conventional three-electrode configura-

tion. The Teflon-covered platinum wire electrode supporting the membrane served as a working electrode. An identical Teflon-coated platinum wire was used as the counter electrode. The reference electrode Ag/AgCl (saturated KCl) was isolated from the cell by an agar bridge. The measuring cell was surrounded by a water jacket to maintain stable temperature, and the cell with jacket was then placed into a Faraday cage. All experiments were carried out at room temperature (21.0 ± 0.2)°C.

The EIS experiments were performed at a frequency range of 100 mHz - 10 kHz, at 15 steps per decade. Impedance was measured with an applied bias voltage 0 mV, at sinusoidal excitation amplitude of 50 mV. The measurement was performed 10 times at each frequency, and averaged during the run. The smoothed EIS data were analyzed using complex non-linear regression least square (CNRLS) fit to a model represented by an equivalent electrical cir-

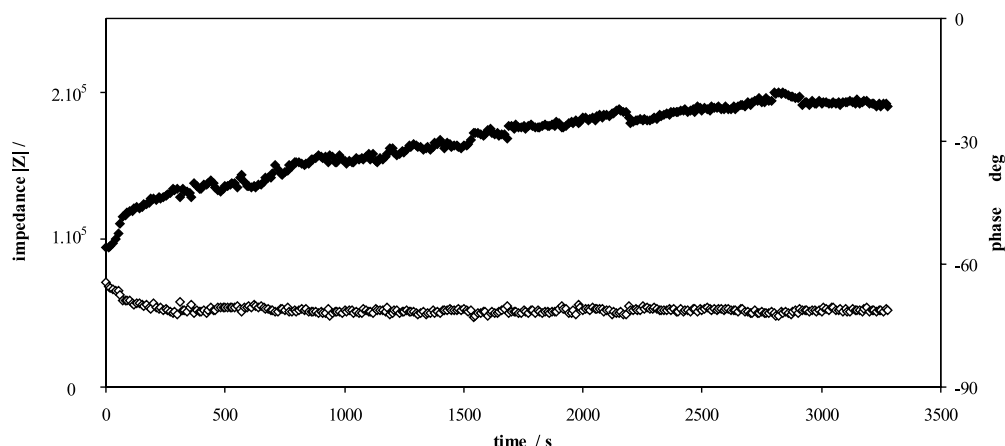


Fig. 1: The time variation of impedance $|Z|$ (\blacklozenge) and phase shift φ (\diamond) of s-BLM developing on platinum support in 100 mmol.l⁻¹ KCl, the amplitude of the applied a.c. signal $U=50$ mV, $f=10$ kHz, $U_{\text{bias}}=0$ mV.

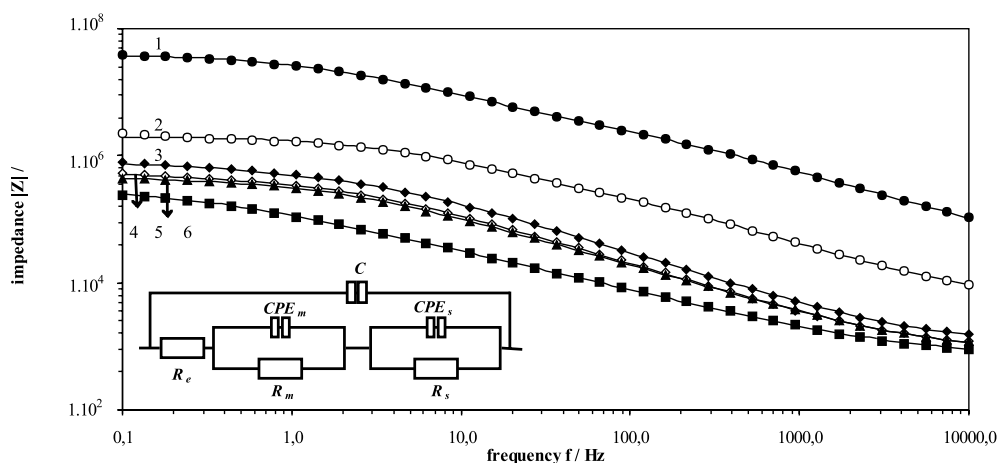


Fig. 2: Effect of D-glucose on the plots of impedance $|Z|$ of s-BLM on platinum in 100 mmol.l⁻¹ KCl: 1. s-BLM, 0 mmol.l⁻¹ glucose, 2. s-BLM, 3 mmol.l⁻¹ glucose, 3. s-BLM, 5 mmol.l⁻¹ glucose, 4. s-BLM, 10 mmol.l⁻¹ glucose, 5. s-BLM, 50 mmol.l⁻¹ glucose, 6. bare platinum, 0 mmol.l⁻¹ glucose. The amplitude of the applied a.c. signal $U=50$ mV, $U_{\text{bias}}=0$ mV. (—) fit to the equivalent circuit model using CNRLS regression. Inset: An equivalent circuit for metal-supported lipid membrane.

cuit. The software used for data analysis was a commercial program from Zahner Elektrik.

Results and discussion

Fig. 1 shows the typical time course of the impedance and phase angle during the developing of the lipid bilayer on the support. Both the impedance values and the phase values were constant, and both values also corresponded to the steady state of the membrane. Stable membrane structures were in most cases reached within an hour. After stability was reached, it was long lasting maintained under the unchanging external conditions. For most of the s-BLM's, membrane degradation was not observed during a time interval of 24 hours.

Fig. 2 (curve 1.) shows AC impedance spectroscopy of an s-BLM that was immersed in 100 mmol.l⁻¹ KCl for approximately 2 hours. For the data analysis we chose a simple electrical equivalent circuit (in the inset of Fig. 2). The model describes the most important properties of a lipid membrane which is supported on metal. The electrical circuit consists of the resistance R_e , which corresponds to the ohmic behavior of the electrolyte. The parallel arrangement of the resistance R_s and the constant phase element CPE_s represents the contribution of the electrode - electrolyte interface. The parallel arrangement of the resistance R_m and a constant phase element CPE_m represents the impedance of the lipid film at the interface between the electrolyte and platinum. C_c is the stray capacitance of the measuring cell.

The Nyquist plot of the measured impedance spectrum of s-BLM on the metal (not shown) corresponds with the suppressed arc. The arc can be formally described by introduction of a constant phase element (CPE) instead of the capacitance. The appearance of the suppressed arc indicates a distribution of relaxation times of the circuit. There are two possible explanations for the appearance of the arc. One explanation attributes it to the properties of the metal electrode supporting the membrane, especially to the electrode's porousness and rough surface (6). The other explanation is that it reflects the imperfect organization of the lipid bilayer on the electrode's rough surface.

To estimate the fractional coverage of the electrode, it is useful to employ Nagel and Scott's theory (7). By assuming that ion transport occurs only at the defect sites of the lipid layer, it is reasonable to express the fractional coverage of the electrode as: $\theta = 1 - (R_s^{bare}/R_m)$, where $R_s^{bare}=0.65$

$k\Omega.cm^2$ represents the bare electrode - electrolyte resistance obtained by fitting the impedance spectrum of bare platinum to the equivalent circuit, and where R_m corresponds to the membrane resistance.

The table compares the s-BLM lipid coverage values with the glucose treated lipid membranes values.

As a preliminary check of membrane quality for bio-sensing, the membrane - D-glucose interactions were studied. The membrane parameters were followed using impedance spectroscopy. Fig. 2 exhibits the impedance spectra of supported lipid bilayer in 100 mmol.l⁻¹ KCl before and after the addition of D-glucose. The same membrane was used for all measurements by continuous increasing of glucose concentration. It can be seen from the spectra, that glucose led to significantly change the membrane parameters. CNRLS regression results of s-BLM and s-BLM treated with 3 mmol.l⁻¹ D-glucose is given in the Table. At a concentration of 3 mmol.l⁻¹, the membrane resistance drops to a value 3.90 $k\Omega.cm^2$, significantly decreases the fractional coverage of the electrode and consequently the ion permeability of the lipid layer increase. The continuous increasing of glucose leads to the total destruction of the lipid membrane. The phospholipid portion of s-BLM is not sufficiently flexible to "withstand" the perturbing molecules. The electrical resistance and the capacitance of the membrane are significantly affected by the glucose and the structure of the s-BLM was disrupted for the concentration of glucose exceeding 10 mmol.l⁻¹.

Conclusions

In spite of some shortcomings, s-BLM's proved to be an appropriate model for the study of lipid membrane - D-glucose interactions. The shortcomings were the roughness of the metal support, and the lack of homogeneity in the monolayer or multilayer lipid structures.

We found evidence that glucose influences the properties of s-BLM's in physiologically relevant concentrations. But we also observed that the influence of the glucose is different if s-BLM's are modified with anthraquinone-2-sulphonic acid [4], where the membrane current was reduced after the glucose application reached 10 mmol.l⁻¹.

The results nevertheless support suggestions (2) that sugars, either free in solution or covalently linked to membrane constituents, can affect the properties and stability of bilayers. The results also indicate that glucose initiated

Tab. 1: CNRLS fitting results.

	R_m/Ω	$R_m/k\Omega.cm^2$	CPE_m		$C_m/\mu F.cm^2$	d/nm	θ
			$V=C_m(x/d)/pF$	$\alpha = 1-(x/d)$			
s-BLM	39.70	78.01	439	0.711	0.77	2.4	0.9916
s-BLM + 3mmol.l ⁻¹ glucose	1.99	3.90	4970	0.736	9.58	0.2	0.8328

* α - approximation of penetration depth x of conduction into an insulating surface layer of thickness d ;
 $Z_{CPE} = 1/(\omega_0 V(j\omega/\omega_0)) = 2\pi.1000.$

changes of the impedance characteristics of s-BLM's make it reasonable to use s-BLM's for biosensing.

Acknowledgement

This work was supported by internal grant 26/2002-2005 from the Faculty of Medicine of P. J. Safarik University, Kosice, Slovak Republic.

References

1. Bordi F, Cametti C, Gliozzi A. Impedance measurements of self-assembled lipid bilayer membranes on the tip of an electrode. *Bioelectrochemistry* 2002;57:39-46.
2. Crowe JH, Crowe LM, Carpenter JF et al. Interaction of sugars with membranes. *Biochim Biophys Acta* 1988;947:367-84.
3. Han X, Wang E. Ion-channel sensing of ferricyanide anion based on a supported bilayer lipid membrane. *Anal Sci* 2001;17:1171-4.
4. Laputková G, Sabo J. Cyclic voltammetry study of glucose and insulin interactions with supported lipid membrane. *Bioelectrochemistry* 2002;56:185-8.
5. Laputková G, Sabo J. Effect of increased glucose concentration on the supported bilayer lipid membrane. *Transactions of the Universities of Košice* 2000;58:42-6
6. MacDonald JR. *Impedance spectroscopy*. New York: John Wiley and Sons, 1987:346.
7. Nagle JF, Scott HL. Lateral compressibility of lipid mono- and bilayers: Theory of membrane permeability. *Biochim Biophys Acta* 1978;513:236-43.
8. Sabo J, Ottova A, Laputkova G, Legin M, Vojcikova L, Tien HT. A combined AC-DC method for investigation supported lipid membranes. *Thin Solid Films* 1997;306:112-8.
9. Salamon Z, Tollin G. Surface plasmon resonance studies of complex formation between cytochrome c and bovine cytochrom c oxidase incorporated into a planar lipid bilayer. II Binding of cytochrome c to oxidase-containing cardiolipin/phosphatidylcholine membranes. *Biophys J* 1996;71:858-67.
10. Tien HT, Salamon Z. Formation of self-assembled lipid bilayers on solid substrates. *Bioelectroch. Bioener* 1989;99:211-8.

***Galina Laputková,
Faculty of Medicine,
Department of Biophysics,
Tr. SNP 1, 040 11 Košice,
Slovak Republic.
e-mail: laputk@medic.upjs.sk***

ASSESSMENT OF CELLULAR DAMAGE BY COMET ASSAY AFTER PHOTODYNAMIC THERAPY IN VITRO

Jaroslav Maceček¹, Hana Kolářová¹, Jitka Psotová², Robert Bajgar¹, Martin Huf¹, Pavla Nevřelová¹, Marek Tomečka¹, Jiří Mosinger³

Palacky University in Olomouc, Faculty of Medicine, Czech Republic: Department of Medical Biophysics¹, Department of Medical Chemistry²; Charles University in Prague, Faculty of Science, Czech Republic: Department of Inorganic Chemistry³

Summary: The aim of this study was analysis of DNA damage in the cell line of the human melanoma G361 after photodynamic therapy (PDT) by comet assay. Photodynamic therapy is based on cytotoxic action of sensitizers (10 μM ZnTPPS₄ fixed into 1 mM cyclodextrin hp β CD) and light with a suitable wavelength. Single-cell gel electrophoresis (SCGE, comet assay) is a rapid and sensitive method for detecting DNA strand breaks at the level of single cells. Great amount of DNA damage was detected with the dose of irradiation of 0.1; 0.5 J and 2.5 J.cm⁻². Only radiation dose of visible light in the presence of sensitizers can induce DNA breaks of tumour cells. Cells with DNA damage appear as fluorescent comets with tails of DNA fragmentation. In contrast, cells with undamaged DNA appear as round spots, because their intact DNA does not migrate out of the cell.

Keywords: Comet assay; Photodynamic therapy; Sensitizer; DNA damage; Cyclodextrine (CD)

Introduction

The Comet assay provides a very sensitive method for detecting strand breaks. It is based on the alkaline lysis of labile DNA at the damaged sites. Cells are immobilized in thin agarose matrix and placed on the microscope underlying slides and subsequently lysed by alkaline buffer. When subjected to electrophoresis, the unwound, relaxed DNA migrates out of the cells. After staining by nucleic acid stain, we can distinguish between undamaged and damaged cells using inverted fluorescent microscopy in dependence of the dose of irradiation.

Photodynamic therapy is new and promising modality for selective irradiation of malignant neoplasms especially superficial skin cancer (1). It is based on cytotoxic action of sensitizers in the oxygen-rich environment. Sensitizers are organic dyes that bound to a cell and are excited by light source with a suitable wavelength. The majority of sensitizers are relatively lipophilic and are reported to localize predominantly in the cytoplasm or cytoplasmatic organelles (2). The sensitizer molecules lose their energy after absorption of a quantum of light by transferring to oxygen forming singlet oxygen (¹O₂). The singlet oxygen is very reactive and rapidly reacts with a number of biological molecules, including membrane lipids, proteins and nucleic acids. The changes in their structure often trigger apoptosis

(programmed cell death). Detection of apoptotic cell death in the single cells and tissues has become of paramount importance in many fields such as cancer biology. Apoptosis together with necrosis of tumour cells is expected as a therapeutic effect in photodynamic therapy (3). A potential benefit of PDT is that it causes minimal damage to healthy tissue.

Melanoma cells are cultivated with sensitizer ZnTPPS₄ [(zinc(II)-5,10,15,20-tetrakis(4-sulphonatophenyl) porphyrine) fixed in cyclodextrin carrier hp β CD. These substances create complexes with good penetration through the cell membrane. After sensitizer uptake the cells are excited by appropriate light and marked by fluorescent dye (4). The goal of this presented work was investigation of efficiency of photodynamic therapy by means of comet assay.

Material and methods

About 2 million cells of human melanoma (cell line G361) were cultivated in DMEM with 10 μM ZnTPPS₄ and 1 mM hp β CD for 48 hours at 37 °C. Then the growth medium was replaced by fresh medium without sensitizer and cells were irradiated by visible light at room temperature. The doses of irradiation were 0.1; 0.5; 2.5; 12.5 and 60 J.cm⁻². Cells cultivated in medium alone, in medium with sensitizer and without sensitizer with the maximum dose of

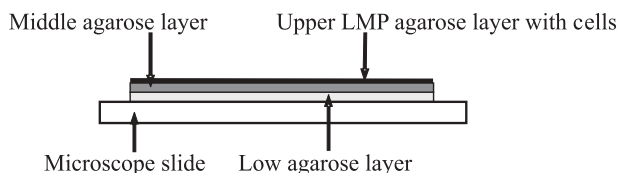


Fig. 1: Diagram of a comet slide.

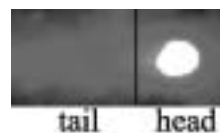


Fig. 2: DNA breaks represented by comet.

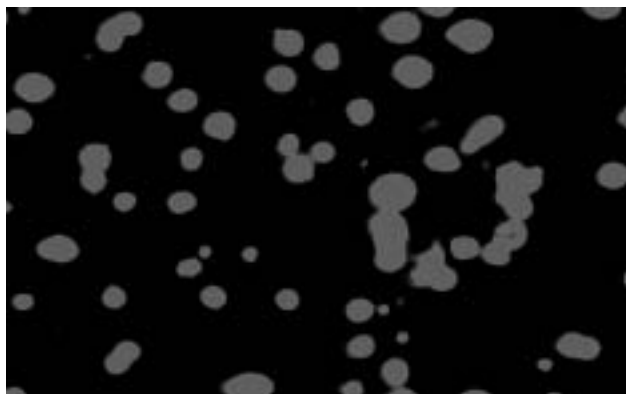


Fig. 3: Typical picture of the undamaged DNA in control samples (G361 cells).

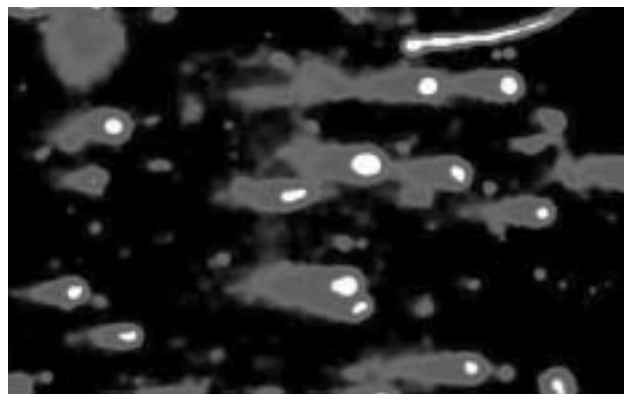


Fig. 4: DNA breaks represented by comets. (PDT of G361 cells; irradiation dose 0.5 J.cm⁻²).

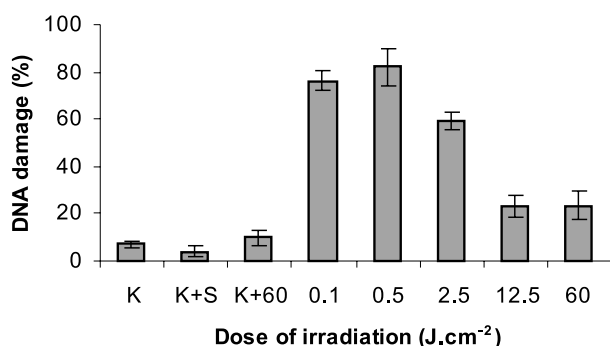


Fig. 5: Percentage occurrence of DNA damage in the dependence of the irradiation dose (K = control; S = sensitizer).

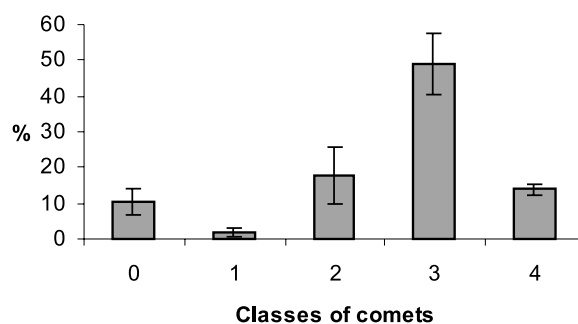


Fig. 6: Percentage occurrence of different stages of DNA damage. (irradiation dose 0.5 J.cm⁻²).

irradiation were used as the controls. Other cells were cultivated in medium with sensitizer and were irradiated by different light dose. After irradiation cells were cultivated for next 24 hours at 37 °C and after this period their damage was assessed by comet assay.

On the microscope slides precoated with 1% standard agarose in H₂O were applied 85 µl of 1% standard agarose in PBS and, while still liquid, covered with a cover slip. Slides were placed in fridge for at least 5 min to solidify agarose. Cells were trypsinated, collected by centrifugation and dispersed in 2ml PBS by vortexing. 20 µl of this solution (2.10⁴ cells) was added to 85 µl of 1% LMP agarose in PBS at 37°C. Finally 85 µl of the mixture were transferred on each slide (Fig. 1) and placed to the fridge for next 5 mi-

nutes. Microscope slides were immersed in lysis buffer (2.5 M NaCl, 100 mM EDTA, 10 mM Tris and 1% Triton X-100; pH = 10) at 4°C for 1 hour. Slides were gently placed on platform in electrophoretic tank and immersed in cool electrophoresis solution (300 mM NaOH, 1 mM EDTA) for 40 minutes. Electrophoresis was run 30 minutes at 2.5 V.cm⁻¹. After electrophoresis the slips were washed 3x5 min with buffer (0.4 M Tris; pH = 7.5) at 4°C and stained by ethidium bromide (20 µg/ml) for the visualization of DNA comet.

It is possible to analyse comets representing different levels of DNA damage quantitatively without image analysis software according to standard method (5). This method classifies comets into classes from class 0 (undamaged, no

discernible tail) to class 4 (almost all DNA in tail, insignificant head) (5). Each comet (Fig. 2) is given based on its pattern a value according to level of DNA damage. We worked with fluorescent microscope, CCD camera and Olympus Micro Image software.

Results

The control samples were used to detect undamaged DNA (Fig. 3). In Fig. 4 we can see DNA of cancer cells as comets visualised by ethidium bromide. Belong to great amount of DNA damage representing by comets from class 1 to 4 was detected at the irradiation dose of 0.5, followed by 0.1 and 2.5 J.cm⁻² (Fig. 5). This low radiation dose induce DNA breaks, which correspond to comets belonging to class 3, less 2 and 4 (Fig. 6).

Discussion and conclusions

Assessment of cellular damage by comet assay is valuable method for detecting DNA breaks. Irradiation of cells can result in a few kinds of reaction. Very low dose of irradiation have no large damage effect on target cells. On the other hand high dose of irradiation cause cell death via necrosis. The major effort of PDT in the field of cancer diseases is to induce cell death mediated by apoptosis. The apoptotic mechanism accompanies DNA fragmentation. The comet assay seems to be good and mainly rapid method to detect DNA cleavage. Moreover our results shows

that low radiation dose of visible light (0.1–0.5 J.cm⁻²) can be use for PDT of tumour cell line G361 using as the sensitizer molecular complex 10 μM ZnTPPS₄ with 1 mM cyclodextrin carrier hpβCD.

Acknowledgement

This work was supported by the grant project of the Grant agency of Czech Republic No. 203/02/1483 and Ministry of Education MSM No. 153100008.

References

1. Agarwal R, Korman NJ, Mohan RR et al. Apoptosis is an early event during phthalocyanine photodynamic therapy-induced ablation of chemically induced squamous papilomas in mouse skin. *Photochem Photobiol* 1996;63(4):547–52.
2. McNair FI, Marples B, West CML, Moore JV. A comet assay of DNA and repair in K562 cells after photodynamic therapy using haematoporphyrin derivate, methylene blue and meso-tetrahydroxyphenylchlorin. *Br J Cancer* 1997;75(12):1721–9.
3. Kessel D, Luo Y. Initiation of apoptosis versus necrosis by photodynamic therapy with chloroaluminium phthalocyanine. *Photochem Photobiol* 1997;66(4):479–83.
4. Mosinger J, Kliment V, Sejbal J et al. Host-guest complexes of anionic porphyrin sensitizers with cyclodextrins. *J Porphyrins Pthalocyanines* 2002;6:513–25.
5. Piperakis MP, Visvardis EE, Tassiou AM. Comet assay for nuclear DNA damage. *Methods Enzymol* 1999;269(20):184–94.

*Mgr. Jaroslav Maceček,
Palacky University in Olomouc, Faculty of Medicine,
Department of Medical Biophysics,
Hněvotínská 3, 775 15 Olomouc,
Czech Republic.
e-mail: macecele@tunw.upol.cz*

REPORT ON THE COURSE OF STUDY BZ-1003-BR FOLLOWING THE CHANGES IN AIRWAYS IN STUTTERERS WITH THE HELP OF PULSE OSCILLOMETRY (MASTER SCREEN IOS)

*Josef Pešák¹, Tomáš Grézl¹, Ludmila Hurtová¹, Lenka Modráčková² and working group**

Palacky University in Olomouc, Medical Faculty, Czech Republic: Institute of Medical Biophysics¹; Palacky University in Olomouc, Faculty of Education, Czech Republic: Department of Musical Education²

*Dagmar Vodičková, Zlín; Zdeňka Skeřilová, Ostrava; Dagmar Pluháčková, Břeclav; Renata Rokytová, Kroměříž; Dana Popelářová, Staré Město u Uherského Hradiště; Marcela Kozáková, Prostějov

Summary: Stuttering affects people all over the world. At the age of six years, about 1.5 percent of children suffers from stuttering. Although stuttering resolves spontaneously upon reaching adulthood in approximately 80% of those affected, it continues to have significant health and social consequences. So far, its etiology remains unknown. The organic differences in those with stuttering and those free of speech problems have been evaluated. As a result of these examinations, it has been hypothesized that stuttering results from functional pneumoobstruction of the tracheobronchial tree in the peripheral respiratory passages. As for now, no similar therapeutic procedure, using a bronchodilating agent in the treatment of stuttering, has been described. Preliminary findings of a pilot study (15,16) are surprisingly positive. In October of 2003, a multicenter open clinical trial (Stage III) to verify the effect of a sympathomimetic agent formoterol was initiated. The study is being realized in six centers in Moravia and enrolls approx. 40 patients (children, adolescents and young adults). First experience and initial evaluation of the cohort are presented here.

Key words: Stuttering; Bronchodilatation; Pulse oscillometry

Introduction

Stuttering is a very sad problem for people affected by this speech impediment. We can mention that the evidence of this handicap has been known for more than 4 millenniums. This is an important reference for following connections and links associated with stuttering on time axis backward. The second interest is the information that localizes areal occurrence of the most various names for stammering. Richard Kitchen and Van Riper (1) in their work *The Nature of Stuttering* (1982) gathered up the marks for stammer virtually all over the world:

- in Europe near 21 nationalities,
- in the East near 15 state formations, from which entirely of 11 languages at Indians,
- in Africa near 10 nationalities,
- on American continent in 4 regions, from which only at original inhabitants - at 11 American-Indian tribes and
- in Pacific in 3 insular territories.

From the etymological point of view are all these expressions synonyms of the substantive stuttering (that is in

a quantity of 75) of miscellaneous onomatopoeic appellations. For instance: Czech word *koktat* (to stammer) means to pronounce *ko-ko-ko*, as a comparison to *kohout* (a cock). (*Kohout* - in old Czech *kohút* - has Slavonic onomatopoeic basis *ko-ko*, which means cock that is gathering his hens.) (2).

Altogether they are primitive imitations of iterative utterance when the speech fluency is disturbed by stammer.

Stammer is a noticeable speech and communication impediment that occurs in time and place and that is so general that there is an assumption that the cause of this disorder could be also one of the most general. Proportionally to the previous supposition, there is a possible general biophysical interpretation (3) that was later presented at neurological forum (4) and afterward even at The Department of Respiratory Diseases and Tuberculosis, Teaching Hospital in Olomouc (5). Hypothetical etymology of the word stuttering was published in *Medical Hypotheses* (6). Subsequently, other reports were published (7,8,9).

On the basis of the Paediatric clinic seminar with the main topic called „children and teenage stammering“, there

was a block of the lectures about children speech disorders on XXIst Days of Clinical and Practical Paediatrics, part of which was an information about stuttering (10). In presented note and in the following performances there were reports about the first experience with stammer therapy (11,12).

On the basis of previous findings, a clinical trial was proposed and approved by the Ethics Committee of the Teaching Hospital and the Faculty of Medicine, Palacký University, Olomouc (13). The company ZAK-PharmaServices s.r.o. prepared the final protocol of the study evaluating the effectiveness and safety of a sympathomimetic agent formoterol in the alleviation of speech non-fluency (14).

The aim of the present contribution is to refer on the clinical study project and methods; the results, both preliminary and final ones, will be reported later.

Present description of therapy with the assistance of bronchodilatation after more than one year of usage of formoterol in the case of the same female subject (13 years) as in previous citations (10,11) is given in reports (15) and (16).

Material and methods

Protocol (14) defines the Teaching Hospital in Olomouc as the central specialized facility. Evaluation of the treatment will involve initial biochemical test, neurological tests EEG and EMG. Further on, test of heart rate variability VSF by the VarCor PF-5 instrument and the speech records of chosen subjects, and spirometric tests with the assistance of instrument MasterScreen IOS (specific functional parameters of lung - rate of flow volume and peripheral limitations of small airways) will be performed. The program of impulse oscillometry IOS provides a reliable analysis of pulmonary distribution disorders, including impairment of the mechanics of breathing. Graphic presentation modelling the lungs gives a rapid overview of the level of pulmonary functions. The respiratory flow is superposed by short-term test impulses. Accurate measuring of flow signal together with resulting response of pulmothoracic pressure brings about the respiratory impedance. Impulse oscillometry is a most useful tool for differential diagnostics of diseases of pulmothoracic system. It is highly sensitive in registering peripheral limitation of respiratory tract, instability



Fig. 1. Detailed view of spirometric investigation.

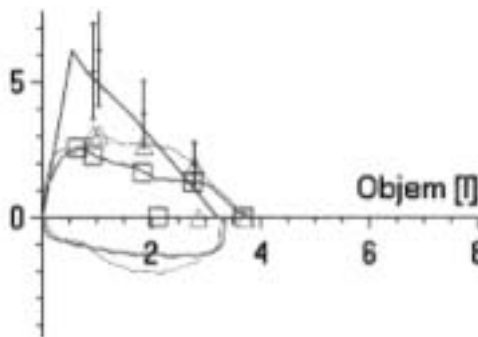


Fig. 2. Entry of the instance of discharge measurement of the volume in a stutterer.

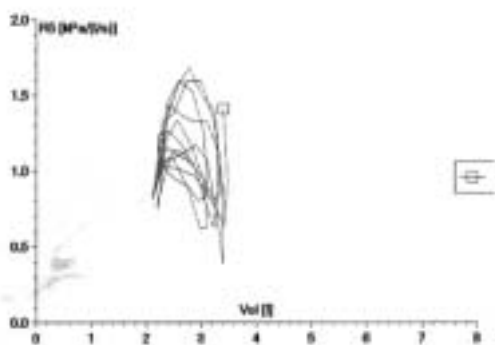


Fig. 3. Entry of the instance of resistance in upper airways of a stuttering subject.

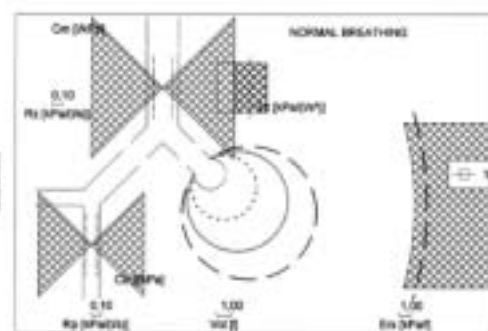


Fig. 4. Entry of the instance of registration of obstructions in airways.

of bronchial tract (air trapping) as well as in determination and differentiation of extrathoracic stenosis. Its sensitivity makes it able to register even the changes considered as physiological from the respiratory point of view, but typical for subjects suffering from the speech fluency disorders.

Figure 1 presents a detailed view of spirometric investigation. Above mouthpiece in top part above trapezoidal tesserae, outer generator equipment Master Screen IOS is fixed. Following figures show examples of investigation records. Fig. 2 a flow volume, Fig. 3 retrained, incarcerated air in small airways, and Fig. 4 an illustrative entry of obstructions in airways.

Number of experimental centres finally stabilized at 6. They are localized in six Moravian towns from Břeclav to Ostrava. The first test was realized on November 11th and on February 25th we decided to finish entrance test with the number of 42 surveyed subjects. New centres were opened after above mentioned entrance tests in experimental centres by a monitor (ZAK-PharmaServices). The process of opening the therapy in separate centres continues while the first patients are almost ready for the second visit in these centres, as it has been supposed in The Scheme of the study progress. These time periods between particular visits in the centres happen due to the consumption of 60 Foradil[®] capsules with the minimal dose of formoterol 12 µg/capsule.

Subjects were chosen by physicians with specialization in phoniatrics (co-authors of the contribution) in six centres of the opening multicentric study BZ-1003-BR. According to the age, group I involved 28 boys (\bar{x} = 11.357 years, s = 2.683 years) and 8 girls (\bar{x} = 13.625, s = 3.248 years) and group II (18–25 years) consisted of 5 men (\bar{x} = 21.5 years, s = 2.683) and 2 women (\bar{x} = 19.5, s = 2.18 years). Spirometric investigation was effected by pulsed oscillometer Master Screen IOS Kurka Jaeger. Then the investigation of flow-volume and inconstancy of bronchial organism was performed. (Air trapping - incarcerate air in small airways), as well as the spirometric investigation at 43 stutterers. This investigation also followed 1) "voluminous" position V of peak-flow at expiration PEF_R, 2) peripheral limitation of inspiratory tract by IOS method, 3) central R_z and peripheral R_p resistance of the airways, 4) positions of characteristic waveforms of general inspiratory speed R₅ and distal capacitance X₅. All monitored values exceeded tolerance limits. Tetanic syndrome was discovered during the investigation in 37 subjects (86%).

Conclusion

Pathological findings at monitored inspiratory functions were registered in 43 observed stuttering subjects.

One patient (female, 21 years) had to be excluded from the study due to increased parameters THS (8.128 mU/l - physiol. range 0.35–5.5) and T3 (FT3) (7.06 pmol/l - physiol. range 3.54–6.47).

References

1. <http://mankato.msus.edu/dept/comdis/kuster/words.html>.
2. Holub J, Leyer S. Stručný etymologický slovník jazyka českého. Praha: SPN, 1978.
3. Pešák J. Balbuties, vada řeči & biofyzikální hypotéza její neznámé etiologie. In: Rosina J, ed. Sborník abstrakt XXIV. Dny lékařské biofyziky, konference s mezinárodní účastí. Praha: Ústav lékařské biofyziky UK, 2001.
4. Pešák J, Bartek J, Zatloukal J. Neuropatofyziologický pneumoobstrukční faktor u balbuties. In: Kuchár M, ed. 48. Společný zjazd slovenskej a českej spoločnosti pre klinickú neurológiu. Nové Zámky, 2001.
5. Pešák J. Hypotetický pohled na etiologii balbuties. Odborný seminář Kliniky TBC a respiračních nemocí, Klinika plicních nemocí a TBC, LF UP a FNO v Olomouci, Olomouc 5. 12. 2001.
6. Pešák J. Pneumoobstruction of the tracheobronchial tree as a hypothetical cause of balbuties. Medical Hypotheses 2002;59(4):458–61.
7. Pešák J, ed. Hypotéza pneumoobstrukční etiologie koktavosti. In: Sborník přednášek 9. semináře univerzitního Společenství pro studium hlasu a řeči. Olomouc: Ústav lékařské biofyziky LF UP v Olomouci, 2002.
8. Pešák J. Hypotéza pneumoobstrukční etiologie koktavosti. In: Dlouhá O, Lašfovka M, eds. Novinky ve foniatрии 2002. Praha: Galén, 2002.
9. Pešák J. Koktavost, balbuties: K popisu současné situace. In: Pešák J, ed. Sborník přednášek SEMINÁŘE DĚTSKÉ KLINIKY s hlavním tématem „balbuties, koktavost u dětí a mladistvých“. Olomouc: Ústav lékařské biofyziky LF UP v Olomouci, 2003.
10. Pešák J, Maňásková E. Koktavost. *Pediatric pro praxi* 2003;4(3):171.
11. Pešák J. Primární experiment klinického zmírňování (odstraňování) neplynulosti řeči u dětí a mladistvých s balbuties. In: Pellant A, Chrobok V, eds. Sborník abstrakt 66. kongresu České společnosti otolaryngologie a chirurgie hlavy a krku ČLS JEP s mezinárodní účastí k příležitosti 100 let založení Nemocnice Pardubice. Hradec Králové: NUCLEUS HK, 2003.
12. Pešák J. Ověřování klinického odstraňování (zmírňování) neplynulosti řeči u dětí a mladistvých s balbuties. In: Lejska M, ed. Sborník 1. česko-slovenského foniatrického kongresu a XIV. celostátních foniatrických dnů Evy Sedláčkové, Brno: Audio-Fon Centr s.r.o., 2003.
13. Rozhodnutí Etické komise Fakultní nemocnice a Lékařské fakulty UP v Olomouci, čj. 46/03. Ověřování klinického odstraňování (zmírňování) neplynulosti řeči u dětí a mladistvých s balbuties. Olomouc 2003.
14. Protokol: BZ-1003-BR Ověřování vlivu bronchodilatace na plynulost řeči u nezletilých i dospělých s balbuties, Součást výzkumného záměru MSM 152100018, ZAK-Pharma Services s.r.o., Finální verze 03.11.03, Brno 2003.
15. Pešák J. Zmírňování zadržávání v řeči u dětí a mladistvých s balbuties po aplikaci β_2 sympatomimetika formoterol. *Klin Farmakol Farm* 2004;18(1): 19–20.
16. Pešák J. Preliminary experience with formoterol for the treatment of stuttering. Letter to the Editor. *Ann Pharmacother* 2004;38(7–8):1323.

Prepared under the sponsorship of the research task MSM 152100018 "Integrated study of voice and speech".

*Doc. RNDr. Josef Pešák, CSc.,
Palacky University Olomouc,
Faculty of Medicine,
Institute of Biophysics,
Hněvotinská 3, 775 15 Olomouc,
Czech Republic.
e-mail: pesak@tunw.upol.cz*

STABILITY OF BOVINE CYTOCHROME *c* OXIDASE AS STUDIED AFTER EXPOSURE TO HIGH HYDROSTATIC PRESSURE

Jana Staničová¹, Andrej Musatov², Neal C. Robinson²

University of Veterinary Medicine, Košice, Slovak Republic; Institute of Chemistry, Biochemistry, and Biophysics¹; The University of Texas Health Science Center, San Antonio, Texas 78229-3900, USA; Department of Biochemistry²

Summary: Structural and functional stability of bovine cytochrome *c* oxidase as a function of exposure to high hydrostatic pressure is reported. The pressure affects the stability of monomeric and dimeric enzyme quite differently. Exposure of the monomeric cytochrome *c* oxidase to pressures higher than 2.5 kbar causes dissociation of subunits III, VIa, VIb, VIIa with a 35–50 % decrease in electron transport activity. Dimeric enzyme is more resistant to high hydrostatic pressure since subunits III and VIIa do not dissociate and the electron transport activity loss is minimal.

Key words: Cytochrome *c* oxidase; High hydrostatic pressure; Dimer; Monomer; Electron transport activity; Subunit dissociation

Introduction

Cytochrome *c* oxidase (CcO[§]; Ec 1.9.3.1) is the terminal enzyme of the inner mitochondrial electron transport chain (18). Bovine heart CcO is consisted of 13 different subunits (6) and the enzyme is almost always dimeric in three-dimensional lattice as it was obtained from crystallographic data (15).

The three largest subunits (I-III) are encoded by mitochondrial DNA and are synthesized in the mitochondria. They constitute the functional core of the enzyme and include all of the redox-active centers. The smaller subunits (IV-VIII) are nuclear encoded and most likely have a structural and/or regulatory role (4,5).

Treatment of CcO with physical (high hydrostatic pressure) or chemical (chaotropic agents, e.g., urea - 13, peroxidation by hydrogen peroxide - 9) factors enables to study the structural effects. Consequently, the relation between structural changes and enzymatic activity may be determined. We report the effects of hydrostatic pressure on electron transport activity and structural composition of CcO. Our approach is the study of pressure influence on CcO in view of different behavior of dimeric and monomeric CcO forms.

Materials and methods

Materials. Bovine cytochrome *c* oxidase was prepared from Keilin-Hartree heart particles by the method of Fowler

et al. (2) with modifications described by Mahapatro and Robinson (8). The final oxidase pellet was solubilized in 100 mM phosphate buffer, pH 7.4 containing 1 % sodium cholate and 1 mM EDTA. Individual drops of purified enzyme (25 mg/mL protein) were quickly frozen by pipetting the solution into liquid nitrogen and stored at -80 °C. Cytochrome *c* oxidase concentrations were calculated on the basis of $\epsilon_{422} = 1.54 \times 10^5 \text{ M}^{-1}\text{cm}^{-1}$ (16). Horse heart cytochrome *c* (Type III) was purchased from Sigma Chemical Co. Reduced cytochrome *c* was freshly prepared by dithionite reduction, and an excess dithionite was removed by G-25 Sephadex gel filtration. Initial concentrations of ferrocyanochrome *c* were determined using $\epsilon_{550} = 21 \text{ mM}^{-1}\text{cm}^{-1}$. All other chemicals were reagent grade.

Methods. The high hydrostatic pressure experiments were performed as described in (11). Kinetics measurements and fluorescence spectra were recorded, respectively. In case of kinetics measurements tryptophan fluorescence was monitored ($\lambda_{\text{ex}} = 295 \text{ nm}$, $\lambda_{\text{em}} = 326 \text{ nm}$) as a function of time. Fluorescence spectra of tryptophan were recorded in emission range 300–500 nm using excitation wavelength 295 nm.

Determination of cytochrome *c* oxidase activity. Molecular activity of CcO was assayed spectrophotometrically at 25°C with 25–30 μM ferrocyanochrome *c* as a substrate in 25 mM phosphate buffer, pH 7.0, containing 1 mg/mL dodecyl maltoside. Molecular activities were calculated by the pseudo-first-order rate of oxidation of ferrocyanochrome *c* by

[§]Abbreviations: CcO, bovine heart cytochrome *c* oxidase; EDTA, ethylenediaminetetraacetic acid; FPLC, fast performance liquid chromatography; HPLC, high performance liquid chromatography; SDS-PAGE, sodium dodecyl sulfate polyacrylamide gel electrophoresis

1.75 nM cytochrome *c* oxidase (1). The activity of the purified enzyme was 300–350 s⁻¹ to an accuracy of ± 5%.

HiTrapQ FPLC ion exchange chromatography. Anion exchange chromatography on the HiTrapQ column was a modification of the method developed for a MonoQ FPLC column (7) and was used as described in (7).

Analysis of subunits. Nuclearly encoded subunits (subunits IV–VIII, nomenclature according to Kadenbach et al. (6) were determined by C₁₈ reversed phase HPLC (7). Absorbance intensity of subunit Vb was taken as the intensity standard for the chromatogram normalization. Determination of three mitochondrially encoded subunits (subunits I–III) was performed by SDS-polyacrylamide gel electrophoresis on 15% acrylamide gels that contained 2 M urea in addition to 0.1% SDS (12). Subunit content was determined by scanning on Personal Densitometer SI (Molecular Dynamics) using ImageQuant version 5.2 software.

Results

Monomeric and dimeric CcO were prepared by manipulating the concentrations of dodecyl maltoside and sodium cholate; high concentrations of dodecyl maltoside (5–10 mM) produce monomeric CcO while a mixture of dodecyl maltoside and sodium cholate produce dimeric CcO [10]. Homogeneity of the monomeric or dimeric forms was confirmed by sedimentation velocity as previously described (17).

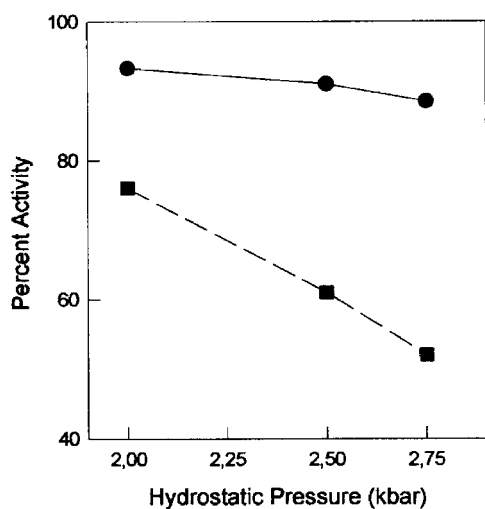


Fig. 1: Dependence of dimeric and monomeric cytochrome *c* oxidase activity on high hydrostatic pressure. Dimeric CcO (5 μM) (circles) was prepared in 20 mM Tris-Cl pH 7.4 with 1mg/mg protein dodecyl maltoside in absence of dialysis. Monomeric CcO (5 μM) (squares) was prepared with 5mg/mg protein dodecyl maltoside followed by dialysis overnight in 20 mM Tris-Cl pH 7.4 with 0.1mg/mL dodecyl maltoside.

Effect of high pressure on the electron transport activity of cytochrome *c* oxidase. Molecular activity of dimeric and monomeric CcO was assayed spectrophotometrically and obtained results showed a significant difference in the pressure-induced effect of dimer, and monomer, respectively. Exposure of dimeric CcO to pressure causes minimal loss of activity of enzyme (7–13% at the pressures 2.00–2.75 kbar) (Fig.1). On the other hand the same pressures induce remarkable decrease in activity of monomeric CcO (24–48%) (Fig.1). From these results we can conclude that dimeric CcO is functionally more stable than monomeric one if both forms are exposed to the equal hydrostatic pressure.

Effect of high pressure on the structural composition of cytochrome *c* oxidase. We used HiTrapQ ion exchange chromatography, combined with C₁₈ reversed-phase HPLC and SDS-PAGE for quantitatively assessing a subunit content of CcO. Chromatographic elution of purified CcO from a HiTrapQ FPLC ion exchange column allows a separation of intact 13-subunit CcO complex from a form that is missing subunits (7). Figure 2a shows HiTrapQ FPLC elution of dimeric CcO after exposure to high hydrostatic pressure 2.5 kbar. Protein eluted as the peak A and a small peak B without a significant difference between pressure-treated CcO and control sample (Fig. 2a). The gel electrophoresis and C₁₈ HPLC chromatography confirmed that peak A contains intact 13-subunit complex and peak B contains 11 subunits and is completely devoid of subunit VI and VIb.

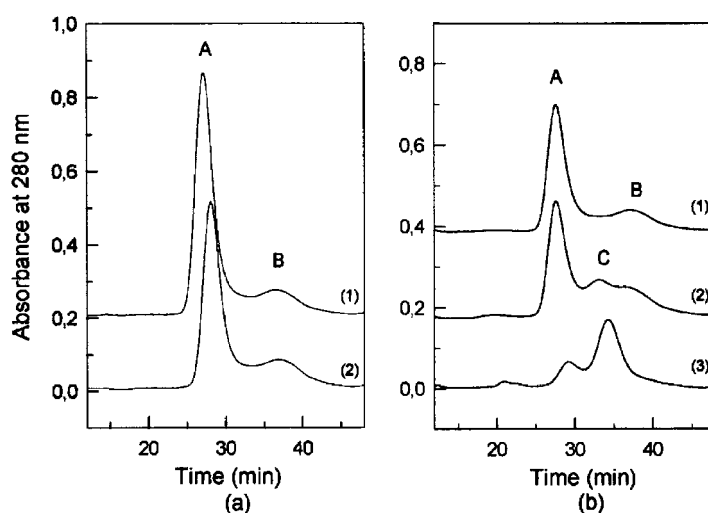


Fig. 2: HiTrapQ FPLC ion exchange chromatography elution of dimeric (a) and monomeric (b) cytochrome *c* oxidase as measured after exposure to high hydrostatic pressure. Both forms were prepared as described in Fig. 1. The elution gradient was as described previously (7). HiTrapQ elution of dimer (a) after exposure to 2.5 kbar is represented by trace 2. Trace 1 shows the elution of control sample. The elution of monomer (b) after exposure to 2.00 kbar is represented by trace 2, and to 2.5 kbar by trace 3. Trace 1 shows elution of sample in absence pressure.

Different situation became when the monomeric CcO was exposed to high hydrostatic pressure (Fig. 2b). Increase of pressure to 2.5 kbar caused a remarkable change in the chromatographic elution of monomeric CcO (Fig. 2b trace 3). As it can be seen from figure, the peak C was the most intensive and the peak B completely disappeared.

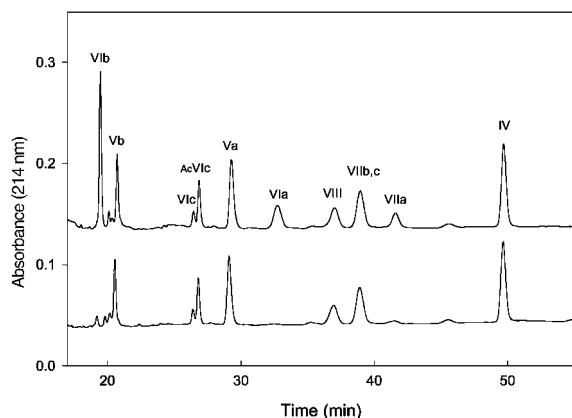


Fig. 3: Subunit content of two forms of CcO after exposure to high hydrostatic pressure as determined by reversed phase HPLC. Upper trace: subunit content of HiTrapQ Peak A, which is the intact 13-subunit CcO. Lower trace: subunit content of HiTrapQ Peak C, which is the subunit depleted form of CcO. The method quantitatively determines the content of the 10 nuclear encoded subunits (subunits IV through VIII), but does not detect the mitochondrially encoded subunits I, II and III (refer to Fig. 4 for their analysis).

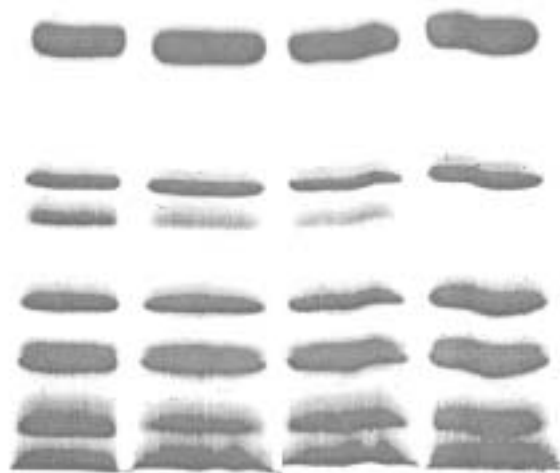


Fig. 4: SDS-PAGE subunit content of HiTrapQ elution peak A (13-subunit intact form) of pressure-untreated monomeric CcO (column 1), peak A of pressure-treated (2.5 kbar) monomeric CcO (column 2), peak B (11-subunit form) of pressure-untreated CcO (column 3), and peak C of pressure-treated CcO (column 4). Conditions SDS-PAGE are described in Methods.

Reversed-phase C_{18} HPLC enables to determine the 10 nuclear encoded subunits (IV - VIII), which are very difficult to separate by SDS - PAGE (7). We used this method for a determination of monomeric CcO subunit composition of eluting protein shown in Fig. 2b (peaks A, C) (Fig. 3).

The chromatographic analysis of the peak C shows a loss of subunits VIa, VIb, VIIa (Fig. 3). Content of subunit VIIa was only 17% from that in the absence pressure and the intensity of subunits VIa (2%) and VIb (8%) decreased enormously (Fig. 3). Similar results were obtained when monomeric CcO was exposed to 2.75 kbar pressure. From our findings, we can conclude that the most of the monomeric CcO exposed to pressure 2.5 kbar and higher values occurs in the form, which is missing subunits VIa, VIb and VIIa (Figures 2b and 3).

Determination and quantitation of the three largest subunits (I - III) was provided by SDS-PAGE. The composition of the monomeric CcO exposed to 2.5 kbar eluting in the HiTrap elution as peaks A, C (Fig. 2b, trace 3) as well as the control enzyme resulting in peaks A, B is shown in Fig. 4, columns 1-4.

The intact 13-subunit control CcO eluted as peak A is presented in column 1 in Fig. 4 and the intact 13-subunit complex of CcO exposed to 2.5 kbar is shown in column 2. Although we can see a small difference in intensity of subunit III band between control sample and sample exposed to pressure, the subunit III is 96% the control sample. Remarkable change was recorded in case of peak C. Subunit III band of the pressure treated enzyme completely disappeared (Fig. 4, column 4) and the percent of this subunit is only 6% the control CcO. From results obtained using SDS-PAGE it is clear that not only subunits VIa, VIb, VIIa but also subunit III is missing in peak C elution of monomeric CcO. We can conclude: the exposure of monomeric CcO to pressure higher than 2.5 kbar leads to changes of its composition and therefore, disturbs a structural integrity of monomeric enzyme. With dimeric enzyme, only subunits VIa and VIb dissociate, neither of which is essential for full electron transport activity.

Discussion

High hydrostatic pressure was used as a physical factor for a study of possible different behavior of dimeric and monomeric CcO. Both forms of CcO were estimated from point of view of its partial functional stability (pressure effect on redox- state of CcO (unpublished results) and electron transport activity; proton pumping has not been estimated) and structural stability (pressure effect on subunit dissociation). We found that high hydrostatic pressure affects the structural and functional stability of monomeric and dimeric CcO quite differently.

The chemical effects on the structure and enzymatic activity of dimeric CcO were investigated (9,13,14). Treat-

ment of dimeric CcO with chemical factors (removal of cardiolipin -14, treatment with urea -13, hydrogen peroxide -9) has important consequences on the structure and function of dimeric enzyme. From our results and considering findings in (14) we can suppose partial dissociation of subunits VIa and VIb due to hydrostatic pressure, which is finished on chromatographic column. In accordance with (14), the decrease in electron transport activity of dimeric CcO due to high pressure was not significant. The exposure of dimeric CcO to chemical factors has more consequences than the exposure to hydrostatic pressure. Possible explanation can be different acting of the pressure. In summary, dimeric form of enzyme is very stable when exposed to high hydrostatic pressure.

The different situation is when the monomeric CcO is treated with high hydrostatic pressure. The exposure of monomeric enzyme to hydrostatic pressure causes dissociation of subunits III, VIa, VIb, VIIa with a significant decrease in electron transport activity. Also the percent of reduction is higher when monomer is exposed to pressure. The subunits VIa and VIb are not responsible for the loss of activity (14) of enzyme. It is known that the dissociation of core subunit III does not alter electron transport activity of CcO (3). From our results we can suppose that the dissociation of subunit VIIa causes significant decrease in enzymatic activity of monomeric CcO. These findings are consistent with results obtained by exposure of CcO to urea (13).

In summary, we can conclude that high hydrostatic pressure perturbs functional (electron transport activity) and structural integrity of monomeric CcO, while dimeric form is more resistant to pressure. Monomeric form of CcO is more fragile than dimeric CcO- this fact can contribute to the general assumption that dimeric form of CcO occurs in vivo.

Acknowledgements

This work was supported by a research grants from National Institutes of Health (NIH GMS 24795) and The Robert A. Welch Foundation (AQ 1481)

The authors especially wish to thank Dr. Mark Panda for his help with the pressure experiments and Ms. Linda Sowdal for technical assistance.

References

1. Dale MP, Robinson NC. Synthesis of cardiolipin derivatives with protection of the free hydroxyl: its application to the study of cardiolipin stimulation of cytochrome c oxidase. *Biochemistry* 1988;27:8270-5.
2. Fowler LR, Richardson SH, Hatefi Y. A rapid method for the preparation of highly purified cytochrome oxidase. *Biochim Biophys Acta* 1962;64:170-3.
3. Haltia T, Saraste M, Wikström, M. Subunit-III of cytochrome-c-oxidase is not involved in proton translocation - a site -directed mutagenesis study. *EMBO J* 1991;10:2015-21.
4. Kadenbach B. Regulation of respiration and ATP synthesis in higher organisms. *J Bioenerg. Biomembr.* 1986;18:39-54.
5. Kadenbach B, Merle P. On the function of multiple subunits of cytochrome c oxidase from higher eukaryotes. *FEBS Lett* 1981;135:1-11.
6. Kadenbach B, Jaraush J, Hartmann R, Merle P. Separation of mammalian cytochrome c oxidase into 13 polypeptides by a sodium sulfate-gel electrophoretic procedure. *Anal Biochem* 1983;129:517-21.
7. Liu YC, Sowdal L, Robinson NC. Separation and quantitation of cytochrome c oxidase subunits by Mono-Q fast protein liquid chromatography and C18 reverse-phase high-performance liquid chromatography. *Arch Biochem Biophys* 1995; 324:135-42.
8. Mahapatro SN, Robinson NC. Effect of changing the detergent bound to bovine cytochrome c oxidase upon its individual electron-transfer steps. *Biochemistry* 1990;29:764-70.
9. Musatov A, Hebert E, Carrol CA, Weintraub ST, Robinson NC. Specific modification of two tryptophans within the nuclear-encoded subunits of bovine cytochrome c oxidase by hydrogen peroxide. *Biochemistry* 2004;43:1003-9.
10. Musatov A, Ortega-Lopez J, Robinson NC. Detergent-solubilized bovine cytochrome c oxidase: dimerization depends on the amphiphilic environment. *Biochemistry* 2000;39:12996-13004.
11. Panda M, Ybarra J, Horowitz PM. Dissociation of the single-ring chaperonin GroEL by high hydrostatic pressure. *Biochemistry* 2002;41:12843-9.
12. Robinson NC, Strey F, Talbert L. Investigation of the essential boundary laeyr phospholipids of cytochrome c oxidase using Triton X-100 delipidation. *Biochemistry* 1980;19:3656-61.
13. Sedlák E, Robinson NC. Removal of bound cardiolipin destabilizes the quaternary structure of bovine heart cytochrome c oxidase. *Biochim Biophys Acta (Suppl.)* 2002;12:119.
14. Sedlák E, Robinson NC. Phospholipase A2 digestion of cardiolipin bound to bovine cytochrome c oxidase alters both activity and quaternary structure. *Biochemistry* 1999;38:14966-72.
15. Tsukihara T, Aoyama H, Yamashita E et al. The whole structure of the 13-subunit oxidized cytochrome c oxidase at 2.8 Å. *Science* 1996;272:1136-44.
16. van Gelder BF. Optical properties of cytochromes from beef heart mitochondria, submitochondrial vesicles, and derived preparations. *Methods Enzymol* 1978; 53:125-8.
17. van Holde KE, Weischet WO. Boundary analysis of sedimentation - velocity experiments with monodisperse and paucidisperse solutes. *Biopolymers* 1978; 17:1387-1403.
18. Wikström M, Krab K, Saraste M. *Cytochrome Oxidase: A synthesis*, London: Academic Press, 1981:136.

**Doc. RNDr. Jana Staničová, Ph.D.,
University of Veterinary Medicine,
Institute of Chemistry, Biochemistry, and Biophysics,
Komenského 73, 041 81 Košice,
Slovak Republic.
e-mail: stanicova@uvm.sk**

SOFTWARE FOR THE ANALYSIS OF SPECIES-SPECIFIC VOCALIZATIONS

Daniel Šuta^{1,2}, Martin Komárek³, Milan Jilek², Josef Syka²

Charles University in Prague, 3rd Faculty of Medicine, Czech Republic: Institute of Medical Biophysics and Informatics¹; Academy of Sciences of the Czech Republic, Institute of Experimental Medicine, Czech Republic: Department of Auditory Neuroscience²; Czech Technical University, Faculty of Electrical Engineering, Czech Republic: Department of Cybernetics³

Summary: Vocalization calls are behaviorally relevant complex sounds that typically contain several harmonics and show frequency and amplitude modulation. In this paper, an introduction to a software tool for the analysis of species-specific vocalizations is presented. The algorithm automatically or under user supervision detects time-varying amplitude and frequency parameters, which can serve for the statistical analysis of calls or as the substrate for the manipulation and synthesis of artificial calls. The described program and its results will be used in studying the representation of complex sounds in the central nervous system.

Key words: Acoustical signal; Communication sound; Neural system; Software; Species-specific vocalization

Introduction

Natural environmental sounds, such as species-specific vocalizations, are behaviorally important sounds with complex acoustical patterns. When studying the neural representation of such spectrotemporally complex stimuli, a fundamental question is to understand which aspect or parameter of the stimulus neurons are sensitive to. This requires the ability to systematically change the stimulus in many aspects. Traditional methods of call modification are based on various filtering strategies or global operations such as signal time reversal, time compression, or time expansion, which are typically performed on examples of representative calls. There are at least two limitations to this approach. First, when an example of the call is used, it may not be statistically accurate in representing a particular type of species-specific vocalizations. Second, there are many aspects of a complex call that cannot be changed by filtering or global operations. In order to address these limitations, a program tool has been developed for analyzing the spectrotemporal pattern of species-specific vocalizations. The design of the program was adjusted for its application in the field of auditory neuroscience.

Materials and methods

The software was programmed in Matlab version 5.3. (and also tested in version 6.5) with the Signal Processing Toolbox as part of a complex software solution for processing communication sounds, containing routines for record-

ing, analysis, modification and synthesis. The user interface employs a graphic environment for the interactive control of sound processing. The file input subroutine can read sound files in the standard wave format (*.wav) or in Matlab binary format.

Before the analysis starts, the segmentation subroutine can be used for separating individual calls or call phrases in the sound record. The segmentation is performed in the time domain, and individual sound segments can be saved into separate files in wave format (wav) or Matlab binary format.

The analysis algorithm is essentially a peak-picking contour extractor. The position of the fundamental frequency as well as the positions of higher harmonics are detected in the short-time sound spectra obtained by windowed fast Fourier transform (FFT). The user can control almost all algorithm parameters, such as the number of points and the overlap of the FFT or the number of harmonics. Individual frequencies are detected as positions of local energy maximums in the sound spectrum. A higher accuracy is obtained by tracking the energy peaks over the entire duration of the sound with a correction performed under the assumption of a continuous time course for all frequencies and the harmonic structure of the spectrum. Any part of the signal whose total energy falls below a certain threshold is assumed to be a silent period and does not affect the analysis algorithm.

Results

The application of the program was tested using calls of adult guinea pigs and very young rats (P10). Figure 1 shows

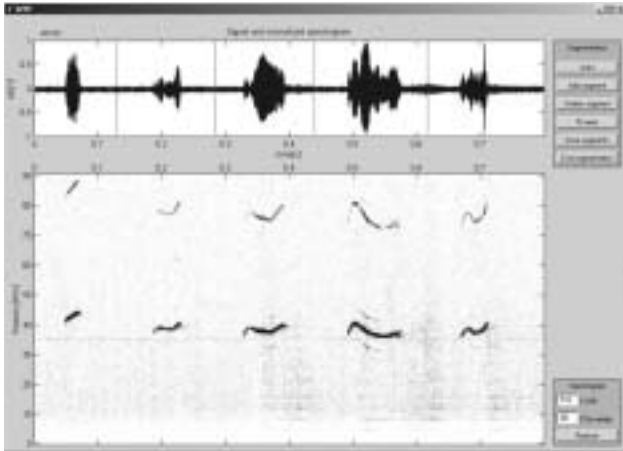


Fig. 1: Copy of the computer screen showing segmentation performed on a ~ 0.8 s long part of a rat vocalization. The upper panel shows the waveform of the signal; the lower panel shows the spectrogram of the signal. Vertical lines in the waveform represent the limits of each time segment as set by the user.

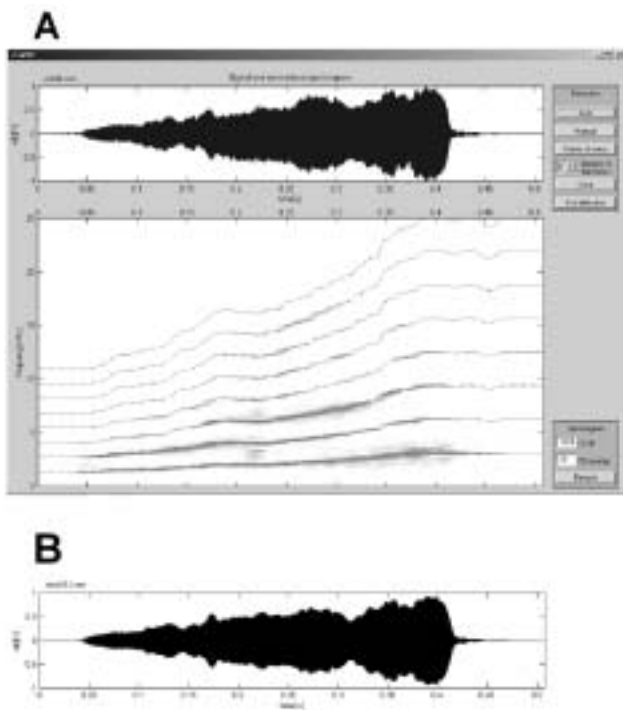


Fig. 2: A. Copy of the computer screen showing the result of signal detection performed on the guinea pig vocalization call 'whistle'. The upper panel shows the waveform of the signal; the lower panel displays the spectrogram of the signal with superimposed lines representing the time courses of individual harmonics as obtained by automatic detection.

B. The waveform of the artificial 'whistle' synthesized from the parameters obtained by the detection algorithm.

the segmentation of a rat vocalization signal sampled at 181 kHz. The signal is graphically represented by its waveform and spectrogram. The signal can be divided into several phrases by automatic operation or manually by introducing marks (shown as vertical lines in the waveform) with a computer mouse. There are two possible reasons to separate individual phrases of calls consisting of many phrases. First, it makes it possible to separate a time segment of interesting signals from uninteresting ones (e.g., a call from noise or another call). Second, if a vocalization consisting of many phrases is divided into individual phrases, the order of phrases can later be easily changed or randomized when altered call is synthesized.

The result of the detection algorithm performed on the guinea pig vocalization call 'whistle' (sampled at 50 kHz) is shown in Fig. 2A. Lines in the spectrogram indicate individual harmonics as found by the automatic detection algorithm. The accuracy of the detected sound parameters is illustrated on the artificial 'whistle' (Fig. 2B), which was synthesized [4] from the detected parameters of the natural 'whistle'. The waveform of the artificial 'whistle' (Fig. 2B) closely resembles the waveform of the original (natural) 'whistle' (Fig. 2A).

The output of the parameter identification module serves for the subsequent statistical analysis of individual types of species-specific vocalizations. The significance of this approach is that it accurately captures the statistical properties of species-specific vocalizations and allows the generation of both representative calls and their artificial variants for studying the representation of this class of complex sounds at various stages of the central auditory system.

Discussion

The algorithm represents a general-purpose solution for the description of species-specific vocalizations, e.g. of bat (3), guinea pig (5,6), rat (4), dolphin (2) or primates (7), but there are also some limitations in its application. First, the procedure assumes an appropriate quality of the recorded sounds. This means a reasonable signal-to-noise ratio and also the isolation of individual calls in the record because an overlap of two or more sounds in the record can lead to improper results (1). The negative influence of these factors can be significantly reduced by user supervision, thus correcting errors in the results obtained by fully automatic detection.

The second limitation is due to the fact that not all communication call types are suitable for 'tone-based' modeling because of their essentially noisy character. Such call types require a different model for analytical description (3). In general, the principle of analytical description can be also applied in the case of 'noisy' calls, but with a more sophisticated algorithm.

References

1. Komárek M. Program tools for processing of the communication sounds of laboratory animals (Diploma thesis). Prague, Czech republic: Czech Technical University, 2003:53pp.

2. Morgenbesser HB, Tyack PL. Synthesis and modification of the whistles of the bottlenose dolphin, *Tursiops truncatus*. *J Acoust Soc Am* 2000;108:407-16.
3. Ohlemiller KK, Kanwal JA, Butman JA, Suga N. Stimulus design for auditory neuroethology: Synthesis and manipulation of complex communication sounds. *Audit Neurosci* 1994;1:19-37
4. Šuta D, Komárek M, Jilek M, Syka J. Software tools for recording and modifying species-specific communication sounds (Abstract). *Plasticity of the Central Auditory System and Processing of Complex Acoustic Signals*, Prague 2003;p56.
5. Šuta D, Kvašňák E, Popelář J, Syka J. Representation of species-specific vocalizations in the inferior colliculus of the guinea pig. *J Neurophysiol* 2003;90: 3794-808.
6. Syka J, Popelář J, Kvašňák E, Šuta D, Jilek M. Processing of species-specific vocalizations in the inferior colliculus and medial geniculate body of the guinea pig. In: Syka J, ed. *Acoustical Signal Processing in the Central Auditory System*. New York: Plenum Press, 1997:431-41.
7. Wang X. On cortical coding of vocal communication sounds in primates. *Proc Natl Acad Sci USA* 2000;97:11843-9.

***Dr. Ing. Daniel Šuta,
Charles University in Prague,
3rd Faculty of Medicine,
Institute of Medical Biophysics and Informatics,
Ruská 87, 100 00 Prague 10,
Czech Republic.
e-mail: daniel.suta@lf3.cuni.cz***

EXAMINATION OF DENTIN SURFACE USING AFM (OUR EXPERIENCE)

Zdeňka Zapletalová¹, Roman Kubínek², Milan Vůjtek², Radko Novotný³

Palacky University Olomouc, Faculty of Medicine, Czech Republic: 1st Clinic of Dentistry¹, Department of Microscopy methods³; Palacky University Olomouc, Faculty of Science, Czech Republic: Department of Experimental Physics²

Summary: Atomic force microscopy (AFM) as one of the techniques of Scanning Probe Microscopy is useful for imaging of surface structure. This method can yield three-dimensional high-resolution topographic images of sample surfaces by using a scanning technique for conductors and insulators on atomic scale. It is based upon mapping of atomic forces on a surface of an investigated sample. The method is useful not only in physics and chemistry; it can be also applied in biological fields. Special construction of AFM scanner enables to follow biological samples in liquid environments. Artifacts caused by dehydration of samples are removed this way. Dentin of human teeth is a vital hydrated tissue. It is strongly sensitive to dehydration and drying that are commonly used in preparation of samples in examinations by Scanning Electron Microscopy (SEM). We describe our experience in examination of dentin surfaces of extracted human third molars using contact method of AFM under moist conditions.

Key words: Atomic Force Microscopy (AFM); Dentin; Smear layer

Introduction

Scanning Probe Microscopy (SPM) is a set of experimental methods used in imaging of surface structures with subatomic resolution (8). Beside physics and chemistry of surfaces the method is useful also in biological sciences.

One of the clones of SPM is Atomic Force Microscopy (AFM). AFM is based on mapping of an atomic-force field on a surface of an examined sample. Atomic forces are tested using a small tip attached on the flexible cantilever that moves above the surface. Attractive or repulsive forces are detected upon flexion of the cantilever with tip. This flexion is monitored using a sensitive usually laser-based detector. Both conductive and nonconductive samples can be studied this way.

Forces deforming a cantilever can have a different physical origin. Mostly van der Waals attractive forces acting between two atoms on larger scales are dominant. Repulsive forces between charged particles are important for shorter distances.

According to the type of the contact between the tip of the cantilever and the sample AFM can operate in three modes:

1. Contact mode:

Distance between the tip and examined surface is so small (they are in contact), that the overall force is repulsive and tends to flex the cantilever out of the surface.

2. Noncontact mode:

In this vibrational technique, an average force between the tip and surface is attractive. The tip vibrates in the di-

rection perpendicular to the surface, value of its amplitude is in order of tens of nm and resonance frequency is 200 kHz. Because there is no mechanical contact it is possible to measure also soft and elastic samples. Their possible contamination is prevented.

3. Intermitent contact mode:

It resembles the previous mode. Amplitudes of tip vibrations are greater and so the tip is in contact with the surface for a small portion of vibration period. This approach is more convenient than contact mode. It is used when damage of the examined sample could be caused by friction or drawing. It is more demanding than noncontact mode.

AFM provides a real topographical three-dimensional image of a sample surface with vertical resolution from 0.1 nm and lateral resolution from 0.1 nm. The obtained resolution depends on a given sample. Good samples can provide even atomic resolution. It gives an image in real time and so can be used also for monitoring of dynamic processes. The greatest advantage of AFM applications in biology is the possibility to image biological samples in vitro and in vivo. A special construction of AFM scanner enables to work directly in liquid environments (9).

Artifacts caused by dehydration of samples are eliminated this way. Imaging using AFM is nondestructive and samples can be visualized several times. Physical or chemical fixations as well as coating of surfaces by sputtering for having a better contrast and conductivity are not necessary.

Dentin of human teeth is a vital tissue that contains a large fraction of water and organic matter. Using the stan-

standard procedure for preparation of dentin samples in SEM (Scanning Electron Microscopy) a sample is dehydrated in graded acetone series, dried and coated in sputtering device after its fixation. The occurrence of artifacts caused by shrinking (15) cannot be eliminated in practice because dentin is strongly sensitive to dehydration.

We have investigated the possibility to examine dentin surface of human teeth under moist conditions using AFM. This method that is not based on aggressive chemicals can help in excluding artifacts.

Method

Human extracted third molars without decay stored in solution of 0.5 % chloramine for the period of less than one month after their extraction at the temperature of 4 degrees of Celsius (according to the rules ISO TR 11 405) have been used. After removing soft tissue and debris anatomical crown and apical part of a root have been separated using a diamond disc. 3-mm high dentin disc has remained after this procedure. A thin layer of cementum on the surface is removed with a low-speed handpiece under water cooling. Then the outer surface is polished by paper discs Sof-Lex (3M ESPE). Every dentin slice is divided into two halves and placed into distilled water in an ultrasonic purified apparatus for 30 minutes. The samples have then been examined by AFM in Laboratory of Atomic Force Microscopy.

AFM Explorer manufactured by ThermoMicroscopes (USA) has been applied using contact mode with tips from silicon nitride (type 1520-00, ThermoMicroscopes). The imaged surface area has gone from 5 to 100 μm and resolution of 300 points per row has been used. Maximum

measurable changes of the surface profile have been 10 μm . Dentin samples have been stored in distilled water and processed under moist conditions.

Results

Figures 1-4 show dentin surfaces and they also demonstrate problems that have been faced using AFM as a method for imaging. A flat dentin surface with well-shown dentinal tubules without smear layer are depicted in Fig. 1. Dentinal tubules as well as obvious drafts caused when preparing a sample are shown in Fig. 2. Dentinal tubules surrounded by a wall (caused probably by mechanical preparation of the sample) can be seen in Fig. 3. Morphology of a dentinal tubulus is visualized in 3D graph in Fig. 4.

Samples were small and that is why they had to be fixed to a bedding in order to allow for a convenient manipulation.

Natural curvature of a tooth root in two planes and a small roughness occurring on dentin surface after removing cementum complicated imaging and could also lead to a damage of the used tip. This problem has been removed polishing the surface by fine paper discs Sof-Lex under water cooling.

We have had to solve the problem of contamination of sample surfaces. If a surface is not clean enough a lot of strips occur in the image; they are caused by small particles that are moved on a surface by the tip. Removal of smear layer that arises on the surface after its instrumentation and prevents dentinal tubules from imaging is necessary. Removal of smear layer as well as plugs in dentinal tubules can be safely reached polishing the samples and subsequently putting them into an ultrasonic bath for 30 minutes. Removal

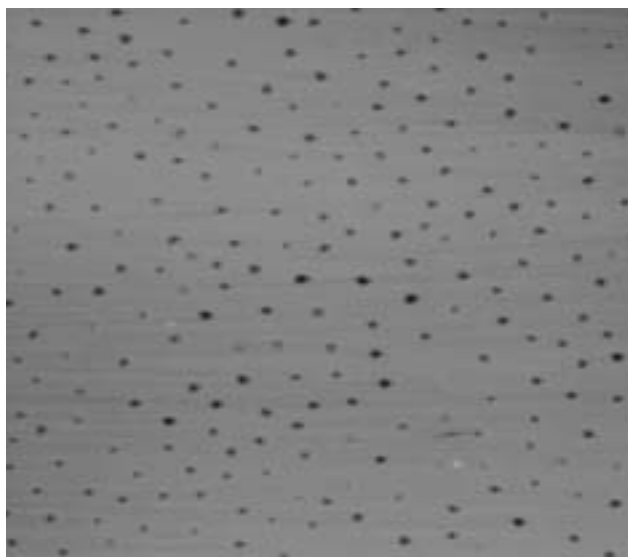


Fig. 1: Picture of a flat dentin surface with opened dentinal tubules without smear layer obtained by AFM (scan area 100x100 μm).

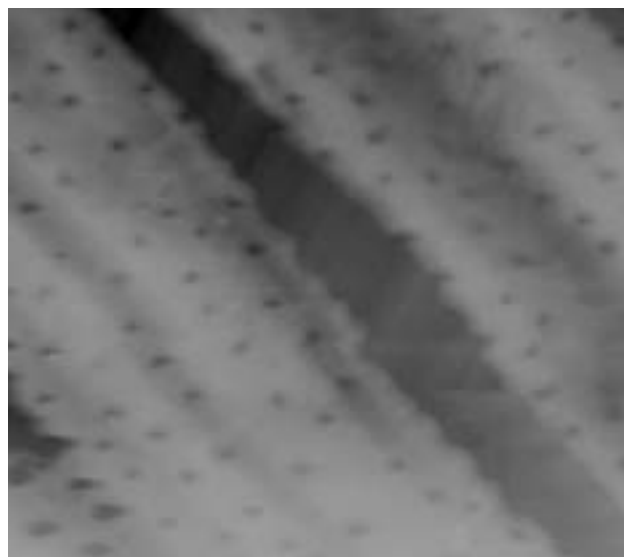


Fig. 2: Visible drafts on a surface of a dentin sample caused by mechanical preparation and depicted by AFM (scan area 100x100 μm).



Fig. 3: Dentinal tubules are surrounded by a wall in this image taken by AFM (scan area 25x25 μm).

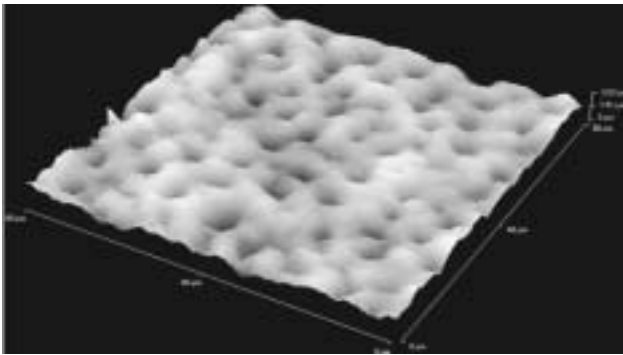


Fig. 4: 3D-image of dentin surface taken by AFM provides full information (scan area 5x5 μm).

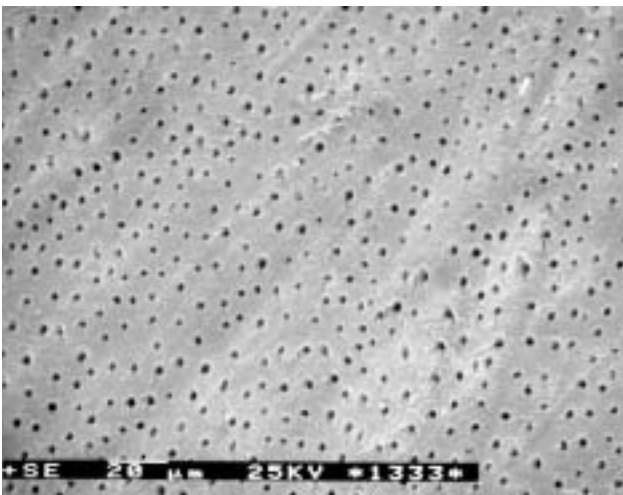


Fig. 5: Dentin surface with open dentinal tubules as seen by SEM; visible drafts remind mechanical preparation; (original magnification x1000, bar represents 20 μm).

of smear layer applying 37 % solution of phosphoric acid or combining phosphoric acid with natrium hypochloride lead to demineralization, event. deproteination of dentin.

Disadvantage of AFM approach is the fact that taking an image requires approx. five minutes. We obtain information about the sample surface just bellow the tip that covers a small area. Information about the rest of a sample surface is missing owing to a small scanned area and this complicates statistical analysis of the surface. Samples have to be moved mechanically bellow the tip which also causes troubles in a real experiment. To compare with Scanning Electron Microscopy (SEM), this method enables to visualize a large area of the surface and a subsequent enlargement of resolution is possible. We show pictures of surface - dentin morphology obtained by SEM for comparison. Samples have been prepared using a standard method for Scanning Electron Microscopy (dehydration in a grated acetone series, drying in CPD-030, coatinge by a 5-nm layer of gold and palladium). Observation has been done using microscope SEM Tesla BS 340. Surface of a dentin sample with well shown tubules is shown in Fig. 5; also evidence about mechanical instrumentation is present. Apertures of tubules are without a smear layer. Surface of dentin shown under a higher resolution is depicted in Fig. 6. Apertures of tubules are mostly covered by smear layer, presence of surface distortions caused by instrumentation is visible.

Discussion and Conclusions

It is evident from literature that AFM is a frequently used method for imaging of dentin. It is mainly useful in studies of a collagen network of dentin and its changes caused by different chemical agents to dentin (3,15). Changes in intertubular and peritubular dentin caused by interaction with phosphoric acid, self-etching primers, conditioners

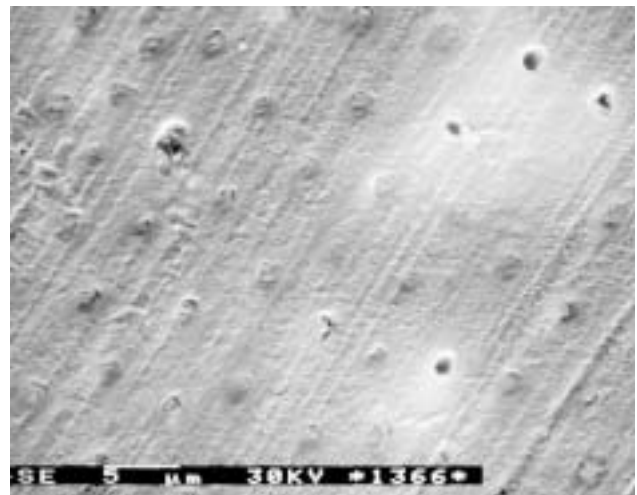


Fig. 6: Dentin surface with concealed apertures of dentinal tubules (original magnification x5000, bar represents 5 μm).

and other agents used in bonding of restorative materials (2,11,14,17,19) can be investigated. Also interaction of dentin adhesives with tooth hard tissues can be observed (1,10,12).

AFM has been applied in investigations of ultra-morphology of superficial and deep dentin and its mechanical properties (6,15). Roughness and elasticity of hydrated peritubular and intertubular dentin has been followed (7). Atomic Force Microscopy enables to observe micromorphology noncarious cervical lesions (13) as well as functional width of the dentino-enamel junction (4). This method also provides information about dentin roughness (16) and enables to register changes in nanomechanical properties of dentin during its storage (5).

We would like to note at this point that AFM has also some limitations. An inevitable use of a cantilever results in many difficulties and restrictions in measurements and sample preparation (20). Furthermore, the high cost of AFM systems prevents their widespread industrial and clinical use, and they are difficult to produce in laboratories that do not specialize in AFM technology (20). When a tip scans across a sample it induces a dynamic interaction force between the tip and the surface (18). The dynamic behavior is complicated and a precise analysis is difficult, but it can influence resolution of the surface image (18).

According to our experience AFM method is not suitable for the estimation of properties of larger areas on a surface. It is time-consuming and requires a flat surface that is accessible to a tip of an AFM microscope. This means a rather strong restriction to flatness of a sample as a whole as well as that concerning flatness of its detailed parts. It is without doubts that AFM brings new possibilities in imaging of dentin surfaces. For this reason, further spreading of this nondestructive method is expected in near future. We can see its main advantage in the fact that this method enables to study wet and chemically non-modified surfaces and so it does not face troubles connected with artifacts caused by dehydration as the other methods do.

This work is supported by the project by IGA no. NK/7710-2/2003 of the Ministry of Health Care of the Czech Republic (Influence of Nd:YAG laser irradiation of cervical dentin of extracted human teeth).

References

1. Cassinelli C, Mora M. Atomic force microscopy studies of interaction of a dentin adhesive with tooth hard tissue. *J Biomed Mater Res* 1994;28:1427-31.
2. El Feninat F, Ellis TH, Sacher E et al. A tapping mode AFM study of collapse and denaturation in dentinal collagen. *Dent Mater* 2001;17:284-8.
3. Habelitz S, Balooch M, Marshall JS et al. In situ atomic force microscopy of partially demineralized human dentin collagen fibrils. *J Struct Biol* 2002;138:227-36.
4. Habelitz S, Marshall SJ, Marshall GW Jr et al. The functional width of the dentino-enamel junction determined by AFM based nanoscratching. *J Struct Biol* 2001;135:249-301.
5. Habelitz S, Marshall GW Jr, Balooch M et al. Nanoindentation and storage of teeth. *J Biomech* 2002;35:995-8.
6. Kinney JH, Balooch M, Marshall GW et al. A micromechanics model of the elastic properties of human dentine. *Arch Oral Biol* 1999;44:813-22.
7. Kinney JH, Balooch M, Marshall GW et al. Hardness and Young's modulus of human peritubular and intertubular dentine. *Arch Oral Biol* 1996;41:9-13.
8. Kubinek R, Vůjtek M, Mašlán M. *Mikroskopie skenující sondou*. Olomouc: Vydavatelství UP Olomouc, 2003:145p.
9. Kubinek R, Vůjtek M, Holubová R et al. Biologické aplikace AFM. *Čes čas fyz* 2003;53(2):109-12.
10. Kwon TY, Imai Y. Effect of ferric chloride/citric acid/phosphoric acid conditioner on adhesion of 4-META/MMA-TBB resin to the tooth. *Dent Mater J* 1999;18:184-93.
11. Marshall GW, Saeki K, Gansky SA et al. AFM study of citric acid-ferric chloride etching characteristics of dentin. *Am J Dent* 1999;12:271-6.
12. Marshall GW Jr, Marshall SJ, Kinney JH et al. The dentin substrate: structure and properties related to bonding. *J Dent* 1997;25:441-58.
13. Marshall GW Jr, Chang YJ, Saeki K et al. Citric acid etching of cervical sclerotic dentin lesions: an AFM study. *J Biomed Mater Res* 2000;49:338-44.
14. Oliveira SS, Marshall JS, Hilton JF et al. Etching kinetics of self-etching primer. *Biomaterials* 2002;23:4105-12.
15. Perdigao J, Thompson J, Toledano M et al. An ultra-morphological characterization of collagen-depleted etched dentin. *Am J Dent* 1999;12:250-5.
16. Rosales JI, Marshall GW, Marshall SJ et al. Acid-etching and hydration influence on dentin roughness and wettability. *J Dent Res* 1999;78:1554-9.
17. Tanumiharja M, Burow MF, Cimmino A et al. The evaluation of four conditioners for glass ionomer cements using field-emission scanning electron microscopy. *J Dent* 2001;29:131-8.
18. Tser-Son Wu, Win-Jin Chany, Jung-Chang Hsu. Effect of tip length and normal and lateral contact stiffness on the flexural vibration response of atomic force microscope cantilevers. *Microelectr Eng* 2004;71:15-20.
19. Van Meerbeek B, Yoshida Y, Snauwaert J et al. Hybridization effectiveness of a two-step versus three-step smear layer removing adhesive system examined comparatively by TEM and AFM. *J Adhes Dent* 1999;1:7-23.
20. Yoshinobu M, Sadao O. Fabrication of micro tactile sensor for the measurement of micro-scale local elasticity. *Sensors Actuators A* 2004;109:202-7.

MUDr. Zdeňka Zapletalová,
Palacky University Olomouc,
Faculty of Medicine, 1st Clinic of Dentistry,
Palackého 12, 772 00 Olomouc,
Czech Republic.
e-mail: zdenzap@tunw.upol.cz